DEVELOPMENT OF CEMENTITIOUS COMPOSITES WITH ELECTROSTATIC DISCHARGE CAPABILITY

ELEKTROSTATİK YÜK BOŞALTMA KABİLİYETİNE SAHİP ÇİMENTO BAĞLAYICILI KOMPOZİTLERİN GELİŞTİRİLMESİ

DAMLA NUR ÇELİK

PROF. DR. MUSTAFA ŞAHMARAN

Supervisor

Submitted to
Graduate School of Science and Engineering of Hacettepe
University as a Partial Fulfillment to the Requirements for be
Award of the Degree of **Doctor of Philosophy in Civil Engineering**

2024

This thesis is dedicated to my parents, Sevgi – İbrahim ÇELİK, who worked with me like PhD students during my experimental studies throughout the pandemic, for their endless support and encouragement. This achievement would not have been possible without them.

ABSTRACT

DEVELOPMENT OF CEMENTITIOUS COMPOSITES WITH ELECTROSTATIC DISCHARGE CAPABILITY

DAMLA NUR ÇELİK

Doctor of Philosophy, Department of Civil Engineering

Supervisor: Prof. Dr. Mustafa ŞAHMARAN

October 2024, 336 pages

In daily life, electrostatic charges occur due to natural physical events and accumulate as static charges when people come into contact with objects and devices. If these charges cannot properly transfer from the floor to the ground, these can cause financial losses by damaging electronic devices and endanger life safety due to sparks. This problem is critical, especially in structures such as hospitals, the electronics industry, the petrochemical industry, production facilities, and military defense structures. The fact that 60% of the malfunctions in the electronics industry occur due to electrostatic discharge is of great importance in removing the static electric charge from the environment, especially on the floors of critical structures. In this context, the coating composite with superior performance, which meets the current requirements of the construction industry, is expected to be both economical and sustainable. This thesis study aims to (i) develop an early age high strength matrix mixture and (ii) obtain electrostatic discharge capability by incorporating single, double, and triple conductive materials into the developed cementitious composite. As a result of the thesis study, the main matrix was developed, the flow diameter of the mixture was measured as 41.5 cm, and the flow

time was measured as 3.75 seconds. The matrix's two-hour compressive strength was determined to be 32.73 MPa, its one-day compressive strength to be 36.90 MPa, and its ninety-day compressive strength to be 86.10 MPa. The one-day electrical resistance value of the matrix mixture without conductor addition was 15.40 MΩ and showed insulating properties. Among conductor-based samples, the lowest electrical resistance value was measured from the B6(2) sample as 200.5Ω after 180 days. The dispersion of the conductors significantly affected the short- and long-term electrical conductivity performance. Carbon fiber was the most effective conductor in single, double, and triple conductor additions. The BAC1022 (1) sample best preserved the mechanical and electrical performance among the mixtures exposed to different environmental conditions and harmful solutions. The composite developed in this thesis study offers a cost-effective solution compared to currently used systems. Thanks to its high mechanical performance, it can be applied directly on the ground without disrupting production. Furthermore, its high mechanical performance under various harsh conditions ensures long-term maintenance of electrical conductivity. Comprising a single layer, it is suitable for field applications, presenting a significant opportunity. In this way, the electrostatic discharge problem likely to occur in critically essential structures can be prevented with cementitious-based composites, thus preventing loss of life and property.

Keywords: Ternary-based systems, Early age high strength performance, Conductive materials, Electrical conductivity, Fresh properties

ÖZET

ELEKTROSTATİK YÜK BOŞALTMA KABİLİYETİNE SAHİP ÇİMENTO BAĞLAYICILI KOMPOZİTLERİN GELİŞTİRİLMESİ

DAMLA NUR ÇELİK

Doktora, İnşaat Mühendisliği Bölümü

Tez Danışmanı: Prof. Dr. Mustafa ŞAHMARAN

Ekim 2024, 336 sayfa

Günlük yaşamda elektrostatik yükler, doğal fiziki olaylar sonucu oluşmakta ve insanların eşyalar ve cihazlarla temas etmesiyle statik yük olarak birikmektedir. Bu yükler, uygun şekilde döşemeden toprağa aktarılamazsa, özellikle hastaneler, elektronik endüstrisi, petro-kimya endüstrisi, üretim tesisleri ve askeri savunma yapıları gibi kritik öneme sahip yapılarda elektronik cihazlara zarar vererek maddi kayıplara sebebiyet verirken, aynı zamanda oluşan kıvılcımlar sebebiyle can güvenliği de tehlikeye atılmaktadır. Bu nedenle, inşaat sektörünün mevcut gereksinimlerine sahip, üstün performans özellikli, ekonomik ve sürdürülebilir kompozitin geliştirilmesi kritik yapılar için önemli bir yere sahiptir. Bu tez çalışması ile (i) erken yaşta yüksek dayanıma sahip matris karışımı geliştirilmesi ve (ii) geliştirilen çimento bağlayıcılı kompozite iletken malzemelerin tekli, ikili ve üçlü ilave ederek servis ömrü boyunca elektrostatik yük boşaltma kabiliyeti kazandırılması amaçlanmıştır. Tez çalışması sonucunda geliştirilen ana matris karışımın yayılma çapı 41,5 cm ve yayılma süresi 3,75 saniye ölçülmüştür. Matrisin iki saatlik basınç dayanımı 32,73 MPa, bir günlük basınç dayanımı 36,90 MPa ve doksan günlük

basınç dayanımı 86,10 MPa olarak tespit edilmiştir. İletken ilave edilmemiş matris karışımının bir günlük elektriksel direnç değeri 15,40 MΩ olarak ölçülmüş ve yalıtkan özellik göstermiştir. Ana matris karışıma iletken malzemelerin ilave edilmesiyle en düşük elektriksel direnç değeri 180 gün sonunda B6(2) numunesinden 200,5Ω olarak ölçülmüştür. Kısa ve uzun dönemde yüksek elektriksel iletkenlik performansı iletkenlerin dağıtım şeklinden önemli ölçüde etkilenmiştir. Tekli, ikili ve üçlü iletken ilavelerinde en etkili iletken, karbon lif olmuştur. Farklı ortam koşullarına ve zararlı çözeltilere maruz bırakılan en iyi elektriksel iletkenlik performansına sahip karışımlar arasında mekanik ve elektriksel performans en iyi BAC1022(1) numunesinde korunmuştur. Mevcut tez çalışması tarafından geliştirilen kompozitin hali hazırda kullanılan sistemlere göre uygun maliyetli çözüm sunması, yüksek mekanik performansı sebebiyle üretimi aksatmadan zeminde kullanılabilmesi, uzun dönemde çeşitli zararlı koşullar altında elektriksel iletkenlik performansını koruyabilmesi, tek katmandan oluşması ve sahada uygulanabilmesi gibi özellikleri sebebiyle zemin uygulamalarında büyük bir fırsat sağlayacağına inanılmaktadır. Bu sayede, kritik öneme sahip yapılarda oluşması muhtemel elektrostatik yük boşalımı problemi çimento bağlayıcılı kompozitlerle engellenerek can ve mal kayıplarının önüne geçilebilecektir.

Anahtar Kelimeler: Üçlü sistemler, Erken yaş yüksek dayanım, İletken malzemeler, Elektriksel iletkenlik, Taze özellikler.

ACKNOWLEDGEMENT

First and foremost, I would like to express my deepest appreciation to my supervisor, my idol in life, for guiding me through the most challenging moments, including my education, and for his unwavering support and interest. It was a great honor and pleasure to work with him.

I would like to extend my sincere thanks to Prof. Dr. İsmail Özgür YAMAN, Assoc. Prof. Dr. Alper ALDEMİR, Assoc. Prof. Dr. Mustafa Kerem KOÇKAR, and Assoc. Prof. Dr. Gökhan DURMUŞ for being on my thesis jury and for their constructive comments. It has been an honor to have them on my defense committee. I would also like special thanks to Assoc. Prof. Dr. Gürkan YILDIRIM, Dr. Mehmet Kemal ARDOĞA, Asst. Prof. Hüseyin ULUGÖL for their constructive criticism and valuable feedback, which enhanced the quality of this research.

I would like to thank all members of the Concrete Research Laboratory at the Department of Civil Engineering, Faculty of Technology, Gazi University for their support. I would especially like to extend my appreciation to my colleagues Tuğba YILDIZLI, Rüya KILIÇ DEMİRCAN, Pınar Sezin ÖZTÜRK KARDOĞAN, Ahmet ERDAĞ, Onur ÇAVUŞOĞLU, Murat PINARLIK, Coşkun ÇAKMAK, Anıl ÖZDEMİR, and Özgün BOZDOĞAN for their supportive throughout and provided a stimulating academic environment.

I would also like to extend my sincere gratitude for the support provided by the Scientific and Technical Research Council of Turkey (TÜBİTAK) for financially supporting my thesis under the 119M175 project. The grant helped facilitate my research-related activities.

I would also like to thank TÜBİTAK Department of Science Fellowships and Grant Programs (BİDEB) for financial support within the scope of the 2214-A International Research Fellowship Programme for PhD Students. I am grateful for the invaluable support the Oregon State University provided throughout the research process. The facilities and resources offered were beneficial and have been instrumental in completing this research project successfully. During the program, I would also like to thank my supervisors, Prof. Dr. Burkan İŞGÖR and Prof. Dr. Jason WEISS, for supporting the project and helping me gain a versatile perspective and experience.

I would also like to thank the Weiss and İşgör Research Group members for their contributions to my experimental studies, and my friends Rojbirin and Şervan BARAN, Nur Sena BALLIOĞLU, Ludovica LELA, and Feyza ŞAHAN for their unwavering support in the USA.

Finally, I would like to express my gratitude to the founding leader of the Turkish Republic, Mustafa Kemal ATATÜRK, and his companions for everything they did and for inspiring me to do better.

Endless thanks,

Damla Nur ÇELİK

October 2024, Ankara

TABLE OF CONTENTS

LIST OF TABLES

LIST OF FIGURES

SYMBOLS AND ABBREVIATIONS

Symbols

^{o}C	Centigrade Degree
%	Percent
V	Volt
R	Resistance
g	Gram
μm	Micro-meter
mm	Milli-meter
cm	Centi-meter
m	Meter
s	Second(s)
min	Minute(s)
h	Hour(s)
MPa	Mega-pascal
Ω	Electrical Resistance (Ohm)
kΩ	Kilo-ohm
MΩ	Mega-ohm
GΩ	Giga-ohm
TΩ	Tera-ohm

Ω.cm	Electrical Resistivity (Ohm.cm)
W	Watt
Rpm	Revolutions Per Minute
Sm^{-1}	Conductivity
kHz	Kilo-hertz
GHz	Giga-hertz
dB	Decibel
Al	Aluminum
Si	Silicon
Ca	Calcium
OH	Hydroxide
Au	Gold
CO_2	Carbon Dioxide
$Ca(OH)_2$	Calcium Hydroxide
SiO_2	Silicon Dioxide
Al_2O_3	Aluminum Oxide
Na_2O	Sodium Oxide
CaO	Calcium Oxide
CA	Calcium Monoaluminate
CT	Perovskite
C_2S	Dicalcium Silicate

C_3S	Tricalcium Silicate
C_3A	Tricalcium Aluminate
C_4AF	Ferrite
C_2AS	Gehlenite
SO_3	Sulfur Trioxide
TiO_2	Titanium Dioxide
Fe_2O_3	Iron Oxide
Al_2O_3	Aluminum Oxide
$CaSO_4$	Anhydrate
$CaSO_4.0.5H_2O$	Hemihydrate
$CaSO_4.2H_2O$	Gypsum
$CaCO_3$	Calcite
C_4AH_{13}	Tetracalcium Aluminate Hydrate
$Al(OH)_3$	Gibbsite
C_3AH_6	Tricalcium Aluminate Hydrate
C_2AH_8	Dicalcium Aluminate Hydrate
C_2ASH_8	Strätlingite
$C_{12}A_7$	Mayenite
CAH_{10}	Calcium Aluminate Decahydrate
C_3FT	Ferro Perovskite
Li_2CO_3	Lithium Carbonate

$C_6H_8O_7$	Citric Acid
FeSi	Ferrosilicon

Abbreviations

ESD	Electrostatic Discharge
UV	Ultraviolet
CAC	Calcium Aluminate Cement
PC	Portland Cement
CŠ	Calcium Sulfate Source
w/c	Water-to-Cement Ratio
s/c	Sand-to-Cement Ratio
kN/s	Kilonewton per Second
A/l	Area-to-Length Ratio
C-S-H	Calcium-Silicate-Hydrate
C-A-S-H	Calcium-Aluminate-Silicate-Hydrate
GGBFS	Ground Granulated Blast Furnace Slag
FA	Fly Ash
RHA	Rice Husk Ash
SF	Silica Fume
XRD	X-ray Diffraction

XRF	X-ray Fluorescence
EDX	Energy-Dispersive X-ray
SEM	Scanning Electron Microscopy
TEM	Transmission Electron Microscopy
ITZ	Interfacial Transition Zone
AFm	Monosulfate
Aft	Ettringite
SF	Steel Fiber
CF	Carbon Fiber
MCF	Milled Carbon Fiber
PVA	Polyvinyl Alcohol
CB	Carbon Black
CNT	Carbon Nano Tube
CNF	Carbon Nano Fiber
MWCNT	Multi-Walled Carbon Nano Tube
GNP	Graphene Nano Platelet
RCF	Recycled Carbon Fiber
WWE	Waste Wire Erosion
SMA	Shape Memory Alloy
GO	Graphene Oxide
RH	Relative Humidity

SP	Superplasticizer
HRWRA	High Range Water Reducing Agent
NFS	Naphthalene Superplasticizer
PCC	Polycarboxylate Superplasticizer
SA	Setting Accelerator
SRA	Setting Retarder Additive
SCC	Self Compacting Concrete
ER	Electrical Resistance
AC	Alternating Current
DC	Direct Current

1. INTRODUCTION

The electrostatic discharge, commonly known as ESD, has been an interesting issue since it was discovered by Thales of Miletus in 600 B.C.E with the electrostatic attraction between amber and hay [1]. In the past, it was one of the most common problems in electrical devices with static electricity or electrostatic discharge [2–4]. Still, this continues to be a problem because of today's technology scaling, higher frequency requirements, and increasing customer expectations [1,5,6].

There are two sources of damaging ESD-generated events: human- and equipment-based. These phenomena occur when a charged person touches an electrical device, or a circuit element of a device can cause ESD to receive damage to other elements. Mainly, electrostatic discharge events occur in daily experience. When an ESD event occurs, the human body can reportedly generate static charge levels that range up to 30,000 volts by simply walking on a floor, touching the doorknob, plugging your palm reader into its socket, getting in a car, pumping gasoline in a car, and putting the key in the ignition [2,7,8]. Static charge can accumulate in the human body through interactions with physical phenomena. The human body cannot see, feel, or hear ESDs much below the potential of 3000 - 4000 volts. In fact, for these levels, it may not be necessary to touch any device physically; a charged body can cause these voltages [4]. The total energy can be discharged into an electrically grounded body or electronic device with periods measured in picoseconds and several kilowatts of power, which might be sufficient to cause failure [7]. To make a long story short, ESD can be responsible for direct, indirect, and latent failures in microelectronic devices (such as IC failures) because of the trends toward higher speed and smaller device sizes and operation of these systems[2,4,6,9].

Literature estimates that between 40 - 60% of equipment failures can be attributed to ESD phenomena [3,10]. This formation harms many valuable electronic equipment and endangers the safety of people who use the devices, apart from causing millions of dollars in additional costs every year in the world. The ESD can be even more dangerous if sparks occur in factories that specialize in producing explosives or armories. If a spark discharge occurs near explosive materials, even a low-energy spark, in the range of 2–3 mJ, can be

sufficient to trigger primary explosives or fires, potentially leading to detonation, which can significantly damage the surrounding area and loss of life. [11].

Because of the problems and risks that ESD might cause, it is necessary to have systems that will ensure that the static load generated in the environment is directly removed from the area and given to the soil to prevent the static electricity charge from accumulating on people from turning into sparks and not harming people and not causing any deterioration. In the literature, ground connection, anti-static working clothes and shoes, anti-static furnishing, ESD-resistant microelectronics, and anti-static floor or ground methods are preferred to remove the static charge in a healthy way from the environment and sustain an anti-static environment [12–15].

Among these methods, coating designs with anti-static capability are among the most preferred methods in critical buildings. The static charge is removed in the construction sector using conductors using epoxy, plastic, and vinyl-based antistatic capability coatings [16–18]. The most important aim is to meet the targeted ESD standards in coating design [19–23]. For this purpose, coatings were designed to apply to the flooring with different binders and conductive materials. Besides providing anti-static capability, it was also designed to be used for repairing the surfaces of damaged and worn floors to obtain flexible, pressure-resistant, crack-free, abrasion-resistant floors on the surface [24].

Currently, epoxy-, plastic- and vinyl-based coatings have disadvantages as well as advantages during application. The fact that these coatings are multi-layered, the application processes are long, and the raw material cost prices of the chemicals as binders and conductors to sustain conductivity put the coating in a disadvantageous position. In addition, the chemical-based coating's surfaces are rapidly damaged due to harmful environmental conditions and contact with UV rays, causing the electrostatic conductivity of the coating to be lost over time. These coatings, which enable problems to be solved in the short term, do not fully meet the desired requirements when the total service life of the structures is considered [25].

From a general perspective, although floor applications are not of great importance, it is clear that any malfunction or technical problem on the floor will disrupt this service and cause severe financial losses. At the same time, it endangers life safety in possible sparks and explosions. To overcome the disadvantages of chemical-based antistatic floor designs, developing new-generation cementitious composites with electrostatic discharge capability in critical buildings is a major step toward sustainable construction.

1.1. Scope of the Thesis

This thesis study adopts a holistic approach to development, offering advanced solutions for a more economical, healthier, and sustainable process for anti-static flooring, addressing various performance objectives: (I) valorization of ternary systems through the development of early age high strengths cementitious composites alternative to chemical-based composites (II) utilization of different types of cement and chemical additives to obtain such as high flowability and crack-free as well as chemical resistant with a primary focus on fresh/rheological properties due to their importance for proper applicability in fabrication (III) development of anti-static protection capability cementitious composite by incorporating single, double, and triple conductors to the system (IV) evaluation of the electrical performance of cementitious composites with anti-static protection capability under various environmental conditions and chemical solutions in the early and long term.

1.2. Contributions

This thesis study is novel in that using cementitious materials to develop anti-static floor designs with conductive additives combines the advantages of cementitious material properties, early age high-strength properties, does not require maintenance, reduces the expenses of raw materials, and has easy/fast applicability, early and long term ESD protection under harsh conditions compared to chemical binder-based floor designs in critical buildings. It promises profitable and circular value chains of materials and products with novel designs compared to traditional floor systems due to its high-performance properties other than electrical conductivity.

The main goals aimed to be achieved in this thesis study for the developed new generation floor design to replace the currently used chemical binder-based coating designs are listed below:

- The cementitious composite to be used as a binder in the coating design must have early and later age high strength, resistance to harmful environmental conditions, high flowability, crack-free, and smooth surface properties.

- Determining the appropriate mixing method and optimum conductive utilization rate to minimize the cost of the composite.

- Evaluation of the long-term electrically conductive performance of anti-static protection capability of composite properties under harmful chemical environments and the effects of humidity and temperature.

- Merging different superior performance features products without compromising on performance features such as long service life and sustainable ESD protection in the same design.

1.3. Organization

The organization of the thesis is as follows:

In the 1st section named “Introduction”, this section provides an overview of the main problems addressed in the thesis, along with the objectives and scope of the study.

In the 2nd section named “Literature Review”, this section provides a comprehensive review of existing literature on ternary systems, early age high-strength composites, conductive materials, and the electrically conductive performance of cementitious composites is presented.

In the 3rd section named “Materials and Methods”, this section informs the materials used in the study, including various types of cement, chemical additives, sand, and conductive materials. It also outlines the testing methods employed to evaluate the rheological, mechanical, and electrical properties of the developed cementitious composites.

In the 4th section named “Results and Discussion”, this section provides the results obtained from the experimental studies that are presented and discussed in detail. This section includes sub-sections covering the development of cementitious-based mortar mixtures with early age high-strength properties and the addition of conductive materials into cementitious mortar by single, double, and triple for the impact of moisture and temperature conditions on composite performance, and the effects of aggressive chemical solutions on composite performance.

In the 5th section named “Conclusion”, this final section summarizes the conclusions drawn from the experimental studies and discusses these concerning the existing literature.

2. LITERATURE REVIEW

The ESD phenomenon is one of the most important physical phenomena that causes 40 - 60% of equipment failures in the electronics industry [3,10]. It can occur easily in daily life, and people do not feel static charge levels of up to 30,000 volts [1,2,7,26]. The total energy can be discharged into a person or electronic device within seconds. Thus, ESD is primarily responsible for electronics failure and fire due to sparks occurring on devices [11]. It can endanger a person's life and waste money because of the breakdown of the devices. Nowadays, this is still a major problem, especially in critical buildings with technological improvements [1,6]. There is a requirement for systems that will directly remove electrostatic charges from the working area in critical buildings. Even though different precautions were taken in the past, one of the most used solutions is chemical binder-based ESD protection capability coating designs [16,27,28]. Due to the disadvantages of chemical binder-based flooring systems, these systems are not sustainable for meeting anti-static protection in the long term [25]. Considering all these drawbacks, researchers have been investigating the usability of other binder-based coating designs in this field. Modified cementitious composites incorporating conductors can solve the ESD problem in critical building floor applications [29,30].

The literature review was carried out in two main stages. The first part of the literature review focused on investigating the early age high strength of cementitious composites. The second part included the possible ways to provide anti-static protection capability to these composites, studying the factors that could impact this performance negatively.

2.1. Cementitious Binder System

Since the invention of traditional cement in early 1824, cement and related products have become the most important industrial products today [31]. Concrete products are the second most globally consumed material after water by mass because ingredients are easily accessible, have good environmental adaptability, and are cost-effective [32]. With technological developments, traditional concrete composite's physical, mechanical, and

durability performance can be improved to superior functional properties by modifying raw materials, chemicals, and mineral additives. Therefore, European standards state a minimum service life of at least 75 years for public concrete structures [33]. However, it has been observed that many structures begin to deteriorate after 20 or 30 years due to the combined effect of mechanical loading and environmental conditions [34]. Service life varies between the interior and exterior of buildings depending on the deterioration. Environmental conditions, which negatively affect buildings, do not have as much effect on interior sides as on exterior sides.

It is preferred that some of the buildings' interior sides should have long service life such as in hospitals, the electronics industry, explosives production facilities, the petrochemical industry, precision production facilities, and military defense structures. Because the interior side of buildings is exposed to chemicals and different ambient conditions, the floors are one of the most affected structural elements for the interior sides of critical buildings [35]. There are high technological devices in such critical or public buildings, so any negative possibilities that may occur on the interior side may result in service disruption for a long time and high costs for replacement or repair [36]. Therefore, the floor system must be designed to increase its service life and resist environmental impacts besides the ESD protection capability. In addition, it must be opened in a minimum time to avoid service disruption after applying coatings on the floors.

Early age high strength cementitious composites, which have become essential in recent years, are widely used in repairing structures such as the construction industry in military airports, some industrial buildings, concrete roads, etc. [37]. In the literature, various strength values are determined for the repair studies. Parker and Shoemaker [38] stated that road patch repair materials had at least 13.80 MPa compressive strength to resist cracking, abrasion, deterioration, and disassembly immediately after traffic opening. Zia et al. [39] stated that early age high strength concretes should reach a compressive strength value of at least 20.70 MPa within the first 4 hours and at least 34.50 MPa within the first 24 hours. The New Jersey Transportation Department [40] found that a minimum compressive strength of 20.70 MPa and flexural strength of 2.41 MPa after 6 hours for “quick concrete mixes” developed in the mid-90s. The Federal Highway Administration

[41] stated that fast-setting capability concrete mixtures to be used as repair materials had to reach at least 6.90 MPa after 3 hours and 20.7 MPa compressive strength after 24 hours. The California Transportation Department [42] claimed extensive highway pavement repairs should have at least 2.76 MPa flexural strength before being opened to traffic. According to the Michigan Transportation Department [43], rapid-setting materials used in structural concrete repairs had to reach at least 13.80 MPa after 2 hours, 17.20 MPa after 4 hours, and 31.00 MPa compressive strength after 28 days. Larmie [44] observed that 11.00 MPa or less compressive strength in 4 hours in order to meet the wheels pressure applied by aircraft wheel on the runway would be sufficient for rapid runway repair. Arslan [45] investigated using self-compacting concrete as a quick repair composite for aircraft runway. The composite was developed using calcium aluminate cement, basalt, silica aggregate, calcium chloride, sodium aluminate, and lithium carbonate as setting accelerators and polycarboxylate-based chemical additives as plasticizers. Sahmaran et al. [46] developed early age high strength ductile cementitious composites with more than 20.00 MPa compressive strength and more than 6.00 MPa flexural strength after 6 hours. In repair applications widely used for different projects nowadays, various minerals and chemicals or techniques must be used along with traditional concrete components to achieve high-strength properties at an early age. The following solutions are generally used to obtain early age high strength in various ranges depending on the application area and conditions [47].

-Early age high strength cement (ex. CEM I 52.5R type Portland Cement)

-Special types of cement, such as ternary-based systems

-High dosage of cement

-Low water/binder ratio

-Chemical additives (setting accelerators, high water reducers, setting retarders, etc.)

-Silica fume (or other additional mineral additives)

-High degree of hydration level

-High curing temperature

One of these solutions, ternary-based systems consisting of a mixture of early age high-strength capability of Calcium Aluminate Cement (CAC) and Portland Cement (PC) with a Calcium Sulfate Source (C$), have been frequently studied in recent years.

2.1.1. Calcium Aluminate Cement (CAC)

TS EN 14647 defines calcium aluminate cement (CAC) as a hydraulic binder and finely ground inorganic substance that, when mixed with water, forms a paste that sets and hardens through hydration reactions. It is a material that maintains strength and stability thanks to the stable, hydrated phases formed after hydration [48]. Literature studies indicated that calcium aluminate cement was invented in 1888 [49]. In patent, it mentioned that alumina-rich calcium aluminates had excellent cementing properties. However, the commercialization of the CACs began with Bied's studies in Lafarge company laboratories at Le Teil, France [50]. After this study, in 1908, Bied got a patent that was related to the manufacturing process for cement produced with bauxite, or other aluminous and ferruginous material of low silica content, which was burned with limestone [51]. Unlike Portland cement, this invented cement had significant properties such as high sulfate resistance and rapid set. At the same time, Henry S. Spackman and Ellis W. Lazell invented a cementitious material using hydraulic calcium aluminate compounds, which were prepared by calcining finely ground lime and bauxite or kaolin, high alumina clays, and high alumina slags in 1908 [52]. In the literature, it was known as 'High alumina cement' in the early years, and then it was named 'Calcium aluminate cement' in the 1970s [53,54].

Between the Word Wars, calcium aluminate cement provided rapid hardening properties for road repair and durability properties for undersea. After the World War II destruction, a requirement for urgent construction occurred, which caused the widespread usage of CAC in prestressed beams in the United Kingdom and Spain [55]. However, several structural failures originated from gradual strength loss due to the conversion process of CAC hydration, and also its higher cost limited the usage of CAC for structural applications [31].

Since the 1980s, the usage of CAC has started to spread because of its unique properties, such as the ability to harden even under low-temperature conditions, shrinkage compensation, rapid strength development, and resistance to a wide range of chemically aggressive conditions [31,53,56,57]. Also, CAC has been preferred in different applications recently, such as rapid repair mortars, refractory and sewer pipe linings, high-tech tile adhesives, floor screeds, and self-leveling coatings in the construction sector [53,58,59]. The demand for calcium aluminate cement has steadily grown over the last few years, reaching one million tons globally between 2021 and 2022 [60].

2.1.1.1. Raw Materials, Chemistry, Manufacturing, and Physical Characteristics of CAC

Regarding raw materials in its production and main phase composition, CAC differs from traditional PC in the construction industry. Two main raw materials are used to produce CAC industrially: limestone as a calcareous source and bauxite as an alumina source. Since CAC contains a high amount of alumina content, alumina and bauxite are vital for production. Although it is widely distributed and usually occurs with silica (as in clays), bauxite is the only suitable mineral available commercially for large-scale cement production. [55]. The alumina content (Al_2O_3) of the raw materials used leads to minor differences in the compounds formed in the production of CACs. Therefore, as the primary raw material has high Al_2O_3 content with minor impurities in production, purer sources of materials, such as low-iron bauxites, alumina, and lime-containing iron, are preferred. However, a considerable amount of Fe_2O_3 (10 – 20%) and several percent of TiO_2 can be present in a CAC system [31,53,59].

In literature studies, there are four main grades of CACs regarding the used raw materials and their proportion [59]. The main variants of CAC clinkers are given in Table 2.1. The aluminate content directly affects the physical and chemical properties of CACs. The color of standard CAC, which has the lowest aluminate content (38 - 40% Al_2O_3), is dark grey. As such, it has a darker color than the ordinary PC. Since ferruginous bauxites are generally preferred in standard CAC-type production, Fe_2O_3 content can be found in the system up to 20%, and TiO_2 content can be up to 3%. As the aluminate content increases

up to 80%, the color of the cement changes from dark to white in CACs. Its main reason is that very pure raw materials must be used to obtain high alumina content, and their iron content should remain very low. Although the application areas of CACs are generally similar, the 70 and 80% high alumina content CACs are explicitly used for refractory purposes. In contrast, the standard and medium CACs are preferred for other purposes, such as repairing mortar and self-levelling. In terms of SO_3 content, a low ratio is critical as it increases sulfate resistance among all CACs [53,56,61].

Table 2.1. Main variants of CAC clinkers [61]

Grade	**Standard 40**	**Medium 50**	**High 70**	**High 80**
Al_2O_3	36-42	48-60	65-75	>80
CaO	36-42	36-42	25-35	<20
SiO_2	3-8	3-8	<0.5	<0.2
Fe_2O_3	12-20	1-3	<0.5	<0.2
TiO_2	<3	<2	<0.005	<0.005
MgO	<1	≈0.1	≈0.1	<0.1
Na_2O	≈0.1	≈0.1	<0.3	<0.2
K_2O	≈0.1	≈0.05	≈0.05	≈0.05
Color	Grey or buff to black	Light buff or grey to white	White	White
Main Use	Concrete and formulated mortars, Peri-refractory	Refractory concrete and formulated mortars	Refractory concrete and formulated mortars	Refractory

Aluminate content also directly affects the manufacturing process of the CACs. However, the CAC clinker is in the form of a wholly fused melt that requires a specially designed furnace that reaches up to 1550 °C, depending on the chemical composition of the CAC clinker. The higher aluminate grades are usually manufactured in rotary kilns like Portland cement, although the product is much lower volumes than it. The final product of CAC clinker is getting quite strong at the end of the production process. Therefore, more energy is needed to grind the CAC clinker than the PC. In addition, the CAC clinker does not contain any calcium sulfate source and mineral additions during grinding [59].

The physical and mechanical properties of CAC types vary depending on the raw material. The specific gravity of CACs varies between 3100 – 3500 kg/m^3 and it is slightly higher than PC [58]. Standard CACs have the highest specific gravity due to their iron content [59]. According to the TS EN 14647 standard, the Blaine surface area of standard CACs should be between 250 – 400 kg/m^2 with a typical residue of 4% on a 90 μm sieve and 20% on a 45 μm sieve [48]. However, surface fineness can be achieved up to 800 m^2/kg in CAC grains, especially with the increase of Al_2O_3 ratio [55]. The flowability value of CACs is significantly higher than PCs at a constant water/cement ratio, and it has a self-levelling ability. While the initial setting time of CACs is approximately 2 hours longer than PCs, the final setting time is approximately 5 hours earlier than PCs [48,58,62]. Although the CAC's setting time starts later than the PC's, the hardening and strengthening period is relatively short. Thus, the 24-hour mechanical performance of CAC is nearly the same as the 28-day mechanical performance of PC [62].

2.1.1.2. General Mineralogical Composition of CAC

In order to understand the hydration mechanism of CAC, it is necessary to know the phases that form as a result of its clinker production. Although principal oxides such as Al_2O_3, CaO, SiO_2, Fe_2O_3, and other minor oxides in CAC clinker are similar to PC clinker, the ratios of oxides in the clinker are quite different [61].

While lime and silica contents are high in PC clinker, alumina, and lime are high in CAC clinker. Therefore, the mineralogical composition of CAC clinker is quite different from that of PC. The increase in the Al_2O_3 ratio and burning temperature lead to changes in the amounts of particular phases, such as hydraulic cement minerals, water, and formed hydrates [63–65]. In general, five main phases are formed by lime and alumina in CAC clinker: calcium monoaluminate (CA), mayenite ($C_{12}A_7$), dicalcium silicate (C_2S), gehlenite (C_2AS) and ferrite (C_4AF) [66,67].

Standard grades CACs containing up to 41% Al_2O_3 have more complex mineralogy, forming more phases due to high amounts of Fe_2O_3. Among the phases, CA is one of the

first phases, with up to 60% content to precipitate from the melt-in the clinker. This is followed by C_2AS (12%), C_2S (9%), small amounts of $C_{12}A_7$, and other minor phases. The 1–3% of Fe_2O_3 is included in solid. Apart from the phases, other minor phases include perovskite (CT) up to 6%, plechroite (Q-phase) up to 6-7%, ferro-perovskite (C_3FT), ferrite (C_4AF), spinel and wustite (f) [59]. The CA is the main phase that gives cementitious properties in CACs. CA phase can have setting times of tens of hours, allowing time to prepare and place mortars, and it can be castable and let them harden quickly when the presence of small amounts of $C_{12}A_7$, the rate of strength development is relatively high at an early age due to the high reactivity of CA phase [53,58,59]. Although $C_{12}A_7$ (mayenite) can occur in small quantities in CAC clinker, it is the most reactive calcium aluminate phase. Therefore, it accelerates the rate of the hydration mechanism and decreases setting time without any strength improvement. The amount of this component is strictly limited to prevent early stiffening or flash setting. However, calcium sulfate source incorporation into CAC can be used as rapid hardening mortars [61,68]. The C_2S phase, formed by lime and silica in clinker, has hydraulic binding properties and behaves similarly to PC hydration. With the contact of clinker with water, the hydration rate of C_2S is slow and thus contributes to the compressive strength of the composite at later ages [31,58]. Silica is usually present as C_2S, C_2AS (gehlenite), or both; the C_2AS phase can be high in AI_2O_3 and low in SiO_2. Pure C_2AS has little or no hydraulic activity, but the impure compound found in CACs may not be so unreactive. Like C_2S, the C_2AS sets slowly and contributes to the strength after a considerable period [53,55]. Other minor oxides are usually present in solid solutions. Plechroite (Q-phase), which has a fibrous form in sections, can occur in different ratios but shows very little hydraulic binder property. However, the CA phase is much reduced when plechroite is found, and the strength is usually lowered. In addition, Perovskite (CT) can occur in clinker, but it has no hydraulic properties. C_4AF (ferrite) contributes no or little to the setting and strength development [31].

In literature studies, the hydration reaction of CAC is also wholly different from that of PC. The CA is the highest phase (up to 60%) in the clinker and has hydraulic properties. A hydroxylated surface layer ($Ca[Al(OH_4)]_2$) is developed between CA and water [59]. As the dissolution process continues, the Ca^{+2} and Al $(OH_4)^-$ concentrations increase rapidly, then begin to precipitate out of the water solution in new chemical combinations,

i.e., CAH_{10}, C_2AH_8, C_3AH_6, and AH_3 and amorphous alumina gel-phases and the pH of the system's pH reaches twelve [56,64]. These products' rate of hydration and related physical properties are affected by the hydration ambient temperature, w/c ratio of mixture, and Al_2O_3 content of CAC clinker. The hydration mechanism reactions of CAC clinker based on temperature are given below [65,69].

First, the CA (mono aluminate) phase reacts with water rapidly and produces CAH_{10}, which has excellent binding properties at below 15 °C:

$$CA + H \rightarrow CAH_{10}$$

If the temperature is above 15 °C, C_2AH_8 is also formed with CAH_{10}. In addition, the content of C_2AH_8 increases with temperature rise, and it becomes dominant with AH_3 at above 25 °C.

$$2CA + 11H \rightarrow C_2AH_8 + AH_3$$

In addition, alumina gel transforms with time from an amorphous state to form hexagonal crystals of gibbsite (Al $(OH)_3$).

$$AH_x\ (alumina\ gel) \rightarrow \gamma - AH_3(gibbsite) + (x-3)H$$

If the temperature is above 40 °C, the CA phase transforms into C_3AH_6 directly during early hydration.

$$3CA + 12H \rightarrow C_3AH_6 + 2AH_3$$

Based on the ambient temperature, C_2AH_8, CAH_{10}, C_3AH_6, and Al $(OH)_3$ are formed as main hydration products. Among the combinations, while C_2AH_8 and CAH_{10} phases are

metastable, C_3AH_6 and AH_3(generally amorphous) phases are stable phases at ambient temperatures. The reaction products are metastable and can cause the following reactions:

$$3CAH_{10} \rightarrow C_3AH_6 + 2AH_3 + 18H$$

$$3C_2AH_8 \rightarrow 2C_3AH_6 + AH_3 + 9H$$

From the reaction of alumina gel, CAH_{10}, and C_2AH_8, the C_3AH_6 phase occurred. CAH_{10} or C_2AH_8 phases slowly transform into C_3AH_6 (or more rapidly if exposed to above 28 °C or higher temperatures), with a cubic structure called hydrogarnet. The crystallisation of AH_3 gel to gibbsite is also highly temperature dependent and sluggish at ambient temperatures. They are known as conversion reactions. There are two results from the conversion reaction. Firstly, water is formed as a product of the conversion reactions. Secondly, the conversion products are denser than the hexagonal hydrates. Since these reactions occur after the cement has set and hardened, the concrete overall dimensions are fixed, resulting in cracks. Cracks accuse of a loss in strength and the possibility of microcracks developing. In addition, the hydrogarnet's weak bonding capacity and it's the low surface area also contribute to the loss of strength. Overall, the reaction strengths of the aluminate hydrates are thought to be in the order $CAH_{10} > C_2AH_8 > C_3AH_6$ [70] Aside from the loss of strength, increased porosity also leads to increased permeability, so dissolved salts, acids, or alkalis in groundwater are more likely to attack the concrete and, if any, steel reinforcement [31,53,56,63]. Except for these reactions, the C_2F, iron analogue of the hydrogarnet phase, can also lead to the following reaction:

$$3C_2F + xH \rightarrow 2C_3FH_6 + F + (X - 12)H$$

After the main CA reaction in the system, Strätlingite forms because of the interaction of β-C_2S, alumina, and water. This reaction prevents strength reduction of the mixtures due to the conversion process:

$$\beta - C_2S + A + 8H \rightarrow C_2ASH_8$$

Unlike PC hydration, Portlandite ($Ca(OH)_2$) does not exist in the CAC hydration. This makes CACs resistant to aggressive solutions. The formation of aluminum hydroxide gel also provides resistance to dilute acids and sulfate. Therefore, the CAC can be used in industrial applications such as flues, sewers, effluent tanks, coal hoppers, ash sluices' flues, oil refineries, breweries, dairies, and tanneries [55,70]. The CAC hydration and its properties are also strongly dependent on temperature due to the conversion reaction. The setting time of the CAC clinker varies significantly with the ambient temperature. For example, the setting starts after 8 hours, and the final setting is completed after 24 hours between 25 - 30°C. Although the setting time is later than the PC, the strength development is relatively quick. When the temperature rises above 30 °C, the setting time is shortened thrice [53].

2.1.2. CAC and PC Combination Systems

Because the hardening time of CAC clinker varies depending on temperature and both strength loss and porosity increase due to the conversion reaction, it is impossible to use only CAC when developing early age high strength mixtures. Although CACs have high-performance properties, the CAC is approximately 4 - 8 times more expensive than a PC. Therefore, using CAC in different combinations has become a frequent application for obtaining long service life with high mechanical properties and cost-effectiveness in early and late age. These combinations can be mixed with calcite, ground granulated blast furnace slag (GGBFS), metakaolin, silica fume, calcium sulfate ($C\acute{S}$), pulverized fuel ash, fly ash (FA), $CaCO_3$, sodium silicate, etc [53,58,60].

Bensted [53] explained early age mechanical properties of these systems with experimental results. To accelerate the hydration rate of CACs, PC was replaced with CAC in different proportions. When PC was in major, the performance of the mixture was similar to the PC hydration mechanism. The setting time was significantly shortened even when the CAC:PC ratio was 5:95. The CAC significantly shortened the setting time due to ettringite formation in the first hydration stage. However, the mix was workable and had sufficient time for application and finishing. When CAC was used up to 25%, the mechanical properties of the mixture were approximately five times lower than the

only CAC-used mixture. The 24-hour compressive strength was measured as 5.5 MPa when the CAC:PC ratio was 25:75. When CAC was in major, the performance of the mixture was similar to the CAC hydration mechanism. Even if a PC was used up to 20%, the setting could be swift, and flash settings can occur. The setting time of the mixture varied at different levels. The setting was accelerated by ettringite formation due to the reaction of CAC with calcium sulfate and calcium hydroxide contained in PC. Although up to 60% PC use contributed to early-age strength, 24-hour and later-age compressive strengths were lower than only the CAC-based mixture. The optimum CAC:PC proportion ratio was 40:60 for achieving early strength and workability.

Ramachandran [70] mentioned that PC-CAC-based expansive cements can be traced back to the 1920s. The proportion of two types of cement directly affected the setting time, and it could be modified with the ratios. Therefore, the fast setting was a problem, limiting the application of these systems.

Gu et al. [71] investigated early strength development and hydration of blended systems. They prepared mixtures in different PC/CAC ratios (92.5/7.5, 80/20, and 20/80). They observed microstructural changes and phases using conduction calorimetry, X-ray diffraction, and scanning electron microscopy. They claimed that the mechanical properties of the blended systems changed with the PC/CAC ratio. The results showed that only 80/20 - PC/CAC mixture had early age strength compared to others. Because of the rapid formation of a large amount of needle-like ettringite crystals, this contributed to the quick set. The presence of CAC delayed the PC hydration. Thus, it had lower compressive strength than others for the 72^{nd} day.

Amathieu et al. [72] proposed a hydration mechanism of rapid setting in PC/CAC binders. According to the results, when sufficient CAC was added, a flash setting occurred, and it was not known if it was related to the ettringite formation or the C_4AH_{13} formation from the C_3A phase. It was stated that the amount of CAC needed to produce rapid setting depended on the nature of CŚ in the PC. This amount was higher when CŚ was present as gypsum or hemihydrate and lower when anhydrite was present.

The combination of PC and CAC forms a large amount of aluminate phase in the matrix. Usually, calcium sulfate is added at specific rates during clinker production in order to prevent the sudden setting formation of C_3A in the PC. The formed aluminate phases react rapidly with the available sulfate source to form ettringite; therefore, the amount of gypsum in the PC is not enough to stop the C_3A component [73]. Since the amount of gypsum coming from the PC is insufficient for aluminate coming from the CAC, flash setting occurs in the system. For this reason, it is aimed to prevent flash setting formation by adding a CŚ source to the blended system in the literature studies.

2.1.3. CAC, PC, and CŚ Combination Systems

Using CAC, PC, and CŚ in the mixtures are known as ternary systems in the literature. The hydration reaction of the mixture occurs differently than that of either of the individual binders. While hydration reactions occur in ternary systems, various ions originate from the components. The ions are mainly released from the C_3A phase in PC and the CA phase in CAC. Since the reaction rate of tricalcium aluminate (C_3A) is the highest, the rate is reduced by using mostly gypsum (sometimes hemihydrate is also used) as a CŚ source in PC-based mixtures. Typically, approximately 2 to 3% gypsum was added to commercial PCs before grinding to prevent flash setting during cement hydration [55,74,75]. The two main hydrated sulfate phases formed in the hydration of PC using a $CaSO_4$ source are AFt (ettringite) and AFm (monosulfate). When the PC clinker comes into contact with water, first, the C_3A phase reacts with the gypsum to form AFt (ettringite) immediately. If the supply of sulfate ions runs out, any AF_t formed reacts with any remaining C_3A to form the AF_m (calcium aluminate monosulfate) [68,69]. However, a large amount of calcium aluminate phase is formed in the matrix by adding PC to CAC cement. The formed aluminate phases react rapidly with the available sulfate source to form ettringite; therefore, the amount of gypsum in the PC is insufficient to stop the C_3A component [73]. Therefore, a CŚ source is used to prevent flash settings that may occur in binary mixtures, which CAC and PC used, and to reduce monosulfate phase formation. In order to understand the hydration reaction of ternary systems (PC, CAC, and CŚ), it is essential to know the reactions in detail. The first reactions in the ternary system when the mixture is in contact with water are generally summarized below [59,68]:

Available sulfate and Ca^{+2} ions from both CŚ and PC sources react with the CA phase from CAC to form ettringite (AFt):

$$(3-n)CA + 3C\acute{S}H_x + nCa + (32+3n)H \rightarrow C_3A(CaSO_4)_3H_{32} + (2-n)AH_3$$

If CŚ supply is consumed completely, the CA phase reacts further with ettringite to form calcium monosulfate (AFm):

$$6CA + C_3A.3C\acute{S}H_{32} + 16H \rightarrow 3C_3A.C\acute{S}H_{12} + 4AH_3$$

Ettringite is the main hydrate, which first formed around CAC particles, giving the initial setting of the paste. This fact is probably due to the dissolution rates of the CŚ and calcium aluminate phases. Because of the rapid hydration behavior of CAC+PC, the formation of ettringite controlled with calcium, sulfate, and aluminate ions in the liquid phase is apparently the key to delaying the setting. The pre-formed layer of hydration products on the non-hydrated CA particle surface effectively delays the setting time by controlling the aluminate ion concentration in the pore solution. A slow diffusion process controls the dissolution of aluminate ions into the liquid phase [68]. It was observed that since insufficient use of the amount of CŚ led to the consumption of all aluminates and mono sulfoaluminate would occur in the system, the amount of CAC and CŚ had a vital role in the system [76]. For this reason, the ettringite formation has been frequently investigated in literature studies, as it is a vital and well-understood part of understanding the early age strength mechanism in ternary systems. Without CŚ source, the amount of alumina in the solution is relatively high. This alumina prevents the C_3S hydration by adsorption on reactive sites, which results in low long-term strength compared to pure PC. Ettringite formation is mainly attributed to the calcium sulfate source. CŚ can be found in gypsum, hemihydrate, and anhydrite forms in the construction industry. Calcium sulfate, which exists as gypsum at ambient temperatures, changes form as the temperature increases. The decomposition of $CaSO_4.2H_2O$ (gypsum) under the conditions of two consecutive reactions, firstly $CaSO_4.0.5H_2O$ (hemihydrate) then $CaSO_4$ (anhydrite) being formed [74]. All sources of calcium sulfate mentioned eventually revert to gypsum in the setting,

and the transformation rate depends on the calcination conditions [77–79]. The reactions are given in the below:

$$CaSO_4.2H_2O \rightarrow CaSO_4 + 2H_2O$$

$$CaSO_4.2H_2O \rightarrow \beta - CaSO_4.0.5H_2O + 1.5H_2O\ (100 - \ 150\ ^\circ C)$$

$$\beta - CaSO_4.0.5H_2O\ \rightarrow \gamma - CaSO_4 + 0.5H_2O\ (150 - \ 197\ ^\circ C)$$

$$\gamma - CaSO_4\ \rightarrow \beta - CaSO_4 + 0.5H_2O\ (375\ ^\circ C)$$

Although CŚ sources provide the same ions in water solution, Ca^{+2} and SO_4^{-2}, their dissolution rates and solubilities differ. It significantly affects the formation of ettringite and its associated characteristics [59,80,81]. Lamberet [68] (2005) claimed that instead of gypsum, other forms of calcium sulfate could be used, such as hemihydrate ($CaSO_4.0.5H_2O$) or anhydrite ($CaSO_4$). The relative dissolution rate of the CŚ source was measured as hemihydrate > gypsum > anhydrite. This solution rate was a key parameter in understanding early precipitation of ettringite formation and its location, which depended on the ionic concentration in the interstitial solution [82,83]. Since the amount of ettringite formation parallelled the dissolution rate, the highest formation was expected from mixtures prepared with α-hemihydrate. Hewlett [55] stated that the added calcium sulfate affected the CAC-based mixtures' setting behaviour. A small amount of CŠ retarded setting time; it was lower than 30 min. Among CŠ sources, the hemihydrate type was the most effective in acceleration, and the anhydrite type had a minor influence on setting time. Due to its accelerating effect, it influenced the workability and fluidity of mortars and simultaneously increased the heat of hydration. The nature of the added calcium sulfate strongly influenced the quantity and morphology of ettringite and related properties in the mixture [84]. Early age hydration mechanism of ternary-based systems, formation of ettringite and other phases, and the effect of CŚ source and its amount on the physical, mechanical, and chemical properties of mixtures have been some of the most frequently studied subjects in the literature.

Lamberet [68] studied the hydration mechanism and microstructural development of ternary-based systems with predominantly CAC + CŚ generally as hemihydrate with minor PC and major PC with minor CAC and calcium sulfate usually as anhydrite. In PC-rich systems, the CAC ratio varied between 6.9 – 30% by weight. According to the results, other forms of calcium sulfate could be used, such as hemihydrate $CaSO_4.0.5H_2O$ or anhydrite $CaSO_4$ instead of gypsum on the ternary-based systems. The hydrates formed at a very early age depend on the ionic concentration in the interstitial solution. While gypsum and hemihydrate usage were more rapidly soluble than the calcium aluminate, the solution was rich in Ca^{2+} and SO_4^{-2} and deficient in Al^{+3}, and short stubby crystals of ettringite were formed. In contrast, anhydrite usage was less rapidly soluble than the calcium aluminate, calcium sulfate solubilization was the limiting parameter, and it led to the growth of long, thin needles of ettringite.

Torréns-Martín et al. [78] conducted calorimetric studies of ternary binders based on PC, CAC, and CŚ. Several mixtures were prepared in ratios of 100, 85/15, and 75/25 of PC/CAC with 0, 3, and 5% of CŚ source. The results showed that the studied ternary systems yielded an extra amount of ettringite and changed the reaction mechanism concerning PC-based systems.

Evju and Hansen [85] studied the expansive properties of ettringite in a ternary-based mixture. They prepared a paste of 25 wt.% CAC, 12.5 wt.% PC, 12.5 wt.% β-calcium sulfate hemihydrate and 50 wt.% water was studied at 20 °C and 100% relative humidity (RH). According to thermal conduction calorimetry results, the first peak in the heat rate curve included contributions from mechanical mixing, initial wetting, and dissolution plus the formation of ettringite and gypsum, the second maximum involved the replacement of gypsum by ettringite, and the third corresponded to the formation of aluminate-AFm.

Evju and Hansen [86] studied the expansive properties of ettringite in ternary systems. The mixtures were prepared with 50 wt.% CAC, 25 wt.% PC and 25 wt.% CŚ sources. As a CŚ source, ß-hemihydrate, anhydrite, and a combination were used. The results showed that only ß-hemihydrate usage led to expansion due to the interaction of crystals

growing on cement grains. Although ettringite crystals grew in only anhydrite usage, there was no expansion in the matrix.

Sang and Liu [87] studied the properties of ternary-based grouting composite. The optimum mix was found to be the one which was prepared with 33.4% wt. of PC, 6.0% wt. of CAC, 6.7% wt. of CS̄, 52.6% wt. of sand, 16% wt. of water, and 1.3% wt. of agents. The mixture showed high strength but slight expansion at the same time. Among mixtures with higher CAC and calcium sulfate content, it had higher early strength, but its strength in the long term was reduced.

Martin et al. [88] studied the impact of calcium sulfate forms and additions on the hydration and properties of ettringite-based systems. Two calcium sulfate sources (hemihydrate and anhydrite) were used. Hemihydrate was found to have high dissolution kinetics to avoid the limitation of sulfate ions to be dissolved in the pore solution. In contrast, anhydrite was determined to ensure sufficient sulfate content in the long term due to its low kinetic dissolution.

Qoku et al. [89] studied the impact of sulfate sources on the hydration of ternary pastes of PC, CAC, and CS̄. In the mixtures, CAC- and PC-rich systems were designed with gypsum and anhydrite addition. The results revealed that anhydrite-based mixtures released the highest amount of ettringite. In contrast, the gypsum-based mixtures developed a higher AFm phase content and amorphous hydrates in the long-term hydration. This difference was attributed to the faster dissolution rate of gypsum. Previous studies revealed that the formation and rate of ettringite strongly depended on the solubility and dissolution of the CS̄ source. Consequently, it was found that CS̄ source directly affected the early age performance of ternary-based mixtures.

Besides the ettringite (AFt) and mono-sulfate (AFm) formation, after the main CA reaction is completed, metastable phases of other hydrated phases can occur in ternary systems. C_2AH_8 and C_4AH_{13} are metastable phases that spontaneously transform into the

fully hydrated, thermodynamically stable cubic hydrogarnet phase (C_3AH_6). However, metastable phases do not form significantly, except for only CAC-based mixtures [90].

$$2\mathrm{CA} + 21H \rightarrow C_4AH_{13} + C_2AH_8$$

$$C_4AH_{13} + C_2AH_8 \rightarrow 2C_3AH_6 + 9H$$

After the main CA reaction is completed in the system, Strätlingite (C_2ASH_8) is also formed, resulting from the interaction of β-C_2S, alumina, and water. In the long term, C_2AH_8 can transform into C_3AH_6(hydrogarnet) phases for different temperature ranges.

$$\beta - C_2S + A + 8H \rightarrow C_2ASH_8$$

In ternary systems, gibbsite ($Al(OH)_3$) can also present due to AFt and AFm formations. In addition, alumina gel transforms to gibbsite in below.

$$AH_x\ (alumina\ gel) \rightarrow \gamma - AH_3(gibbsite) + (x-3)H$$

After the first stage of the hydration mechanism is completed, PC-based reactions continue. PC contributes to the calcium ions in the solution and brings some silicate ions, forming C-S-H gel and portlandite ($Ca(OH)_2$).

$$C_2S + 2H \rightarrow C-S-H + CH$$

$$C_3S + 3H \rightarrow C-S-H + 2CH$$

The hydrated phases of ternary systems are quite different from those of pure CACs. The relevant properties of the ternary system, such as rapid setting, rapid hardening, rapid drying, and shrinkage compensation, show that it can be used where high strength is

targeted at an early age. However, the proportional ratio of components affects the physical and mechanical properties of the mixture. For this reason, many researchers have identified CAC/PC/CŚ as three different zones using a triangular diagram. The main hydrates that form is shown in Figure 2.1 [59].

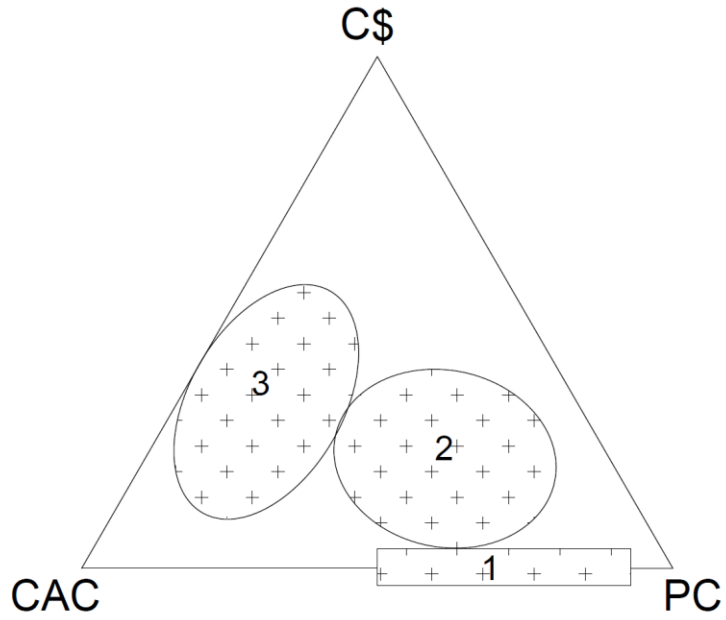

Figure 2.1. PC/CAC/CŚ Equilibrium Phase Diagram [59]

The first zone (1) represents blended PC and CAC mixtures. As given in Section 2.1.2, these systems are generally unsuitable for use in widespread areas due to flash setting or hardening in a few minutes. Only moderate strengths can be gained, which is mostly lower than PC. In addition, the absence of shrinkage compensation limits their use to small applications.

The second zone (2) represents the ternary system consisting of PC(major), CAC(minor), and CŚ. In this system, the amount of ettringite formation increases with using CŚ source at early ages. Because of the ettringite formation, aluminate ion concentration remains low in the solution. Therefore, lowering the aluminate concentration minimized the slowdown of the C_3S hydration rate. In this way, early age high strength can be achieved by using a PC-rich ternary system (≈20 MPa at 3 h). The strength development of mixtures occurs in two stages. Initial strength development occurs due to ettringite

formation in the first 24 hours. The 28-day strength development of the mixture occurs due to the formation of C-S-H gel by the C_3S and C_2S reaction due to the PC-rich content after the first day. Apart from the early age mechanical performance, the risk of possible cracks can be limited, and large horizontal surfaces compensate for shrinkage due to ettringite formation at early ages.

The third zone (3) represents the ternary system having PC(minor), CAC(major), and CS̀. The CAC-rich system makes the alumina concentration the main phase in the solution. Due to the high content of the CA phase, ettringite formation increases significantly at an early age. It has higher early strength, better shrinkage compensation, and rapid mixture drying than the second zone. Due to this performance, it is pretty common in flooring applications. However, the formation of metastable phases increases with the CAC-rich system, and these can transform into the C_3AH_6 phase based on temperature, which causes a loss in strength in the long term. In addition, high alumina content negatively affects the long-term strength of the mixture as it slows down the C_3S and C_2S reaction of PC. Besides these disadvantages, the cost of the mixture increases due to the high price of CACs [78].

2.1.4. Utilization of Mineral Additives in Ternary System

Supplementary materials are incorporated into ternary systems or pure CAC systems as minor components to improve performance properties that limit the use of ternary systems' widespread applications, such as low long-term strength, low durability, expansion mechanism, and fast setting. In literature, experimental studies have been carried out using supplementary materials such as fly ash (FA), metakaolin, ground granulated blast-furnace slag (GGBFS), lime, rice hush ash (RHA), silica fume, and quartz sand and scientific understanding of their influence on the ternary system of hydration mechanisms.

Bensted [53] stated that CACs could be blended with supplementary materials such as GGBFS, slag, metakaolin, FA, silica fume, etc. Supplementary materials could improve

the long-term compressive strength of mixtures against pure CAC systems if the ambient temperature were moderated. Hydrogarnet formation related to conversion reactions was insignificant within blended mixtures. Instead of metastable phases, little CH and alkalis were present in these systems.

Kırca [58] stated that lime could be incorporated into the CAC-based mixtures for rapid strength development. Due to the lime addition, the system's pH value increased, leading to accelerated hydration. It also affected the setting time and hardening properties of mixtures.

Bentivenegra [61] stated that GGBFS compensated the conversion reaction in pure CACs for the long-term strength at ambient or moderately elevated temperatures. However, blended systems with GGBFS and CAC had lower strength than pure CACs in the short term. When calcium aluminates reacted with amorphous silica from GGBFS, C_2ASH_8 (strätlingite or gehlenite) was formed. Strätlingite had higher stability than the hydrogarnet phase. Thus, the blended system did not show any compressive strength loss.

Fernandez-Carrasco and Vázquez [91] investigated the reactions of FA with CAC and CS̀. CAC-rich and FA-rich designs were used with gypsum added to different ratios in the mixture. In order to minimize the effect of the clinker in ternary systems, the FA was incorporated instead of PC as raw material in this study. The results showed that only the hydrogarnet phase was detected in the CAC-rich samples among mixtures. The conversion reactions were not observed in other mixtures. The main product was ettringite in all mixtures. The effect of fly ash content on the hydration reaction did not depend on the FA/CAC ratio, but there was a tendency for ettringite content to increase with FA content. It was proved that the incorporation of FA in the ternary mixtures was an alternative way to develop ettringite-based products.

Idrees et al. [92] investigated the hydration behaviour of CAC mortars with mineral additives at different curing temperatures. In order to determine the effect of mineral additives, the mortars were prepared by using constant CAC content, and the sand was

replaced by class F-FA as 10, 30, 60%, GGBFS as 10, 30, 60%, and silica fume as 5, 10, 15%. As a result, the replacement of sand with mineral additives accelerated the rate of hydration in all types of mineral additives. %10 replacement of sand by FA and GBFS resulted in 7 and 16% increases in compressive strength, respectively, at 20 °C. On the other hand, the replacement of silica fume had relatively lower strengths, but it showed improvement in strength at a later age.

Li et al. [93] investigated the effects of slag on the degradation mechanism of PC, CAC, and gypsum-based ternary systems under multiple erosive ions for the repair of concrete in marine engineering. This study conducted experiments on hydration products, morphology, and mechanical performance of samples. The results indicated that incorporating the slag ratio significantly improved samples' durability and mechanical performance in the erosion environment. While SO_4^{-2} enhanced the stability of ettringite, it was slightly reduced by the additional Mg^{+2} in corrosive solution.

Liao et al. [94] studied the hydration of calcium aluminate cement pastes containing silica fume using non-contact electrical resistivity measurement at an early age. When silica fume was incorporated into the mixture, Strätlingite (C_2ASH_8) formation inhibited the conversion of the metastable phases (CAH_{10} and C_2AH_8) into the stable hydrogarnet phases. This study replaced silica fume with CAC at 0, 5, 10, and 20% (wt. of binder). According to the results, the hydration mechanism of samples accelerated with 24 hours as the silica fume ratio increased in the mixture. It also inhibited the conversion of metastable CAC hydrates (CAH_{10} and C_2AH_8) to C_3AH_6 through filling, seeding, and reacting with CAC, thus reducing the heat of hydration.

2.1.5. Utilization of Chemical Additives in Ternary System

Chemical additives are common in CAC-based mixtures like cementitious composites to adjust properties such as setting, rheology, strength, and adhesion in the fresh state. Retarders, accelerators, water reducers, fluidifies and plasticizers, air entraining and foaming agents and latex and formulated resins can be used alone or combined for different purposes in CAC-based mixtures [55].

Cement type, high dosage cement, and low water/cement ratio are essential to achieve early age high strength in CAC-based mixtures. As the amount of cement increases, mixing water decreases, and thus, the flowability of the mixtures is negatively affected [95]. Additionally, combinations of different chemical additives are used to obtain higher early age strengths. For example, water-reducing or superplasticizer additives increase mortars' flowability and early age strength by reducing the amount of water needed. Accelerators accelerate hydration reactions and increase strength at an early age; thus, these reduce the initial setting time [96]. Desired matrix properties can be achieved by using chemical additives such as setting retarder additives to prevent rapid setting and adjust the hardening time [97].

Among chemical additives, retarders and accelerators are significant components in improving strength, setting time, workability, and expansion-related properties. Set accelerators are used to increase the hydration rate and enhance mixtures' early age strength. In contrast, retarders may reduce CAC's average rapid hardening properties, like rapid setting and flowability. In the long term, accelerator additives may result in lower strength than those without additives, while higher strengths can be obtained with retarder additives. Therefore, the accelerator and retarder can obtain early and highly comparable strengths in a CAC-based mixture. In addition, these additives affect the workability or rheology of mixtures differently. Therefore, water reducers may combine with others to enhance the physical properties of mortars. The retarders and accelerators mostly used in CAC systems are summarised in Table 2.2 [55].

Literature studies showed that combinations of chemical additives were used to prepare cementitious composites. Saglam et al. [98] studied the effect of polycarboxylate-based additives on workability and early strength properties. Polycarboxylate-based superplasticizers, besides naphthalene, melamine, and lignosulfonate-based superplasticizers, were developed in the construction industry. The results showed that polycarboxylate-based additive could be used with cements. Incompatibility of cement and additives resulted in low strengths at one and seven days. For this reason, it was concluded that different types of superplasticizers had to be used, and the mixture should be prepared with the most appropriate one when designing the matrix.

Table 2.2. Various accelerators and retarders in CAC-based mixtures [55]

Accelerators	**Retard at low concentrations and accelerate at high concentrations**	**Retarders**
Lithium hydroxide	Magnesium chloride	Sodium borate
Lithium carbonate	Calcium chloride	Sodium chloride
Lithium sulfate	Barium nitrate	Sodium nitrate
Lithium chloride	Acetic acid	Potassium sulfate
Lithium nitrate	Calcium sulfate hemihydrate	Potassium chloride
Calcium hydroxide	Calcium formate	Barium chloride
Potassium hydroxide		Sodium gluconate
Potassium carbonate		Sodium citrate
Sodium hydroxide		Citric acid
Sodium carbonate		Hydrochloric acid
Sodium sulfate		Glycerine
Sulfuric acid (very dilute)		Sugar

Niziurska et al. [99] investigated the influence of lithium carbonate on the phase composition of calcium aluminate cement paste. The mixtures were prepared with 0.03% addition of Li_2CO_3. In this study, they claimed that very little addition of lithium carbonate caused a significant effect on the reaction rate of CAC phases. According to the results, both calcium monoaluminate and C_2AH_8 formations significantly accelerated in the first hydration mechanism of CAC. Moreover, the addition of lithium carbonate caused a significant acceleration of hydrate conversion into the C_3AH_6 hydrogarnet phase. In terms of heat of hydration, the mixture with Li_2CO_3 addition produced lower heat than the control mixture due to the inhibition of further hydration of grains coated by a layer of rapidly growing reaction products.

Godek et al. [100] investigated polycarboxylate-based superplasticizer selection for ready-mixed concrete industry and performance in self-compacting concrete (SCC) production. Among three polycarboxylate-based superplasticizers, the most appropriate superplasticizer was selected based on the rheological behaviour of fresh cement paste with fluidity, workability behaviours, and mechanical properties. The results showed that

SCC maintaining self-compatibility up to 1 hour at C30/37 strength could be prepared by SV type polycarboxylate based superplasticizer.

Demir and Sevim [101] examined the effect of lithium salts on sulfate cement mortars in terms of strength and setting times. Four different lithium additives (Li_2SO_4, $LiNO_3$, Li_2CO_3, and LiBr) were added to the cement at 0.5, 1, 1.5, and 2% by mass. The results showed that Li_2CO_3, among the other lithium additives, effectively reduced the initial and final setting times. In contrast, $LiNO_3$ and LiBr additives gave the best results regarding strength and length change when tested for 1% additive ratio by mass. Among the lithium salts, the incorporation of 2% Li_2CO_3 reduced the initial and final setting time from 150 to 20 minutes and from 230 to 50 minutes, respectively.

Li and Hao [102] experimentally studied the preparation of a new mortar mixture with an early age high strength using ternary systems. The best results were obtained in a mixture of 67% calcium sulfoaluminate cement, 23% aluminate cement, and 10% gypsum. The effects of different types of retarders, lithium carbonate (accelerator), and superplasticizers on the setting time and mechanical properties of the composite were also investigated. In this study, six different retarders were used in the mixtures. As a result of experimental studies, the initial and final setting time of the mixture increased with the increase of the retarder. In addition, the best results were obtained when 0.4% borax, 0.02% lithium carbonate, and 1.2% naphthalene-based superplasticizer additive were used.

Zhang and Cai [103] studied the effects of chemical additive types on cement performance. The mixtures were prepared with Naphthalene Superplasticizer (NFS) and Polycarboxylate Superplasticizer (PCC); coagulant: lithium carbonate (Li_2CO_3). The results showed that superplasticizers seriously enhanced the fluidity of cement paste. As superplasticizer content increased, the initial and final setting times of the mixture got longer. In terms of best fluidity, the optimum dosage of chemical additives was 0.4 - 0.6% and 0.01% for NFS and Li_2CO_3, respectively. In terms of setting time, it was reduced by about 85.9%, and the final setting time was reduced by about 82.2% at a 0.35% ratio of Li_2CO_3 addition.

Gwon et al. [104] investigated the combined effects of set retarders and polymer powder on the properties of calcium sulfoaluminate and PC-blended cement systems. Retarders controlled the rapid setting properties of high alumina cement systems to provide sufficient workability. They stated that the effect of retarders on the age-dependent properties of mixtures was rarely investigated. The results indicated that the retarders delayed early-age strength development via inhibiting ettringite formation. However, the final strength was increased due to lower porosity and denser structure with the evolution of hydration products.

Coppola et al. [105] investigated the influence of lithium carbonate and sodium carbonate on physical and elastic properties and carbonation resistance of calcium sulfoaluminate-based mortars. The experimental results showed that lithium carbonate and sodium carbonate accelerated the hardening process, improved the early age strength, and reduced porosity content. In addition, sodium carbonate also reduced the water absorption, the carbonation rate, and the shrinkage of mortars with no change in setting times and the workability.

2.2. Electrostatic Discharge Capability of Cementitious Composite

Concrete is the most popular construction material due to its easy-to-reach ingredients, good environmental adaptability, low cost, and high compressive strength [106–108]. Various chemicals and mineral additives with high-quality industrial products have been used to impart additional functional properties to traditional concrete mixtures. With technological development, the utilization of an optimum amount of nano- and micro-sized different types of highly conductive fillers can enhance electrical properties of cementitious composites such as conductivity, electromechanical and electromagnetic behaviours, as well as mechanical properties such as tensile ductility, flexural and compressive strength, toughness by improving post-cracking ductility and control cracking, and reduced drying shrinkage [107,109,110].

Typically, the average electrical resistivity of cementitious composites (paste, mortar, and concrete) ranges between 10^2-10^9 Ω.cm depending on the mixture composition, which means that it is a poor semiconductor or insulator material at dry state [29,111,112]. However, this behaviour can be modified by the utilization of conductive materials with different scales in the mixture compositions [113,114]. In the 1990s, Chen and Chung [110] revealed a study on carbon fiber reinforced concrete for smart structures capable of non-destructive flaw detection. It was first reported that the fiber-based cementitious composite can sense strain and damage by its change in electrical resistance. Nowadays, modified cementitious composites are possibly used for grounding systems [29,30,115], de-icing/self-heating [116–120], electromagnetic shielding [121–123], cathodic protection [124,125], strain-sensing [126,127], traffic monitoring [30,128,129], and self-monitoring [130–132].

One of these applications is a grounding system, which paves the way for ESD problems by providing anti-static protection capability to cementitious composites. The grounding system is crucial in structures such as hospitals, operating rooms, and x-ray rooms, critical industrial facilities such as the electronics industry, explosive material production facilities, petrochemical industry, and military defense structures, especially those that require good electrostatic discharge capability. Almost every piece of electrical equipment needs grounding systems to eliminate static electricity, provide personal safety, and protect against several detrimental conditions that can cause sparks and explosive materials [133,134]. Usually, 2 – 3 mJ low energy may lead to sparks that initiate the primary explosion. Because of this low energy, the electrostatic discharge problem is mainly associated with physical phenomena that accumulate person or staff evacuating energy up to 8.3 - 20 mJ to the electronic equipment [11,135]. Although various applications are used to solve the ESD problem among engineers, chemical and cementitious binder-based applications are prevalent because they do not require any additional precautions. However, epoxy and chemical binder-based traditional grounding systems can mostly be preferred in ESD problems; the service life of systems can be shortened because of harmful environments (chemicals, moisture, and temperature effect), staff mistakes (cutting or damaging floor at working), and poor mechanical properties these systems could be ineffective to sustain electrostatic discharge protection [25,136]. Besides a chemical binder-based grounding system, the first electrically

conductive concrete was patented on January 19, 1965, with the number 3,166,518 [137]. With the improvement of concrete technology, researchers have studied the properties of electrically conductive cementitious composites for different purposes mentioned in the upper part. Within the design of electrical, physical, and mechanical properties of the cementitious composite, the low resistivity and high conductive pathway between paste or mortar and conductors can be achieved by incorporating conductive materials or embedding electrodes underground to prevent ESD failures [115,138,139]. Cementitious composites can be used for electrostatic protection with modifications. However, higher costs of conductors, mixed proportion of composite, mechanical and physical properties of composites, and environmental effects have prevented its widespread use in critical building flooring applications as a ground system.

2.2.1. Measurement of Electrical Resistivity of Cementitious Composites

The electrical resistance of the concrete is defined as the resistance against the current when a voltage is applied to a concrete mass. It can also be defined as contact electrical resistance which refers to the resistance of an interface between two objects when a current is passed across the interface in a direction [140]. In order to measure the electrical resistivity of concrete samples, Ohm's law can be applied to experimental studies in the literature. Firstly, a specific voltage is applied between two sides of the specimen. Then, the current is measured by equipment. Ohm's law states that the voltage is directly proportional to the current passing through the concrete sample, if all physical conditions and temperatures remain constant [115,141]. Based on the measured value of current and voltage difference, electrical resistivity (ρ) and electrical conductivity (σ) can be calculated based on the following equations:

$$V\,(V) = I \times R \quad (1)$$

$$R\,(\Omega) = \frac{V}{I} \quad (2)$$

$$\rho\,(\Omega.\,\mathrm{cm}) = R * A/l \quad (3)$$

$$\sigma = \frac{1}{\rho} \quad (4)$$

Where (V) is the voltage, and (I) is the current, (R) is the resistance defined as ohm (Ω). (l) the length is the distance between two inner electrodes of the specimen, defined as cm, and is perpendicular to the specimen's cross-sectional area (A), defined as cm^2. (ρ) is the resistivity defined as Ω.cm. Electrical conductivity is inversely proportional to electrical resistivity [107,115,142,143]. The electrical conductivity (or the electrical resistivity value) is directly related to the electrical performance of the conductive concrete [134]. The lower the electrical resistivity of concrete mixtures, the more effective and higher the electrical conductivity inside the matrix or on the surface. Therefore, it is required to aim low resistivities from mixtures to develop electrically conductive concrete for ESD problems.

In order to determine the electrically conductive performance of cementitious composites, the experiment should be conducted accurately. However, the resistivity value from test results is not definite value because some of the factors that affect the measurement, such as the geometry of the specimen, test method, test equipment, type of power supply, voltage, current and frequency range, contact of the electrode, numbers of electrode, moisture and temperature effect, saturation degree of specimens [134,144]. Two main reasons for the measurement differences are based on the sample's type of power suppliers and electrode arrangements. It is schematically shown in Figure 2.2, adapted from [139]. In electrical resistivity measurements, the power supply can be divided into its current frequency, alternating current (AC), and direct current (DC). Researchers widely prefer both power suppliers in studies, and various results have been revealed in the literature. Tian and Hu [134] revealed that measured electrical resistivity results from AC were lower than about one-third of DC under the same conditions. Vossoughi [109] claimed that DC often measured electrical resistivity with two electrodes connected to the specimen. Although DC was used in measurements, a stable value might not be determined from a single measurement due to polarization occurring at electrodes. Fiala et al. [145] claimed that DC was a fast and simple method. However, an error could occur due to a polarization of electrodes. At the same time, AC was a more complex method and was not affected by polarization effects, and it provided logical information about

electrical performance. Chuang et al. [107] revealed that AC was often used in the measurements because it could prevent polarization due to charge carriers moving back and forth as the voltage polarity varied. In addition, DC was simpler and less expensive than the AC method. Sassani et al. [144] used low-current and low-voltage in the AC method with 1000 Hz frequency, and the applied geometry factor (A/I) provided measurement stability and avoided polarization problems. Dong et al. [113] claimed that the DC method could generate serious polarization in the sample and significantly affected the resistivity measurements. Since the amount of voltage was reduced to zero within a short time using the DC method, it caused severe errors and gave wrong electrical resistivity results. In the AC method, the capacitive and skin effects could cause a fluctuation in resistivity measurements. The capacitive effect could be reduced when the higher frequencies were applied to specimens. However, the skin effect might come into force when the frequency reached a threshold. Therefore, AC frequency should be selected where electrical resistance remains constant.

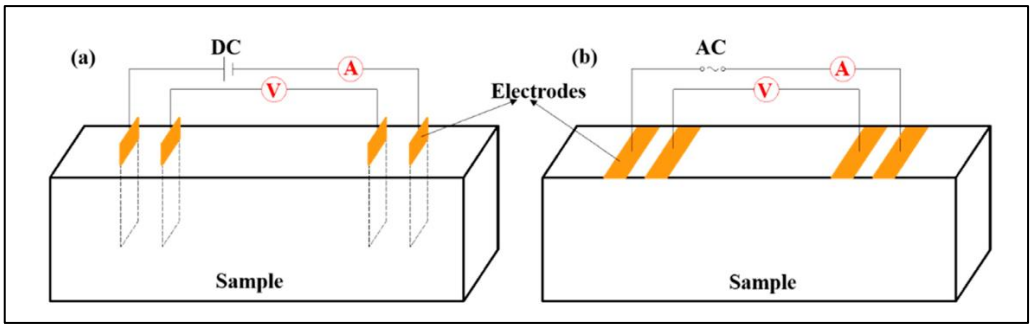

Figure 2.2. Different electrode arrangements and resistivity measurement methods a) DC method, b) AC method [139]

Another main factor is the number of probes adopted as the two-pole method and the four-pole method (Wenner probe method), respectively, based on the electrode arrangement and layouts for the contrast test. It is schematically shown in Figure 2.3, adapted from [134]. Four electrical contacts are used in the four-probe method: the outer two are used for passing current, while the inner two are used for measuring voltage. In the two-probe method, only two electrical contacts are used at the two ends of the specimen so that each contact is both for passing current and voltage measurement. In studies, two and four probes are embedded into cementitious mortars, and various results

have been revealed in the literature. Tian and Hu [134] revealed that measurement results changed slightly. However, the electrical resistance value of the four-probe method was smaller than the two-probe method. The four-probe method had a higher accuracy due to error elimination, which was caused by the contact resistance of the electrode in the two-pole test. Thus, it reflected the actual resistivity of specimens. Two probes could be preferred in normal conditions, while the four-probe method could be preferred for higher accuracy. Zhu and Chung [146] claimed the two-probe method also had contact resistance. When large sizes and various geometries of concrete structures were used, the ideal case of electrical contact configuration should be considered. Moreover, measuring surface resistance—using a surface current facilitated by electrical contacts placed on the same surface—could be more straightforward to implement than measuring volume resistance, which required electrical contacts that ideally ensured a uniform current density distribution throughout the volume during resistance measurement. Wang and Aslani [115] revealed that the resistance value of specimens via the four-probe method was smaller than that via the two-probe method since it could eliminate the contact resistance between the electrode and cementitious composite, thus reflecting the actual resistance of the material. However, the two-probe method was preferred for test convenience, although the four-probe method had higher accuracy.

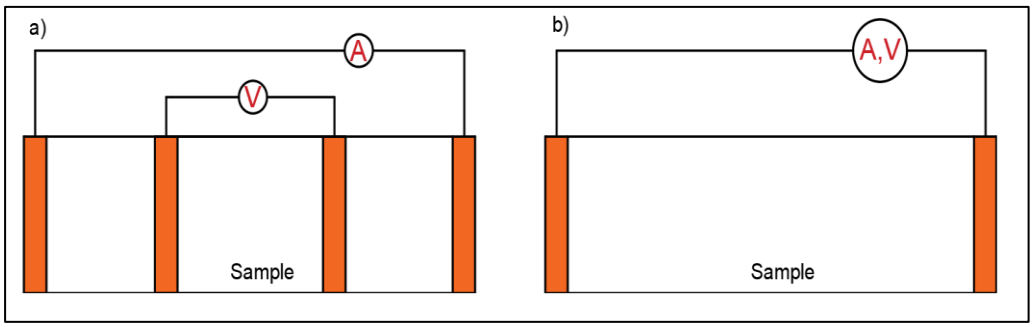

Figure 2.3. Placement of probes inside of sample a) Four-probes method, b) Two-probes method [134]

Effects of other factors on the electrical resistance measurements have been also investigated, and the results are revealed in the literature. Tian and Hu [134] claimed that higher voltages would decrease the resistivity of conductive concrete without power supply types. In order to obtain actual electrical resistivity results, the value should be

stable over 10 V. Fiala et al. [145] stated that electrical resistance could be measured by a device with a frequency range of 10 Hz – 300 kHz. In high-resistance specimens, impedance characteristics at low frequencies could not be measured due to the limited range of devices. Typically, impedance was a measure of the opposition to electrical flow and was described as, in ohms, while impedance and resistance were the same for DC systems, the reactance affected the resistance due to the frequency-dependent contributions of capacitance and inductance. In the case of dried specimens, the absolute values of the resistance and the reactance dependence on the frequency (range 1 kHz – 100 kHz) exhibited a decrease of about 2–3 orders of magnitude.

2.2.2. Electrical Resistivity Specifications for Cementitious Composites

There are various standards in literature for the use of cementitious composites as coatings with electrostatic protection capability in the grounding system of critical structures to solve ESD problems by providing electrical conductivity.

ANSI/ESD S6.1-2005 standard, which was revised in 2019 by the Electrostatic Discharge Association, specifies the parameters, materials, equipment, and test procedures necessary to choose, establish, verify, and maintain an Electrostatic Discharge (ESD) Control grounding system for use within an ESD Protected Area (EPA) for protection of ESD susceptible items. According to the requirements, the resistance shall not be greater than 1 MΩ between the ground and related materials [19].

The Air Traffic Organization Policy by the U.S. Department of Transportation Federal Aviation Administration, published in 2017, mandated standard lightning protection, transient protection, grounding, bonding and shielding configurations and procedures, and control of electrostatic discharge (ESD). This standard systematically minimized electrical hazards to personnel, electromagnetic interference, and damaged to facilities and electronic equipment from lightning, transients, ESD, and power faults. Devices with a sensitivity of less than +/- 200 V required additional ESD protection measured than those specified in this standard. In addition, the surface resistance of grounding systems

to prevent ESD phenomena shall be greater than 1 MΩ and less than 1 GΩ. A minimum of five readings should be selected at different locations on the floor surface [21].

ASTM F150-06 standard, which was reapproved in 2018, covered the determination of electrical conductance or resistance of resilient flooring in either tile or sheet form for applications such as hospitals, computer rooms, clean rooms, access flooring, munition plants, or any other environment vulnerable to personnel-generated static electricity. According to the standard, conductive and dissipative floorings should have a resistance between 25 kΩ - 1 MΩ and 1 MΩ - 1 GΩ, respectively. The standard also included the testing procedure. In order to measure the electrical resistance of conductive floors, the electrodes should be placed at least one in. (25.4 mm) from an edge of the area to be tested and 36 in. (914.4 mm) apart. The meter should be set to 10 V, and readings should be taken 15 seconds after voltage application or after the reading reaches equilibrium. If the reading was below 1 MΩ, recorded the reading. If the reading was higher than 1 MΩ, the voltage should be modified to 100 V and repeated the measurement [22].

In the Occupational Health and Safety Regulations of the Machinery and Chemical Industry Institution, which was published in Türkiye, 2002, the conditions were determined within the scope of the safety measures to be taken in workplaces where flammable-explosive-dangerous and harmful substances were used. Floor systems on which explosive materials were produced and used should be made of conductive materials, and their electrical resistance should be at most 500 kΩ in the long term. In areas where the electrical facility is 220 V, the electrical resistance of the conductive floor or coating (shoes + floor) must be at least 25 kΩ. All conductive floors had to be measured in terms of electrical resistance after installation and before work was started. After that, measurements should be made yearly, and the results should be recorded [23].

Vijayaraghavan et al. [147] revealed that charge buildup on people could be reduced using conductive flooring or coating. The electrical resistance value of the floor should be less than 1 MΩ at points approximately 1 m apart for this method for a practical coating application. At the same time, the resistance should be more than 25 kΩ to avoid shock to personnel.

The Neutral Electrical Code (NFPA 70), published in 2016, covered general and specific requirements for grounding and bonding electrical installations and specific requirements in-house. According to the regulations, all electrically conductive objects in the spraying area, except those objects required by the process to be at high voltage for the process shall be electrically connected to the ground with a resistance of not more than 1 MΩ [148].

EN 1081 and TS EN 1081 standards, revised in 2020, determine the electrical resistance in resilient, laminate, and modular multilayer floor coverings. In a resistance meter device, three voltage grades should be used: 10 V, 100 V, and 500 V. These ranges change from dissipative to conductive behavior in materials. For an open circuit, the tolerances shall be 10 V, 100 V, and 500 V for the resistances lower than 1 MΩ, between 1 MΩ and 100 GΩ and higher than 100 GΩ, respectively. In terms of the conductive flooring system, the electrical resistance values should be lower than 1 MΩ [149].

2.2.3. Utilization of Conductive Materials into Cementitious Composites

Conductive cementitious composites can be produced incorporating micro-sized steel fiber(SF), carbon fiber(CF), milled carbon fiber(MCF), nano sizes-carbon black(CB), steel slag, steel shavings, graphite powder, carbon nanotube(CNT), carbon nanofiber(CNF), graphene nanoplanet, electrically conductive additives, alkaline slag binders, and conductive aggregates to composites.

Dehghanpour et al. [111] studied electrically conductive concrete with a laboratory-based investigation and numerical analysis approach for the anti-icing method on airport runways. In this study, 6-mm and 12-mm long CFs (0.2, 0.5, and 1% volume of total mixture), NCB (0, 3, 6, and 10% weight of the binder), SF (2% weight of the binder) and waste wire erosion (WWE) (1.5% weight of the binder) were combined in different proportions. Electrothermal tests of conductive concrete slabs were carried out in a cooling chamber at -10 °C. Experimental results revealed that the best conductive performances were obtained from three different mixtures, which contained 6% CB, 1%

CF-based specimen, and the combination of 6% CB and, 0.2% CF-based specimen, and 1.5% WWE-based specimen. The lowest resistivity was measured as 80 Ω.cm in cylinder specimens and 357 Ω.cm in slab specimens for the mixture containing 6% CB and 1% CF mixture.

Banthia et al. [114] studied the electrical resistivity of carbon and steel both in mono and hybrid (combination) forms in micro-fiber reinforced cement. Micro-carbon and steel fibers were incorporated into mixtures up to 5%. The experimental study showed that electrical resistivity was significantly reduced with fiber addition. In mono-fiber additions, the carbon fibers were more effective than the steel fibers in improving conductivity. However, the conductivity of CFs was much lower than steel fibers. In hybrid-fiber additions, the effect of CFs was efficient, like in the case of mono-fiber addition. However, an optimum incorporation ratio of CFs should be considered to create a conductive fiber network and provide inter-fiber connectivity in hybrid systems, which was used to enhance the conductivity of SFs.

Wu et al. [116] studied three-phase composite conductive concrete for pavement de-icing. In the study, steel fiber (between 0.6 and 1.2%), carbon fiber (between 0.2 and 0.8%), and steel fiber-graphite (between 2 and 8%) were incorporated into mixtures to obtain conductivity performance. Besides homogeneous dispersion of the CF, volume fraction ratio and concrete voids directly affected conductivity in the results. The best result was obtained for the mixture which contained 1% volume of SF, 0.4% volume of CF, and 4% content of graphite, and the specimen had a resistivity of 322 Ω.cm and compressive strength of 40 MPa after 28 days.

Sassani et al. [118] studied carbon fiber-based electrically conductive concrete for salt-free de-icing of pavements. An optimum CF ratio was determined to provide electrical conductivity in cementitious paste, mortar, and concrete with possible minimum fiber usage. The 6-mm long chopped CF was embedded into a mixture of up to 1% volume. The results showed that the matrix type affected the conductivity of cementitious composites. The percolation threshold of CFs was determined as 0.25 - 1%, 0.6 - 1%, and 0.5 - 0.75% volume for paste, mortar, and concrete mixtures, respectively.

Donnini et al. [120] aimed to explore the mechanical, electrical, and self-sensing properties of cement-based mortars with short carbon fibers at different dosages (2, 3, and 4% by weight of cement). According to the results, the electrical resistivities of samples decreased for 60 days. However, it reached a stable value when the number of CFs in the mixture was sufficient in terms of electrical conductivity, and its resistivity decreased to half compared to mortar without fibers. The best results were obtained with 3% CF addition, and resistivity decreased to below 150 Ω·cm. However, the resistivity did not decrease further after the 3% addition.

El-Dieb et al. [138] conducted an experimental investigation examining the impact of various conductive fillers—steel shavings, carbon powder, and graphite powder—used as partial replacements for fine aggregate (at 1, 3, 5, and 7% by volume) on the electrical, physical, mechanical, and durability properties of structural concrete. The findings demonstrated that structural concrete with favourable electrical conductivity could be achieved for diverse applications by selecting appropriate types and proportions of conductive fillers. However, the conductors affected the mechanical strength of mixtures negatively, and this reduction increased with the rate of conductors. Carbon powder had the most minor negative effect on mechanical strength among fillers. In terms of electrical performance, steel shavings could not be used to produce composites for structural applications, while the graphite and carbon powders could be used up to 7% by volume of sand, which provided the best performance.

Meehan et al. [140] investigated electrical-resistance-based sensing of impact damage in carbon fiber-reinforced cement-based materials. In this study, 5-mm and 7-mm sizes of three types of short carbon fibers were used in the amounts of 0, 0.50, 1.00, and 1.50% by weight of cement. So as to obtain sensing behaviour, electrical resistivity should be in the range of $10^4 – 10^5$ Ω.cm. According to the results, this range was obtained for 5-mm and 7-mm long CFs at 0.5% and 1.0% additions, respectively. The mixtures, which contained 5-mm and 7-mm long carbon fibers in 1.5% and 0.5% additions, were less effective due to low mortar resistivity of about 10^3 Ω.cm. In addition, there was no sensing ability without fiber incorporation.

Zhou et al. [143] investigated the electrical properties of low-dosage carbon nanofiber/cement composite in terms of percolation behavior and polarization effect. In the study, CNFs were used in the amounts of 0, 0.01, 0.05, 0.1, 0.2, 0.3, and 0.5% by weight of cement. Regarding the results, the percolation threshold was as low as 0.05% of CNF addition. Although there was a slight fluctuation for 0.1% dosage of addition, the resistivity results of the sample were reached stable after 0.5% addition. Above this amount, the electrical resistivity result was the same with the dosage of 0.1%. It was found that this was effective for developing cost-effective electrically conductive cementitious composite.

Fiala et al. [145] experimentally studied the electrical properties of steel-fiber reinforced concrete. In the study, three types of SFs were added to obtain conductive properties in 0.5, 1.0, and 2.0% of volume. As a result, concerning the utilization of SF in the concrete mixture for railroad ties applications in-situ conditions, changed in electrical resistivity depended on the volume fraction ratio of fiber.

Chiou et al. [150] studied the electromagnetic interference shielding with carbon fiber-reinforced cement. In this study, the 3-mm CFs, effective on electromagnetic interference shielding due to their short size, were added into the mixture in the amounts of 0.5, 1, 2, 3, and 4% by weight of the cement. The best result was obtained with 0.5% CF addition, and chemical agents improved the interference shielding effectiveness of cement mortar with an increase of 10 dB or more in the frequency range of 1.0 to 2.0 GHz for a 4 mm thickness.

Zuofu et al. [151] investigated two methods to increase the electrical conductivity of conductive concrete using carbon fiber (CF). Besides carbon fiber addition, various chemical additives and silica fume were added to the mixture in different ratios to desire better homogeneity of fibers. The best result was obtained for the mixture containing 0.58% CF (by volume) and 20% silica fume. This mixture showed an excellent electrical conductivity and a superior mechanical strength. The results showed that CF could be dispersed in two methods: increasing the water amount to dissolve the methylcellulose and preparing the carbon fibers before mixing.

Li et al. [152] investigated the effect of compressive strain on the electrical resistivity of carbon black-filled cement-based composites. In this study, CB was used in the amounts of 5, 10, 12, 15, 20, and 25% by the weight of cement. The results indicated that the tunnelling effect was dominant when the amount of CB was lower than the percolation threshold. In contrast, percolation phenomena played a critical role when the amount of CB was higher than the percolation threshold. The percolation threshold of CB was determined to be between 7.22 to 11.39 % by volume. The contact resistivity of fillers was found to have a dominant role in conductivity.

Wen and Chung [153] studied the partial replacement of carbon fiber with carbon black in multifunctional cement–matrix composites. In the study, CB (0.5 to 2% of the weight of cement) and CF (0.5 to 3.5% of the weight of cement) were added to the mixture. The results showed that CF was more effective than CB in terms of conductivity. Among replacement ratios, 50% CF replacement with CB lowered the cost and increased the workability besides electrically conductive behaviour among all mixtures. The addition of both CF and CB caused the decrease in compressive strength, strain at failure, and density of the mixtures.

Xiaoming et al. [154] the electrical conductivity and piezoresistivity of carbon fiber graphite cement-matrix composites with carbon fiber content (1% by the weight of cement), graphite powder contents (0 - 50% by the weight of cement) and cementitious capillary crystalline waterproofing materials (4% by the weight of cement) were studied. Although electrical performance was improved by increasing graphite content, the percolation threshold of graphite content was found to be about 20% addition. As a result, the piezoresistive effect was obtained for the mixture, which contained 1% by weight of cement of carbon fibers and ranges from 20% or 30% by weight of the cement of graphite powders.

Qin et al. [155] studied the electrical conductivity of additive fillers in carbon fiber-cement-based composites. In this study, three types of mixtures were prepared: (1) carbon fiber was added in the amount of 0.1, 0.2, 0.4, 0.6, 0.8, 1.0, and 1.2% by weight of cement with different w/c ratios of 0.45, 0.50, 0.55. (2) graphite was added at 10, 15, 20, 25, and

30% by weight of cement with different carbon fiber content for a w/c ratio of 0.50. (3) multi-walled carbon nanotube (MWCNT) was added to 0.1, 0.2, 0.5, 1.0, 2.0% by weight of cement with 0.4% by weight of the cement carbon fiber at a w/c ratio of 0.40. According to the results, the mixture, which contained 0.4% carbon fiber and 0.5% multi-walled carbon nanotubes addition, showed an excellent electrical conductivity of 33.65 Ω·cm. In contrast, the excessive addition of MWCNTs into a mixture with carbon fiber rapidly increased electrical resistivity. When the CF was below the percolation threshold (0.4% CF), graphite additions up to 30% were provided to obtain lower electrical resistivity, which reduced dramatically from 3991.44 Ω·cm to 524.33 Ω·cm. There was no effect on the electrical conductivity for graphite with above the 0.4% CF addition due to an increase in porosity.

Zakaria et al. [156] studied the effect of the milled carbon fiber (MCF) addition as a secondary filler on the electrical conductivity of graphite/epoxy composites for electrically conductive material. In this study, an average of 165-µm lengths of MCFs were incorporated up to 8% by weight of cement. In terms of electrical conductivity, the best results were obtained for 2% MCF addition by the weight of cement. The agglomeration of MCFs in higher additions affected the electrical conductivity negatively due to its shape. The MCF had a cylindrical, rod-like shape, which differed from hollow CNTs. According to the results, MCF had the potential to be the main filler in a conductive polymer composite system like CNTs.

Han et al. [157] studied the reinforcement effect and mechanism of carbon fibers on mechanical and electrically conductive properties of cement-based materials. In the study, 3-mm and 6-mm CFs were added in the amounts of 0, 0.2, 0.5, 0.8, 1.1, 1.5, and 2.0% weight of the cement. The results indicated that increasing the number of fibers enhanced compressive strength and electrical conductivity. The lowest electrical resistivity result was obtained for 2% CF addition for both sizes due to the tunnel effect and lapping CFs into the mixture. Compared with the two sizes, 6-mm long CFs established a steadier conductive pathway easily.

Al-Dahawi et al. [158] studied the electrical percolation threshold of cementitious composites possessing self-sensing functionality with carbon-based materials. In this study, various conductive materials such as multi-walled carbon nanotubes (CNTs), graphene nanoplatelets (GNPs), and carbon black (CB) as the nano-scale materials, 6- and 12-mm long carbon fibers (CF6 and CF12) as the micro-scale materials were used. The CNT was added up to 1%, CNP and CB were added up to 5% (weight of binder (PC+FA) for CNT, GNP, and CB. The addition rate for CF was up to 2% (volume of mixtures for CF). In terms of improving self-sealing performance and electrical performance, the percolation thresholds of mixtures were obtained for CNT, GNP, CB, and CFs as 0.55%, 2.0%, 2.0%, and 1.0%, respectively.

Shi et al. [159] investigated the mechanical and electrical characterization of steel fiber- and carbon black-engineered cementitious composites. In this study, two types of self-sensing cementitious composites were prepared: SF (0.58%) and CB (1.75%) additions with an amount of 1.75% PVA addition. Although both conductors can improve mixtures' flexural strength and electrical conductivity, the SFs had better performance due to the bridging phenomenon with its higher length. In addition, surface resistance results showed similar behaviour in case of cracking.

Kim et al. [160] studied the electrical characteristics of hierarchical conductive pathways in cementitious composites incorporating carbon nanotubes and carbon fibers. In the study, CF was added to a mixture ranging from 0.1% to 0.5% by weight of the cement with the constant 0.5% CNT incorporation. Regarding the results, CF was the most fundamental material to obtain conductivity performance. Both CF and CNF-based mixtures were more stable than the mixtures without CF. In addition, increasing the number of CFs in the mixture with CNT extended the electrically conductive pathway at a higher w/c ratio. This improvement decreased the unfavourable effects of the w/c ratio, electrolytic pore solution, and temperature.

Jiang et al. [161] compared cementitious composites' compressive strength and electrical resistivity with different nano- and micro-fillers. In this study, various conductors such as nano-SiO_2, nano-TiO_2, carbon nanotubes (CNTs), and carbon nanofibers (CNFs) were

incorporated into the mixture at dosages of 0.1, 0.5, and 1.0% by weight of the cement. In addition, 3-mm and 6-mm long carbon microfibers (CFs) were added in the amounts of 0.5, 1.0, and 1.5% by the weight of cement. Among all conductors, the CFs improved mixtures' compressive and flexural strength. In terms of reinforcing effect, micro-fibers showed better performance than nano-fillers. The percolation threshold was determined to be 0.5% for both CNFs and CFs mixtures and 1% for the CNTs mixtures in terms of electrical conductivity. Although CNFs did not have a significant effect on the compressive strength of composites, they provided the best improvement in reducing electrical resistivity.

Zhang et al. [162] studied the effect of mix proportion and production methods on cementitious composites' mechanical and electrical properties with nano/fiber fillers. In this study, Nano-SiO2 and carbon nanotubes (CNTs) were incorporated up to 0.5%, and 3-mm long carbon fiber (CF) was incorporated up to 1% into the mixtures. Experimental results showed that the percolation thresholds were determined to be 0.1%, 0.1%, and 1% by the weight of the cement for NS, CNT, and CF, respectively. Among all the conductors, the best mechanical strength and conductivity performance were obtained with a 1% CF addition, achieving a strength of 152.69 MPa and a conductivity of 0.1258 S/m after 28 days.

Faneca et al. [163] studied the development of conductive cementitious materials using recycled carbon fibers (RCF). In this study, four types of RCFs were utilized at 0.1 to 1.4% by volume. The results indicated that electrical resistivity reduced in the range of 3 – 0.6 Ω·m with the RCF addition of between 0.2 to 0.8% by volume.

Uygunoglu and Simsek [164] investigated the mechanical, physical, and electrical properties of graphene-oxide-blended mortars. In this study, electrical conductivity was measured at different frequency values (0.1, 1, 10, and 100 kHz) using graphene oxide at dosages of 0.0, 0.5, 1.0, 1.5, and 2.0% by the weight of cement. Regarding the results, graphene oxide could enhance mixtures' electrical conductivity due to the filler's structural nature. The electrical resistivity of the reference sample was measured as 85 Ω.m at 0.1 kHz frequency for the seven days; this result decreased to 55 Ω.m using a 2%

addition of filler. Increasing frequency decreased resistivity more than other factors. In addition, the compressive strength increased by 44% compared to the reference mixture, especially with 0.5% of the graphene oxide usage.

Wang et al. [165] studied the effects of carbon fibers and carbon nanofibers on electrical conductivity of concrete. In the study, CFs and CNFs were utilized in mixtures in ratios of 0.1, 0.2, 0.3, 0.4, and 0.5%. Regarding the results, increasing volts decreased resistivities independently of the type of fiber. In addition, the resistivities of mixtures had an increased trend line with curing age. In the first seven days, resistivity increased faster, but after this age, it increased slower. Higher fiber content improved electrical conductivity significantly. However, CFs were more effective in creating electrically conductive pathways than CNFs.

Dehghani and Aslani [166] studied the effect of SMAs, SFs, and CFs on fresh, mechanical, and electrical properties of cementitious composites. In this study, steel and SMA fibers were added at volume fractions ranging from 0.25 to 1.50% at 0.25% intervals. Additionally, 12.7-mm long CFs were incorporated at low volume fractions ranging from 0.1 to 0.6%, with 0.1% intervals. This was done to achieve a lower percolation threshold and minimize the adverse effects of fibers on the workability of cementitious composites. According to the results, CF addition seriously influenced the flowability and corresponding workability of the mixtures, while SMA and SFs slightly improved the flowability of the mixtures. Regarding the results, up to %1 addition of SMA and SFs modestly lessened the compressive strength of mixtures. After that limit, the strength was improved with increasing fiber content. Furthermore, incorporating SMA and SFs did not substantially influence the electrical conductivity of composites up to 1.5% addition. However, the %0.1 content of CF addition affected electrical performance considerably. The optimum CF dosage was found to be 0.3% in terms of electrical conductivity.

Akbar et al. [167] investigated microstructural changes and mechanical performance of cement composites reinforced with recycled carbon fibers (RCFs) (length of 80–100μm). In the study, the RCFs were incorporated into mixtures up to 1.5% volume fractions at an

increasing rate of 0.25%. The results indicated that the best result and reinforcing effect were obtained by adding 1% by volume of the RCF. The flexural and compressive strengths were improved by 82% and 47%, respectively, compared with the reference mixture.

2.2.4. Percolation Threshold Phenomena

In literature studies, the electrical conductivity of composites undergoes significant changes with the incorporation of single or combined types of conductive materials, each in various geometries, into the cementitious matrix at different volume fraction ratios. Nevertheless, research studies have revealed that the geometric properties of the conductor and its distribution in the matrix are more influential factors than the conductivity and usage rates of the conductors themselves [138]**.** The reason is the mechanism that occurs when incorporating conductive materials into the matrix of cementitious composites. In the literature, this mechanism is called the conductive pathways theory, tunnelling effect theory, field emission theory, or percolation threshold [115]. The percolation threshold phenomenon is the volume fraction above which the fibers touch one another, forming a continuous electrical path [109]. The theory can be explained by Figure 2.4 [109,115,142,168].

Stage 1 is the insulated phase, indicating that conductive materials like carbon fiber are incorporated into the mixture in less than the optimum ratio. The lower quantity of fibers results in a wide average distance between two adjacent fibers, preventing electron transfer in this region and forming an insulating zone.

Stage 2 is a transition phase. With an increase in the content of conductive material, the average distance between two adjacent fibers decreases sufficiently for electron transfer. As the number of conductors per unit volume increases in the composite, overlapping occurs between some fibers in the transition zone. The reduction in distance between adjacent fibers and the formation of overlapping and contact between fibers facilitate the transmission of electrons, creating a conductive pathway or tunnel effect in this region

since the primary electric conduction relies on the transfer of electrolyte ions and conductive material. The conductivity undergoes significant changes by several orders of magnitude when the fiber's volume reaches a critical value. This zone is referred to as the percolation threshold zone. Percolation theory provides insight into the minimum amount of conducting filler required to convert an insulating matrix into a conducting one.

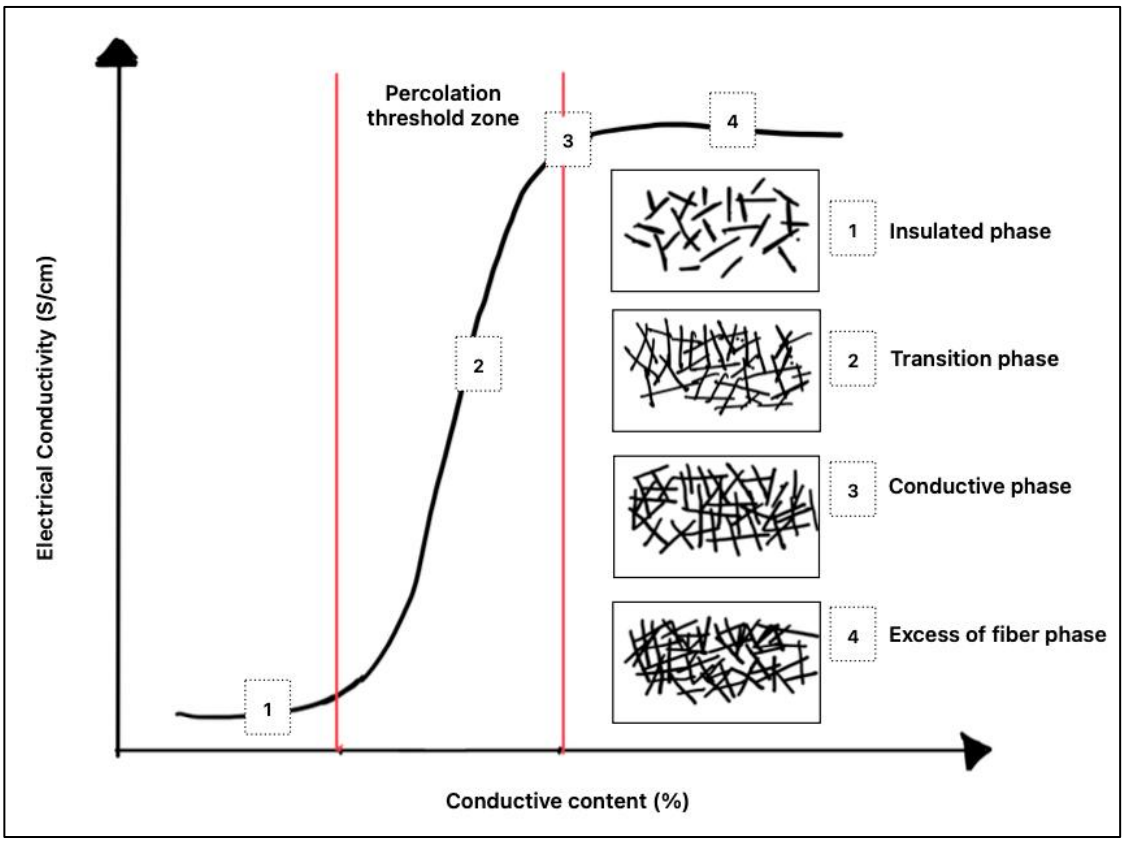

Figure 2.4. Theory of percolation threshold zone [109,115,142,168]

Stage 3 is the conductive phase, where the composite achieves maximum conductivity performance. In this region, electrical conductivity surpasses the levels observed in the percolation threshold, primarily because of forming the shortest continuous conductive path with the maximum utilization of conductors. Here, conductive materials align in lines, making contact with each other and frequently overlapping.

Stage 4 is the excess of the fiber phase. It is observed that incorporating more conductors into the matrix beyond its maximum level does not improve conductivity and reaches stability. In this region, there is no distance between the fibers, and the conductive

materials are in complete contact, overlapping [109,113,120,157,169]. In conclusion, increasing the conductor ratio does not improve the electrical performance of the cementitious composite beyond the maximum point. Since a continuous conductive path can be established even at lower ratios in the percolation threshold zone, using the appropriate ratio of conductors is crucial for enhancing the cost-effectiveness of the cementitious mixture.

The effects of various factors on the percolation threshold zone are frequently investigated in the literature. These factors include the type of conductive material, the use of combined conductors in single, double, and triple configurations, and the geometric properties of conductors such as length, radius, aspect ratio, and particle size [115,122,137,138,142,170–175]. Other influential factors involve the incorporation ratio of conductors, the distribution of conductors in the matrix, the method of distributing conductors, the mixing method, the orientation of conductors, the mix proportion of the mixture, and the type of cement [144]. These factors significantly impact the percolation threshold area, specifically the electrical conductivity performance of the mixture. These factors also affect the other physical and mechanical properties of cementitious composites.

Chen and Chung [110] stated that fiber dispersion is vital to obtaining electrically conductive performance. It was claimed that chemical and mineral additives such as methylcellulose, latex, or silica fume could be used to improve dispersion behavior.

Dong et al. [113] claimed there was less probability for the agglomeration of CF with a higher aspect ratio in composite, thus increasing the dispersion of fibers. Generally, the use of conductive fibers with a larger aspect ratio tended to lower the percolation threshold by providing more potential conductive passages and thus improved the conductivity performance of cementitious composite, while it could also lead to reduction the contact of fibers and matrices, resulting in weaker cohesion and caused lower mechanical properties.

Wang and Aslani [115] mentioned that the dispersion of CFs in the matrix was significant in terms of conductivity performance. While well-dispersed CFs showed more conductive pathways in the matrix, poorly dispersed CFs were in a fasciculus state. They were separated by thin cement wall layers, preventing electron transfer via a conductive pathway. In conclusion, homogenous dispersion and preventing agglomeration were significantly required for electrically conductive concretes.

Han et al. [139] studied the effect of fillers' dispersion, electrode arrangement, electrical resistivity measurement methods, curing age, moisture content, and temperature on the performance was analyzed during the preparation and application. According to results, carbon-based conductive materials were ideal for cementitious composition. In addition, longer CF length and higher aspect ratio caused higher conductivity and a smaller percolation threshold. However, carbon-based materials were dispersed in water poorly due to their hydrophobic properties. In addition, their large aspect ratio caused the agglomerations in the matrix and negatively affected the mechanical and electrical performance of mixtures. Therefore, the dispersion of fibers in the matrix homogeneously became the most critical problem in the preparation.

Wang et al. [169] claimed that electrical pathways could not be established below the percolation threshold, and even higher lengths of fibers were used. They observed a negative relationship between fiber length and the percolation threshold. In conclusion, the electrical conductivity performance was strongly dependent on two main factors: the incorporation ratio of fibers and the length of the fibers.

Research studies have revealed that the percolation threshold region is influenced by various factors, resulting in variable electrical conductivity performance. Nevertheless, it has been emphasized that the most critical factor is the dispersion method of the conductive materials into the matrix. To accurately determine the percolation threshold of cementitious composites, it is essential to uniformly and effectively disperse conductive materials throughout the matrix. The fibers' dispersion directly impacts the final composite's fresh, mechanical, and electrical properties [107,113,115,116,159,168,176].

2.2.5. Chemical Approaches of Dispersion Methods of Conductive Materials into the Cementitious Matrix

In literature studies, different techniques provide electrical conductivity performance to cementitious composites. Physical and chemical methods achieve the most effective and uniform dispersion of conductive materials within the matrix. The chemical approach involves using appropriate amounts of high-range water-reducing additives [120,157,166,177,178], various dispersants [126,153,155,169,179], and mineral additives [107,153,172,180,181] are used. A general summary of chemical and mineral additives commonly used in the literature is provided in Table 2.3 [115,168].

The combined use of chemical and mineral additives is observed to significantly alter the mixtures' physical, mechanical, chemical, and electrical properties. Chung [182] stated that fiber dispersion was enhanced by various methods via additives (such as silica fume, acrylic particle dispersion, methylcellulose solution, and silane) and fiber surface treatment (such as ozone treatment).

Chuang et al. [107] stated that silica fume addition was required to obtain a homogeneous dispersion of fibers. It was explained that conductivity could be sustained through ion migration by pores in the gel matrix. The total porosity of the matrix was reduced, and the composite's density was increased with silica fume content in the cementitious matrix. In conclusion, denser microstructure led to increased resistance of the composite due to the difficulty of migration ions. Thus, the resistivity of the composite was increased as well.

Dong et al. [113] stated that supplementary cementitious materials like silica fume, fly ash, and slag greatly affected the electrical properties and piezoresistivity of cementitious composite. The research identified that silica fume incorporations had lower electrical resistance results than reference composite. Typically, additives had non-conductive properties and were used in the cementitious matrix at small scales. Nevertheless,

conductive fillers showed a filling effect and reduced size and the total amount of porosity, resulting in improved piezoresistivity of sensors.

Table 2.3. Chemical approaches for dispersing conductive materials [115,168]

Category	**Dispersion Material**
Chemical additive	Water-reducing agent
	Methylcellulose
	Polycarboxylate based high range water reducing additive
	Polycarboxylic-acid based superplasticizer
	Naphthalene-based water-reducing additive
	Superplasticizer
	Dispersive agent
	Hydroxyethyl cellulose
	Naphthalene sulfonate
	Defoamer
	Carboxy-based methylcellulose
	Acrylic dispersion
	Latex
Mineral additive	Silica fume
	Fly ash
	Granulated blast furnace slag
	Silica sand

Wang and Aslani [115] stated that silica fume could be used to enhance the dispersion performance of functional fillers. When silica fume was incorporated at 10% of the weight of cement, it could mechanically weaken the agglomeration into smaller sizes. In the case of silica fume use within the hydration reaction of cement grains, more C-S-H gel and smaller pores of matrix occurred. This improved bonds between functional fillers and the matrix, resulting in higher mechanical strength. Up to 30% incorporation of silica fume, agglomerated fillers could be completely dispersed as individual fibers or particles. Although no large clumps were observed, the increased conductive fillers tended to agglomerate and caused the declined compressive strength. Nevertheless, higher silica fume usage could cover the cement grains and influence the hydrate reaction. Though the conductivity performance of composites increased with the addition of silica fume, silica

fume should not be used in large amounts because of its adverse side effects on mechanical properties. In conclusion, optimum silica fume usage was defined to be between 10 – 15% to obtain higher conductive materials dispersion and improve mechanical and electrical conductivity properties.

Kim et al. [183] studied the enhanced effect of carbon nanotubes on cement composites' mechanical and electrical properties by incorporating silica fume. In the study, the effects of silica fume addition on the porosity, compressive strength, and electrical resistance of the CNT/cement composites were then systematically investigated. Silica fume was added to amounts of 0, 10, 20, and 30% by weight of cement in the composites. Regarding the results, CNTs were not easily dispersed and tended to agglomerate without silica fume addition. With silica fume in small amounts, agglomeration started to dissolve in the matrix, affecting both mechanical and electrical conductivity positively. In the higher amount of silica fume usage, CNTs dispersed in the matrix homogeneously and decreased the electrical resistance of mixtures. In conclusion, it was observed that silica fume addition had a direct positive effect on the mechanical and electrical properties of composites.

Bai et al. [184] revealed that optimum silica fume usage could improve the pore structure of the cementitious matrix. Using silica fume up to a certain amount could enhance compressive strength and increase the cementitious composite's electrical conductivity performance. However, exceeding this optimal silica fume content impacted mechanical and electrical performance negatively.

Dong et al. [185] investigated the effects of silica fume on physicochemical properties and piezoresistivity of intelligent carbon black-cementitious composites. In this study, silica fume was added to the mixture in amounts of 0, 5, 10, and 20%. The results showed that electrical resistance was reduced with the increasing amount of silica fume. It also caused a decrease in the flowability of the mortar. In particular, 10% silica fume incorporation had the highest compressive and flexural strengths on 28 days, reaching 43.40 MPa and 3.10 MPa, respectively. Moreover, micropores and CB agglomerations

were found in the matrix without SF addition. Whereas denser structures and well-dispersed CB nanoparticles were obtained with a 5 and 10% addition of silica fume.

2.2.6. Physical Approaches Dispersion Methods of Conductive Materials into the Cementitious Matrix

In the literature, various mixes are used to perform the electrical conductivity of cementitious composites. Both physical and chemical approaches are utilized to achieve the most effective and uniform dispersion. The physical approach distributes fibers throughout the matrix using various mechanical mixing methods. Researchers have explored the fact that combining the physical and chemical approaches provides electrical conductivity performance on composites. Extensive studies in the literature have identified three primary mixing methods for dispersing nano- and micro-sized conductive materials in cementitious mixtures: the first admixing method, the synchronous admixing method, and the latter admixing method [163,168]. The schematic representation of these mixing methods is shown in Figure 2.5.

The mixing process of the first admixing method is as follows: Step 1 includes mixing conductive materials with an aqueous solution. The solution can include chemical additives, such as high-range water-reducing additives and various dispersants. Step 2 includes adding binding materials with mineral additives into a mixing bowl, and Step 3 includes adding aggregates into a mixing bowl.

The mixing process of the synchronous admixing method is as follows: Step 1 includes mixing conductive materials with binding materials and, if any, mineral additives. Step 2 includes adding aggregates into a mixing bowl. Step 3 includes adding an aqueous solution, including chemical additives, high-range water-reducing additives, and various dispersants.

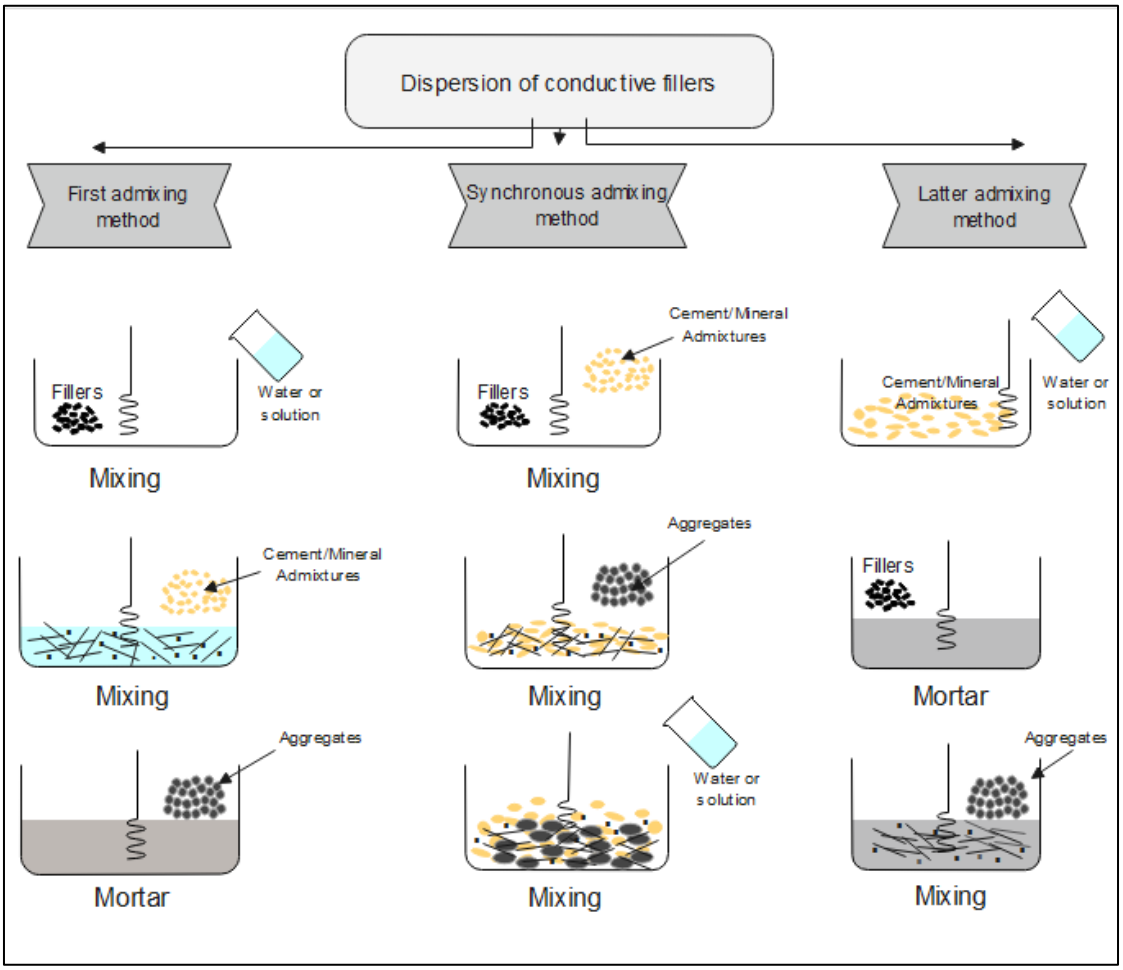

Figure 2.5. Different dispersion methods of conductive materials [115]

The mixing process of the latter admixing method is as follows: Step 1 includes mixing binding materials with mineral additives (if any) and an aqueous solution, including chemical additives, high-range water-reducing additives, and various dispersants. Step 2 includes adding conductive materials into the mixing bowl. Step 3 includes adding aggregates to the mixture. The literature contains comprehensive data on the electrical performance of cementitious mixtures prepared with conductive materials using these mixing techniques. Detailed information about these studies is provided in Table 2.4.

Table 2.4 shows various micro- and macro-sized conductive materials added in single, double, and triple matrices to improve the electrical performance of composites with different mixing methods. In addition to mixing methods, researchers also preferred using mineral and chemical additives to create conductive networks by homogeneously

dispersing conductive materials throughout matrices. The electrical resistance/resistivity results were mainly affected by conditions such as conductor type, utilization rates, and the mixing method. In comparison to micro-sized conductive materials, carbon fiber in mixtures containing single and multiple additions of conductive materials demonstrated the most effective electrical performance. Among nano-size conductive materials, carbon-based ones significantly changed the electrical conductivity performance. The best electrical performance was obtained by adding conductive materials to the matrix in a wide range of 30%. The results showed that similar values were measured from the same type of conductive material at different contents. Physical and chemical approaches also significantly affected resistance/resistivity differences. Among the physical approaches, the first admixing method was mostly preferred to disperse the nano-sized conductive materials [107,151,155,157,177,186]. As for micro-sized conductives, there was no dominant mixing method. Moreover, mixtures were often formulated with mineral additives such as silica fume, fly ash, or blast furnace slag to enhance the performance of the mixture [131,159,187,188].

.

Table 2.4. Dispersion methods for conductive materials

Reference	Type of conductive material	Type of binder	Type of chemicals additives	Mixing methods	Electrical performance	Percolation ratio
Li et al. [152]	Carbon black	Cement	Defoamer, Water-reducing agent	First admixing method	10^2 Ω·cm	7.22–11.39% (by weight of cement)
Monteiro et al. [177]		Cement	Polycarboxylate based water-reducing agent	First admixing method	9700 Ω	6.5% (by weight of cement)
Monteiro et al. [189]		Cement	Water-reducing agent	Latter admixing method	1.43×10^4 Ω	7.0% (by weight of cement)
Chuang et al. [107]	Carbon fiber	Cement, Silica fume	Hydroxyethyl cellulose, Naphthalene sulfonate	First admixing method	3.6 kΩ.cm	0.6% (by weight of cement)
Donnini et al. [120]		Cement	Superplasticizer	Latter admixing method	<150 Ω·cm	3% (by weight of cement)
Zuofu et al. [151]		Cement, Silica fume	Defoamer, Methylcellulose, High range water-reducing agent	First admixing method	$<10^2$ Ω·cm	0.58% (by volume of mixture)
Han et al. [157]		Cement	Water-reducing agent	First admixing method	5 kΩ·cm	2.0 % (by weight of cement)
Wang et al. [169]		Cement	Methylcellulose fiber dispersant	First admixing method	0.1 Ω.cm	2–3% (by weight of cement)
Liu et al. [190]		Cement, Silica fume	Superplasticizer	Synchronous admixing method	8 Ω.cm	2% (by volume of mixture)

Table 2.4. Dispersion methods for conductive materials (continued)

Shi et al. [159]	Steel fiber	Cement, Fly ash	Superplasticizer	Latter admixing method	37.5 kΩ	0.58% (by volume of mixture)
	Carbon black			Synchronous admixing method	57.5 kΩ	1.0% (by weight of cementitious materials)
Banthia et al. [114]	Carbon fiber, Steel fiber	Cement, Silica fume	Not given	Not given	10^2–10^3 Ω·cm	2% carbon and 1% steel fiber (by volume of mixture)
Nalon et al. [127]	Carbon black nanoparticles	Cement	Superplasticizer	First admixing method	1.7–2.1 Ω.cm	8% (by weight of cement)
Qin et al. [155]	Graphite, Multi-walled carbon nanotubes, Carbon fiber	Cement, Silica fume	Dispersant	First admixing method	33.65 Ω·cm	0.4% carbon fiber, 0.5% multi-walled carbon nanotubes
					524.33 Ω·cm	0.4% carbon fiber, 30% graphite
Wen and Chung [153]	Carbon black, Carbon fiber	Cement, Silica fume	Water-reducing agent, Defoamer	First admixing method	3.55×10^2 Ω.cm	1.5% carbon fiber, 2.0% carbon black (by weight of cement)
Dehghani and Aslani [166]	Shape memory alloy, Steel fiber	Cement, Fly ash, Silica fume, Granulated blast furnace slag	Polycarboxylate-based HRWRA, Polyether-based superplasticizer and viscosity modifying agent	Latter admixing method	Did not improve conductivity	Up to 1.5% (by volume of mixture)

Table 2.4. Dispersion methods for conductive materials (continued)

El-Dieb et al. [138]	Steel shavings, Carbon powder, Graphite powder	Cement	Not given	Synchronous admixing method	5×10^2 Ω·cm	7% (by volume of mixture)
Al-Dahawi et al. [131]	Carbon nanotubes, Graphene nanoplatelets	Cement, Fly ash, Silica fume	Polycarboxylate-ether-based high range water reducing additive	First admixing method	497 Ω·m	0.25% (by total weight of cementitious material)
	Carbon fiber			Synchronous admixing method	185.5 Ω·m	0.5% (by volume of mixture)
Wu et al. [116]	Steel fiber, Carbon fiber, Graphite	Cement	Naphthalene superplasticizer, Dispersive agent	Not given	322 Ω.cm	1% steel fiber, 0.4% carbon fiber, 4% graphite (by weight of cement)
Akbar et al. [167]	Milled recycled carbon fiber	Cement, Silica fume	Polycarboxylic ether superplasticizer (PCE)	Synchronous admixing method	-	1% (by volume of mixture)
Fulham-Lebrasseur et al. [191]	Carbon fibers, Steel fibers, Graphite powders, Copper powder, Graphene	Cement, Silica fume	Superplasticizer and Methylcellulose	Latter admixing method	177 Ω.cm	18.2% conductive aggregate, 10.8% graphite, 1.36% steel fiber, 0.1% graphene (by volume of mixture)

2.2.7. Effects of Types of Conductive Materials on the Properties of Cementitious Composites

Because cement-based composites usually exhibit high electrical resistance as Mega-Ω range within a short period, composites get insulators. Consequently, changing the electrical behaviour of the mixture by adding conductive materials to cementitious composites has been frequently studied in the literature. The electrical conductivity of cementitious composites increases with the higher content of conductives independently from the conductive type. However, the degree of conductivity performance of the composites is significantly influenced mainly by the type of conductive material and its incorporation dosages [115,138]. Commonly used conductive materials are metal and carbon-based sources. Metal-based materials typically include steel fiber, slag, metal oxide, and nickel powder. In contrast, carbon-based materials encompass carbon fiber, carbon nanotube, carbon black, graphene oxide, and milled carbon fiber. Carbon fibers are one of the most used to impart electrical conductivity properties among all conductive materials.

In literature studies, carbon fibers have been demonstrated as the most effective conductive material for providing electrical conductivity. Including an appropriate amount of CFs significantly reduces the electrical resistivity of cementitious composites in an extensive range, making them suitable for various applications. Additionally, CFs offer numerous advantages in terms of mechanical, physical, and durability performance. Firstly, CFs substantially enhance the mechanical performance of cementitious composites; in other words, they lead to high elastic modulus, flexural strength, toughness, creep resistance, and excellent tensile strength. CFs serve as reinforcement, inhibiting microcrack susceptibility and fatigue cracking development and expansion. Among conductive materials, a higher amount of fiber can be found in the matrix because of the lower density of CF. Therefore, its strength-to-density ratio is one of the highest among all fibers. CFs are also inert in aggressive environments, abrasion- and corrosion-resistant, stable at high temperatures, medically safe, high corrosion resistant, and more chemically stable than glass fibers in alkaline environments. CFs also have superior properties in terms of durability performances, such as low drying shrinkage, freeze-thaw

resistance, high specific heat, low thermal conductivity, and weak thermoelectric behavior. On the other hand, the drawbacks of CFs have also been investigated in the literature. The large aspect ratio of CFs and higher contents can easily lead to agglomeration in the matrix. This agglomeration primarily reduces the flowability of the fresh mortar, decreases the mechanical, and increases the electrical resistivity of cementitious composites. Additionally, CFs have a higher cost, limiting their essential usage in most large-scale applications in construction projects [107,109,110,115,120,139,144,166,170,192,193].

Another carbon-based fiber is produced by chopping carbon fiber into micro-sized, called milled carbon fiber (MCF). The technical properties of MCF are identical to carbon fiber, except for the size of the fiber. MCF is cylindrical and rod-like, distinguishing it from hollow CNTs. Consequently, it holds high potential to serve as the main filler, like other nano-scale conductive materials [194]. Incorporating MCF into cementitious composite at high contents could enhance the mechanical properties as well as electrical conductivity performance [195].

One of the conductive materials frequently preferred is steel fiber as a metal product in literature. SFs are embedded into cementitious composite mixtures to obtain electrical conductivity performance while improving the mechanical performance of mixtures. Because of its higher mechanical strength, SF can improve the tensile strength of composites by preventing the progression of deterioration in case of cracking and post-cracking, impact, and toughness strengths. SFs reduce the electrical resistivity of composites in magnitude of 2- or 3-times order and can be used in various applications where electrical conductivity is needed. In addition, the cost of SF is relatively lower than that of other types, and it provides cost-effective composites. However, there are some disadvantages of SFs, as well. The length of SF is relatively longer. It has a higher density than others, making it prone to agglomeration due to the large aspect ratio and segregation due to its higher unit weight. Therefore, the electrical resistivity of composites can show variability with the positions of fibers. Additionally, metals and the conductive materials based on them can easily be influenced by the corrosive environment, causing deterioration of the conductors. Thus, the electrical resistivity value increases with the

curing time of SFs used in electrically conductive cementitious composites due to the gradual rusting of SFs, which subsequently blocks all possible conductive paths [114–116,139,145,196].

Nano-scale conductive materials can also be used with micro-sized conductive fibers to enhance the electrical conductivity performance of cementitious composites. Carbon black (CB), carbon nanotube, steel shaving, or graphene oxide are used in a large amount due to their high conductivity performance for cementitious composites. CB has a higher specific surface area and lower cost, as well as good conductivity [139]. CB exists in a porous agglomerated form within the nanoparticles. This is due to the highly compressible nature of CB, leading to its spread. Its spreadability contributes to improving the electrical conductivity of composites [139,153]. High amounts of carbon black are produced by recycling waste tires using the pyrolysis process [111]. Although CB exhibits high electrical conductivity performance, its conductive efficiency is lower than that of micro-sized conductive materials due to its low aspect ratio [115]. Therefore, a relatively large amount of CB should be used to achieve conductivity performance. However, excessive CB behaves like defects in the matrix, adversely affecting mechanical performance. Although CB contributes less to the mechanical properties when compared to other materials, it can still serve as an effective conductive filler due to its better dispersion and lower cost [139].

One-dimensional carbon nanotubes (CNT), also known as carbon nanofibers, exhibit good mechanical and thermal properties and excellent electrical performance. CNTs possess a large aspect ratio, outstanding conductivity, and a low percolation threshold. When stress is applied to composites, electrical resistivity can change at different levels, demonstrating a piezoresistive effect in CNTs. However, due to their higher aspect ratios and strong van der Waals interaction, the CNTs are prone to agglomeration [176,183,197].

Graphene oxide (GO) is a carbon-based product that is lightweight and strong. It has superior properties such as transparency, inertness, density, high electrical conductivity, and thermal conductivity performance [164]. Owing to its two-dimensional structure, GO

exhibits a high specific surface area, enhancing cementitious composites' compressive and tensile strength. However, GO can decrease mixtures' consistency due to its high specific surface area. Thus, chemical additive needs to be used in these mixtures to compensate [194].

Steel shavings are a by-product of steel fibers. The properties of steel shavings closely resemble those of steel fibers. The specific gravity of steel shavings is higher than that of other nano-scale conductive fillers and even fine aggregates. Therefore, plasticizers are unnecessary when using steel shavings due to their segregation trend. Furthermore, the specific surface area of steel shavings is the lowest among all nano-scale conductive materials [138]. In addition, a large content of conductive filler should be used to create a conductive path in the matrix due to its relatively small particle size. For this reason, both the cost-effectiveness of nano-sized fillers compared to fibers and their positive impact on the conductive paths due to the synergistic effect between fillers and fibers, using nano-sized fillers in combination with fibers rather than alone have been interesting in the literature [115,176,198].

2.2.8. Effects of Physical Properties of Conductive Materials on the Electrical Conductivity Performance of Composites

Conductive fillers exhibit positive and negative effects on the electrical, mechanical, and physical properties of the matrix, mainly depending on the type and content of the conductors. In the literature, researchers also mentioned that conductive nature length, radius, aspect ratio, and particle size also affected these performances of composites. Chuang et al. [107] stated that higher lengths of carbon fiber could form a conductive network easily by overlapping. Thus, conductivity performance was getting stronger with higher lengths of fibers. In conclusion, the smaller the electrical resistivity results were measured.

Vossoughi [109] investigated the factors affecting the electrical performance of carbon fiber-reinforced concrete. The results showed that the water/cement and sand/cement

ratios were almost independent of electrical performance. Electrical conductivity performance could be affected by fiber length. Longer fibers provided a lower incorporation ratio to establish electrically conductive pathways. However, it was found that the longer fiber length and increasing incorporation ratio were prone to increase air void content and resulted in decreasing compressive strength.

Dong et al. [113] claimed that longer fiber length (SF or CF) had a remarkable effect on altering composites' resistivity and piezoresistivity properties because of conductive passage generation. At the same time, the aspect ratio of conductive materials affected dispersion, orientation, and coagulation performance in the composite.

Banthia et al. [114] concluded that in composite materials, the length and distribution of fibers had a critical role compared to the conductivity of fibers. Consequently, hybrid-fiber composites exhibited superior conductivity behaviour than mono-fiber systems.

Wang and Aslani [115] claimed that many factors affected the electrical conductivity of cementitious composites significantly, such as filler concentrations, fiber/particle diameter, fiber length, filler dispersion method, sand-to-cement ratio, water-cement ratio, aggregate-to-cement ratio, water content, curing age, temperature.

El-Dieb et al. [138] claimed that the electrical resistivity of cementitious composites was greatly affected by many factors, such as the content of aggregate, w/c ratio, sand-to-cement ratio, and air voids. Regarding the results, the conductivity of concrete was influenced by the type and number of fillers used and the homogenous dispersion of fillers. This homogeneity was affected by factors such as mix proportions, filler content, and the admixing method.

Sassani et al. [144] studied the influence of mix design variables on the engineering properties of carbon fiber-modified electrically conductive concrete. 6-mm and 12-mm lengths of carbon fibers were incorporated at 0.1, 0.55, and 1.0% (by volume) ratios into the mixture. In the study, carbon fiber dosage, fiber length, coarse-to-fine aggregate

volume ratio, and chemical additive dosages were investigated experimentally. Among mixing variables, in order of most to least significant, fiber content, coarse-to-fine aggregate volume ratio, fiber length, and conductivity-enhancing agent dosage influenced electrical resistivity. In terms of fiber length, the 12-mm fibers showed a positive effect on electrical conductivity but had a negligible effect on strength properties. Considering factors related to mixing and implementation, a 6-mm fiber length was recommended for overall suitability.

Wen and Chung [153] claimed that conductive fillers, such as graphite powder, were less effective in electrical performance due to their low aspect ratio. Among micro-sized fibers, carbon fibers were more effective than steel fibers, attributed to the crucial fiber–fiber contact, as opposed to the fiber-matrix contact that governed the piezoresistivity between steel fiber- and cement. However, fillers were more cost-effective than fibers, and their high use did not significantly impact the total cost of the mixture. Therefore, combining fibers with fillers could provide an advantage from an economic point of view. Furthermore, fillers might enhance the electrical conductivity between adjacent fibers, resulting in a synergistic effect.

Han et al. [157] found that carbon fibers with two different lengths (3-mm and 6-mm) exhibited the same average center-to-center spacing, decreasing with higher CF content. Nonetheless, longer fibers showed a higher potential to establish bridging and conductive paths even at a low incorporation of 0.2%. In conclusion, a 6-mm length of CF demonstrated superior conductivity in cementitious composites, especially at lower addition levels.

Dehghani and Aslani [166] noted that the percolation threshold zone initiated between 0.5% and 1% addition of carbon fiber (with a diameter of 7-15 μm and a length of 1 - 6 mm). However, this zone could vary based on the type of cementitious composite, the aspect ratio of carbon fiber, and its length. The results showed that the percolation threshold decreased with longer carbon fibers. Nevertheless, the longer carbon fibers posed challenges in terms of fiber dispersion, significantly reducing the workability and

flowability of the matrix. Consequently, chemical and mineral additives were necessary for use in the composition.

Payakaniti et al. [176] stated that reinforced-cementitious composites could be produced with particulate, short, or continuous fiber. In terms of civil engineering applications, short fibers were most favourable due to cost efficiency, ease of handling, and manufacturing.

Chung [182] stated that different diameters existed for conductive fillers. It was stated that nanofibers with around 0.1-mm diameters were less effective than microfibers as a reinforcement. However, they were more effective in terms of electromagnetic shielding due to their small diameter and the skin effect (the tendency of alternating high-frequency currents). The small diameter of fiber generally had a higher aspect ratio, but it was a barrier to homogeneous dispersion of fiber. Similarly, smaller fiber lengths had a lower aspect ratio. Thus, the fiber dispersion for these fibers was easier. In conclusion, agglomeration of fibers could occur with the fibers having a small diameter or high length clinging to one another.

Monteiro et al. [189] revealed that CF could be combined with CNT, SF, and CB in cementitious composites. Because of their aspect ratio, fibers generally resulted in larger improvements in electrical conductivity.

Ding et al. [193] stated that combined nanocarbon black and short carbon fibers showed both enhancement of conductive pathways of CF using NCB and improved mechanical properties of composites.

Ivaturi et al. [199] investigated the distribution of milled carbon fibers as a function of their length on S-glass fabric and its effect on the electromagnetic properties of S-glass epoxy composites. MCFs were made by chopping carbon fibers to five different lengths, namely 7-, 20-, 60-, 200-, and 400-μm, and these were used to fabricate electrically conductive epoxy composites. The study indicated that 400-μm length of milled carbon

fibers had better conductive performance than other lengths. The efficiency of conductive paths improved due to the increased interconnectivity of fiber in the matrix.

Notani et al. [200] studied the effect of carbon-fiber properties on volumetric and ohmic heating of electrically conductive asphalt concrete. In this study, 3-, 6-, and 12-mm lengths of carbon fibers were incorporated into mixtures 1% by the total binder volume. Regarding the results, the effect of the length of the fibers was evaluated in terms of related properties. With the increasing fiber length, air voids of matrix voids in the mineral aggregate and voids filled with asphalt were increased. In addition, the electrical conductivity performance of mixtures enhanced with the smallest length of the fiber, and it improved the heat-generation efficiency.

In literature, researchers mentioned that air voids and their size in the matrix formed due to conductor usage also affected the electrical conductivity and related performances of composites. Chung [25] revealed that the resistance of the specimen was relatively higher when voids occurred in the matrix because air, being an electrical insulator, led to higher resistance compared to the more conductive other ingredients.

Chuang et al. [107] stated that the air void ratio affected the properties of cementitious composites. Carbon fiber could be added to composites until the air void content became excessively high. When the air void content increased because of fiber addition, it negatively affected many properties, such as compressive strength and electrical performance. Besides the air void content, the workability of the mortars decreased with the fiber content.

Wu et al. [116] stated that higher graphite content caused lower compressive strength among steel fiber, carbon fiber, and graphite additions. When the mixture contained 6% graphite, it had more voids because of poor workability, which could also block the conductive path, resulting in a large resistivity. In addition, the number of voids was considerably reduced with the increase in sand ratio. So, a low sand ratio caused the formation of voids or gaps in the concrete, which affected the electrical properties.

Chung [170] stated that excess carbon fiber usage tended to excessively high air void content. When the total air void increased with fiber dosages, it tended to have a negative effect on compressive strength and workability behaviour besides the cost of the mixture. In addition, fiber content increased with the aggregate's particle size, resulting in decreased flexural strength. It was also claimed that as the specimen size increases, it resulted in the decline of the tensile and flexural strengths except for electrical properties, with the size effect becoming more significant.

Chung [201] stated that higher fiber dosages than critical content had some disadvantages on the properties of cementitious composites. With the increasing amount of fiber, material costs increased, consistency decreased, and the air void content increased, resulting in reduced compressive strength and increased electrical resistivity.

In literature, researchers mentioned that amount of water content in the matrix also affected the electrical conductivity and related performances of composites. Sassani et al. [144] observed that complete electrical contact was established between the electrodes and the concrete matrix when voids were filled with water. Therefore, higher saturation and elevated temperature reduced resistivity in cementitious composites. Electrolytic conduction occurred through capillary water when the degree of saturation exceeded 40%. Therefore, to ensure consistent measurements, promote electrolytic conduction, and eliminate surface moisture's effects, all specimens should be kept in a saturated surface-dry condition at an ambient temperature of 23 °C.

Wang and Aslani [115] stated that a high water-cement ratio was beneficial to achieve well dispersion of conductive fillers. Besides dispersion, the water-cement ratio was the main factor in providing sufficient mixture workability. In the case of poor workability, fillers were used at higher dosages, and the formation of conductive networks and mechanical strength was affected negatively. Hence, the water-cement ratio should be adjusted for both workability and dispersion sides in the cementitious mixtures.

Diaz et al. [173] claimed that the incorporation of fibers made the microstructure more porous and caused larger pores. In the cementitious composites, porosity and pore diameter were reduced using dispersants. In conclusion, addressing the negative and positive effects of fiber length, aspect ratio, air voids, and water content was crucial. Therefore, these factors should be considered in the development of electrically conductive cementitious composites, taking into account both economic and scientific considerations.

2.2.9. Effects of Environmental Factors on the Electrostatic Discharge Capability of Cementitious Composites

Researchers mentioned that conductive types and content, physical properties of conductive materials, air and water content might affect related performance of mixtures. In addition, studies also observed that environmental conditions such as curing age, moisture-, water- content, and curing age may negatively affect the electrically conductive performance of composites [202].

Studies on the effects of ambient temperatures on the electrical behaviour of composites have been frequently carried out in the literature. Wang and Aslani [115] stated that ambient temperature influenced the electrical performance of composites. Electrical resistivity decreased at higher temperatures first, then it increased suddenly. When the ambient temperature was lower than the specific limit, the electron absorbed heat energy and transferred it to kinetic energy. It increased the tunneling effect, resulting in a decrease in resistivity. While higher temperatures caused vaporing pore waters and resulted in higher resistivity.

Kim et al. [160] stated that ambient temperature influenced the electrical resistivity of cementitious composites. In the study, all specimens were oven-dried for 24 h at 50 °C to minimize the influence of the evaporation of the electrolytic pore solution, which increased the electrical resistivity. In conclusion, the electrical resistivity of a composite

with an electrically conductive filler could be varied with the thermal expansion coefficients of the filler and the matrix.

Payakaniti et al. [176] stated that the electrical resistivity of composites was influenced by curing temperature at low CF dosages. However, the effect of curing temperature on the resistivity diminished after the 0.4% CF dosages. The electrical resistivity could be varied in both curing temperature and CF contents. When the temperature was higher than 60 °C, electrical resistivity was higher, and the resistivity was more stable with time than with 25°C.

Dong et al. [185] claimed that higher temperatures caused a polarization effect and resulted in higher resistance of cementitious composites. Han et al. [139] stated that the temperature affected the resistivity of composites. Temperature variations tended to change the spacing between conductive fillers and the distribution of the conductive network. On the other hand, the temperature could also change the electronic transition and the conductivity of the tunnelling effect. So, the temperature could increase or decrease the conductivity, depending on the dominant effect. The electrical conductivity performance might change with the filler type, temperature range, and matrix microstructure. Studies have shown that temperature variations can affect the electrical resistance of composites. For this reason, it is necessary to determine whether the electrical performance is sustainable by the resistivity values of cementitious composites at different temperatures.

Another factor is the ambient water and dry conditions that can affect composites' electrical conductivity. Wang and Aslani [115] noted that saturation and dry conditions influenced the conductive pathway in the cementitious matrix. Under full saturation conditions, conductive current could pass through voids filled with water, resulting in continuous conductivity performance. Conversely, conductivity might stop or be hindered when voids occurred in the matrix without water under dry conditions, led to a sharp increase in electrical resistivity. In conclusion, undried composites exhibited lower electrical resistivity, up to three orders of magnitude, compared to dried composites, as water, an excellent conductor, facilitated the passage of current.

Han et al. [139] stated that overlapping filler conduction, tunnelling effect conduction, and free ionic conduction were most easily affected by the moisture content of the matrix. Ambient humidity affected the internal moisture content and changed conductive paths, resulting in variations in electrical resistivity. In addition, this difference could change with the content of the conductive filler. When the conductive filler content was lower than the percolation threshold area, an increase in moisture content improved conductivity performance. When the higher conductive filler was used in the matrix, the influence of moisture content was weaker. Studies have shown that the amount of dry and moisture conditions could affect the electrical resistance of composites.

Li et al. [203] investigated the electrical properties of cement-based composites filled with carbon black under long-term wet and loading conditions. The results indicated that water content had direct negative effects on the electrical conductivity performance of specimens. This outcome was attributed to the polarization effect, intended to increase water content. Additionally, the resistance of specimens increased over time due to the polarization phenomenon. Strong polarization effects occurred in environments with higher water content, resulting in higher resistance over time. In conclusion, this adversely impacted the actual resistance of the specimen, even limiting the use of the composite as a strain-sensing material.

Chen et al. [204] revealed that the resistivity of the system was increased abundantly at lower moisture content. Due to its changing water content, moisture content should be considered during resistivity measurements. The measurements were unstable or undetected when the specimens were oven oven-dry or in the air at 40% RH condition. While these measurements were conducted at surface saturated or wet conditions, the results were similar. Therefore, specimens could be wetted prior to the resistivity measurements.

The other factor is the curing regime and age, which can affect composites' electrical conductivity. Chuang et al. [107] observed that the resistivity of specimens tended to change with curing time due to the long hydration process. According to the results, when the incorporation ratio of CF changed between 0 and 0.6%, the resistivity increased

significantly until 28 days, and it became stable after 84 days. These results explained with the hydration process. During continuous hydration, free water was gradually reduced in the matrix, and this free water was converted into adsorption water or gel water from a larger dielectric constant. Therefore, the conductive pathway was blocked because the interface layer on the fiber surface became thicker. Fibers became isolated, and the absolute barrier between them grew due to weakened conductivity. In such a situation, electrons could not jump by the tunneling effect. However, the incorporation of CF ranged from 0.8 to 1%, the resistivity increased sharply until seven days, and it became stable behaviour after 84 days. The conductivity of specimens was slightly affected by the curing age of the higher dosage of CF. The distance between fibers narrowed when the amount of CF was used higher than the percolation threshold. So, electrons could quickly transfer with a conductive pathway. In conclusion, the conductivity performance of composites was hardly influenced by the curing age when fibers were used at higher dosages than the critical value.

Han et al. [139] claimed that the curing age influenced the resistivity of the composite. It was found that longer curing age tended to higher resistivity. Many solution-containing ions existed because of the low hydration degree and higher porosity found at an early curing age. This led to ionic conduction being carried out quickly, which was essential to obtaining the conductive path of cementitious composites. According to the literature, external factors may negatively affect the electrical conductivity performance of cementitious mortar. For this reason, it is necessary to determine whether the electrical performance is sustainable by the resistivity values of cementitious composites at different conditions. In conclusion, the developed electrically conductive coating design for ESD problems in floor applications of critical buildings must have short and long-term high electrically conductive performance properties.

Chen et al. [142] stated that cementitious composites had a continuous long hydration time. Therefore, hydration time and relative humidity could influence the electrical conductivity performance of the system due to the changes in the microstructure of the system.

Al-Dahawi et al. [158] measured the electrical resistivity of four carbon-based fillers up to 180 days of curing. It was revealed that the electrical resistivity increased with time due to the continuous hydration of the cementitious matrix. In addition, the total amount of porosity and moisture content was reduced with continuous curing age, resulting in a loose pore network. Moreover, hydration products were gradually to wrap conductive fillers within the curing age. Thus, these effects caused a disconnect in the conductive pathway and resulted in higher resistivity.

Lee et al. [205] studied the fluctuation of electrical properties of carbon-based nanomaterials/cement composites with different factors. In this study, the fluctuation was observed as follows: 1) ununiformed dispersion of CNM in a cement matrix, 2) cracking: disconnection of CNM network, 3) growth of hydration products: tunnel blockage effect, 4) debonding of electrodes, 5) interfacial void around composite sensors, 6) moisture contents in cement composite (also correlated with polarization and ion flow). According to the results, the electrically conductive network of fillers dispersed in the cement matrix had three types of mechanisms of electrical flow. First was direct conduction due to physical contact between the CNMs, and this was not disturbed by other external factors, except the loss of conductivity of CNMs themselves. The second was electron flow through ions in the pore solution of the cement matrix. This was influenced by the internal moisture content and the tunneling effect caused by the third. In terms of water content, the electric properties of cement composites were strongly influenced by moisture content in the pore networks, as the pore solution contained a high concentration of ions. In addition, the hydration products, including calcium silicate hydrates, had nano-sized particles filled between CNMs, which might block the tunnelling pathway with a continuous hydration process. This could be called the ‘tunnel blockage effect’.

3. EXPERIMENTAL STUDIES

3.1. Materials

In this section, the features of the materials used to develop new-generation cementitious composites with electrostatic discharge capability are explained in detail. This includes information on cementitious mixtures (cement types and sand), mineral and chemical additives, and conductive materials (carbon fiber, steel fiber, and milled carbon fiber).

3.1.1. Cement Types

In the thesis study, two types of cement, calcium aluminate cement and Portland cement, were preferred to obtain the ternary system. High-early strength CEM I 52.5R type White Portland cement (PC), which was produced by Turkish Çimsa Cement Company, was used in the development of early age high strength cementitious composite. Among different proportions of Al_2O_3-based calcium aluminate cements (CAC), Isıdaç 40 and Isıdaç 50 type of cement were supplied from Turkish Çimsa Cement company, while Secar 51 and Secar 80 types of cement were supplied from French Kerneos company in the experimental study. The CAC types of cement used are concordant with TS EN 14647 [48]. The CEM I 52.5R cement used in concordant with EN 197-1, and ASTM C150 standards [206,207]. Digital images are shown in Figure 3.1. While PC is white, the CAC varies from dark gray to white color with increasing aluminate content (Al_2O_3). Subsequently, the specimens were dried overnight in an oven before the analysis. Energy dispersive X-ray analysis (EDX) is performed with SEM or TEM.

In addition, the oxide compositions determined by X-ray fluorescence (XRF) analysis are given in Table 3.1, the technical properties obtained from the manufacturers are given in Table 3.2, and the particle size distributions of the types of cement determined by the laser diffraction method are shown in Figure 3.2. The same preparation procedure was used for EDX analysis before testing the specimens. In XRF analysis, a wavelength of 0.1-50 Å was used, while during the laser diffraction method, a particle size range

sensitivity of 0.02 to 4000 µm was employed. All microstructure analyses were conducted during the thesis study at HUNITEK laboratory, Hacettepe University.

Therefore, the application process time of the prepared mixtures must be adjusted correctly, and cement types must be used in optimum proportions to achieve the target of high early-age strength. Regarding Table 3.2, CEM I 52.5R type cement and Secar 80 type CAC (80% Al_2O_3) have higher surface areas, increasing the mixtures' water requirement. Thus, the workability of the mixtures should be improved by using appropriate chemical additives. Regarding mechanical properties of cements , the compressive strength results of cement types with 40 - 50% Al_2O_3 can be obtained greater than 20 MPa at 6 hours and greater than 60 MPa at 24 hours. However, there is no compressive strength for CEM I 52.5R type PC and SECAR 80 type CAC (80% Al_2O_3) at 6 hours. Therefore, using the correct type of CAC is essential in composites with the aim of early age high strength. Regarding the particle size distributions of cement, CEM I 52.5R type PC has the smallest particle sizes. Among CACs, the particle size distribution of cement decreases as the aluminate content increases. This also results in increasing the water content of the mixture.

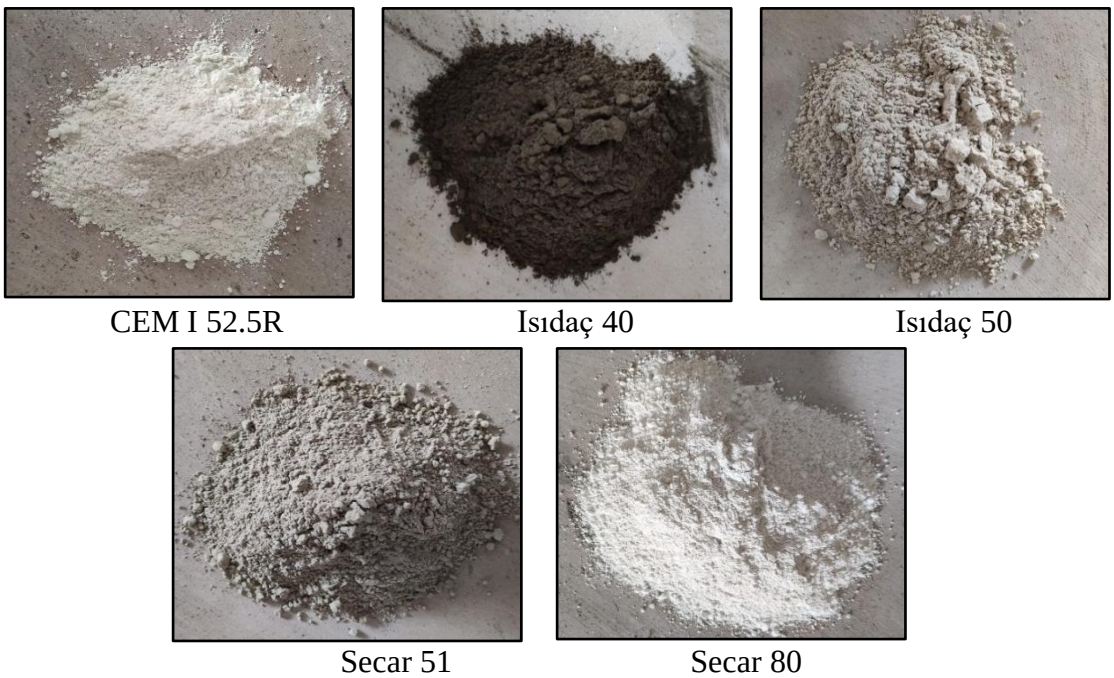

Figure 3.1. Digital camera images of different cement types

Table 3.1. Chemical compositions of ingredients, %

Ingredients, %	**SiO_2**	**Al_2O_3**	**Fe_2O_3**	**CaO**	**MgO**	**K_2O**	**Na_2O**	**SO_3**	**P_2O_5**	**TiO_2**	**Cr_2O_3**	**Mn_2O_3**	**$CaSO_4.$ ½ H_2O**
CEM I 52.5R	21.91	4.23	0.26	65.38	0.34	0.36	0.40	4.03	0.06	0.12	0.0052	0.0049	-
Isıdaç 40	3.93	39.81	17.64	35.71	0.76	0.16	0.08	0.01	0.06	1.92	0.0746	0.0968	-
Isıdaç 50	4.01	53.12	1.22	36.98	0.62	0.62	-	0.03	0.12	2.55	0.0800	0.0100	-
Secar 51	4.73	50.56	2.50	38.11	0.58	0.28	0.07	-	0.03	2.60	0.0880	0.0436	-
Secar 80	0.44	77.57	0.20	18.78	0.35	0.03	1.02	-	-	0.04	0.0137	0.0101	-
Quartz Sand	99.50	0.14	0.04	0.02	0.02	0.04	0.05	-	-	0.01	-	-	-
Silica Fume	91.32	0.32	0.98	1.03	0.93	1.14	0.66	0.19	0.10	-	0.0051	0.09	-
α-hemihydrate	-	-	-	-	-	-	-	-	-	-	-	-	98.00

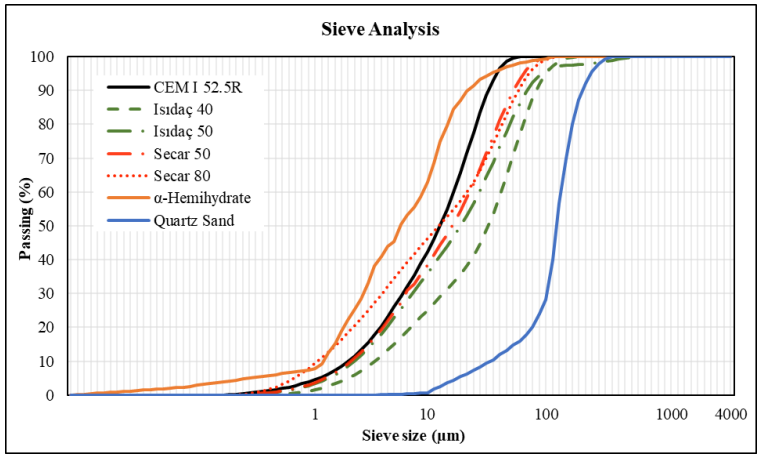

Figure 3.2. Particle size distributions of ingredients

Table 3.2. Physical and mechanical properties of ingredients

Ingredients	CEM I 52.5R	Isıdaç 40	Isıdaç 50	Secar 51	Secar 80	Quartz Sand	Silica Fume
Physical Properties							
Specific gravity (g/cm^3)	3.06	3.25	≤3.03	3.04	3.19	2.65	2.32
Blaine fineness (cm^2/g)	4600	3000	≥3500	3750-4250	-	-	19080
Initial setting (min)	100	280	≥300	190-270	≥45	-	-
Final setting (min)	130	295	≤500	210-300	≤170	-	-
Loss on ignition (%)	3.20	0.30	-	-	-	-	1.86
Insoluble residue (%)	0.18	-	-	-	-	0.15	-
Mechanical Properties, MPa							
6 hours	-	≥28	≥20	≥5	-	-	-
1 day	-	≥60	≥60	≥65	≥16.50	-	-

3.1.2. Mineral Additive

In this study, silica fume was used as a mineral additive to prepare cementitious composites. Considering the literature studies, silica fume was preferred to obtain denser matrix strength, improve compressive strength at early and later ages, and facilitate the homogeneous dispersion of conductive materials in the matrix. Silica fume is an ultra-fine powder that reduces high-purity quartzite with coal and wood particles in electric arc furnaces while producing silicon metal or ferrosilicon (FeSi) alloys. The silica fume was obtained from ELKEM, a Norwegian company. Silica fume has a particle diameter range of 100-150 nm and is concordant with the ASTM C204 and ASTM C618 standards [208,209]. The digital camera image of the silica fume is shown in Figure 3.3. The chemical oxide composition of silica fume is given in Table 3.1, and its physical and mechanical properties are given in Table 3.2. Higher fineness of silica fume causes the increasing water requirement of the matrix; therefore, water-reducing chemical additives should be used, and appropriate amounts of silica fume should be added to the matrix.

Figure 3.3. Digital camera image of silica fume

3.1.3. Aggregate

Compared to traditional concrete, coarse aggregate usage has not been preferred. The total amount of aggregate in the mixtures has been limited, and a high proportion of binder material has been preferred. Thus, quartz sand was selected to improve the early age high strength of composites, to reduce and minimize the pores, and to enhance the dispersion of conductive materials homogeneously in cementitious composites. In this context, micro-quartz sand was used with the largest particle size of 600 μm in the mixtures. Quartz sand is quartz (SiO_2) particles smaller than 2-mm, formed as a result of the decomposition of quartz-rich magmatic, metamorphic rocks. It is a building material that is pure white, 99% pure and can be mined in crushing and screening machines to the desired particle size. The micro-sized quartz sand was obtained from the Pomza Export Company in Türkiye. The chemical oxide composition of quartz sand is given in Table 3.1, its physical and mechanical properties are given in Table 3.2, and the particle size distribution of the quartz sand determined by the laser diffraction method is shown in Figure 3.2. The digital camera image of the quartz sand is shown in Figure 3.4.

Figure 3.4. Digital camera image of quartz sand

3.1.4. Calcium Sulfate Source

The calcium sulfate source (CŚ) was used to improve the performance properties of early age high strength cement. In this context, it was decided to use a calcium sulfate source as a component of the ternary system to prevent flash setting, extend the application time of the mortar, and achieve high strength development at the final setting time. Gypsum, hemihydrate, and anhydrate types are used as calcium sulfate sources in the industry. However, it was decided to use α-type hemihydrate due to its high dissolution rate compared to other types of calcium sulfate [68,82,83]. The α-type hemihydrate was obtained from the Baldudak Company in Turkey. The chemical oxide composition of α-type hemihydrate is given in Table 3.1, its technical properties are given in Table 3.3, and the particle size distribution of the α-type hemihydrate determined by the laser diffraction method is shown in Figure 3.2. The digital camera image of the α-type hemihydrate is shown in Figure 3.5.

Figure 3.5. Digital camera image of α-type hemihydrate

Table 3.3. Technical properties of α -type hemihydrate

Properties	**Unit**	**Value**
Flowing diameter	mm	190±20
Initial setting	min	10±3.50
Final setting	min	Max 30
Tensile strength	MPa	7.85
Compressive strength	MPa	18.63
Linear Expansion	%	0.36
Water Absorption	%	25

3.1.5. Chemical Additives

The combination of different chemical additives was preferred to simultaneously provide superior performance properties such as early age high strength, flowability, smooth surface, and resistance to chemical reactions to the cementitious composite with anti-static protection capability developed within the scope of the thesis. In this study, the minimum water content and high amounts of binder were preferred in the matrix to achieve high early age strength in cementitious composites. By reducing the amount of water in the mixture and incorporating mineral additives and conductive materials into the mortar, the water demand of the matrix will increase. For this reason, besides covering the water requirement of the matrix, the high-range water reducer additive (HRWRA) was used to provide flowability and enhance the homogeneous dispersion of conductive materials. During the development of early age high-strength cementitious composites, HRWRA was obtained from various companies and different types in the experimental study. As a result of the experimental study, polycarboxylic ether-based HRWRA with commercial code EBA 1447, obtained from BASF Construction Chemicals, was selected since it increased the workability of the mortar mixture and affected the matrix strength less negatively than other additives. The digital camera image of HRWRA, produced as a yellowish powder, is shown in Figure 3.6. The technical specifications of HRWRA are provided by the company and are given in Table 3.4.

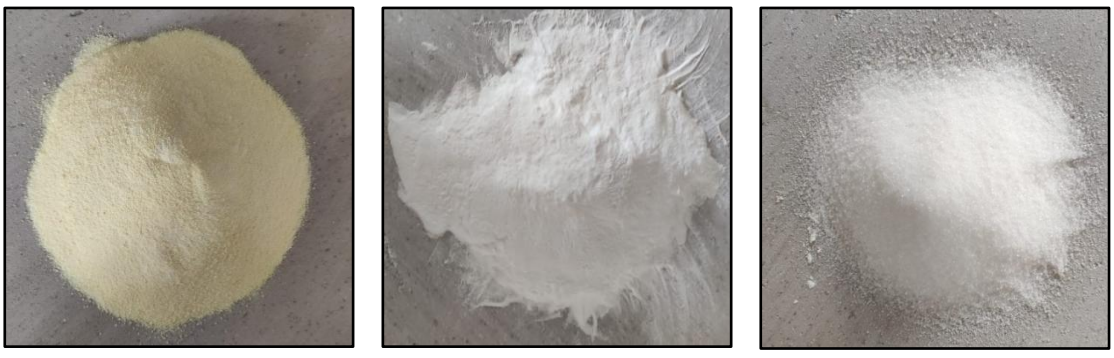

Polycarboxylic Ether-Based High-Range Water Reducer (HRWRA)

Lithium Carbonate (Li_2CO_3)-Based Set Accelerator

Citric Acid ($C_6H_8O_7$)-Based Set Retarder

Figure 3.6. Digital camera images of chemical additives

In the thesis study, the minimum water content and high amounts of the binder were preferred in the matrix to achieve high early age strength in cementitious composites. Considering the binder in the matrix, the CAC with a high aluminate ratio and PC having a higher strength class were preferred to achieve high strength at an early age. However, a setting accelerator additive was used to obtain higher strengths in a much shorter time and to make the composite ready for use quickly after the application was completed. In this context, the lithium carbonate (Li_2CO_3) based setting accelerator (SA) additive supplied by Ata Kimya company was used in the experimental studies. The digital camera image of SA, produced as a white powder, is shown in Figure 3.6. The technical specifications of SA are provided by the company and are given in Table 3.4.

Table 3.4. Technical properties of chemical additives

Properties	**Set accelerator (SA)**	**Set retarder (SRA)**	**HRWRA**
Color	White	White	Yellow
Solubility	Insoluble in water	Soluble in water	Soluble in water
Melting point (°C)	720	135-152	20
Relative density (kg/l)	2.11	1.54-1.66	1.18-1.24
Volume density (kg/m$^{3)}$	640	-	300-600
Degradation point (°C)	380	345	-
Solubility value (G/100G H_2O 20°C)	1.30 g/100 ml	67.60 g/100 ml	-
Appearance	Powder, granule powder	Powder, granule powder, crystal	Powder

In the thesis study, the minimum water content and high amounts of the binder were preferred in the matrix to achieve high early age strength in cementitious composites. Considering the binder in the matrix, the CAC with a high aluminate ratio and PC were preferred to achieve early age high strength. Along with the SA additives and high amounts of aluminate cement used to obtain higher strength, a setting retarding additive was used in the matrix mixture to prevent the flash setting and to extend the setting time. In this context, citric acid ($C_6H_8O_7$) based setting retarder additive (SRA) of the Peramin brand, supplied by Ata Kimya company, was used in the experimental study. The digital

camera image of SRA, produced as tiny white particles, is shown in Figure 3.6. The technical specifications of SRA are provided by the company and are given in Table 3.4.

3.1.6. Conductive Materials

It is aimed to develop an electrical conductivity cementitious composite that sustains electrical performance in the short and long term. The composite should also resist humidity, water, temperature, and aggressive environment. According to literature studies, electrically conductive carbon fiber (CF), brass-coated steel fiber (SF), and milled carbon fiber (MCF) were incorporated into the cementitious composite to provide anti-static protection capability. The scope of this section is aimed to create optimum electrically conductive pathways with conductive materials to be incorporated as inert material to the main cementitious mortar, which has an early age high strength, flowability, and crack-free surface.

Incorporating micro-sized carbon fiber, which showed the highest electrical performance at the lowest contents in the literature, was preferred to provide electrical conductivity capability to the cementitious mortar mixture. In this context, CF was selected with a 12-mm length and a length/diameter ratio 1700, supplied by ELG company with the product name CARBISO CT IM56D-06. Digital camera images of carbon fibers and the different scales of scanning electron microscopy (SEM) images are shown in Figure 3.7. The technical specifications of CF, provided by the company, are given in Table 3.5.

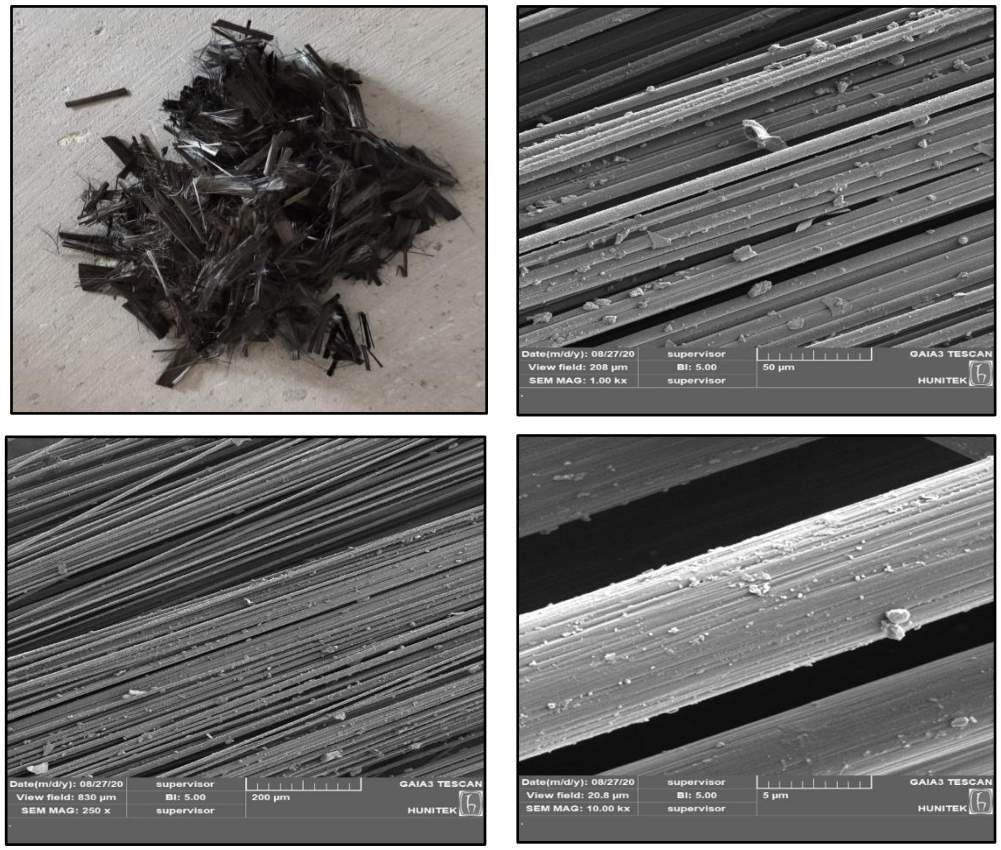

Figure 3.7. Digital camera images of carbon fiber and SEM images from different scales

Incorporating micro-sized brass-coated steel fiber, which showed high electrical performance in the literature, was preferred to provide electrical conductivity capability to the cementitious mortar mixture. SF had a length of 35 mm and an aspect ratio of 65, and it was supplied by BEKAERT company with the product Dramix 3D. Digital camera images of steel fibers and the different scales of scanning electron microscopy (SEM) images are shown in Figure 3.8. The technical specifications of SF are provided by the company and are given in Table 3.5.

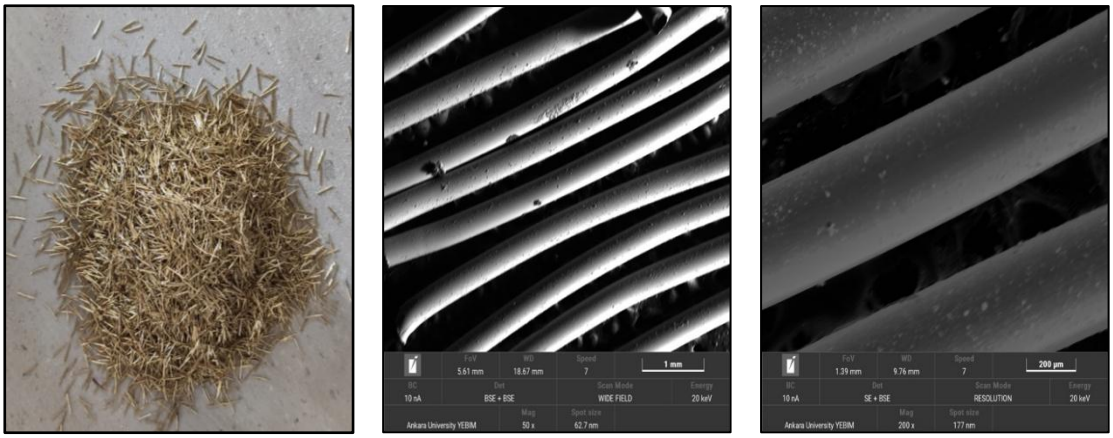

Figure 3.8. Digital camera images of brass-coated steel fiber and SEM images from different scales

Table 3.5. Technical specifications of conductive materials

Properties	**Carbon Fiber**	**Steel Fiber**	**Milled Carbon Fiber**
Diameter	7 µm	0.55 mm	7 µm
Density	1.70 - 2.00 g/cm^3	-	1.80 g/cm^3
Length	12 mm	35 mm	100 µm
Aspect ratio	1700	65	14
Tensile strength	4633 MPa	1550 MPa	3470 MPa
Elastic modulus	288 GPa	200 GPa	246 GPa

Incorporating micro-sized milled carbon fiber, which showed high electrical performance in the literature, was preferred to provide electrical conductivity capability to the cementitious mortar mixture. In the literature, various fillers are frequently used in different types and contents to enhance the conductive path created by microfibers. However, the incorporation of milled carbon fibers, which are chopped by milling carbon fibers, has recently been preferred in the literature. In this context, MCF was selected with a 100-µm length and a length/diameter ratio of 14, supplied by ELG company with the product name CARBISO TM MF-80. Digital camera images of milled carbon fibers, along with the different scales of scanning electron microscopy (SEM) images, are shown in Figure 3.9. The technical specifications of MCF are provided by the company and are given in Table 3.5.

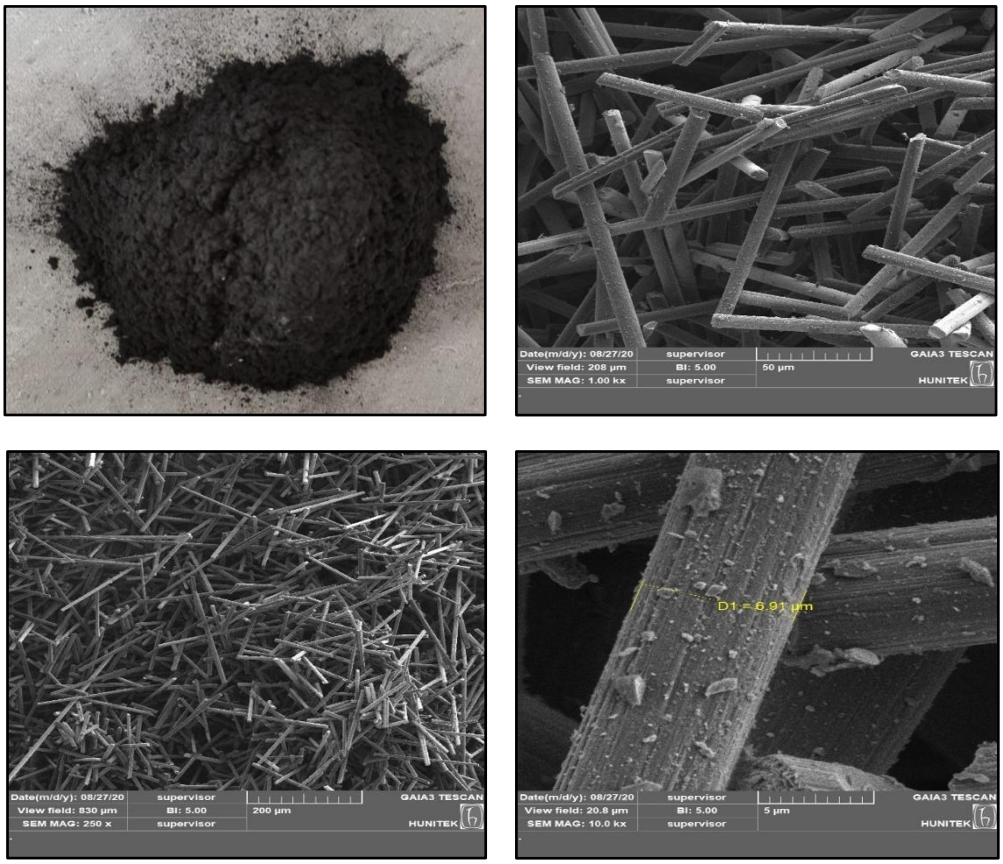

Figure 3.9. Digital camera images of milled carbon fiber and SEM images from different scales

3.2. Methodology

Experimental procedures, including the incorporation of conductive materials, mixing processes, specimen preparations, and experimental setups, are presented in this section.

3.2.1. Methodology of Early Age High Strength Cementitious Composite

The experimental program for the new generation of cementitious composites with anti-static protection capability was conducted based on literature studies. The materials were selected with respect to their physical and chemical properties. It was aimed that the composites with electrostatic discharge capability demonstrate superior mechanical and physical properties of the matrix. The developed composite should be used in a short time once the application is completed. The methodology of the experimental study carried out

to develop composites with sufficient flowability and crack-free surfaces, as well as early age high-strength performance, is shown in Figure 3.10.

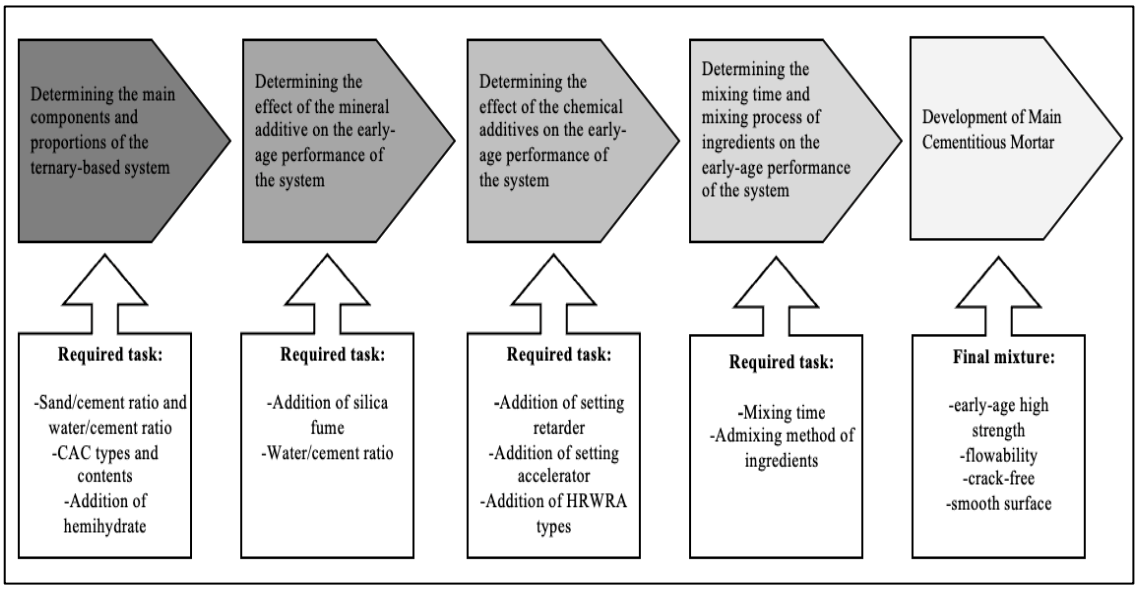

Figure 3.10. Four main steps of tasks to develop main cementitious mortar

According to Figure 3.10, the early age of high-strength cementitious mortar mixture development involves four stages. In the first stage, the sand-cement ratio and water-cement ratio were determined. Subsequently, the contents of the main components of the ternary system were identified, specifying the CAC type along with PC in the main matrix. Moving to the second stage, silica fume was added at different ratios, resulting in a higher water requirement and determining the optimum silica fume content and water-cement ratio. The third stage involved the addition of chemical additives to enhance the workability, flowability, and early age high strength of the ternary system. In the last stage, the admixing process of ingredients and mixing times were determined based on compressive strength results. The final mortar mixture was achieved with the highest early age compressive strength, a crack-free surface, and flowability performance. The developed matrix mixture was prepared as the main matrix, and conductive materials were added based on this matrix mixture.

3.2.2. Methodology of Electrostatic Discharge Capability Cementitious Composite

The experimental program for the new generation of cementitious composites with anti-static protection capability was conducted based on literature studies. The materials were selected with respect to their physical and chemical properties. It is aimed that the composites should demonstrate superior electrical performance in the early and long term without affecting any external factors. The methodology of the experimental study carried out to develop a new generation of cementitious composites with anti-static protection capability is shown in Figure 3.11.

According to Figure 3.11, developing the cementitious composite with electrical conductivity performance involves five stages. In the first stage, conductive materials were individually incorporated into the main matrix mixture developed in the first section, using different mixing methods. The conductive material type, content, and mixing method were selected based on the specimens that showed the best performance. Subsequently, the conductive materials were incorporated into the matrix in a double and triple combination. The type and content of conductive material used in these two sections were determined from the results of the experimental study with the single additions. After three stages, the specimens were selected for electrical, mechanical, and physical properties. Among the selected specimens, the differences between performances under humidity and temperature factors were determined. After completing all the steps, the sustainability of the electrical conductivity performance of the composites was tested by subjecting the mixtures least affected by ambient temperature to long-term acid tests with single, double, and triple conductive material additions. Upon completion of the experimental stages, a cementitious composite with electrostatic discharge capability was developed, considering literature studies.

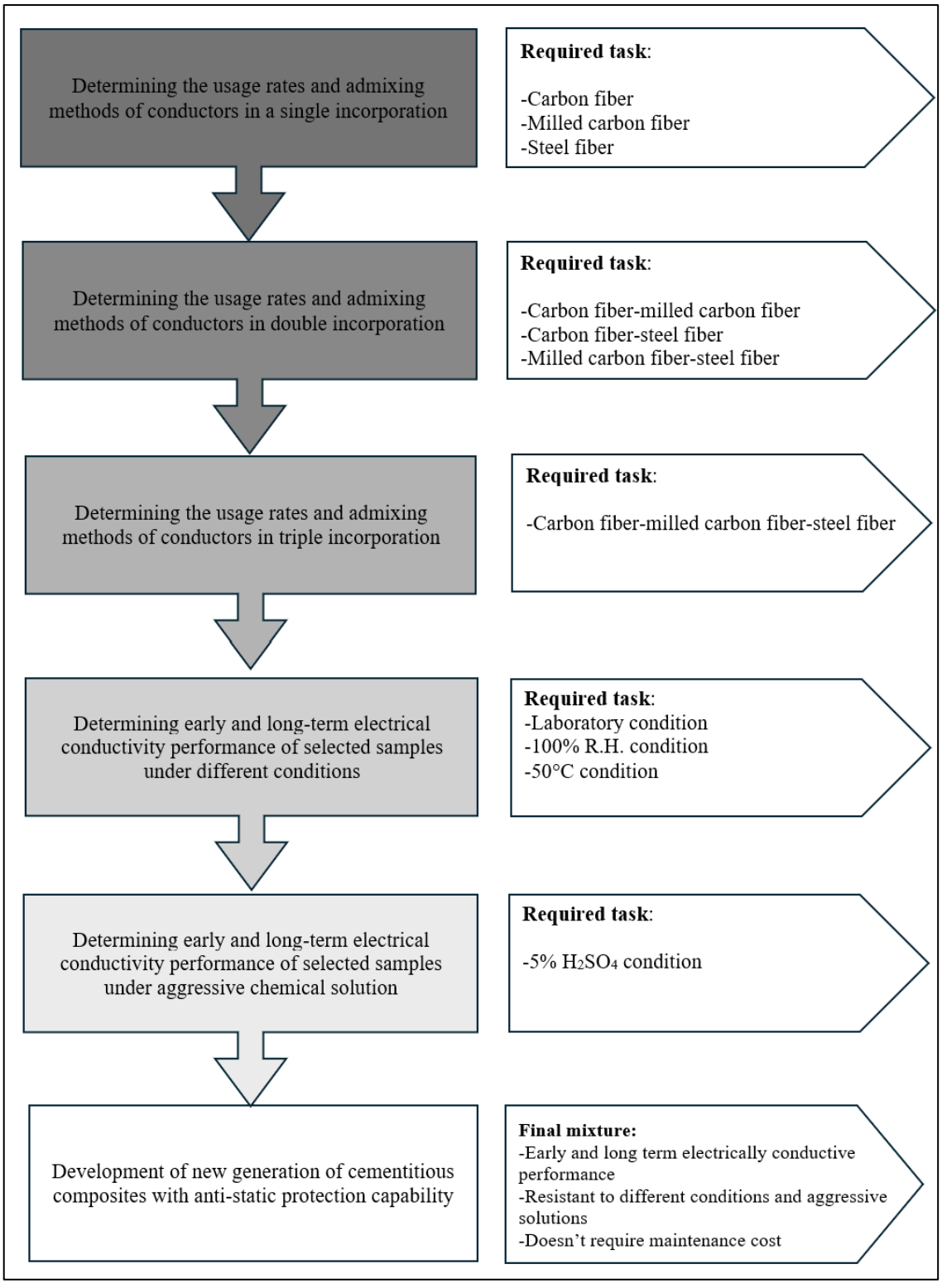

Figure 3.11. Five main steps of tasks to develop electrically conductive cementitious composite

3.2.3. Mixture Proportions of Electrostatic Discharge Capability Cementitious Composite

Mixture proportions of mortars without conductive fibers characterized by high early strength, high flowability, and high electrical conductivity suited for flooring applications are given in Table 3.6. The sand-to-binder and water-to-binder ratios were kept constants for all mixtures at 0.6 and 0.3, respectively. The total weight of binders in the mixtures was considered the total weight of CEM I 52.5R and CAC (Isıdaç 40). The total binder contains 60% PC and 40% CAC, according to the weight of the total binder. In order to prevent flash setting, 15% CŠ by the weight of the CAC was used to mix in all mixtures. In order not to risk the fresh and mechanical properties of the composites and prevent the agglomeration of conductive fibers, 2.5% silica fume and 2.0% HRWRA, 0.2% SRA, and 0.5% SA by the total weight of the binders were used in all mixtures. Mixture proportions were determined based on the mixture, which showed the highest level of flowability and the highest early/final-age compressive strength during the preliminary experimental program. In the thesis study, the utilization rates of conductive materials were selected based on previous literature studies, given in Table 2.4, and the goal of achieving floor coating designs with low cost, lower utilization rates of fibers, and highest electrical conductivity. Therefore, conductive materials were used in the range of 0 - 1%, by the total weight of the binder, with incremental rates of 0.1%.

Table 3.6. Mixture proportion of main cementitious composite

Ingredients	**Amount (kg/m^3)**
CEM I 52.5R	716
CAC	477
α-hemihydrate	72
Sand	716
Silica fume	30
HRWRA	24
Set accelerator (SA)	6
Set retarder (SRA)	2.5
Water	358
Carbon fiber Steel fiber Milled carbon fiber	0-1%

3.2.4. Mixture Preparation Process of Electrostatic Discharge Capability Cementitious Composite

Various mixing methods were applied to obtain homogeneous MCF, CF, and SF dispersion in cementitious matrices. The literature presents different mixing methods for the single, double, and triple incorporation of conductive fibers in matrices, as shown in Table 2.4. After reviewing extensive literature, the first admixing and synchronous admixing methods were selected for MCF-based mixtures. In contrast, the synchronous and latter admixing methods were chosen for CF- and SF-based mixtures. This selection aimed to simplify the mixing process and accurately determine the percolation thresholds for each conductive fiber within a given matrix composition.

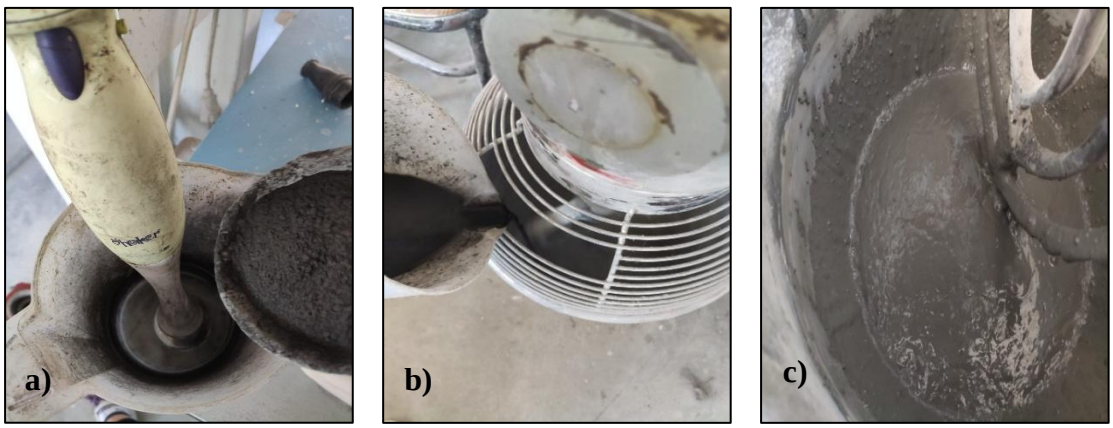

Figure 3.12. a) Mixing the milled carbon fiber with water, b) Adding the solution to the dry mixture, c) Final mortar mixture

In the study, MCF was incorporated into the main matrix mixture using the first (F) admixing method and the synchronous (S) admixing method. In the first (F) admixing method, the preparation process of mixtures was as follows: *(1)* the total amount of MCF with the mixing water was mixed in a hand mixer at 580 rpm for 10 mins (Figure 3.12-a). *(2)* PC, CAC, α-hemihydrate, silica fume, and sand were mixed using a mechanical Hobart N50 model mixer at 136 rpm for 10 mins. *(3)* After completing the first two steps, both mixers were turned off, and half of the amount of HRWRA and the total amount of SRA was added to the dry mixture, and the mixer was turned on. Following this, one-third of the solution prepared in the first step was added to the Hobart mixer within 30 s,

and the mixture was continued to be mixed at 136 rpm for 2 mins (Figure 3.12-b). *(4)* After, another amount of HRWRA and a total amount of SA were added to the mixture, and the mixer was turned on. Following this, two-thirds of the solution prepared in the first step was added to the Hobart mixer within 30 seconds, and the mixture was continued to be mixed at 136 rpm for 3 mins. At this stage, all chemical additives were added to the mortar mixture. *(5)* To obtain a more homogeneous mixture, mixing proceeded at 281 rpm for an additional 3 mins (Figure 3.12-c). *(6)* Finally, the fresh mixture was cast into oiled molds, and no vibration was applied.

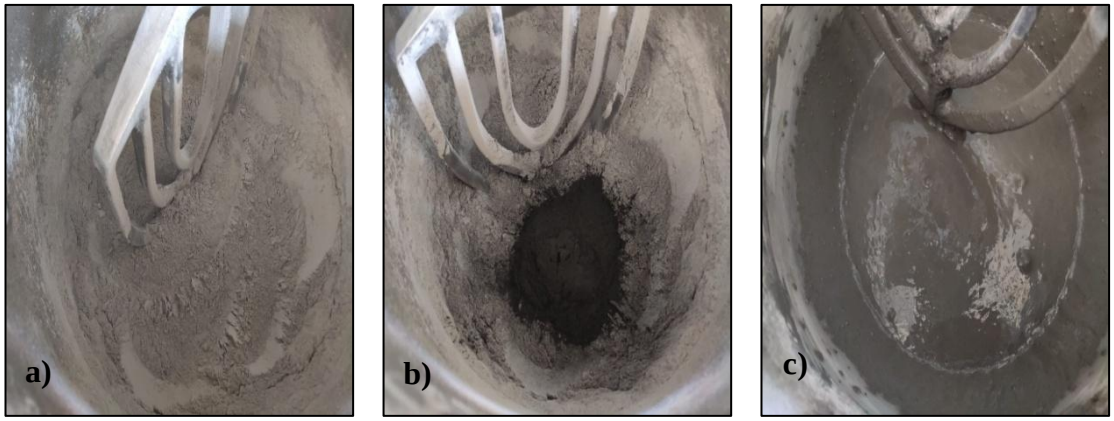

Figure 3.13. a) Mixing the dry mixture, b) Adding the milled carbon fiber to the dry mixture, c) Final mortar mixture

In the synchronous (S) admixing method, the preparation process of mixtures was as follows: *(1)* PC, CAC, α-hemihydrate, silica fume, and sand were mixed using a mechanical Hobart N50 model mixer at 136 rpm for 10 mins and dry mixture was obtained (Figure 3.13-a). *(2)* Then, the total amount of milled carbon fiber was added to the dry mixture and stirred at 136 rpm in a Hobart mixer for 10 mins (Figure 3.13-b). *(3)* After completing the first two steps, both mixers were turned off, and half of the amount of HRWRA and the total amount of SRA was added to the dry mixture, and the mixer was turned on. Following this, one-third of the mixing water prepared in the first step was added to the Hobart mixer within 30 seconds, and the mixture was continued to be mixed at 136 rpm for 2 mins. *(4)* After, other amounts of HRWRA and the total amount of SA were added to the mixture, and the mixer was turned on. Following this, two-thirds of the mixing water prepared in the first step was added to the Hobart mixer within 30 seconds, and the mixture was continued to be mixed at 136 rpm for 3 mins. At this stage, all

chemical additives were added to the mortar mixture. *(5)* To obtain a more homogeneous mixture, mixing proceeded at 281 rpm for 3 mins (Figure 3.13-c). *(6)* Finally, the fresh mixture was cast into oiled molds, and no vibration was applied.

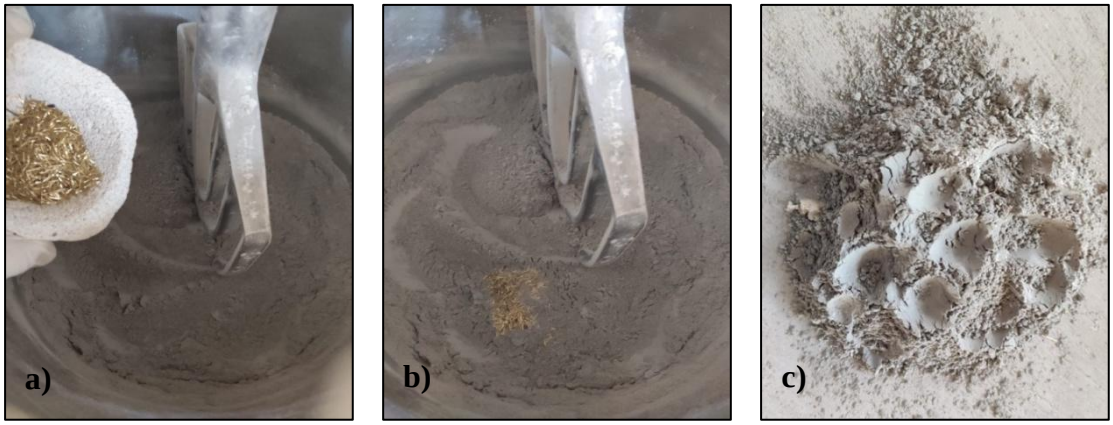

Figure 3.14. a) Mixing the dry mixture, b) Adding the steel fiber to the dry mixture, c) Fiber incorporated mixture

In thesis study, steel fiber was incorporated into the main matrix mixture using the synchronous (S) admixing method and latter (L) admixing method. In the synchronous (S) admixing method, the preparation process of mixtures was as follows: *(1)* PC, CAC, α-hemihydrate, silica fume, and sand were mixed using a mechanical Hobart N50 model mixer at 136 rpm for 10 mins and dry mixture was obtained (Figure 3.14-a). *(2)* Then, the total amount of steel fiber was added to the dry mixture and stirred at 136 rpm in a Hobart mixer for 3 mins (Figure 3.14-b). *(3)* With the completion of the first two steps, mixer was turned off (Figure 3.14-c) and half of the amount of HRWRA, and the total amount of SRA were added to the dry mixture and the mixer was turned on. Following this, one-third of the mixing water prepared in the first step was added to the Hobart mixer within 30 s, and the mixture was continued to be mixed at 136 rpm for 2 mins. *(4)* After, other amounts of HRWRA and the total amount of SA were added to the mixture and the mixer was turned on. Following this, two-thirds of the mixing water prepared in the first step was added to the Hobart mixer within 30 s, and the mixture was continued to be mixed at 136 rpm for 3 mins. At this stage, all chemical additives were added to the mortar mixture. *(5)* To obtain a more homogeneous mixture, mixing was proceeded at 281 rpm for an additional 3 mins. *(6)* Finally, the fresh mixture casted put into oiled molds and no vibration was applied.

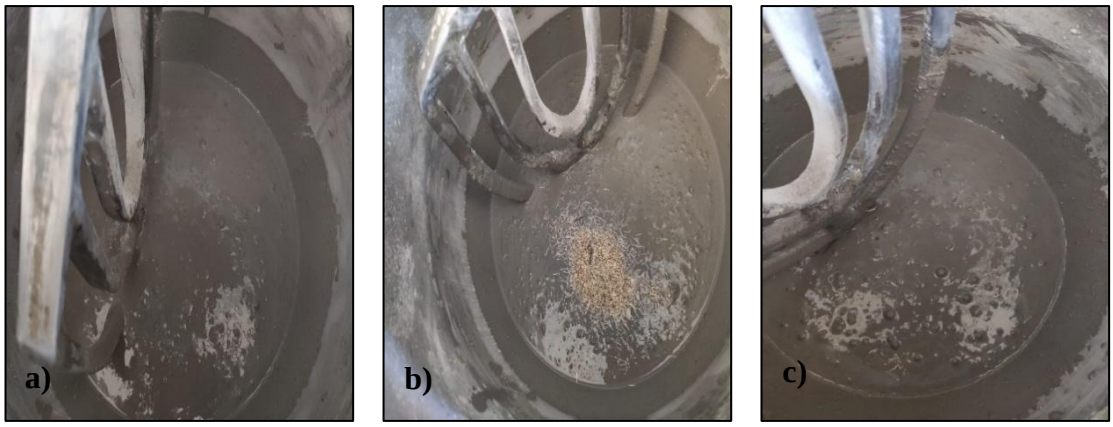

Figure 3.15. a) Obtaining the mortar mixture, b) Adding the steel fiber to the mortar mixture, c) Fiber incorporated mixture

In the latter (L) admixing method, the preparation process of mixtures was as follows: PC, CAC, α-hemihydrate, silica fume, and sand were mixed using a mechanical Hobart N50 model mixer at 136 rpm for 10 mins, and dry mixture was obtained. *(2)* After this step, the mixer was turned off; half of the amount of HRWRA and total SRA was added to the dry mixture and turned on. Following this, one-third of the mixing water prepared in the first step was added to the Hobart mixer within 30 seconds, and the mixture was continued to be mixed at 136 rpm for 2 mins. *(3)* Then other amounts of HRWRA and the total amount of SA were added to the mixture, and the mixer was turned on. Following this, two-thirds of the mixing water prepared in the first step was added to the Hobart mixer within 30 seconds, and the mixture was continued to be mixed at 136 rpm for 3 mins. At this stage, all chemical additives were added to the mortar mixture (Figure 3.15-a). *(4)* After adding a pre-determined amount of steel fiber (Figure 3.15-b) to the prepared mortar mixture to obtain a more homogeneous mortar mixture, mixing was continued at 281 rpm for an additional 3 mins. *(5)* Finally, the fresh mixture was cast into oiled molds, and no vibration was applied (Figure 3.15-c).

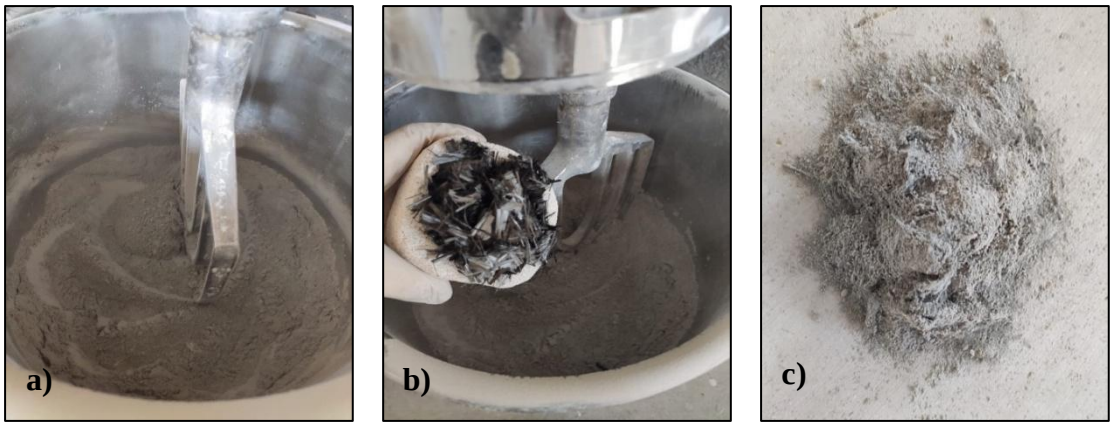

Figure 3.16. a) Mixing the dry mixture, b) Adding the carbon fiber to the dry mixture, c) Fiber incorporated mixture

In the thesis study, carbon fiber was incorporated into the main matrix mixture using the synchronous (S) admixing method and the latter (L) admixing method. In the synchronous (S) admixing method, the preparation process of mixtures was as follows: *(1)* PC, CAC, α-hemihydrate, silica fume, and sand were mixed using a mechanical Hobart N50 model mixer at 136 rpm for 10 mins and dry mixture was obtained (Figure 3.16-a). *(2)* Then, the total amount of carbon fiber was added to the dry mixture and stirred at 136 rpm in a Hobart mixer for 10 mins (Figure 3.16-b). *(3)* After completing the first two steps, the mixer was turned off (Figure 3.16-c), half of the amount of HRWRA and the total amount of SRA was added to the dry mixture, and the mixer was turned on. Following this, one-third of the mixing water prepared in the first step was added to the Hobart mixer within 30 seconds, and the mixture was continued to be mixed at 136 rpm for 2 mins. *(4)* Afterward, other amounts of HRWRA and the total amount of SA were added to the mixture, and the mixer was turned on. Following this, two-thirds of the mixing water prepared in the first step was added to the Hobart mixer within 30 seconds, and the mixture was continued to be mixed at 136 rpm for 3 mins. At this stage, all chemical additives were added to the mortar mixture. *(5)* To obtain a more homogeneous mixture, mixing proceeded at 281 rpm for 3 mins. *(6)* Finally, the fresh mixture was cast into oiled molds, and no vibration was applied.

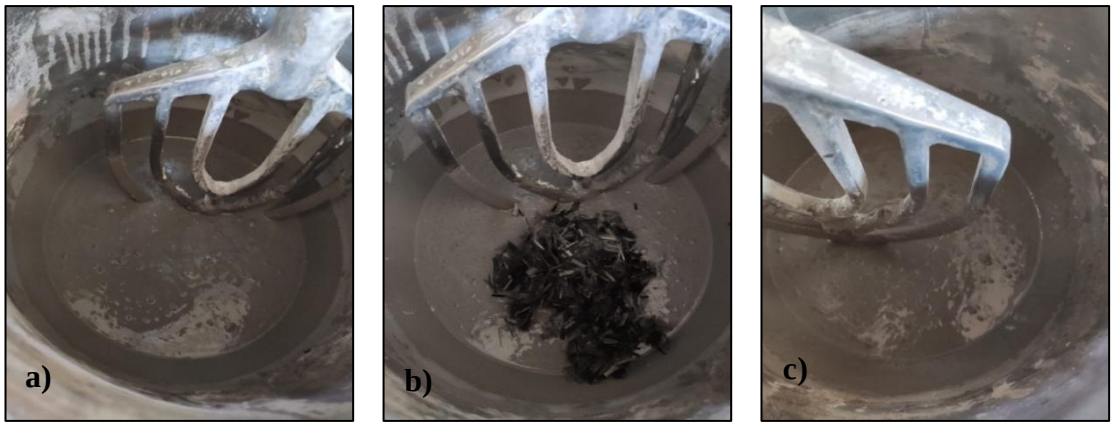

Figure 3.17. a) Obtaining the mortar mixture, b) Adding the carbon fiber to the mortar mixture, c) Fiber incorporated mixture

In the latter (L) admixing method, the preparation process of mixtures was as follows: PC, CAC, α-hemihydrate, silica fume, and sand were mixed using a mechanical Hobart N50 model mixer at 136 rpm for 10 mins, and dry mixture was obtained. *(2)* After this step, the mixer was turned off, and half of the amount of HRWRA and the total amount of SRA were added to the dry mixture, and the mixer was turned on. Following this, one-third of the mixing water prepared in the first step was added to the Hobart mixer within 30 seconds, and the mixture was continued to be mixed at 136 rpm for 2 mins. *(3)* Then other amounts of HRWRA and the total amount of SA were added to the mixture, and the mixer was turned on. Following this, two-thirds of the mixing water prepared in the first step was added to the Hobart mixer within 30 seconds, and the mixture was continued to be mixed at 136 rpm for 3 mins. At this stage, all chemical additives were added to the mortar mixture (Figure 3.17-a). *(4)* After adding a pre-determined amount of carbon fiber (Figure 3.17-b) to the prepared mortar mixture to obtain a more homogeneous mortar mixture, mixing was continued at 281 rpm for an additional 3 mins. *(5)* Finally, the fresh mixture was cast into oiled molds, and no vibration was applied (Figure 3.17-c).

3.2.5. Preparation and Coding of Samples

Fresh mortar mixtures were prepared to determine the mechanical, physical, and electrical performance of the samples prepared within the scope of the thesis study. The prepared mortar was cast into five cube samples with dimensions of 50*50*50 mm, one cylinder

with dimensions of Φ10*20 cm, and one plate with dimensions of 40*40*1 cm for each sample. For each type of test, samples were removed from the molds and cured until measurement time. Different codes were used for each step in the samples. In the first stage of the single conductive material incorporation, the MCF-based mixtures were coded as "C". In these mixtures, the synchronous (S) admixing method was coded as C(1), and the first (F) admixing method was coded as C(2), as shown in Figure 3.18. For instance, "C4(2)" indicates that the mixture contains 0.4% milled carbon fiber and was prepared using the first admixing method.

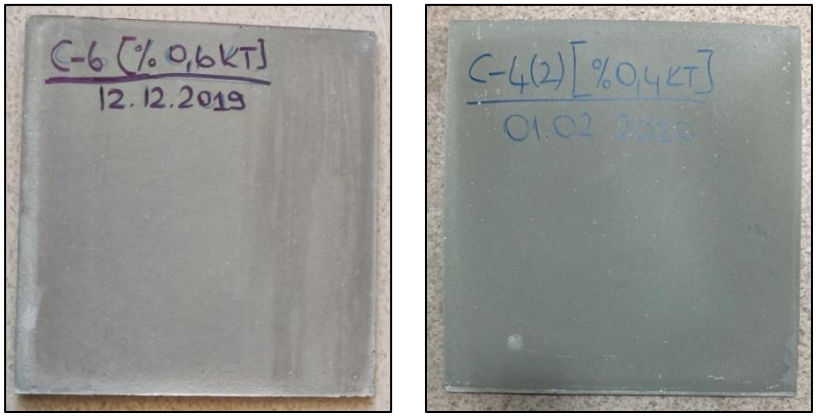

Figure 3.18. The coding of milled carbon fiber-based mixtures

SF-based mixtures were coded as "A". In these mixtures, the synchronous (S) admixing method was coded as A(1), and the latter (L) admixing method was coded as A(2), shown in Figure 3.19. For instance, "A3(2)" indicates that the mixture contains 0.3% steel fiber and was prepared using the latter admixing method.

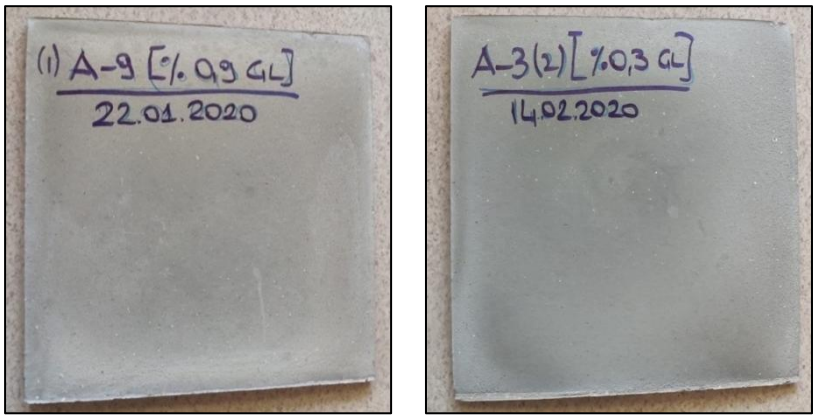

Figure 3.19. The coding of steel fiber-based mixtures

Carbon fiber-based mixtures were coded as "B" among the single conductive material incorporation. In these mixtures, the synchronous (S) admixing method was coded as B(1), and the latter (L) admixing method was coded as B(2), shown in Figure 3.20. For instance, "B2(2)" indicates that the mixture contains 0.2% carbon fiber and was prepared using the latter admixing method.

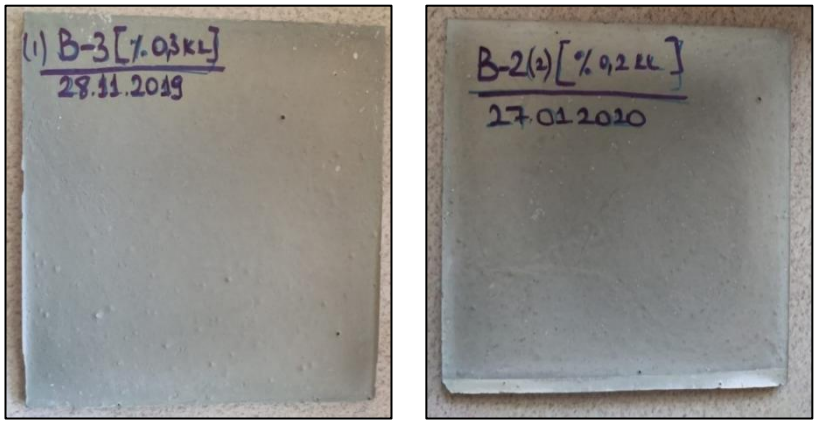

Figure 3.20. The coding of carbon fiber-based mixtures

In the second stage of the thesis study, conductive materials were added to the matrix mixture in double combination. A double combination was applied to the samples, showing higher electrical performance due to the first stage. In experimental studies, the combination of conductive materials was carried out as carbon fiber-steel fiber, carbon fiber-milled carbon fiber, and steel fiber-milled carbon fiber, as shown in Figure 3.21. The mixing method was selected based on the mixing method showing the best electrical performance. Since the lowest ER results were obtained using the latter admixing method in carbon fiber-based mixtures with a single addition, carbon fiber was added to the mixtures only using the latter admixing method in double conductor combinations. On the other hand, steel and milled carbon fiber were added using both mixing methods. For instance, “CB42(1)” indicates that the mixture contains 0.4% milled carbon fiber, which is incorporated into the mixture by the synchronous (S) admixing method and 0.2% carbon fiber. “AB410(2)” indicates that the mixture contains 0.4% steel fiber, which is incorporated into the mixture by the latter (L) admixing method, and 1.0% carbon fiber. “CA62(1)” indicates that the mixture contains 0.6% milled carbon fiber and 0.2% steel fiber, which are both incorporated into the mixture by the synchronous (S) admixing method.

Figure 3.21. The coding of a combination of double conductor addition

In the third stage of the thesis study, conductive materials were added to the matrix mixture in a triple combination. After completing two stages, the samples were determined, showing higher electrical performance and lowest conductor content. The experimental plan prepared for the triple addition of conductors is shown in Figure 3.22. Since the best performance was obtained from carbon fiber-based mixtures, the ratios were determined based on the carbon fiber content. Then, other conductor contents were determined according to the milled carbon fiber and steel fiber ratio, respectively.

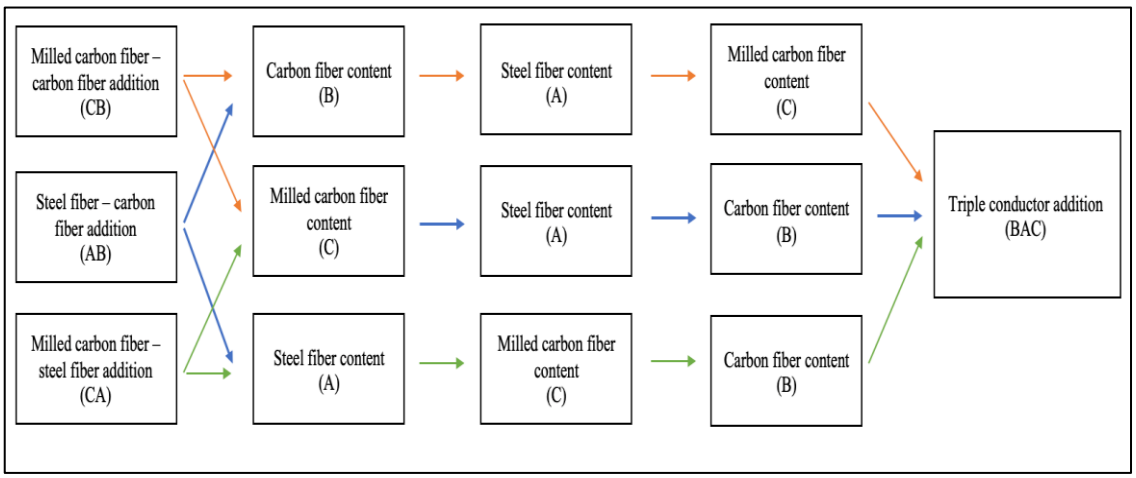

Figure 3.22. Preparation of the experimental plan for triple conductor addition

Figure 3.23 showed triple conductive material was incorporated as carbon fiber-steel fiber-milled carbon fiber in an experimental study. The coding of mixtures is shown in Figure 3.20. For instance, “BAC824(1)” indicates that the mixture contains 0.8% carbon fiber, 0.2% steel fiber, and 0.4% milled carbon fiber. The mixing method was selected

based on the mixing method showing the best electrical performance and higher flowability at the first stage.

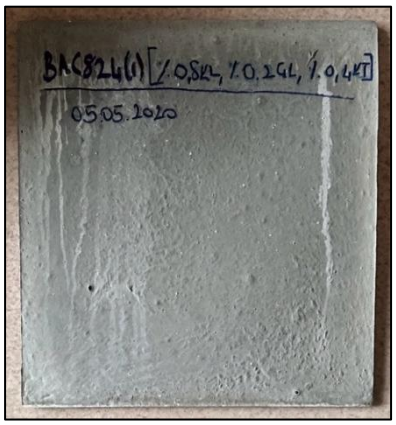

Figure 3.23. The coding of a combination of triple conductor addition

In single, double, and triple additions of conductors to the matrix, the performance of the mixtures was tested in the short and long term. When selecting the mixtures to be tested for humidity and temperature effects, the electrical performance of the mixtures, the lowest level of conductivity, and the economical design were considered. In this context, humidity and temperature tests were applied to three groups. Among groups, carbon fiber-based mixtures were selected from single addition, carbon fiber-steel fiber, and carbon fiber-milled carbon fiber-based mixtures were selected from double conductor addition, and carbon fiber-milled carbon fiber-steel fiber-based mixtures were selected from triple conductor addition. In the first group, samples were kept under laboratory conditions at 23±2 °C and 50±5% RH. In the second group, samples were removed from the mold and immersed in water 3 hours after the casting process. The samples were removed from the water tank on the measurement days and immersed in water again after the measurements were completed. In the third group, the plates were removed from the molds after 3 hours and kept in laboratory conditions at 23±2 °C and 50±5% RH until the measurement day. The samples were kept in the oven at 50 °C for 5 hours on the measurement days. Measurements of the samples were completed after they were removed from the oven. The coding of mixtures is shown in Figure 3.24. For instance, “CB26(1)” was selected among carbon fiber-milled carbon fiber additions. “CB26(1) [lab]” indicates that the mixture kept at laboratory condition, “CB26(1) [100%]” indicates that the mixture kept

at 100% RH condition, “CB26(1) [50°C]” indicates that the mixture kept at 50 °C condition.

Figure 3.24. The coding of mixtures under different environments

After humidity and temperature tests, a sulfuric acid resistance test was applied to selected single, double, and triple conductor-based samples. In order to measure the mechanical and electrical conductivity performance of the coating designs under the influence of various chemicals, samples were kept in a 5% concentrated sulfuric acid solution for 3 months according to the ASTM C267 test method. The prepared solution mixture represented a highly acidic environment and acid attack. The solution was prepared every week. At the end of each period, the samples were kept at 50°C for 24 hours, and their electrical resistance and strength losses were determined. The coding of mixtures is shown in Figure 3.25. For instance, an acid test was applied on the “CB26(1) [H_2SO_4]” sample, which indicates that the mixture was kept under an aggressive solution.

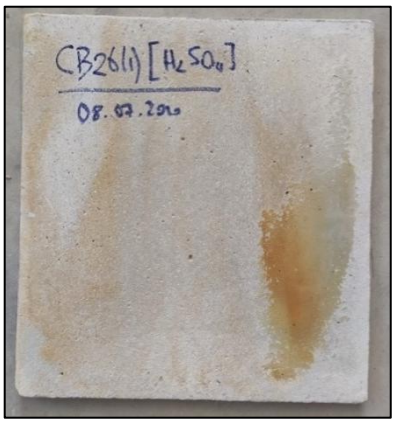

Figure 3.25. The coding of mixtures under an aggressive sulfuric acid solution

3.2.6. Testing

The development of a new generation electrostatic capability of cementitious composite within the scope of the thesis study aims to have superior performance properties that can be used in coating applications of critical structures in the construction industry. In this context, a series of tests were conducted to assess the cementitious mixtures' rheological, mechanical, and electrical properties under various environmental conditions. The rheological properties were primarily measured based on the mixtures' workability, flowability, and applicability. Compressive strength measurements were taken using 50 mm cube specimens cast from the mixtures to represent both early and long-term mechanical performance. Moreover, the electrical resistivity of mixtures was measured by using Φ10x20cm-cylinder and 40x40x1cm-plate casted specimens to represent the electrical performance of mixtures under conditions such as curing time, moisture, temperature, and chemical acid solutions. All these testing procedures used within the scope of this thesis study are detailed in the following sections.

3.2.6.1. Mini Slump Test

Using the EN 12350 standard [210], mini-slump tests were conducted to determine the consistency of the developed mixtures. As part of the flow table test, a truncated cone mold was used, whose dimensions were 200 mm at the bottom, 130 mm at the top, and 200 mm at the height, and the mold was placed on a 700×700 mm smooth plate. The representative images are shown in Figure 3.26-a. Fresh concrete is filled into the mold in two equal layers and compacted by a tamper ten times at each layer. After 30 seconds, the cone was lifted upwards, and the mortar mixture was dropped 15 times. Two perpendicular diameters were recorded on the longest side, and the average of these was used to calculate the flow diameter of the mortar (Figure 3.26-b).

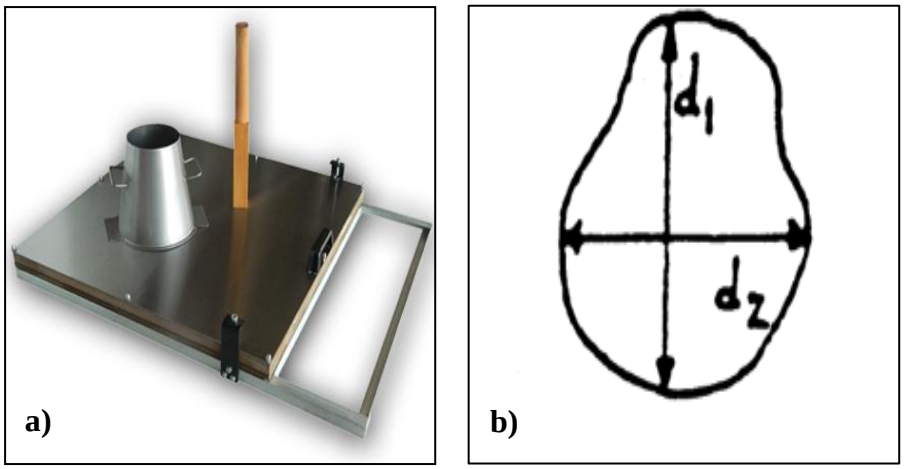

Figure 3.26. a) Representative images showing the details of the flow table test, b) Determination of flow diameter of mortars

The new generation electrostatic discharge capability of cementitious composites is expected to be flowable. Due to the large cone apparatus volume, a high mortar volume is required at the same level in the flow-table test. Therefore, a different test method was used to reduce the amount of mortar. Therefore, the flowing diameter of the mortar was determined using the TS EN 1015-3 test method instead of the flow table test [211]. In this mini-slump flow spread test, a truncated cone mold was used with a bottom diameter of 92 mm, top diameter of 44 mm, and height of 76 mm size. The representative images are shown in Figure 3.27. The specified cone was used to determine the flowability of the mixtures without applying any tamped or dropped process. Since the mortar mixture will flow quickly and have high flowability, the truncated cone was placed on the smooth plate, and the mortar of each specimen was filled with mortar, as shown in Figure 3.28-a. After 30 seconds, the cone was lifted upward. The cone and plate were not tamped to determine the flowability behaviour of the mixture. Flow diameter is defined as the average diameter of the mortar, measured after flow completion.

Figure 3.27. Representative images showing the details of the mini flow table test

At the same time, the slump flow time of mortars was also determined, besides the flow diameter, to represent self-levelling properties. In order to represent the slump flow time of mortars, a truncated cone specified in EN 12350 was used [210]. This test is also known as t500, which represents when the truncated cone is filled with mortar and lifted after 30 seconds without any tamped process, and the mortar reaches 500 mm in diameter. However, due to the high amount of mortar required for the experiment, the slum flow time was determined with a cone with a bottom diameter of 92 mm, top diameter of 44 mm, and height of 76 mm, as shown in Figure 3.28-a. Therefore, the mortar placed in the truncated cone was removed after 30 seconds, and the time was recorded when the mortar reached 250 mm in diameter, and the slump flow rate was determined. In addition, the flow diameter was calculated for each specimen by taking the average of two perpendicular diameters when the flow stopped. The representative image is shown in Figure 3.28-b.

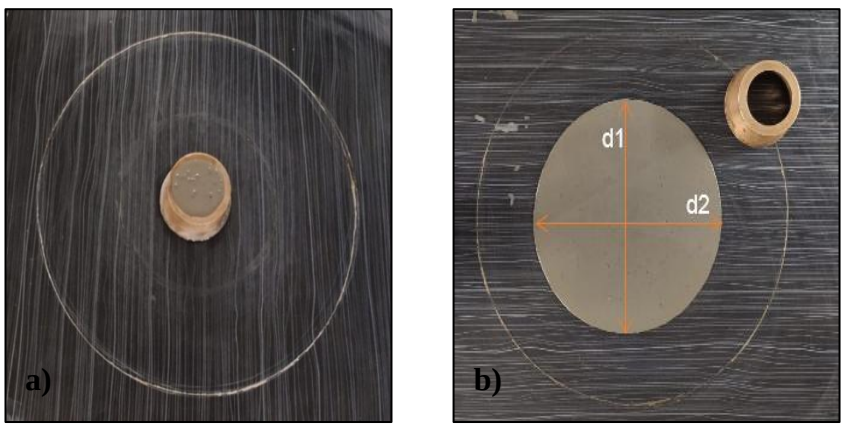

Figure 3.28. a) Placement of truncated cone filled with mortar, b) Representative image showing the determination of flow diameter of mortars.

3.2.6.2. Compressive Strength Test

New generation electrostatic discharge capability of cementitious composites is expected to have high compressive strength properties at an early and later-age. In order to measure the mechanical performance of mixtures, a compressive strength test was performed following the ASTM C109 standard [212]. Regarding the standard, the fresh mortar mixtures were poured into cubic molds measuring 50 mm at each side to determine compressive strength for each specimen, as shown in Figure 3.29-a. Specimens were kept in their molds for 3 h and then removed and kept under laboratory conditions at 23±2 °C and 50±5% RH until the completion of pre-determined testing ages. The compressive strength test was conducted using a 150-ton-capacity hydraulic testing machine with a 0.9 kN/s loading rate after 1, 3, 7, 28, and 90 days of curing, as shown in Figure 3.29-b. The average of six cubes was taken for the compressive strength value of each specimen at different ages (e.g., mixture content, loading direction, testing age, etc.), shown in Figure 3.29-c.

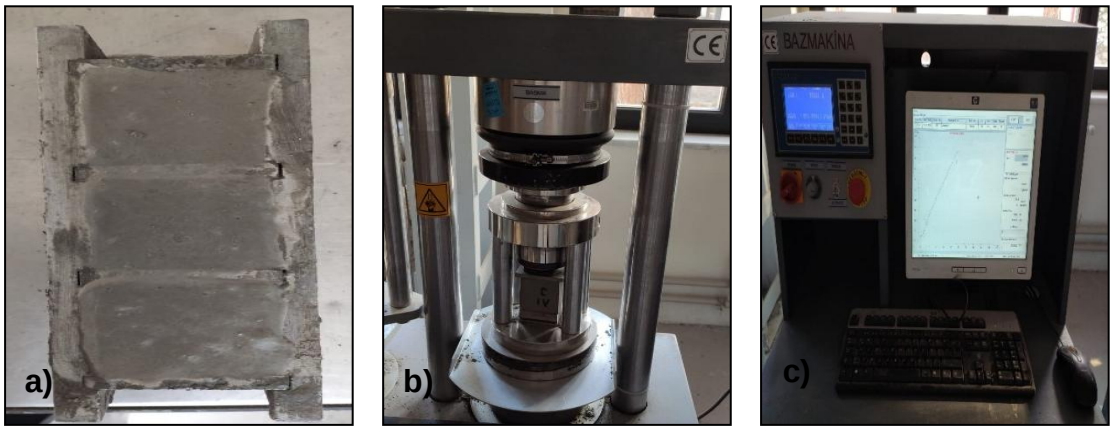

Figure 3.29. a) Cubic samples for the test, b) Compressive strength test machine, c) Test result

3.2.6.3. Testing the Electrical Conductivity Performance of Specimens

Electrical resistivity measurement is a significant parameter in showing permeability and physical and chemical properties of cementitious mortars, especially the pore network, porosity, flexibility, and chemistry of pore solution, as well as the electrical behavior of

composites [213,214]. For this reason, electrical resistance measurements were conducted to obtain a discussion about the electrical and microstructural properties of the coating designs developed within the scope of the thesis. According to ESD standards, the electrical resistance of the electrostatic discharge capability of cementitious composites is expected to be less than 1 MΩ at different hydration levels [19,22,149]. Conductive material combinations and their contents was tested, and a relationship was established between surface resistance values independent of moisture and hydration status. In addition, the distribution of conductive materials was determined by electrical resistance measurements in terms of the homogeneous dispersion of conductors in the cementitious matrix. The electrical resistance values of the specimens were measured on the 1^{st}, 3^{rd}, 7^{th}, 28^{th}, 90^{th}, and 180^{th} days. Two different measurement methods were applied to determine the electrical performance of specimens, such as cylinder and plate samples.

To determine the electrical conductivity performance of the specimens, the resistance values of the cylinder samples were measured according to two-point AC electrical resistance. Different types of conductive materials were incorporated into the matrix in single, double, and triple combinations, and cylinder samples were preferred to determine the percolation threshold of conductive materials and their dispersion in the matrix. In this context, a two-probe concrete resistivity meter with axial configuration was used to collect electrical data. Configurations of such concrete resistivity meters are standard, and test equipment details can be found in Spragg's study [215]. The measurements were made with a GIATEC RCON^{TM} concrete electrical resistance measuring device is shown in the Figure 3.30. GIATEC RCON™ is an instrument developed for electrical resistivity measurement of concrete using the uniaxial method. RCON™ uses the AC impedance technique for accurate and fast readings that can be consistently obtained for a variety of concrete materials. Technical specifications of device are given in Table 3.9.

Figure 3.30. GIATEC RCON^{TM} concrete electrical resistance measuring device

The electrical resistance measuring device can operate at different frequency values (1 Hz - 30 kHz) and the phase angle (0 - 180°) and gives impedance results by applying alternating current (AC). Since the polarization effect is minimized by at least 1 kHz frequency in AC applications, the frequency value was preferred to be 1 kHz in the tests. During this test method, Φ100×50 mm cylindrical samples were placed parallel to each other between two electrodes, and pre-saturated sponges with a height of 10 mm and a diameter of 150 mm were placed between the sample and the electrodes to ensure sufficient electrical contact. Since there was a possibility that electrical resistance measurements could be affected by the sponges, sponges were moistened using a similar amount of water during each measurement. Although electrical resistance measurements of water-saturated sponges were performed, no measurements were recorded. Therefore, resistance measurements taken from the device were directly used to determine the electrical properties of the samples.

Table 3.7. Technical specifications of Giatec RCON device

Properties	**Value**
Working temperature	15 - 45 °C
Working moisture	30 - 80%
Working voltage	100 - 250 V±10%, 60 Hz
Measurement time	5 s
Accuracy	±2%
Phase angle	0 - 180°
Frequency range	1 Hz - 30 kHz

A Φ10*20 cm cylindrical sample was cast for each mixture to determine the electrical resistance value of the mixtures using the device. Then, the sample was removed from the mold, and a 2.5 cm section was cut from the upper and lower layers and divided into three pieces with dimensions of Φ10*5 cm, as shown in Figure 3.31-a. The sections of the samples were numbered starting from the top layer. These sections were kept in an air cure under laboratory conditions until the measurement's day is shown in Figure 3.31-b. The electrical resistance results of the samples were measured on the 1st, 3rd, 7th, 28th, 90th, and 180th days, and the data were recorded. The ER values of sections were compared with each other to determine that the conductive materials were distributed homogeneously.

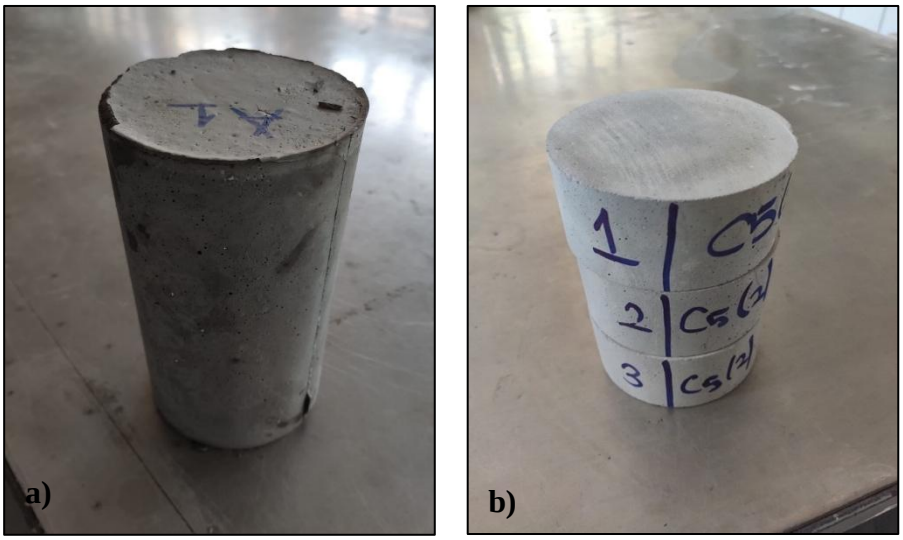

Figure 3.31. a) A cylindrical sample, b) The sections with Φ10*5 cm

In addition to the AC measuring method, the thesis study aims to develop a new generation of electrostatic discharge capability in cementitious mortars by incorporating conductive materials. In order to measure the ER values of plates, the METRISO 3000 ESD surface resistance meter was used, as shown in Figure 3.32-a. High ohmic resistance meter Metriso 3000 measures point-to-point, ground, surface, and volume resistance. Technical specifications of the device are given in Table 3.8.

Table 3.8. Technical specifications of METRISO 3000 ESD device

Properties	**Value**
Test voltage	DC 10 V, 100 V, 500 V
Resistance range	1 Ω - 1.2 TΩ
Working temperature	-10 °C - +70 °C
Working moisture	10 - 90%

Regarding Table 3.8, METRISO 3000 has voltage ranges between 10 V and 500 V and resistance value ranges between 1 Ω and 1.2 TΩ. The device automatically adjusts its voltage depending on the electrical resistance of the measured area. Therefore, the ER values of the plates using 10 V vary between 1 Ω and 100 kΩ, using 100 V varies between 100 kΩ and 1 GΩ, and finally, while using 500 V, they vary between 1 GΩ and 1.2 TΩ. As the ER value of the plate increases, the used voltage increases in the same line. In order to determine the ER values of the plate, probes were placed in the crosses as 1-1 and 2-2, as shown in Figure 3.32-b.

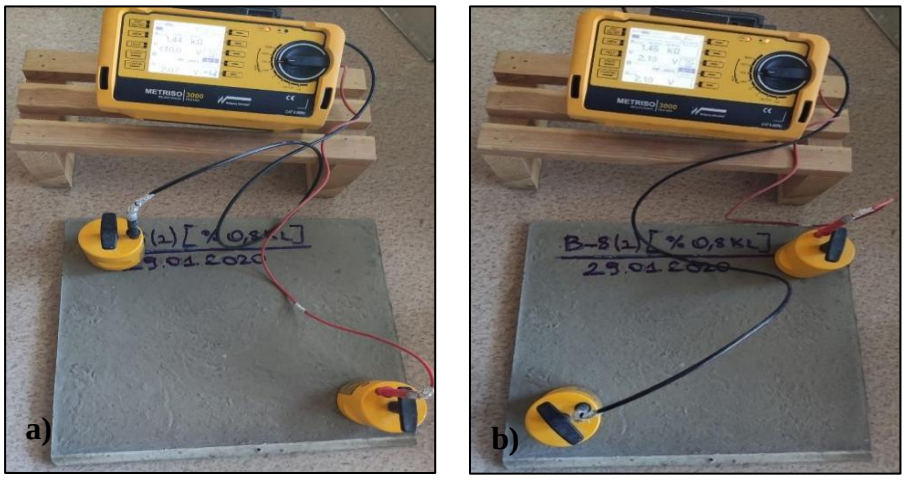

Figure 3.32. a) METRISO 3000 ESD surface resistance meter device, b) Placements of probes

So as to determine the electrical performance of specimens, the fresh mortar was poured into a 400×400×10 mm-plate, as shown in Figure 3.33-a, and kept for 3 hours in the mold, and then removed from the mold. Electrical resistance (Ω) was measured from panel specimens, as shown in Figure 3.33-b. ER values were measured by placing the probes diagonally on the plates at 25-35 cm distance to simulate grounding applications and human steps. The electrical resistance values of the samples were measured on the 1st, 3rd,

7^{th}, 28^{th}, 90^{th}, and 180^{th} days, and the data were recorded as shown in Figure 3.33-c. The electrical conductivity performances of the plates at different hydration stages were compared. In measurements, the aim was to obtain the lowest ER value in a homogeneous conductive material dispersion early and long-term.

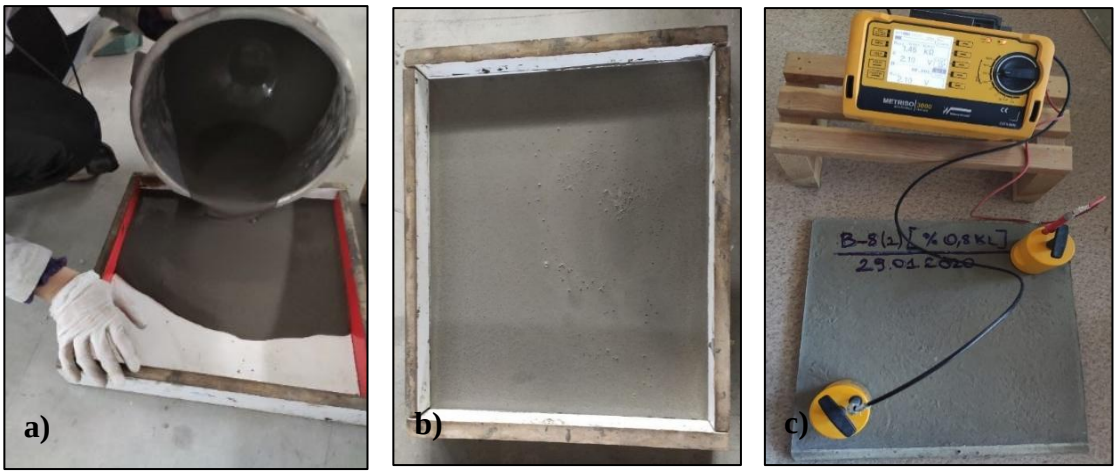

Figure 3.33. a) Placing fresh mortar into the mold, b) View of fresh mortar, c) Measurement of electrical resistance value

3.2.6.4. Determining the Mineralogical Structure of Cementitious Matrix

This thesis study aims to distribute conductive materials homogeneously into the cementitious matrix. Homogeneous dispersion aims to create a magnetic field and to healthily remove the accumulated electrostatic charge in the environment from the field. Therefore, the mineralogical structures of the matrix were examined to determine the distribution of conductive materials in the matrix. In this context, a scanning electron microscope (SEM) was preferred for microstructural analysis of the selected samples obtained after the compressive strength test, as shown in Figure 3.34. This device takes micron-sized images of the composites, and their contents are determined by EDX analysis. The mapping method can identify elements in a certain area by looking at the distribution of the desired nanoparticles and elements. As part of these characterizations, mapping analyses were conducted, and scanning electron microscopy observations were made using energy-dispersive X-ray spectroscopy (SEM/EDX). SEM/EDX analyses were carried out in the Hacettepe University HUNITEK laboratory. After each experimental stage, microstructure tests were applied to the selected samples after the

compressive strength tests were carried out on the 28th day. SEM/EDX analyses were conducted on samples taken from cubic specimens (less than 1 cm in each dimension). Chemical formations, interfacial transition zones (ITZs), and conductive pathways were examined in selected areas. SEM images were captured under low-vacuum conditions at 30 KV voltage with backscattered electron signals using the EDX attachment. In addition, samples from both acid-exposed and non-exposed conditions at the final age were examined under a scanning electron microscope to analyze the interactions of the conductive materials with each other and the microstructural properties of the matrix in detail.

Figure 3.34. A scanning electron microscope (SEM)

4. RESULTS AND DISCUSSION

The development of coating design is a complex process that takes place in more than one phase, beginning with obtaining an early age high-strength cementitious main composite, continuing with the incorporation of conductors, and ending with testing the final composite performance. One of these processes largely depends on the type and amount of ingredients such as cement types, calcium source, and chemical additives, mainly contributing to the early age high strength of the main composite. The other process largely depends on the type and content of the conductive material, the method of admixing the conductors, and the incorporation of conductors in single, double, or triple forms. The conductors are mainly responsible for the electrical conductivity performance and contribute to changes in the rheological, and mechanical properties of the final coating design. The aforementioned tests were performed to examine the rheological, mechanical, and electrical properties of cementitious mortar mixtures; details and discussions are provided in the following sections.

4.1. Development of Cementitious Main Paste Mixture

The first part of the thesis study aimed to develop an early age high-strength cementitious binder matrix. More than one factor can affect achieving early age high strength, as stated in Section 2.1. The main matrix was also expected to have high flowability, crack-free, and acid-resistance performances. The results of the experimental work to obtain the cementitious matrix developed are given in this section.

4.1.1. Determining the Main Components and Proportions of the Ternary-Based System

4.1.1.1. Effects of Sand/Cement Ratio and Water/Cement Ratio on Early Age High Compressive Strength

The optimum sand/cement (s/c) and water/cement (w/c) ratios of the mixtures were determined first. In this part, s/c was used at the ratios of 0.5, 0.6, 0.7, 0.8, 0.9, and 1.0,

and w/c was used at the ratios of 0.55, 0.50, 0.45, 0.40, and 0.35. The 6-hour compressive strength of the pastes was measured. The average of six cubes was taken for the compressive strength value of each specimen. In order to obtain early age high strength, the mixing water was kept to a minimum ratio and the amount of binder was kept to a maximum ratio. Additionally, only CEM I 52.5R PC was used in the mixtures. The effect of sand/cement and water/cement ratio on the compressive strength of mixtures is given in Table 4.1.

Table 4.1. Effects of the sand/cement and water/cement ratio on the compressive strength of mixtures, MPa

s/c ratios	**w/c ratios**				
	0.55	0.50	0.45	0.40	0.35
1.0	12.40	14.1	17	22.4	25.6
0.9	12.10	10.4	16.6	20.8	25.3
0.8	10.50	14.30	15.90	18.60	23.40
0.7	11.60	14.20	15.80	20.00	23.60
0.6	7.20	10.30	11.00	21.70	26.10
0.5	8.70	9.70	15.50	19.00	25.30

According to Table 4.1, the compressive strength of samples increased significantly as the w/c ratio decreased. However, variations of the s/c ratio did not improve a visible change in the compressive strength results. The 6-hour compressive strength was determined to be the highest at 26.10 MPa in the sample, with a w/c ratio of 0.35 and a s/c ratio of 0.6. According to the results, the s/c ratio was determined as 0.6, and the w/c ratio was determined as 0.35 to reduce the pore volume in the matrix and obtain early age high strength.

4.1.1.2. Choosing of CAC with Respect to Mechanical Performance at Early Age and Economy

Early age high strength CACs with varied aluminate (Al_2O_3) ratios from different companies were used, and the effects of the mixtures on compressive strength were determined. Considering the literature studies, a PC-rich ternary-based system was preferred for obtaining economical composites at an early age high strength, high workability, and optimum application time. The CAC type and the lowest CAC ratio were determined in this context. CAC cements were replaced at different rates with PC, considering the workability of the mixtures. Considering the literature studies, α-type hemihydrate (CŠ) was used, which had the highest dissolution rate among calcium sulfate sources for the combined use of CAC and PC in the ternary system [68,82,83]. Due to the addition of gypsum in the production of PC clinker, standard PCs contain a gypsum composition. In preliminary experimental studies, the amount of CŠ was added based on the total binder content (PC+CAC). This addition delayed the setting time of the mixture, combined with the gypsum from PC, resulting in lower early strength. Therefore, CŠ was added to the mixtures only based on the weight of CAC cement in all mixtures. Although the w/c ratio was determined at 0.35 in the first section, it was kept constant at 0.4 to avoid adversely affecting the mixtures' workability. Additionally, the s/c ratio was kept constant at 0.6. The compressive strengths of the mixtures were measured at 3 and 6 hours. The effects of mixtures prepared using Isıdaç 40 type (~40% Al_2O_3) CAC, which was first developed by ÇİMSA cement, one of the cement producers of Turkey, on compressive strength, are given in Table 4.2.

According to Table 4.2, Isıdaç 40 type CAC content gradually positively affected the mixtures' early age compressive strength. Insufficient CŚ ratio in the mixture resulted in a tendency to flash setting and lower strengths at 3 and 6 hours. In addition, the incorporation of sufficient CŚ had a significant positive effect on the 3 and 6-hour compressive strengths of mixtures. Based on the results, the highest compressive strength was obtained from the mixture containing 60% PC, 40% Isıdaç 40 type CAC, and 0.15 CŚ ratio. The compressive strength was measured as 20.90 MPa at 3 hours and 28.7 MPa at 6 hours. Since the compressive strength and cost of the mixture were negatively

affected by the approximately 50% Isıdaç 40 type CAC, the replacement ratio of CAC was not increased after this ratio.

Table 4.2. Effect of the Isıdaç 40 type CAC on the compressive strength of mixtures

Binder Proportions, %		**CŠ ratio**	**Compressive Strength, MPa**	
PC	**CAC (Isıdaç 40)**		**3 hours**	**6 hours**
100	0	0	2.36	21.70
90	10	0	3.73	17.33
90	10	0.05	3.00	20.43
90	10	0.10	4.10	21.70
90	10	0.15	3.80	23.43
80	20	0.05	7.93	23.16
80	20	0.10	4.26	22.46
80	20	0.15	4.60	25.70
70	30	0.05	4.93	5.93
70	30	0.10	13.66	14.70
70	30	0.15	9.56	25.53
60	40	0.05	6.26	6.60
60	40	0.10	7.53	8.43
60	40	0.15	20.90	28.17
60	40	0.20	6.77	25.00
60	40	0.25	5.03	11.33
60	40	0.30	4.70	11.23
50	50	0.10	Flash setting	
50	50	0.15	20.43	23.60
50	50	0.20	9.83	23.30
40	60	0.15	Flash setting	
40	60	0.20	Flash setting	

In order to determine the effect of CAC type on the early age compressive strength performance of mixtures, Isıdaç 50 (~50% Al_2O_3) type CAC developed by ÇİMSA cement was used. In the preliminary experimental study, the mortars were tough, lumpy, and challenging to cast into molds. Therefore, HRWRA was added to the mixtures at 1%

of the total binder (PC+CAC) amount by weight to improve workability. The effects of mixtures prepared using Isıdaç 50 type CAC on compressive strength are given in Table 4.3.

Table 4.3. Effect of the Isıdaç 50 type CAC on the compressive strength of mixtures

Binder Proportions, %		**CŠ ratio**	**Compressive Strength, MPa**	
PC	**CAC (Isıdaç 50)**		**3 hours**	**6 hours**
70	30	0.20	7.67	10.89
60	40	0.10	8.87	13.84
60	40	0.15	13.33	18.85
60	40	0.20	18.13	26.65
50	50	0.10	17.10	25.86
50	50	0.15	24.57	32.65
50	50	0.20	21.70	30.48
40	60	0.15	4.70	6.80
40	60	0.20	12.73	19.68
40	60	0.25	21.90	30.30
30	70	0.20	16.93	20.55

Based on the results, the highest compressive strength was obtained from the mixture containing 50% PC, 50% Isıdaç 50 type CAC, and 0.15 CŚ ratio. The compressive strength was measured as 24.57 MPa at 3 hours and 32.65 MPa at 6 hours. The flash setting formation was prevented by adding CŚ in different proportions. Additionally, HRWRA addition improved the workability of the mixture, and the compressive strength was affected positively. The theoretical expectation is that HRWRA increases flowability, provides better compression and less porosity, and increases strength [45,96,98]. However, in the case of setting retarding effect of HRWRA may also reduce the early strength [97,103]. These effects can vary depending on the mixture proportions. In experimental studies, mixtures were also prepared using imported Secar 51 (~50% Al_2O_3) type CAC developed by KERNEOS Cement, one of the world's largest cement companies. Due to the improper mortar condition in the preliminary experimental study, HRWRA was added to the mixtures 1% of the total binder amount by weight to improve

workability. The effects of mixtures prepared using Secar 51 type CAC, on compressive strength are given in Table 4.4.

Table 4.4. Effect of the Secar 51 type CAC on the compressive strength of mixtures

Binder Proportions, %		**CŠ ratio**	**Compressive Strength, MPa**	
PC	**CAC (Secar 51)**		**3 hours**	**6 hours**
100	0	0.00	2.36	21.70
90	10	0.00	4.00	20.80
80	20	0.00	4.40	6.17
80	20	0.05	4.30	7.00
80	20	0.10	4.40	6.47
80	20	0.15	0.90	6.93
70	30	0.05	5.03	5.07
70	30	0.10	6.67	7.07
70	30	0.15	9.80	10.83
70	30	0.20	2.33	32.33
60	40	0.05	Flash setting	
60	40	0.10	5.17	5.50
60	40	0.15	10.40	12.57
60	40	0.20	11.53	12.90
60	40	0.25	1.20	8.43
60	40	0.30	3.37	13.63
50	50	0.05	Flash setting	
50	50	0.10	9.23	12.37
50	50	0.15	14.63	17.40
50	50	0.20	21.13	27.53
50	50	0.25	13.96	38.63
50	50	0.30	2.26	9.70
40	60	0.15	32.40	41.00
40	60	0.20	44.00	55.00
40	60	0.25	22.16	26.90

According to Table 4.4, the desired results could not be obtained in 3-hour compressive strength up to 50% use of Secar51. However, the 3 and 6-hour compressive strength values increased significantly when the optimum level of CŠ was added with 50% Secar51 in the mixtures. Based on the results, the highest compressive strength was obtained from the mixture which contains 40% PC, 60% Secar 51 type CAC, and 0.20 CŚ ratio. The compressive strength was measured as 44.00 MPa at 3 hours and 55.00 MPa at 6 hours. Although high mechanical properties were obtained in these proportion ratios, the high content of Secar 51 cement could increase the cost of the mixture. To determine the effect of CAC type on the early age compressive strength performance of mixtures, Secar 80 (~80% Al_2O_3) type CAC developed by KERNEOS cement was used. Due to the improper mortar condition in the preliminary experimental study, HRWRA was added to the mixtures 1% of the total binder amount by weight to improve workability. The effects of mixtures prepared using Secar 80 type CAC, on compressive strength are given in Table 4.5.

Table 4.5. Effect of the Secar 80 type CAC on the compressive strength of mixtures

Binder Proportions, %		**CŠ ratio**	**Compressive Strength, MPa**	
PC	**CAC (Secar 80)**		**3 hours**	**6 hours**
100	0	0.00	2.36	21.70
90	10	0.00	0	6.97
80	20	0.00	2.67	3.23
80	20	0.05	1.70	3.40
80	20	0.10	0	0
80	20	0.15	0	0
70	30	0.05	4.53	5.10
70	30	0.10	5.90	6.83
70	30	0.15	2.10	10.43
60	40	0.10	10.93	13.40
60	40	0.15	11.17	14.87
60	40	0.20	0.40	12.90
50	50	0.10	16.90	20.90
50	50	0.15	15.90	22.43
50	50	0.20	4.33	25.30
40	60	0.15	12.23	21.90
40	60	0.20	3.47	33.73

According to Table 4.5, the compressive strength results of mixtures were relatively low compared to other types of CACs. In literature studies, it was mentioned that the matrix becomes more resistant to high temperatures as the aluminate ratio in calcium aluminate cements increased [53,61]. Since these cement types are designed to resist high temperatures rather than early age high strength, their strength values were below the expected level in experimental studies. Based on the results, the highest compressive strength was obtained from the mixture, containing 50% PC, 50% Secar 80 type CAC, and 0.10 CŚ ratio. The compressive strength was measured as 16.90 MPa at 3 hours and 20.90 MPa at 6 hours. The mixing ratios that showed the highest compressive strength at an early age were selected among types of CACs. Besides mechanical performance, the developed matrix mixtures are expected to be economical. Therefore, the price of the types of CACs in 2023 is given in Table 4.6. Current prices were obtained from companies.

Table 4.6. Cement prices and compressive strength values of selected mixtures

Cement Type	**Price of CACs**	**Mixture Proportions,**			**Compressive Strength, MPa**	
		PC, %	**CAC, %**	**CŚ**	**3 hours**	**6 hours**
Isıdaç 40	18000 TL/Ton + VAT	60	40	0.15	20.90	28.17
Isıdaç 50	21000 TL/Ton + VAT	50	50	0.15	24.57	32.65
Secar 51	900 Euro/Ton + VAT	40	60	0.20	44.00	55.00
Secar 80	1300 Euro/Ton + VAT	50	50	0.10	16.90	20.90

Based on the 3-hour compressive strengths, the results were obtained in increasing order of providing mechanical performance from Secar 51, Isıdaç 50, Isıdaç 40, and Secar 80 type CACs. Considering the workability of the matrix of mixtures, the HRWRA addition was required to improve the workability of the mixtures except for Isıdaç 40 type CAC. The final composite is also expected to be prepared with local materials and should have a lower cost than other coating designs at the end of the thesis study. Considering these

criteria and easy accessibility to the materials, Isıdaç 40 type CAC, which had the lowest cost, was preferred to obtain early age high strength.

4.1.2. Determining the Effect of the Mineral Additive on the Early Age Performance of the System

After determining the main components and usage rates of the ternary system, silica fume was added to the matrix as a mineral additive. Although the addition of silica fume aimed to reduce the pore volumes of the mixtures, obtained a denser matrix, and dispersed the conductors more homogeneously into the matrix, the workability was expected to be negatively affected by the silica fume addition [94,114,216]. In these mixtures, the s/c and w/c ratios, where the highest compressive strength was measured in section 4.1.1.1., were preferred to obtain early age high strength. Therefore, the s/c and w/c ratios were kept constant at 0.6 and 0.3, respectively. For this reason, 1.5% HRWRA by the weight of total cement was used until the addition of 2% silica fume, while after this rate, 2.5% HRWRA by the weight of total cement was used in the mixture. Additionally, 0.5% SRA by the weight of the total cement was also used to prevent flash-setting by adding silica fume. Silica fume was added to the mixtures in different ratios at 0.5, 1.0, 1.5, 2.0, 2.5, 3.0, 5.0, 7.0, and 10.0% by weight of the total cement amount. The effects of silica fume addition on the compressive strength of mixtures are given in Table 4.7.

Based on the results, the highest compressive strength was obtained, 26.87 MPa, from the mixture containing 0.5% silica fume addition. However, similar results were obtained at 2 and 3-hour strengths between 0.5 - 2.0% silica fume ratios; the compressive strength decreased by approximately 25% beyond the use of 2.0% silica fume addition due to the increase in HRWRA. Compared to the control mixture, silica fume addition did not affect the early strength significantly. This result was mainly related to the insufficient use of SRA in the hydration reaction. Without SRA addition, the paste became flash setting, and no strength could be measured from the samples. Therefore, the use of silica fume adjusted with the SRA content in the matrix.

Table 4.7 Effect of the silica fume addition on the compressive strength of the mixtures

Silica Fume Content, %	Compressive Strength, MPa	
	2-hours	3-hours
0.0	22.50	29.03
0.5	26.87	27.57
1.0	24.40	25.90
1.5	24.63	25.30
2.0	23.73	24.90
2.5	15.70	20.47
3.0	16.77	22.50
5.0	17.50	22.90
7.0	16.13	23.03
10.0	17.10	25.37

4.1.3. Determining the Effects of the Chemical Additives on the Early Age Performance of the System

Because the desired strength could not be achieved when the flash setting occurred due to the use of PC and CAC in the system, it was necessary to use SRA at an optimal rate to achieve early age high strength. Inadequate use of SRA prevented silica fume from an improved effect on strength performance. Therefore, optimum chemical additive usage rates were determined in silica fume-incorporated mixtures.

4.1.3.1. Effect of the Setting Retarder Addition on the Compressive Strength of the Mixtures

Although CŠ was added to extend the setting time in ternary systems, the flash setting could still occur due to using setting accelerators (SA) and CAC. In addition, the workability and strength of the mixtures were also negatively affected by the addition of

silica fume. Therefore, the effect of SRA usage on early age high strength was determined. In mixtures, 2.5% silica fume content was selected due to its significant effect on the homogeneous dispersion of conductive material to prevent loss of workability and flash setting problems. Based on the literature studies, SRA was added up to 0.5% by weight of the total cement. The effects of setting retarder addition on the compressive strength of mixtures are given in Table 4.8.

Table 4.8. Effect of the setting retarder addition on the compressive strength of the mixtures

SRA Content	**Compressive Strength, MPa**		**Workability**
	2-hours	**3-hours**	
0.0% SRA	25.60	24.33	Workability was good but the mixture set quickly. The surface was rough and had cracks.
0.1% SRA	26.40	25.60	The mixture was flowable, but it set quickly. Casting was easy, the surface was very smooth.
0.2% SRA	33.00	30.13	The mixture was flowable, it set later than 0.1% SRA content. Casting was easy, the surface was very smooth.
0.3% SRA	26.93	36.80	The mixture lost its fluidity, but its workability was good, and it set later than 0.2% SRA. Surface was smooth.
0.4% SRA	24.80	32.70	The mixture lost its fluidity, but its workability was good, and it set later than 0.3% SRA. Surface was rough.
0.5% SRA	15.70	20.47	The mixture lost its fluidity, but its workability was good, and it set later than 0.4% SRA. Surface was rough.

According to the results, the highest compressive strength of 33 MPa was obtained from the mixture containing 0.2% SRA at 2 hours, while the highest compressive strength of 36.8 MPa was obtained from the mixture containing 0.3% SRA at 3 hours. While the SRA ratio improved the strengths by using 0.2% SRA content, the strengths decreased significantly beyond this ratio at 2-hour measurements. Using SRA at more than the

optimum rate prolonged the hydration time of CAC, resulting in lower strength values at the same measurement time. Due to the mixture's characteristics of having flowable mortar, a smooth surface, and early age high strength, the optimum ratio of SRA addition was determined as 0.2% (Figure 4.1).

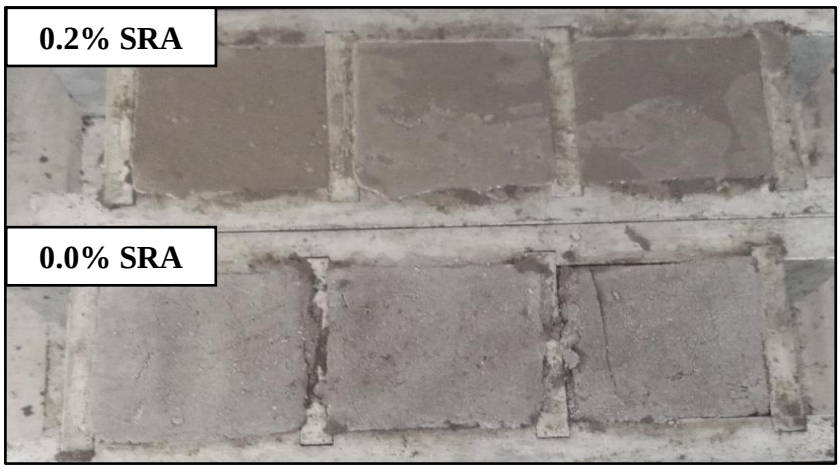

Figure 4.1. The effect of the setting retarder addition on the surface of mixtures

4.1.3.2. Effect of the Setting Accelerator Addition on the Compressive Strength of the Mixtures

SRA addition significantly improved the 2-hour compressive strength results. According to literature studies, early age high strength could be enhanced by using combined setting retarders and setting accelerator additives in ternary systems [96]. In the mixtures, 2.5% silica fume, 2.5% HRWRA, and 0.2% SRA by total cement amount were kept constant. In order to improve the early age compressive strength of mixtures, SA was added up to 1.0% by the weight of the total cement based on literature studies. The effects of setting accelerator addition on the compressive strength of mixtures are given in Table 4.9.

Table 4.9 shows that except for the 0.5% SA addition, there was no significant improvement in strength results with SA use. As the SA ratio increased, it negatively affected its flowability; the paste became rough and had cracks on the paste during the experimental process. Flowability was not at a sufficient level when increasing SA

content. Therefore, before increasing HRWRA content, the effect of the type of HRWRA on the compressive strength and flowability of the mixtures was investigated.

Table 4.9. Effect of the setting accelerator addition on the compressive strength of the mixtures

SA Content	Compressive Strength, MPa	
	2-hours	3-hours
0.00% SA	33.00	30.13
0.05% SA	27.90	28.17
0.10% SA	29.90	32.30
0.30% SA	29.10	30.07
0.50% SA	33.43	32.17
1.00% SA	30.10	32.50

4.1.3.3. Effects of the Types of HRWRA Addition on the Compressive Strength of the Mixtures

So as to use composites in flooring systems, the design should have high flowability performance. Until this stage, C-97 type HRWRA, obtained from the Plustechno company, was used to improve the workability of the mixtures. However, various types and quality HRWRA were obtained from different companies to determine the most suitable additive. For this reason, before increasing HRWRA content, the effect of different types of HRWRA on the mechanical and flowability properties of the mixtures was determined based on the mixture with the highest strength at an early age. In the mixtures, the use of 2.5% silica fume, 2.5% HRWRA, and 0.2% SRA by total cement amount was kept constant. The compressive strength results of mixtures at 2 and 3 hours are given in Table 4.10. In addition, digital camera images of mixtures prepared using different types of HRWRA are shown in Figure 4.2.

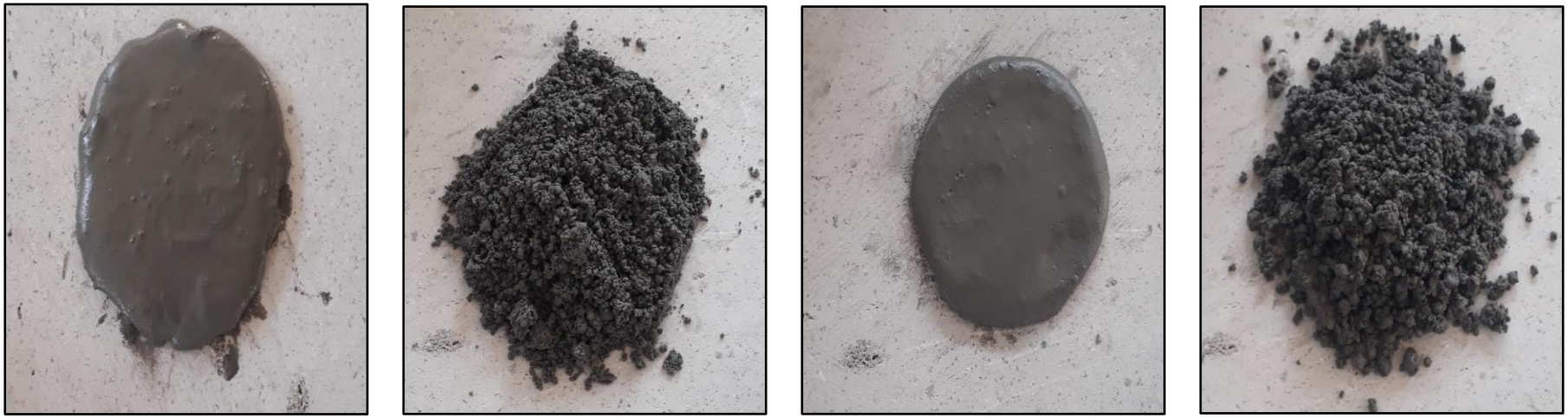

149S (Ata Kimya) | Plus Powder (Plustechno) | Plus C-97 (Plustechno) | Plus UM-P (Plustechno)

Cemeste P-97H (Plustechno) | Cemeste P-67R (Plustechno) | EBA1447 (BASF) | EBA1446 (BASF)

Figure 4.2. Effects of the types of HRWRA on the workability of mixtures

Table 4.10. Effects of the HRWRA types on the compressive strength of the mixtures

Types of HRWRA	**Compressive Strength, MPa**	
	2-hours	**3-hours**
149S (Ata Kimya)	23.87	24.80
Plus Powder (Plustechno)	-	-
Plus C-97 (Plustechno)	33.27	31.20
Plus UM-P(Plustechno)	-	-
Cemeste P-97H(Plustechno)	31.87	32.10
Cemeste P-67R(Plustechno)	-	-
Polycarboxylic ether-based EBA 1447 (BASF)	27.70	26.00
Naftalin EBA 1446 (BASF)	30.20	32.00

According to Table 4.10, strength results varied depending on the HRWRA types. Based on the 2-hour compressive strength results, the highest value was obtained as 33.30 MPa using Plus C-97 type HRWRA. In contrast, the highest flowability was obtained using Polycarboxylic ether-based EBA 1447 supplied by BASF company, as shown in Figure 4.2. Some HRWRAs did not provide workability, and the strength of the mixtures could not be measured. The 2-hour and 3-hour compressive strength of the EBA 1447 HRWRA used sample were measured as 27.70 and 26.00 MPa, respectively. Therefore, polycarboxylic ether-based HRWRA was selected to achieve the goal of a high flowability and crack-free surface for the coating.

4.1.3.4. Adjusting the Amounts of Chemical Additives

So as to enhance the early age strength of cementitious, the optimum usage of chemical additives was determined by using different ratios of a combination of SA and HRWRA. Among the chemical additives, SRA content was kept constant in the mixtures since it negatively affected early age strength after 0.2% ratio significantly. In the mixtures, the use of 2.5% silica fume and 0.2% SRA by total cement amount was kept constant. In mixture proportion, other ingredients were also kept constant. The compressive strength results of mixtures at 2-hours and 3-hours are given in Table 4.11.

Table 4.11. Optimization of chemical additives

Content		Compressive Strength, MPa		Workability
SA	**HRWRA**	**2-hours**	**3-hours**	
0.0%	2.0%	21.97	23.00	Flowable
0.0%	2.5%	21.00	19.93	
0.5%	1.5%	22.67	30.33	
0.5%	2.0%	29.00	29.95	
0.5%	2.5%	26.00	27.70	
1.0%	1.5%	27.90	30.40	
1.0%	2.0%	28.60	28.93	
1.0%	2.5%	23.77	27.80	
1.5%	2.5%	26.93	29.45	Not flowable
2.0%	2.5%	0.00	0.00	Not workable

According to Table 4.11, mostly all mixtures showed sufficient flowability. Based on the compressive strength results and workability behaviour, the best performance was achieved from the sample, which had 0.5% SA and 2% HRWRA. The 2-hour and 3-hour compressive strengths were measured as 29.00 MPa and 29.95 MPa. As a result, the usage rates of chemical additives in the development of early age high strength mixtures were determined as 0.2% SRA, 0.5% SA, and 2% HRWRA.

4.1.4. Effects of the Mixing Time and Mixing Process of Ingredients on the Early Age Performance of the System

4.1.4.1. Determining Mixing Process of the Cementitious Matrix

The impact of the mixing process and duration on the main matrix's flowability and early age high strength was assessed to achieve optimal flowability and mechanical performance for the new-generation cementitious composite. This evaluation aimed to ensure that the performance properties of composites remained unaffected when conductive materials were incorporated to develop a matrix. Before determining the mixing process of the final mixture, the method and content of chemical additives added to the mixture were determined in the last section. In this context, water and chemical

additives were added to the mixture in different ways during the preparation. In order to determine the addition way of chemical additives, a dry mixture (sand, cement, and CŠ) was mixed first. Then, the addition step of chemical additives was carried out after this step. Mixing times were kept constant for this study. The effects of the mixing method on the flowability and early age compressive strength of the mixtures at 2 hours are given in Table 4.12.

Table 4.12. Effect of the addition method of chemical additives on the mixture proportions

Addition method	**Slump Flow Time (s)**	**2-Hours Compressive Strength (MPa)**
Mixing water/3	6.10	29.00
Mixing water/3 + HRWRA	9.20	30.00
Mixing water /3 + HRWRA/2	10.55	32.30
Mixing water /3 + HRWRA/2 + SRA	4.10	30.20
Mixing water/3 + HRWRA/2+ SA	5.80	27.97
Mixing water/3 + HRWRA/2 + SRA + SA	7.75	29.50

According to Table 4.12, slump flow time values were measured between 4.10 and 10.55 seconds depending on the addition of chemicals to the mixtures in different ways. The highest strength was achieved using one-third of the mixing water and half of HRWRA. However, a mixture that contains a third of the mixing water, half of HRWRA, and the total amount of SRA was selected due to the lowest flow time. With the determination of the addition method of chemicals, the preparation process of the final mixture was prepared in four stages. Firstly, the dry mixture was completed. All powder raw materials (PC, CAC, CŚ, and Quartz sand) except chemical additives were added to the mixing bowl and mixed with a mechanical mixer at 150 rpm for 3 minutes, as shown in Figure 4.3.

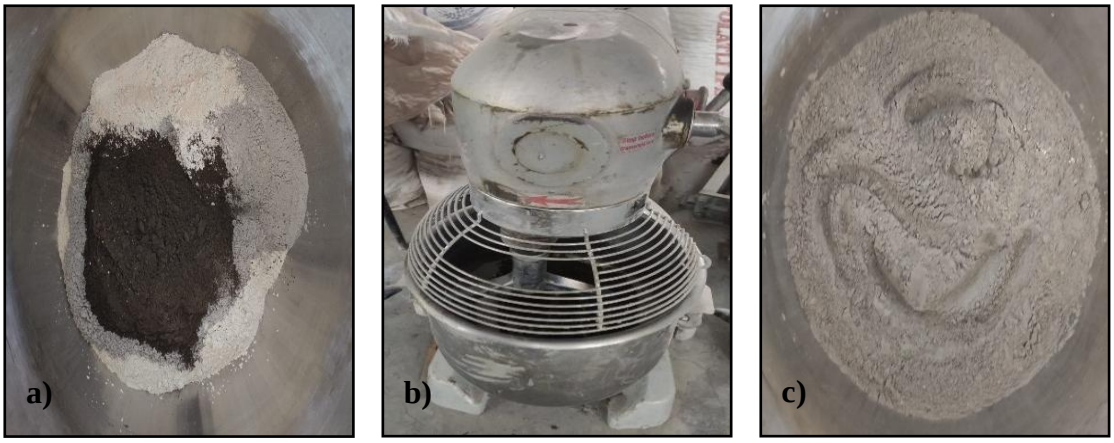

Figure 4.3. a) Adding powder raw materials in a mixing bowl, b) A mechanical mixer, c) Dry mixture

After obtaining the dry mixture, the mixer was stopped, and half of the amount of HRWRA and the total amount of SRA were added to the mixture. Once the mixer was restarted, one-third of the mixing water was added to the mixture within 30 seconds and mixed at 150 rpm for 2 minutes, as shown in Figure 4.4.

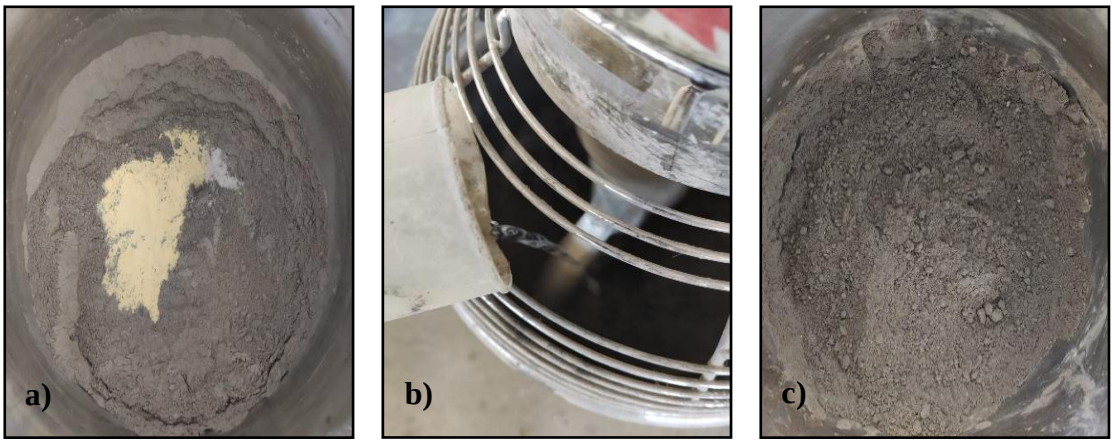

Figure 4.4. a) Adding HRWRA and SRA in a mixing bowl, b) Adding water into the mixture, c) End of the mixing stage

After 2nd stage, the mixer was stopped, and half of the amount of HRWRA and the total amount of SA were added to the mixture. Once the mixer was restarted, one-third of the mixing water was added to the mixture within 30 seconds and mixed at 150 rpm for 3 minutes, as shown in Figure 4.5.

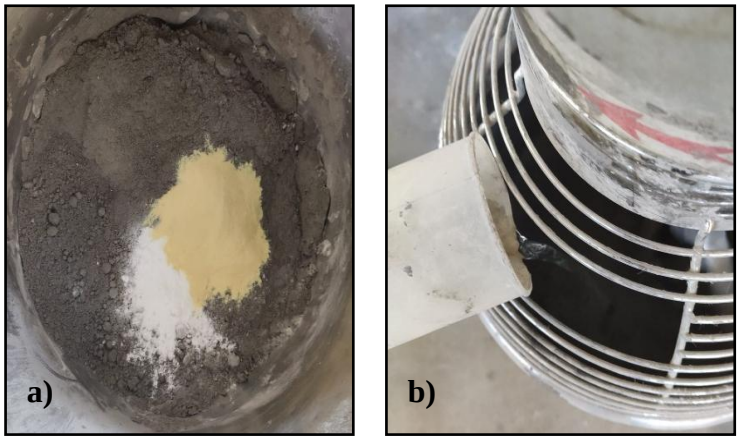

Figure 4.5. a) Adding HRWRA and SA in mixing bowl, b) Adding water into the mixture

The last stage involved mixing the prepared mortar mixture at 265 rpm for 1 minute to obtain homogeneous mortar without clumping, as shown in Figure 4.6.

Figure 4.6. Final mortar mixture

All components, their proportions in the mixture, and the mixing processes of the cementitious main matrix mixture were determined up to this stage. Lastly, mixing times were determined for four mixing stages to ensure a homogeneous distribution of conductors when incorporating conductive materials into the main matrix mixture.

4.1.4.2. Determining Mixing Time of the Cementitious Matrix

There were four main mixing stages in preparing the cementitious matrix mixture, and each mixing time was different. However, considering the effect of mixing times on the workability and mechanical performance of the mortar mixture and the homogeneous dispersion of conductive materials into the mixture, it was decided to determine the optimum mixing time for each mixing stage. In this context, mixing times were varied for all stages of the mixing process. Firstly, the preparation time for the dry mixture varied between 3 and 10 minutes. The effects of mixing time on 2-hour strength and slump flow time are given in Table 4.13.

Table 4.13. Effect of mixing time of 1st stage on 2-hour strength and flowability

Stages (min)				**Slump Flow Time (s)**	**2-Hours Compressive Strength (MPa)**
1st	**2nd**	**3rd**	**4th**		
3	2	3	1	3.80	30.37
5				4.62	30.20
7				3.55	28.80
10				3.55	30.43

According to Table 4.13, the increasing mixing time of the first stage did not significantly affect the flowability of the samples. Literature studies mentioned that conductive materials could be incorporated into a matrix using the synchronous admixing method [138,167,190]. In addition, the highest compressive strength was measured as 30.43 MPa based on the strength results. Besides strength value, obtaining a uniform dispersion of the conductive materials in the matrix, the mixing time of the first stage was selected as 10 minutes. In the second mixing stage, half of the amount of HRWRA and the total amount of SRA were added, and the preparation time for the second stage varied between 2 and 8 minutes in terms of the mixing behavior of the mixture. The effects of mixing time on 2-hour strength and slump flow time are given in Table 4.14.

Table 4.14. Effect of mixing time of 2nd stage on 2-hour strength and flowability

Stages (min)				Slump Flow Time (s)	2-Hours Compressive Strength (MPa)
1st	2nd	3rd	4th		
10	2	3	1	4.39	30.43
	4			18.60	27.30
	6			25.00	26.37
	8			50.10	0.00

According to Table 4.12, the increasing mixing time of the second stage directly affected the flowability and strength of the samples. For this reason, the mixing time of the second stage was selected as 2 minutes regarding both mechanical and physical concerns. In the third mixing stage, half of the amount of HRWRA and the total amount of SA were added to the mixture, and the preparation time for the third stage varied between 3 and 10 minutes in terms of the homogeneity of the mixture. The effects of mixing time on 2-hour strength and slump flow time are given in Table 4.15.

Table 4.15. Effect of mixing time of 3rd stage on 2-hour strength and flowability

Stages (min)				Slump Flow Time (s)	2-Hours Compressive Strength (MPa)
1st	2nd	3rd	4th		
10	2	3	1	4.50	30.43
		5		6.19	30.77
		7		9.19	30.83
		10		18.85	29.20

According to Table 4.15, the increasing mixing time of the third stage affected flowability significantly. However, the compressive strengths of the mixtures mainly remained the same. For this reason, the mixing time of the third stage was selected as 3 minutes regarding physical performance. A mortar mixture was obtained after completing this stage. Additionally, literature studies observed that conductive materials could be incorporated into a mortar matrix using the latter admixing method [166,191], and the preparation time for the final stage varied between 1 and 5 minutes in terms of the mixing

behaviour of the mixture. The effects of mixing time on 2-hour strength and slump flow time are given in Table 4.16.

Table 4.16. Effect of mixing time of the 4th stage on 2-hour strength and flowability

Stages (min)				Slump Flow Time (s)	2-Hours Compressive Strength (MPa)
1st	2nd	3rd	4th		
10	2	3	1	3.28	30.43
			2	4.50	31.90
			3	3.75	32.73
			5	3.75	31.77

According to Table 4.16, the increasing mixing time of the last stage did not significantly affect the flowability and strength of the samples. The results showed that the highest compressive strength was 32.73 MPa for 3 minutes. Therefore, the mixing time of the third stage was selected as 3 minutes to obtain both the highest compressive strength and flowable mortar, as well as dispersion of conductive materials.

4.1.5. Development of Main Cementitious Mortar Mixture

In the first stage of the thesis study, a matrix mixture to which conductive materials would be added was developed. Using optimum raw materials, high flowability, early age high strength, and crack-free surface were achieved. In addition, the mixing method and mixing times for the matrix to have high performance were also determined. The s/c and w/c ratios were maintained at 0.6 and 0.3 for all mixtures. The total weight of binders was calculated as the total weight of CEM I 52.5R and CAC. Both sustain optimum fresh and mechanical performance and prevent the agglomeration of conductive fibers; 2.5% silica fume and 2% HRWRA, 0.2% SRA, and 0.5% SA by the total weight of the binders were used in the mixtures. The mix proportions of the final matrix are given in Table 4.17.

Table 4.17. Mixture proportions of cementitious composites

Materials	**Amount (kg/m^3)**
CEM I 52.5R	716
CAC	477
CŠ	72
Sand	716
Silica fume	30
HRWRA	24
Set accelerator (SA)	6
Set retarder (SRA)	2.5
Water	358

In terms of mechanical performance, the compressive strength results of different ages of the final cementitious composite mixture are given in Table 4.18. Besides mechanical properties, the flow diameter was measured as 41.5 cm, and the slump flow time was measured as 3.75 seconds in the final mix.

Table 4.18. Early and later age of compressive strength results in the final cementitious composite mixture, MPa

Early age Strength Results	**1 hour**	**2 hours**	**3 hours**	**6 hours**	**24 hours**
	0	32.73	33.50	35.80	36.90
Ultimate Strength Results	**1st day**	**3rdday**	**7th day**	**28th day**	**90th day**
	36.90	54.90	63.80	75.10	86.10

Although no strength could be measured at 1 hour, the 2-hour compressive strength was 32.73 MPa, and the one-day compressive strength was 36.90 MPa for the final mix. This difference between 1-hour and 2-hour compressive strength results was due to the type of CAC preferred, Isıdaç 40, and the usage of ternary-based systems. High amounts of ettringite formation occurred at the early stages of the hydration reaction in the ternary system. Thus, the strength of the mixture increased with time shortly [53,78]. In addition, the increased tricalcium silicate (C_3S) and tricalcium aluminate (C_3A) contents contributed to early age high strength [31]. However, as the number of fine particles increased in the mixture, the total amount of voids in the matrix could be filled better or

smaller, and high compressive strength could be obtained with a dense microstructure [217]. In addition to the filling effect, the early age compressive strength of the matrix was improved by providing OH^- ions and extra nucleation sites along with alkalis to the pore solution due to the high surface area of materials [218]. Moreover, early age high strength was achieved with combinations of the optimum usage of the setting accelerator, retarder additives in the ternary system [96]. This means that the reference coating mixture can be serviced within 2 to 3 hours on the surfaces where it is applied. For the reference sample, the compressive strength increased continuously. It was observed that the reference mixture reached 40-50%, 50-60%, 70-75%, and 85-90% of their ultimate compressive strength (90-day strength values) after 1, 3, 7, and 28 days, respectively. As of the 90^{th} day, the strength had reached 86.10 MPa. Considering that the durability of the mixture and its compressive strength properties are directly proportional, the high compressive strength of the developed composite also shows that it is durable [31]. Besides its physical and mechanical properties, the reference mixture's electrical resistance (Ω) results on different measurement days were determined from the coating and cylinder samples. The Electrical resistance (ER) results from the coating sample, which is the reference final cementitious composite mixture at different ages, are given in Table 4.19.

Table 4.19. ER results of coating of the reference mixture, MΩ

Electrical Resistance Results	**1^{st} day**	**3^{rd} day**	**7^{th} day**	**28^{th} day**	**90^{th} day**	**180^{th} day**
	15.40	20.80	33.20	65.40	75.30	104.50

As seen from Table 4.19, the ER value was determined to be 15.40 MΩ on the first day of the reference mixture. ER value on the 180^{th} day increased by seven times, approximately to 104.50 MΩ. The ER results of the anti-static protection capability of cementitious coating designs should be lower than 1 MΩ in every measurement [19,20,148,149]. For this reason, the reference mixture without conductive material incorporation did not show electrical conductivity performance and even had insulating properties. Thus, the aim was to reduce ER results by incorporating conductive materials into the matrix mixture. Moreover, ER results from the cylindrical sample, which is the reference final cementitious composite mixture at different ages, are given in Table 4.20.

Table 4.20. ER results of cylindrical parts of the reference mixture, kΩ

Parts of the cylinder	**1st day**	**3rd day**	**7th day**	**28th day**	**90th day**	**180th day**
Bottom	0.521	0.785	1.500	19.820	162	226
Middle	0.552	0.768	1.350	17.600	168	223
Top	1.600	50.600	90.300	190	626	773

As seen from Table 4.20, ER values of cylindrical parts were increased with curing time. The bottom and middle parts of the reference mixture had approximately similar electrical resistance values regardless of curing time. In contrast, the ER results of the upper part were 4 to 90 times higher than the other parts. The reason was that the upper layer surface was directly exposed to external environmental conditions. According to ER results, the reference mixture generally showed insulating performance that was far from electrically conductive. However, the ER values of the developed coating design were expected to be similar for different parts of coating and curing times in the thesis study. Therefore, ER results were expected to be similar between layers in mixtures with fiber addition. Along with the experimental studies, SEM and EDX analysis were performed to determine the mineralogical structure taken in samples after the 28th-day compressive strength measurement, shown in Figure 4.7.

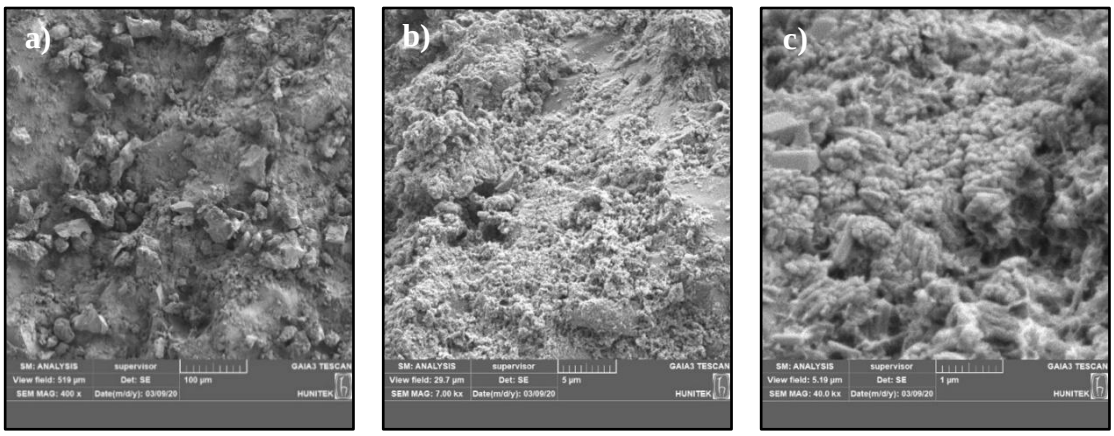

Figure 4.7. SEM images of the reference specimen at magnifications of a) 400 x, b) 7 kx, and c) 40 kx

In Figure 4.7, the microstructure image was obtained by magnification of the reference mixture at different scales. In Figure 4.7-a, complex structures were observed on the examined area for a 400-x scale. Sharp plates and covered or agglomerated structures were formed with smooth surfaces in the area. In order to determine structures, the scale of the existing image was increased. In Figure 4.7-b, the 7-kx scaled image showed higher content of interlocking spiral structures than flat surfaces, compared to a 400-x scaled image. It was predicted that the structures formed here were predominantly C-S-H gel and portlandite formation (CaOH) [31]. Thus, a PC-rich system was preferred in the development of early age high-strength. In the first stages of the hydration reaction, the development of ettringite (AFt) was expected as the main structure, and strätlingite, hydrogarnet, gibbsite, and monosulfate (AFm) structures were expected to be formed due to the use of CAC as the second binder [59,90]. Due to the fact that the matrix was a PC-rich system in the ongoing hydration reaction, it was expected that portlandite formation would be detected along with the formation of a higher proportion of C-S-H gel, ettringite, and monosulfate [89]. In Figure 4.7-b and Figure 4.7-c, the structures were detected as C-S-H gel and portlandite as a secondary product for 28 days. In Figure 4.7-c, it was observed that relatively thicker plates were formed in rectangular shapes as well as the helical structure. Rectangular shapes were referred to as portlandite and gibbsite formations. In contrast, helical structures were referred to as C-S-H gel formation. In addition, no micro-scale pores or cracks in the microstructure were found in the examined area. In order to understand the micro-structure formations in the obtained image more clearly, EDX analysis was also performed, and the formed elements are examined in Figure 4.8.

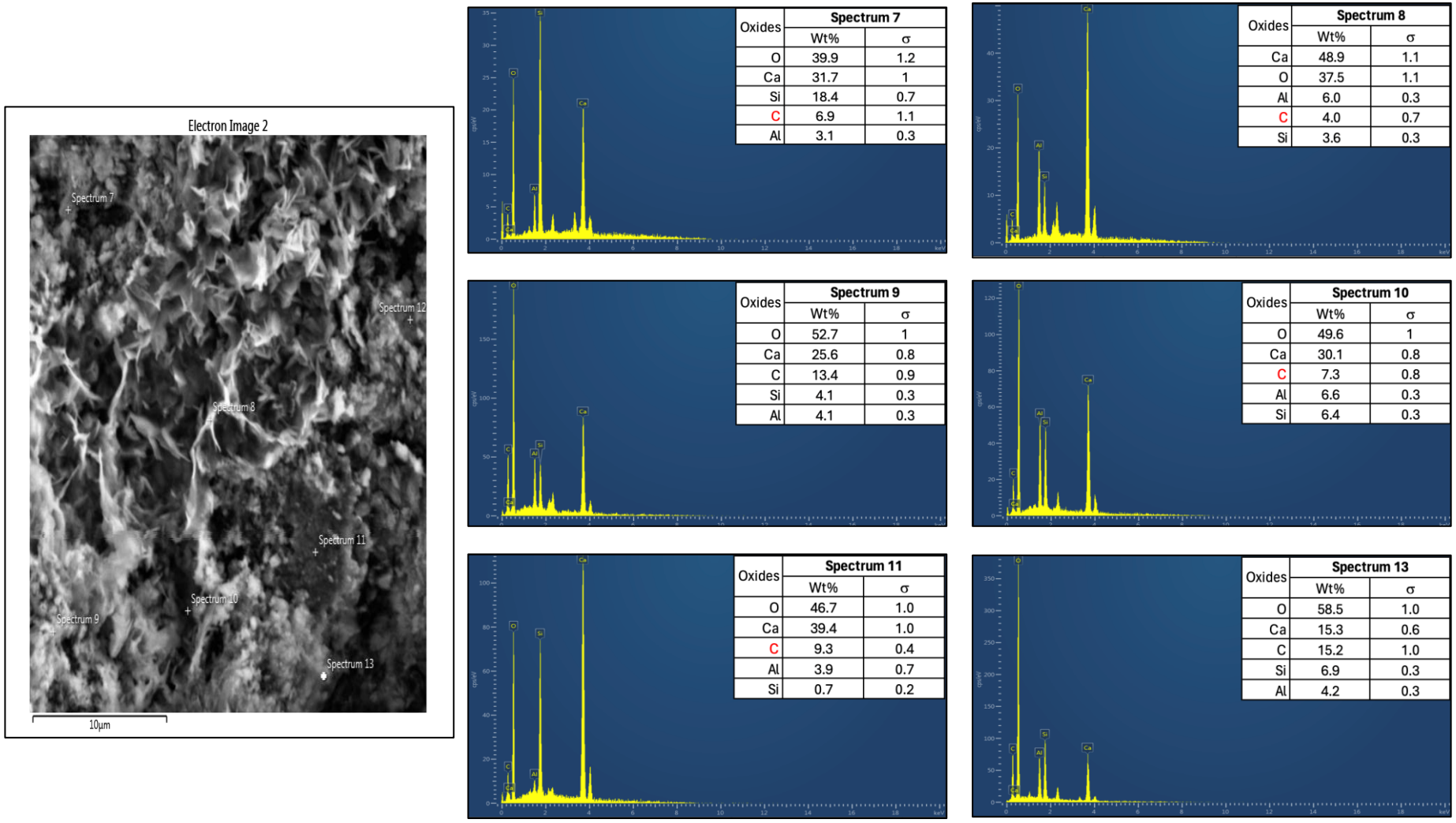

Oxides	Spectrum 7	
	Wt%	σ
O	39.9	1.2
Ca	31.7	1
Si	18.4	0.7
C	6.9	1.1
Al	3.1	0.3

Oxides	Spectrum 8	
	Wt%	σ
Ca	48.9	1.1
O	37.5	1.1
Al	6.0	0.3
C	4.0	0.7
Si	3.6	0.3

Oxides	Spectrum 9	
	Wt%	σ
O	52.7	1
Ca	25.6	0.8
C	13.4	0.9
Si	4.1	0.3
Al	4.1	0.3

Oxides	Spectrum 10	
	Wt%	σ
O	49.6	1
Ca	30.1	0.8
C	7.3	0.8
Al	6.6	0.3
Si	6.4	0.3

Oxides	Spectrum 11	
	Wt%	σ
O	46.7	1.0
Ca	39.4	1.0
C	9.3	0.4
Al	3.9	0.7
Si	0.7	0.2

Oxides	Spectrum 13	
	Wt%	σ
O	58.5	1.0
Ca	15.3	0.6
C	15.2	1.0
Si	6.9	0.3
Al	4.2	0.3

Figure 4.8. EDX analysis results of the points determined by the 10 µm scaled image of the reference sample.

As seen from Figure 4.8, in the elemental examination conducted at various points to determine the structures of different shapes and forms in the examined area, the main phases identified were calcium (Ca), oxygen (O), silicon (Si), aluminum (Al), carbon (C), and low amounts of gold (Au). The reason for the presence of the gold element in the matrix was that the samples were coated with gold before analysis. Additionally, there was a high amount of oxygen (O) in the matrix due to the samples being kept in the laboratory environment and the porous structure of the matrix. In ternary systems, the percentage of Ca ions varied by 25-50%, while Al ions varied by 1-8% due to predominantly PC in the matrix. According to the analysis of the spiral structure (spectrum 7), a high amount of silicon formed. The presence of high amounts of Si in the matrix due to silica fume was an expected result. In the 13th spectrum, a darker-colored formation was observed compared to the other structures. At the same spectrum, 60% of oxygen formed due to the void/crack of the related structure.

4.2. Single Addition of Conductive Material into the Cementitious Matrix

In this study, mixtures containing conductive fibers with different utilization rates were manufactured using three different mixing methods. The mixtures were assessed for physical, mechanical, and electrical properties. Furthermore, SEM/EDX analyses were carried out on the mixtures with the lowest electrical resistivity (ER) values.

4.2.1. Flow Diameter and Flow Time Values of Composites with Single Conductive Material Incorporation

The flow diameter and slump flow time results from mini-slump tests were evaluated for mixtures containing MCF, CF, and SF, which were incorporated into cementitious matrices in single using various mixing methods. The reference sample's diameter and flow time, having no conductive materials, were 41.5 cm and 3.75 seconds, respectively. Among the CF-based mixtures, the samples indicated with "B(1)" were prepared using the synchronous admixing method, and the samples indicated with "B(2)" were prepared

using the latter admixing method. The flow diameter and flow time results for mini-slump tests of CF-based mixtures are shown in Figure 4.9.

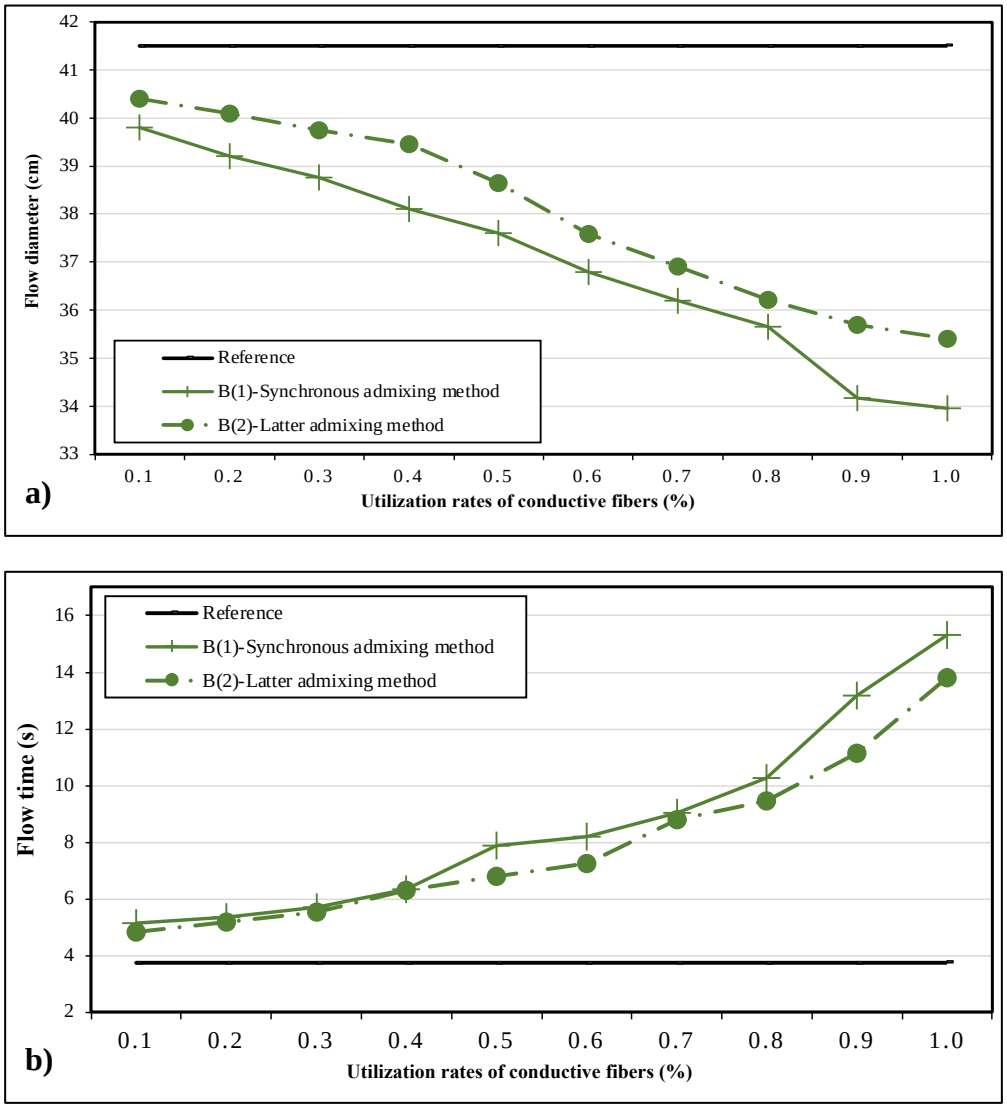

Figure 4.9. a) Flow diameter results for CF-based mixtures, b) Flow time results for CF-based mixtures

As seen from Figure 4.9-a, the highest flow diameter was measured as 40.4 cm from a mixture containing 0.1% CF addition prepared by the latter admixing method. In mixtures prepared by the latter admixing method, the flow diameter of CF-based mixtures decreased by about 12.40%, down to 35.4 cm, and up to 1.0% CF addition. As seen from Figure 4.9-b, regarding the flow time of mixtures, the lowest flow time was measured as around 4.82 s from a mixture containing 0.1% CF addition in both admixing methods. In

mixtures prepared by the synchronous admixing method, the flow time of CF-based mixtures increased by about 217.80%, up to 15.32 s up to 1.0% CF addition. Incorporating CF regardless of mixing method resulted in a significant decrease in flow diameters, which were also lower than the diameter of the reference mixture. Studies have also reported a decreasing trend for flow diameters of CF-based mixtures. Safiuddin et al. [219] mentioned that the workability and density of the fresh mortar were negatively affected by CF addition, so it also increased the air content of the mixtures. Ghanem and Bowling [220] observed a linear relationship between slump and fiber content. An increased amount of CF resulted in higher porosity and air content. Al-Dahawi et al. [158] mentioned that CF's water-holding characteristic negatively affected workability due to the increased water requirement of the mixtures in higher-contents. According to flow time and flow diameter results, the samples prepared with the latter admixing method showed a better flow diameter than the ones with the synchronous admixing method in all mixtures. Incorporating CF into the aqueous mortar mixture led to higher flow diameters than incorporating it into the dry mixture. In the synchronous admixing method, agglomeration was high due to insufficient contact with water. Therefore, the workability of the mixtures was negatively affected by inhomogeneous dispersion and water-holding properties of the fibers. Among the MCF-based mixtures, the samples indicated with "C(1)" were prepared using the synchronous admixing method, and the samples indicated with "C(2)" were prepared using the first admixing method. The flow diameter and flow time results for mini-slump tests of MCF-based mixtures are shown in Figure 4.10.

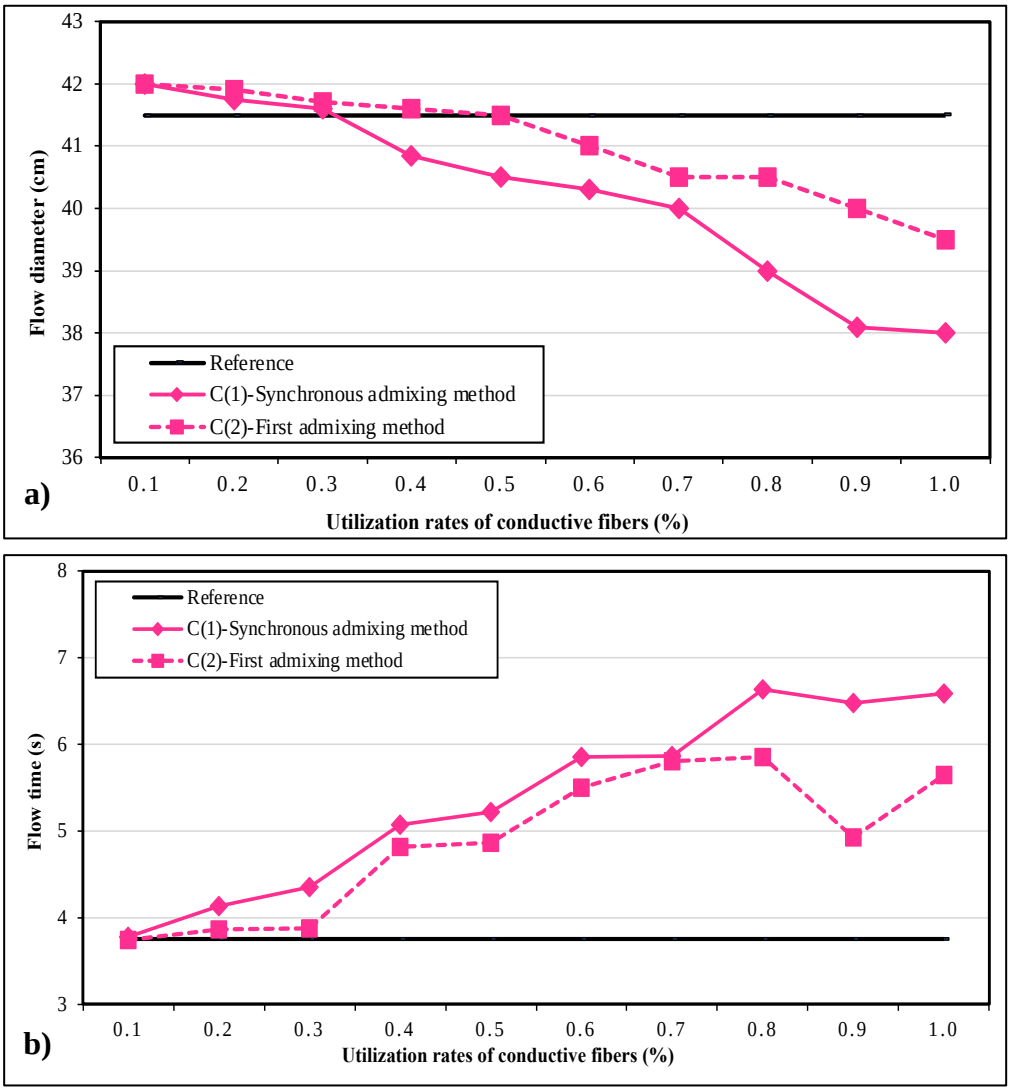

Figure 4.10. a) Flow diameter results for MCF-based mixtures, b) Flow time results for MCF-based mixtures

As seen from Figure 4.10-a, the highest flow diameter was measured as 42.0 cm from a mixture containing 0.1% MCF addition prepared by both admixing methods. In mixtures prepared by the synchronous admixing method, the flow diameter of MCF-based mixtures decreased by about 10%, down to 38 cm, and up to 1.0% MCF addition. As seen from Figure 4.10-b, regarding the flow time of mixtures, the lowest flow time was measured as around 3.78 s from a mixture containing 0.1% MCF addition in both admixing methods and in mixtures prepared by the synchronous admixing method, the flow time of MCF-based mixtures increased by about 74%, up to 6.58 s up to 1.0% MCF addition. Incorporating MCF regardless of mixing method resulted in a significant decrease in flow diameters, which were also lower than the diameter of the reference

mixture. Literature studies indicated that carbon-based materials exhibited water-retention behavior due to their structure and characteristics, adversely impacting the mixtures' workability [158]. The synchronous admixing method led to a lower fluidity between the two mixing methods. One of the reasons why the incorporation of the fibers into a dry mixture affected the fluidity more negatively was the prolonged mixing time, which caused the formation of agglomeration in the matrix due to MCFs holding more water. In addition, carbon fiber addition had a more negative effect on the flow diameter than milled carbon fiber addition. In the literature, similar results have also been reported. Rieger et al. [221] investigated the effect of the short carbon fiber (3mm) and milled carbon fiber ($\leq$ 0.5 mm) on the rheological behavior of the mixture. The results indicated that milled carbon fibers had a minimal impact on flow performance. In contrast, short carbon fibers significantly increased viscosity and reduced workability due to the interlocking mechanism of the fibers. Among the SF-based mixtures, the samples indicated with “A(1)” were prepared using the synchronous admixing method, and the samples indicated with “A(2)” were prepared using the latter admixing method. The flow diameter and flow time results for mini-slump tests of SF-based mixtures are shown in the Figure 4.11.

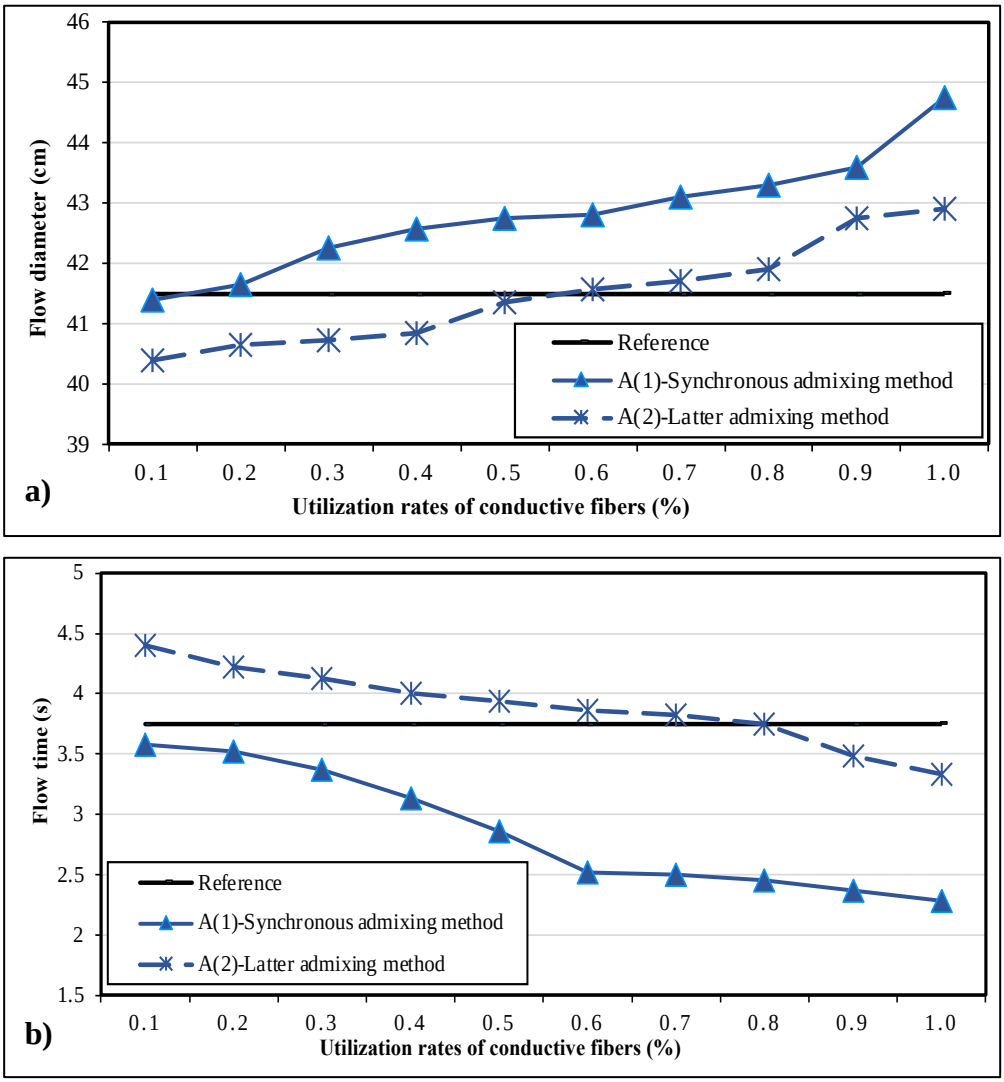

Figure 4.11. a) Flow diameter results for SF-based mixtures, b) Flow time results for SF-based mixtures

As seen from Figure 4.11-a, the highest flow diameter was measured as 44.75 cm from a mixture containing 1.0% SF addition prepared by the synchronous admixing method. In Figure 4.11-b, regarding the flow time of mixtures, the lowest flow time was measured as around 2.28 s from a mixture containing 1.0% SF addition prepared by the synchronous admixing method. With SF addition to mortar mixtures, flowability improved regardless of the mixing method as opposed to MCF and CF. In the latter admixing method, the flow diameter exceeded that of the reference sample after 0.7% SF incorporation. In contrast, synchronous admixing showed a higher flow diameter than the reference sample after 0.2% SF incorporation. Additionally, literature studies have reported an incremental trend with SF addition for flow diameter and flow rate. Majain et al. [222] reported that steel

fibers might negatively affect the workability of the mixture, resulting in segregation and bleeding, especially in higher contents. At the same time, the higher content of steel fiber was also caused by inhomogeneous distribution in the matrix. Ozyurt et al. [223] observed that the workability of the mixtures affected fiber dispersion and tensile strength of steel-based cementitious mortars. There were some reasons for this behaviour. A higher flow diameter was obtained when heavy materials fell into the mortars while lighter materials seeped to the surface [115]. For this reason, it was predicted that the higher density of steel fibers significantly affected the workability compared to other fibers. Secondly, Sameera et al. [224] stated that the performance of concrete structures was improved by using different types of steel fiber. This was due to the shape of the steel fiber, which affected failure modes. Although cementitious mortar's workability and strength properties were mainly dependent on the composition and mixing proportions, the fiber type also impacted these properties. Ramakrishan et al. [225] investigated the performance properties of cementitious composite using four different types of fibers: hooked-end steel, straight steel, corrugated steel, and polypropylene. Among the fibers, balling tendency was observed from straight steel fiber matrix in higher contents. In the case of hooked-end steel fibers, the maximum number of fibers could be incorporated without balling and segregation. In this study, brass-coated straight steel fiber was used as SF in the mixtures. Therefore, it was predicted that the higher flow diameter than the reference sample might also occur due to the shape of the steel fiber. Thirdly, Majain et al. [222] observed that a small aspect ratio of steel fibers could result in a higher flowability of steel fiber-based composites. Alrawashdeh and Eren [226] investigated the mechanical and physical characterization of steel fiber-reinforced self-compacting concrete using different aspect ratios and volume fractions of fibers. Based on the results, the workability and rheology decreased, flexural strength increased, the toughness and the ultrasonic velocity results increased, and the permeability results decreased in the case of an increase in aspect ratio from 60 to 80. In this study, the aspect ratio of the used steel fiber is 65. It was predicted that the flow diameter was higher than the reference mixture in this study because of the physical properties of steel fiber. Nevertheless, the increase detected was more pronounced in the samples (after adding 0.2% SF) prepared using the synchronous admixing method (adding SF to the dry mixture) than in the reference sample. Based on the results, the technical properties of the steel fibers affected the mixture's fresh properties more when the synchronous admixing method was used. On

the other hand, SF showed better adherence in the mixture for mixtures prepared with the latter admixing method when SF first mixed with an aqueous mortar mixture.

In conclusion, the mixing method significantly impacted the workability of fresh mortar. In addition, the synchronous admixing method negatively impacted the fresh mortar properties of the mixtures among all fibers. In MCF and CF-based composites, the synchronous admixing method negatively affected the workability due to the holding water properties and inhomogeneous dispersion of fibers. In the SF-based mixture, the synchronous admixing method significantly improved the flow diameter due to the type and density of the steel fiber and its inhomogeneous dispersion.

4.2.2. Compressive Strength Results of Composites with Single Conductive Material Incorporation

Average compressive strength results of mixtures containing MCF, CF, and SF were measured for different curing ages of 1, 3, 7, 28, and 90 days are shown in Figure 4.12. In the figure, A, B, and C represent steel fiber, carbon fiber, and milled carbon fiber-based mixtures, respectively.

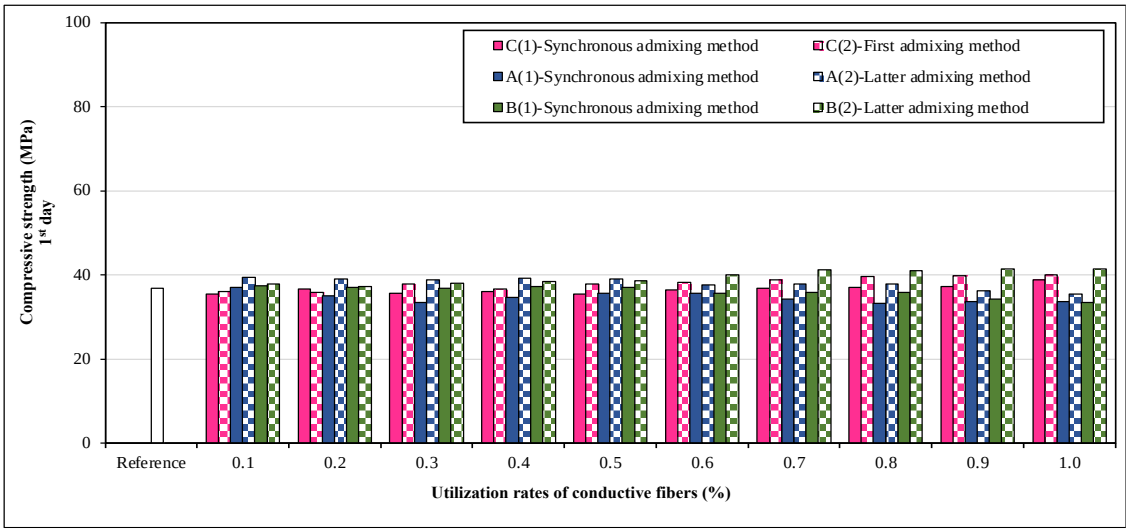

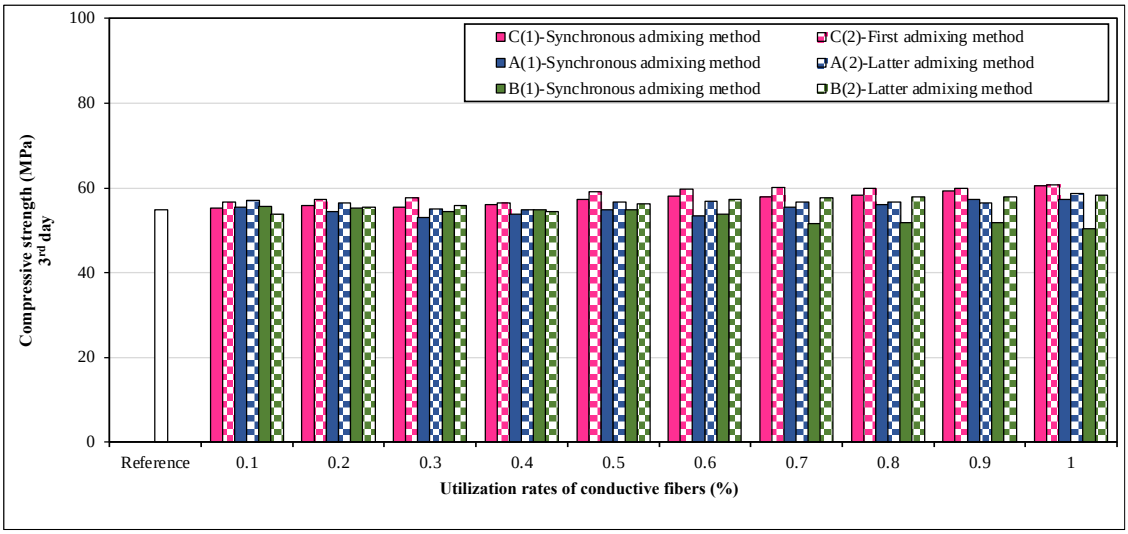
C(1)-Synchronous admixing method
C(2)-First admixing method
A(1)-Synchronous admixing method
A(2)-Latter admixing method
B(1)-Synchronous admixing method
B(2)-Latter admixing method
Compressive strength (MPa) 3rd day
100
80
60
40
20
0
Reference
0.1
0.2
0.3
0.4
0.5
0.6
0.7
0.8
0.9
1
Utilization rates of conductive fibers (%)

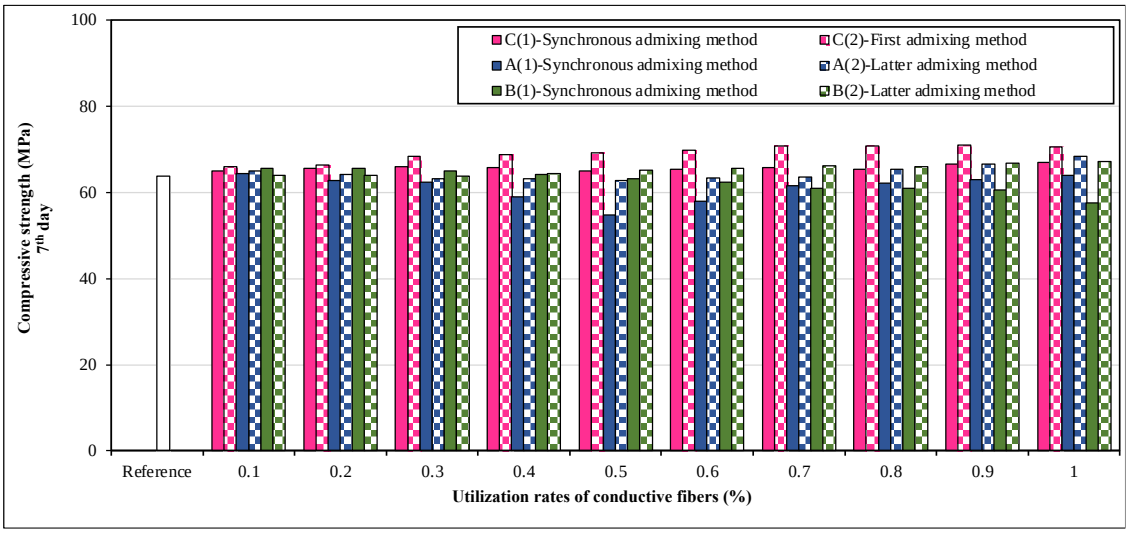
C(1)-Synchronous admixing method
C(2)-First admixing method
A(1)-Synchronous admixing method
A(2)-Latter admixing method
B(1)-Synchronous admixing method
B(2)-Latter admixing method
Compressive strength (MPa) 7th day
100
80
60
40
20
0
Reference
0.1
0.2
0.3
0.4
0.5
0.6
0.7
0.8
0.9
1
Utilization rates of conductive fibers (%)

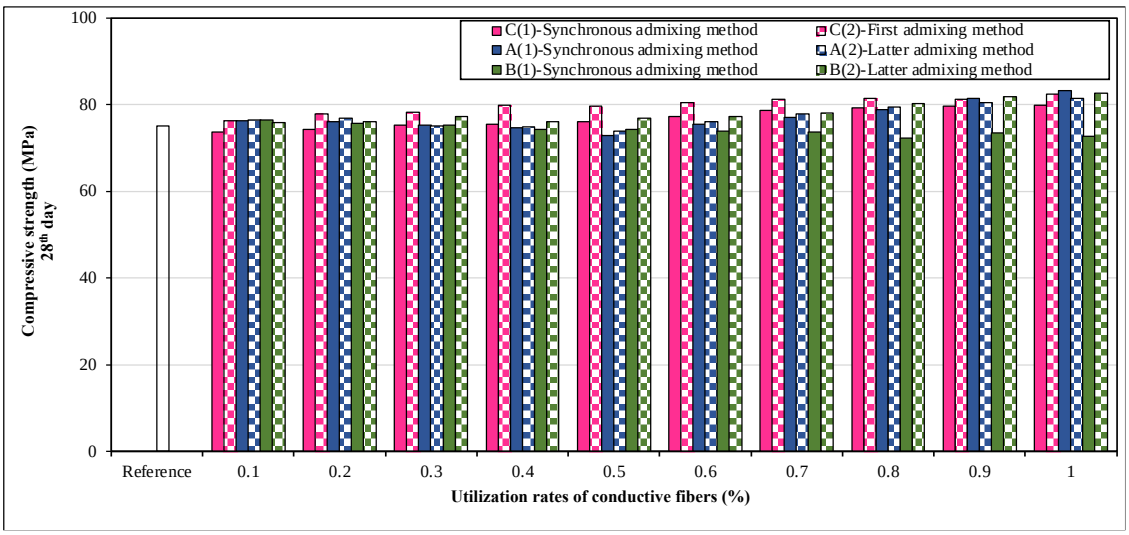
C(1)-Synchronous admixing method
C(2)-First admixing method
A(1)-Synchronous admixing method
A(2)-Latter admixing method
B(1)-Synchronous admixing method
B(2)-Latter admixing method
Compressive strength (MPa) 28th day
100
80
60
40
20
0
Reference
0.1
0.2
0.3
0.4
0.5
0.6
0.7
0.8
0.9
1
Utilization rates of conductive fibers (%)

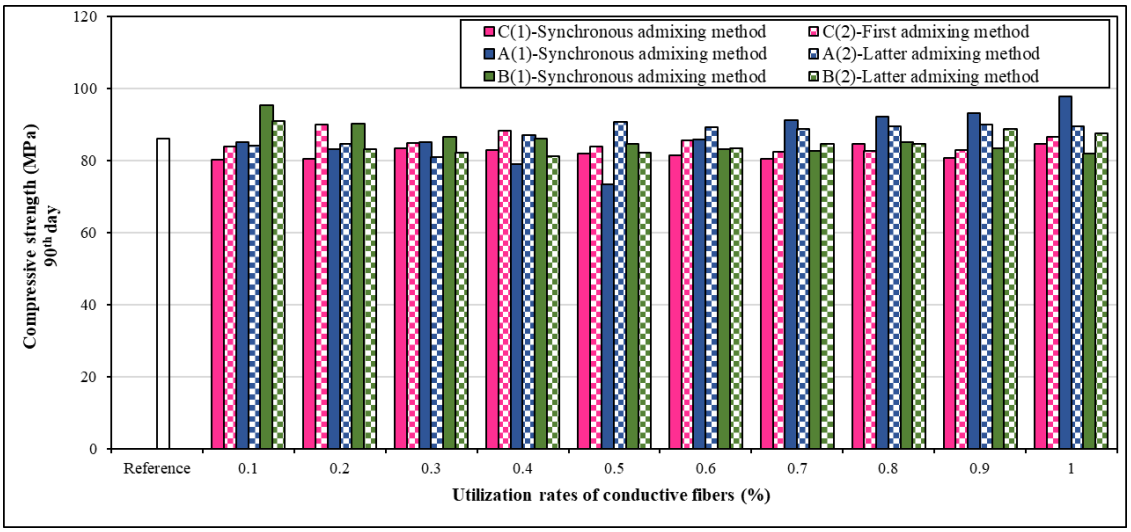

Figure 4.12. Compressive strength results of composites with single conductive material incorporation after different curing ages

It was found that all specimens had an incremental strength trend over time, regardless of the type of fiber or mixing method used. In general, it was observed that all mixtures gained 40-50%, 50-60%, 70-75%, and 85-90% of their ultimate compressive strength (as measured on the 90th day) after 1, 3, 7, and 28 days, respectively. Meanwhile, compressive strength was influenced by conductive fiber type, utilization rate, and the dispersion method. So, the results were obtained in a wide range. As the MCF content increased in the mixtures, compressive strength was improved in the 3-11% range at all ages. The highest strength was measured from a mixture containing 1.0% MCF addition prepared by both admixing methods. Akbar et al. [167] studied the microstructural changes and mechanical performance of recycled MCFs-based cement composites, whose lengths ranged from 80–100 µm. In the SEM images, grooves or small channels of varying depths and widths were visible along the fiber axis of MCFs. These formations were also observed in MCF used mixtures in these systems. MCFs and hydrated cement paste could be mechanically interlocked and better interfacially bonded with these defects and channels, enhancing the structure's compressive strength. These formations with relatively large widths and depths achieved a denser microstructure, providing effective nucleation sites with accumulated hydration products. Therefore, these formations along the fiber axis enhanced compressive strength with the higher content of MCF addition. Regarding the effect of mixing methods on the MCF-based mixtures, mixtures prepared with the first admixing method were slightly higher (1 - 5% higher) than those prepared

with the synchronous admixing method. Higher strength was obtained using the first admixing method by MCFs mixed in the aqueous solution due to uniform dispersion.

Because of the mixing methods, CF-based mixtures had reversed compression strength results for all testing ages. Studies stated that CFs enhanced the cementitious composites' mechanical properties, particularly flexural and compressive strength [227]. There were three main reasons for the improvement in the compressive strength of mixtures with the use of CF: (i) CFs could provide a crack-resistance effect mitigating the initiation and propagation of microcracks in cementitious composites, (ii) CFs absorbed energy by overcoming the fiber pull out or breakage, which can improve the mechanical properties, (iii) some parts of hydration products adhered to CFs enhancing the interfacial bonding between fibers and hydrated cement paste. Jiang et al. [161] investigated the effect of nano- and micro-fibers on cementitious composites' compressive strength and electrical resistivity. In addition to flexural strength, CFs also improved the compression strength of composites in this study. CFs likely prevented longitudinal cracks from developing in specimens under pressure. Han et al. [157] explored that carbon fibers (CFs) improved the mechanical and electrical properties of cementitious materials. SEM images and experimental data demonstrated that this strength improvement was attributed to the fibers' ability to inhibit microcrack growth and absorb energy through fiber pullout.

As for the effect of admixing methods on the compressive strength of mixtures, mixtures prepared using the synchronous method reached higher compressive strengths, up to 0.5% CF addition. In contrast, mixtures prepared using the latter admixing method had higher compressive strengths of up to 1.0% CF addition at all ages. Lower strength in the B10(1) mixture was attributed to the air content, which increased at a higher volume of CF content, and inhomogeneous dispersion or possible agglomeration of fibers. Chung [182] found that the mechanical performance of fiber-based composites mainly depended on the bonding of fiber and matrix, air content, and homogeneity of fiber dispersion. In uniform dispersion of fibers, higher electrical conductivity performance was observed. Chuang et al. [107] observed that increasing carbon fiber (CF) content improved matrix performance up to a certain point. Beyond that, higher fiber content led to more and larger air voids, negatively impacting compressive strength and electrical conductivity

performances. Therefore, using the optimum number of CFs with an effective mixing method for uniform dispersion was recommended. In the literature, similar conclusions were also drawn [198]. In this study, the samples prepared with the latter admixing method had 10 to 20% higher compressive strength than those prepared with the synchronous admixing method at all testing ages. Aside from the mixing method, it was also attributed to the physical properties of fibers due to the reinforcing effect, which directly affected the compressive strength and related properties of mixtures [161]. Lu et al. [228] investigated the effect of different carbon fiber (CF) lengths (3, 6, and 10 mm) on cement composites. In the study, the flexural strength of 0.5% CF addition increased by 7%, 12%, and 16% using 3-, 6-, and 10-mm fibers, respectively. The CFs resisted cracking by reducing microcracks' initiation and propagation, resulting in higher strengths. In addition, some of the 3-mm fibers were broken or damaged during mixing, highlighting potential production errors. In this study, 12-mm length of carbon fibers (CF) were used. Two possible reasons explained the variations in compressive strength results with mixing methods. First, the admixing method likely caused physical damage to the fibers. Second, the synchronous admixing method may have led to insufficient dispersion of CFs, resulting in agglomeration in some regions of the mixtures. CFs did not show sufficient resistance against the growth of microcracks because of the incorporation method, resulting in lower strength. However, In MCF-based mixtures, fiber length did not affect the compressive strength, unlike in CF-based mixtures. The impact of carbon fiber (CF) length on compressive strength due to the synchronous admixing method was not observed in MCF-based mixtures. Although this method negatively affected the strength of MCF-based mixtures, the impact was less severe than in CF-based mixtures. This was likely compared to the 100-micron MCFs because the 12-mm CFs tended to be damaged or break during mixing, agglomerated in some areas, and increased air content.

In SF-based mixtures prepared with both admixing methods, compressive strength slightly increased when SF content exceeded 0.5%, likely due to SF's ability to bridge microcracks during compression. Except for the first day results, varying admixing methods did not critically affect the mechanical performance on all days. However, the latter admixing method reached 5 to 20% higher strength than the synchronous admixing method on all days. The results were linked to the incorporation way of SFs into the mixture. Adding SFs with the synchronous admixing method increased flow diameters compared to the reference sample, impacting the compressive strength results. In contrast,

better results were measured using the latter admixing method, which improved better adherence between the fibers and the mortar. Banyhussan et al. [229] observed that the mortar phase directly affected strength results more than the fibers. While the mixing method significantly influenced the first day strength results, this effect lessened as the hydration process continued.

In summary, although all mixtures increased compressive strength over time, differences were observed depending on the mixing method used. The first admixing method yielded higher compressive strengths for MCF-based mixtures, while the latter admixing method was more effective for CF-based and SF-based mixtures. Across all conductive materials, the synchronous admixing method consistently had lower compressive strength. Adding conductive materials to the dry mixture negatively impacted the microstructure and, consequently, the compressive strength. However, regardless of the mixing method, all mixtures achieved 1-day compressive strengths between 34.00 – 42.00 MPa, indicating that the developed composites could be suitable for use as repair mortar due to their superior flow characteristics and quick setting time.

4.2.3. Electrical Resistance Results of Composites with Single Conductive Material Incorporation

4.2.3.1. Electrical Resistance Results of Coating Samples

The electrical resistance values of the mixtures were determined using two experimental devices. Average electrical resistance (ER) values were measured from the coating sample of CF-, MCF-, and SF-based mixtures after 1, 3, 7, 28, 90, and 180 days of curing. In measurements, ER results of reference samples having any conductive material were 15.4, 20.8, 33.2, 65.4, 75.3, and 104.5 MΩ, after 1, 3, 7, 28, 90, and 180 days of curing, respectively. Starting from the first day of curing, the reference sample had a very high ER value expressed in MΩ after passing time. The ER results of the MCF-based mixtures until the 180th day are shown in Figure 4.13.

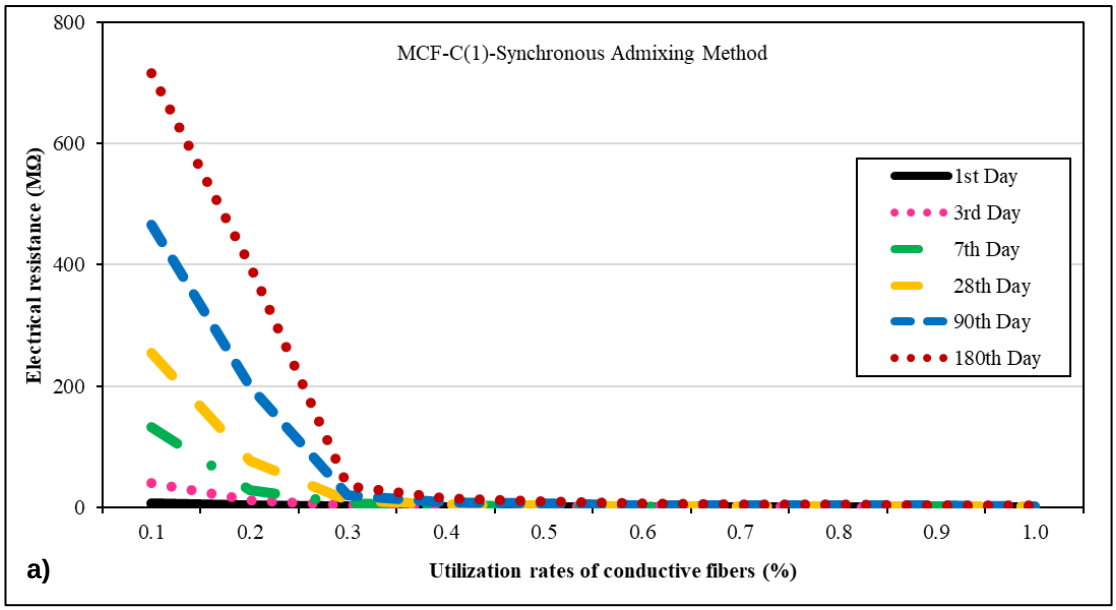
MCF-C(1)-Synchronous Admixing Method
Electrical resistance (MΩ)
800
600
400
200
0
0.1
0.2
0.3
0.4
0.5
0.6
0.7
0.8
0.9
1.0
Utilization rates of conductive fibers (%)
1st Day
3rd Day
7th Day
28th Day
90th Day
180th Day
a)

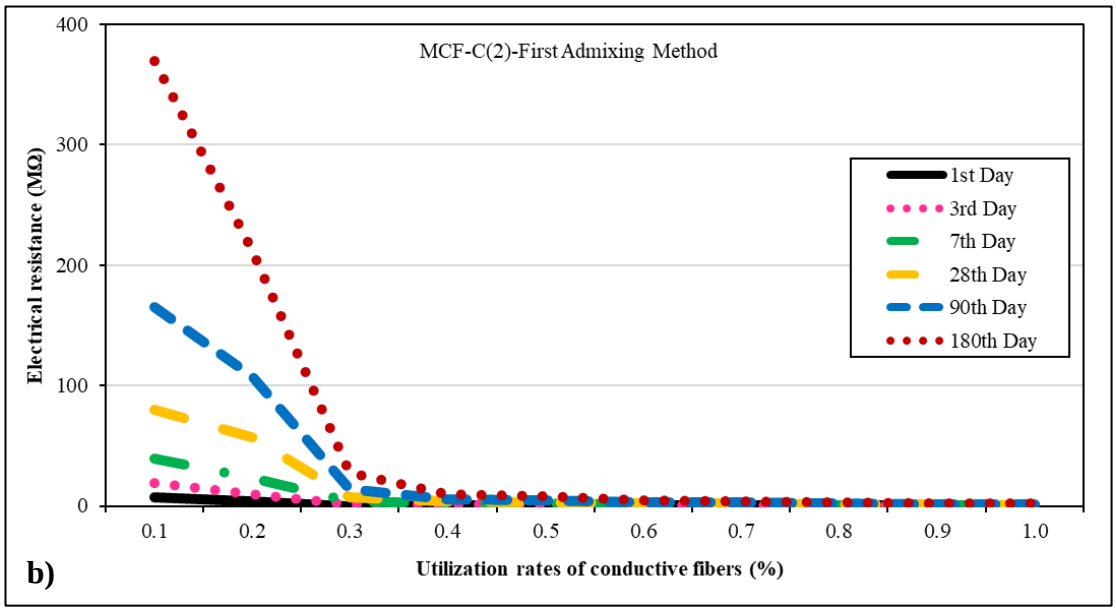
MCF-C(2)-First Admixing Method
Electrical resistance (MΩ)
400
300
200
100
0
0.1
0.2
0.3
0.4
0.5
0.6
0.7
0.8
0.9
1.0
Utilization rates of conductive fibers (%)
1st Day
3rd Day
7th Day
28th Day
90th Day
180th Day
b)

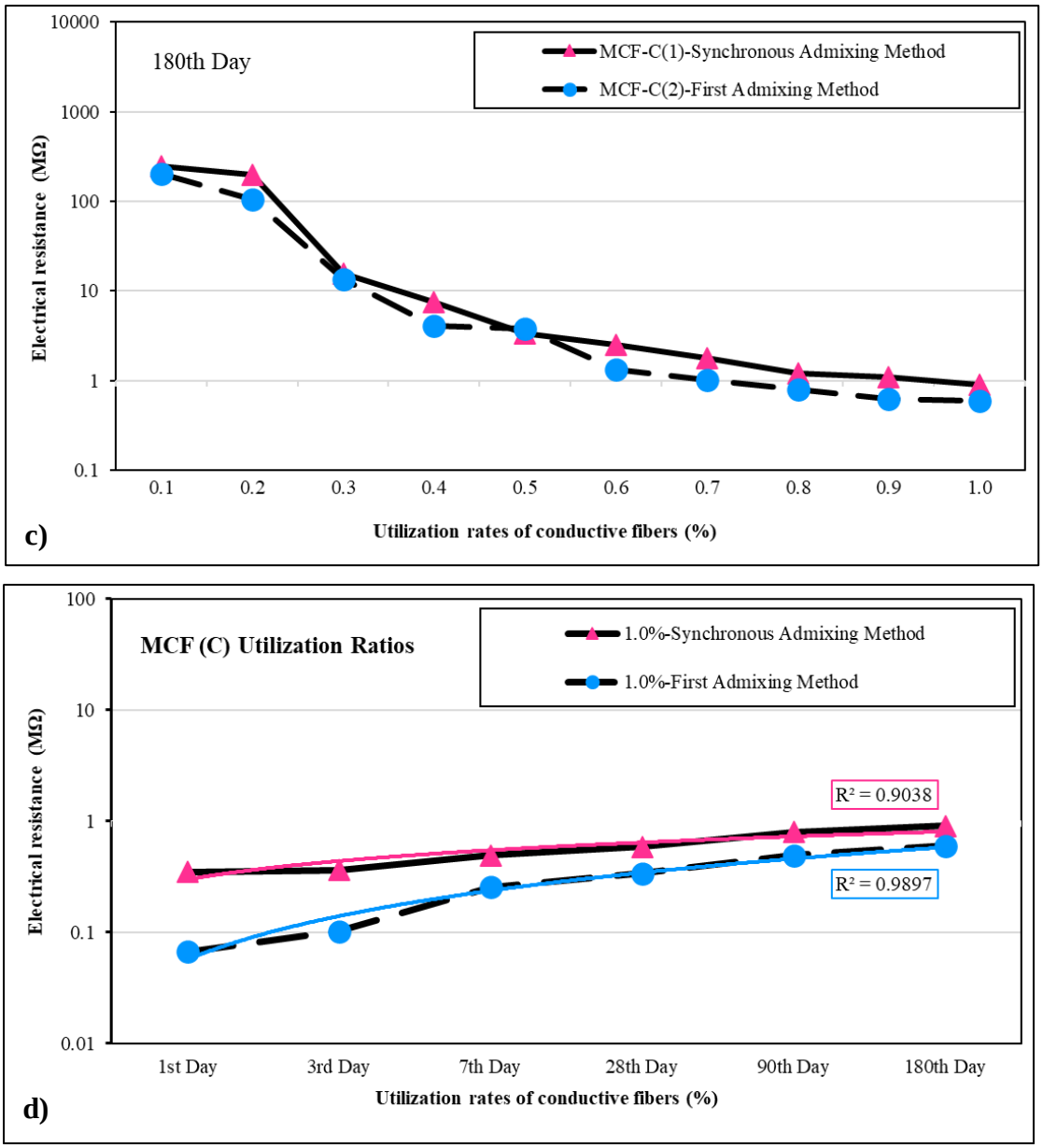

Figure 4.13. Age-dependent ER results of MCF-based composites produced with a) The synchronous admixing method, and b) The first admixing method, Effect of dispersion methods on c) 180-day ER results, d) MCF-based composites having the lowest ER results with age

The effects of the MCF utilization rate and mixing methods on the electrical performance of cementitious composites are shown in Figure 4.13-a and b. As seen from Figure 4.13-a, the 1-day ER of composites using the synchronous admixing method was lower than 1000 kΩ in the presence of MCF exceeding 0.4%. As seen from Figure 4.13-b, the 1-day ER of composites using the first admixing method was lower than 1000 kΩ in the presence of MCF exceeding 0.3%. However, most composites demonstrated insulative

performance because ER values exceeded 1000 kΩ over the long term. Among MCF-based mixtures, the lowest ER value was observed at a 1.0% utilization rate. Based on the ER value limits outlined in relevant standards, the percolation threshold was identified as 0.8% for the first admixing method and 1.0% for the synchronous admixing method [19,20,23,148,149]. So as to obtain high electrical conductivity performance, MCF should be added to a mixture with higher than 1% content. The differences in the 180-day electrical performance results of composites prepared by the synchronous and first admixing methods are shown in Figure 4.13-c. Although neither dispersion method could achieve the desired performance in the long term, the ER results decreased with the incorporation of MCF. Nevertheless, the ER results for all ages were lower in the first admixing method than in the synchronous admixing method because uniform dispersion was obtained when the fibers were mixed with an aqueous solution before being added to the dry mix. Using the synchronous admixing method in MCF-based mixtures, in which fibers were added to dry mix, did not significantly impact the electrical conductivity performance like CF-based mixtures because this method resulted in a lack of conductivity due to the failure to form magnetic paths, insufficient fiber contact with the mixing water, uneven fiber dispersion, and fiber agglomeration within the matrices. No specific utilization rate for MCFs was reported in the literature, and the amount of MCFs ranged from 0.1-16% by weight of total cementitious materials [161,167,230,231]. Although low ER results were observed at MCF utilization rates between 0.11 and 4%, even incorporating up to 1% MCF was not enough for the ESD standards. The limited electrical performance of MCFs was attributed to their short length (100 μm), which restricted the formation of continuous conductive paths. Additionally, using more than 1% MCF increased the overall cost of the composite materials without significant improvements in electrical performance [232,233]. The age-dependent electrical performance of MCF-based composites with the lowest ER results is shown in Figure 4.13-d for different mixing methods. Both methods yielded similar ER results at the specified MCF utilization rates. However, ER values increased over time, likely because the matrices became denser with continuous hydration, which blocked conductive pathways [111,112]. In summary, using MCFs up to 1% was inadequate to provide the electrical conductivity needed for flooring and other construction applications, regardless of the mixing method. The ER results of the CF-based mixtures until the 180th day are shown in Figure 4.14.

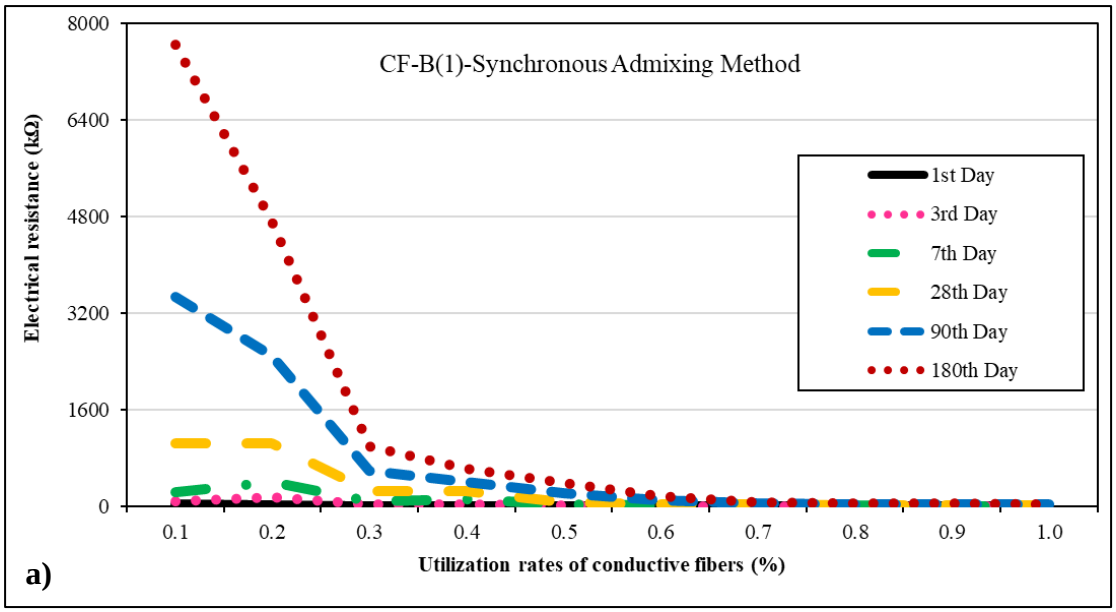
CF-B(1)-Synchronous Admixing Method
Electrical resistance (kΩ)
8000
6400
4800
3200
1600
0
0.1
0.2
0.3
0.4
0.5
0.6
0.7
0.8
0.9
1.0
Utilization rates of conductive fibers (%)
1st Day
3rd Day
7th Day
28th Day
90th Day
180th Day
a)

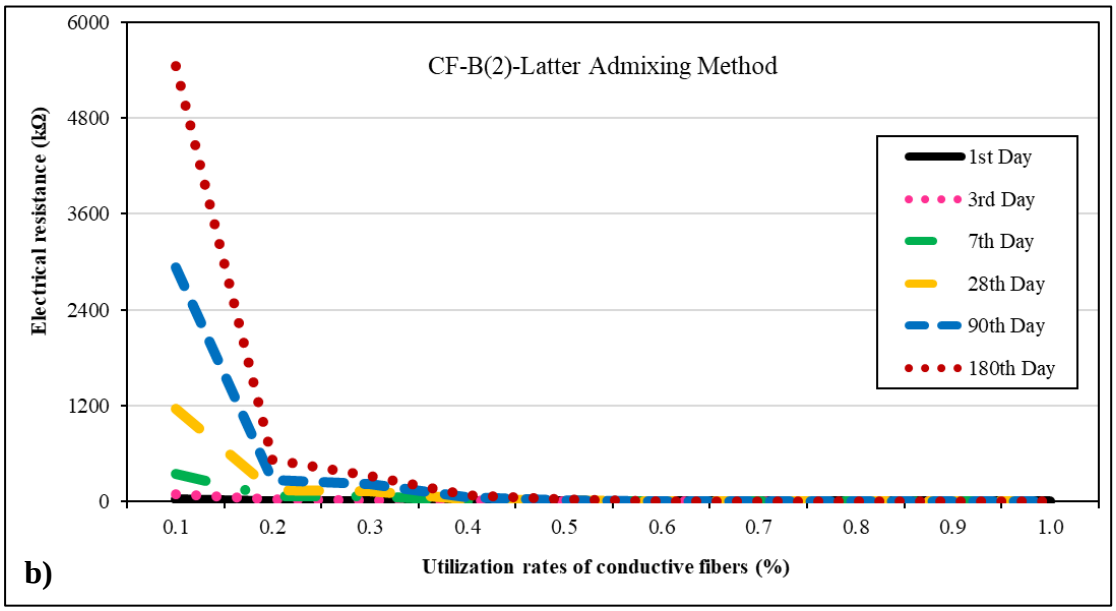
CF-B(2)-Latter Admixing Method
Electrical resistance (kΩ)
6000
4800
3600
2400
1200
0
0.1
0.2
0.3
0.4
0.5
0.6
0.7
0.8
0.9
1.0
Utilization rates of conductive fibers (%)
1st Day
3rd Day
7th Day
28th Day
90th Day
180th Day
b)

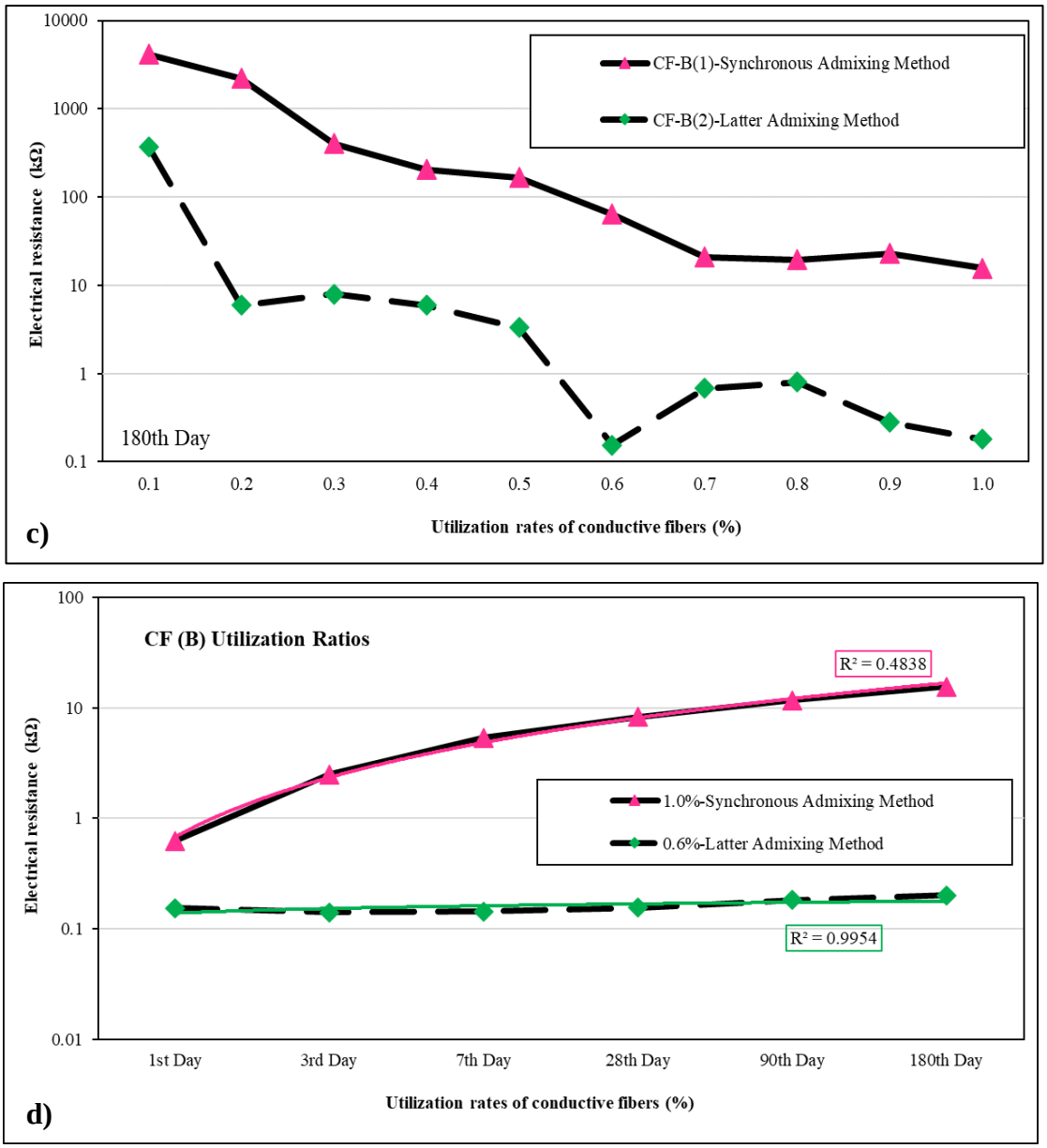

Figure 4.14. Age-dependent ER results of CF-based composites produced with a) The synchronous admixing method, and b) The latter admixing method, Effect of dispersion methods on c) 180-day ER results, d) CF-based composites having the lowest ER results with age

In Figure 4.14-a and b, the effect of CF utilization rate and dispersion method on the time-dependent electrical performance of the composites can be seen. In Figure 4.14-a, the 1-day ER of the composites was measured lower than 30 kΩ with the addition of CF using the synchronous admixing method. The composites demonstrated conductive performance with electrical resistance below the 100 kΩ limit in the long term when 0.6% CF was incorporated into the mixtures. While the lowest ER values were observed with

1.0% CF addition, the percolation threshold was identified at 0.6% CF when using the synchronous admixing method. Beyond this rate, electrical resistance values were reduced minimally. Chen et al. [142] stated that higher CF content generally enhanced the electrical performance of composites. While a higher CF rate could influence the magnetic pathways, exceeding a certain amount of CF did not significantly improve the overall performance of the mixture. In Figure 4.14-b, the 1-day ER of the composites was below 37 kΩ when CFs were added using the latter admixing method. Long-term conductive performance was sustained with a 0.3% CF utilization. While the lowest ER was measured at 0.6% CF, the percolation threshold was identified as 0.3% CF, and the electrical performance of the composites remained consistent beyond 0.6% CF. In Figure 4.14-c, 180-day ER results showed differences between admixing methods. In both methods, ER results decreased with the addition of CFs. However, the latter admixing method yielded better electrical performance due to uniformly dispersed CFs forming the shortest magnetic path at a lower fiber content. Figure 4.14-d shows the age-dependent electrical performance of CF-based composites with the lowest ER results. While similar electrical performance was observed with different mixing methods, the ER results varied with measurement time. However, the ER results remained relatively stable for composites prepared using the latter admixing method at all times. In contrast, composites prepared by the synchronous admixing method showed parabolic increased in ER with age. This behavior was likely due to the denser matrix during hydration, which disrupted the magnetic pathways significantly in the synchronous admixing method [29,110–112,115].Thomoglou et al. [234] stated that adding 0.5% CF into the mixture using the synchronous admixing method resulted in a resistance of 1136 Ω. In addition, ER decreased to 312 Ω in the combination of 0.2% nano-sized multi-walled carbon nanotubes (MWCNTs) and 0.5% CF. Therefore, it was concluded that the hybrid usage of conductive materials provided a more comprehensive conductive network and helped to reduce the resistance value significantly even when the synchronous admixing method was used. According to the literature, CFs were typically added to cementitious matrices in proportions ranging from 0.2 to 5.0% by the weight of the total cementitious content [107,114,158,198], using the first admixing method, the latter admixing method, or the synchronous admixing method [120,151,155,166]. In these studies, low ER results were measured at 0.3 - 3.0% CF utilization rates [169]. On the other hand, the superior electrical conductivity performance was obtained with the lowest CF content in the thesis study without using dispersants, defoamers, high levels of mineral additives, or curing

processes, unlike the literature studies. Additionally, incorporating fibers into the mixtures increased the overall cost of the composites. Therefore, minimizing the use of conductive materials to reduce costs was crucial, especially in large-scale flooring applications [233]. The ER results of the SF-based mixtures until the 180th day are shown in Figure 4.15.

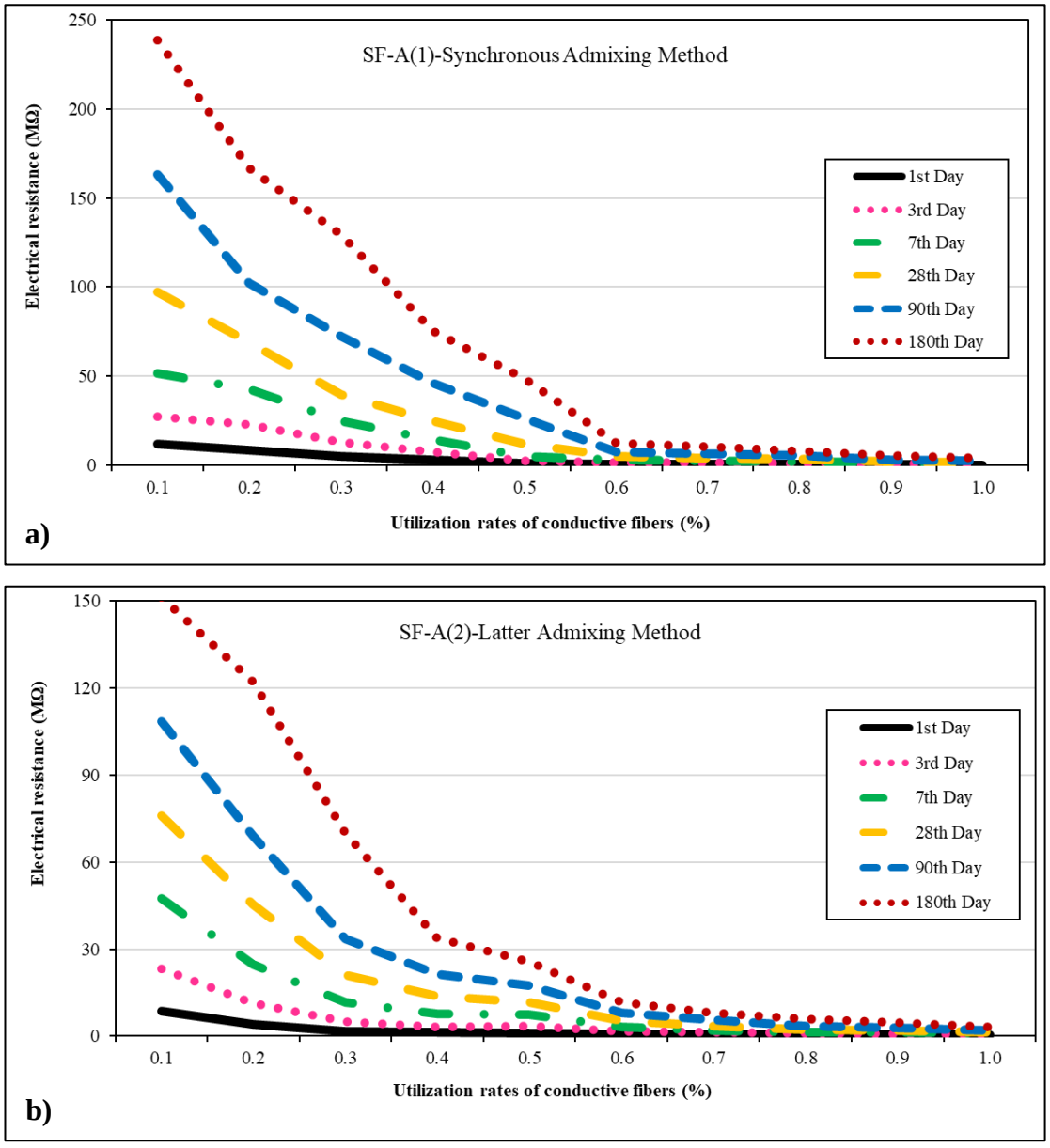

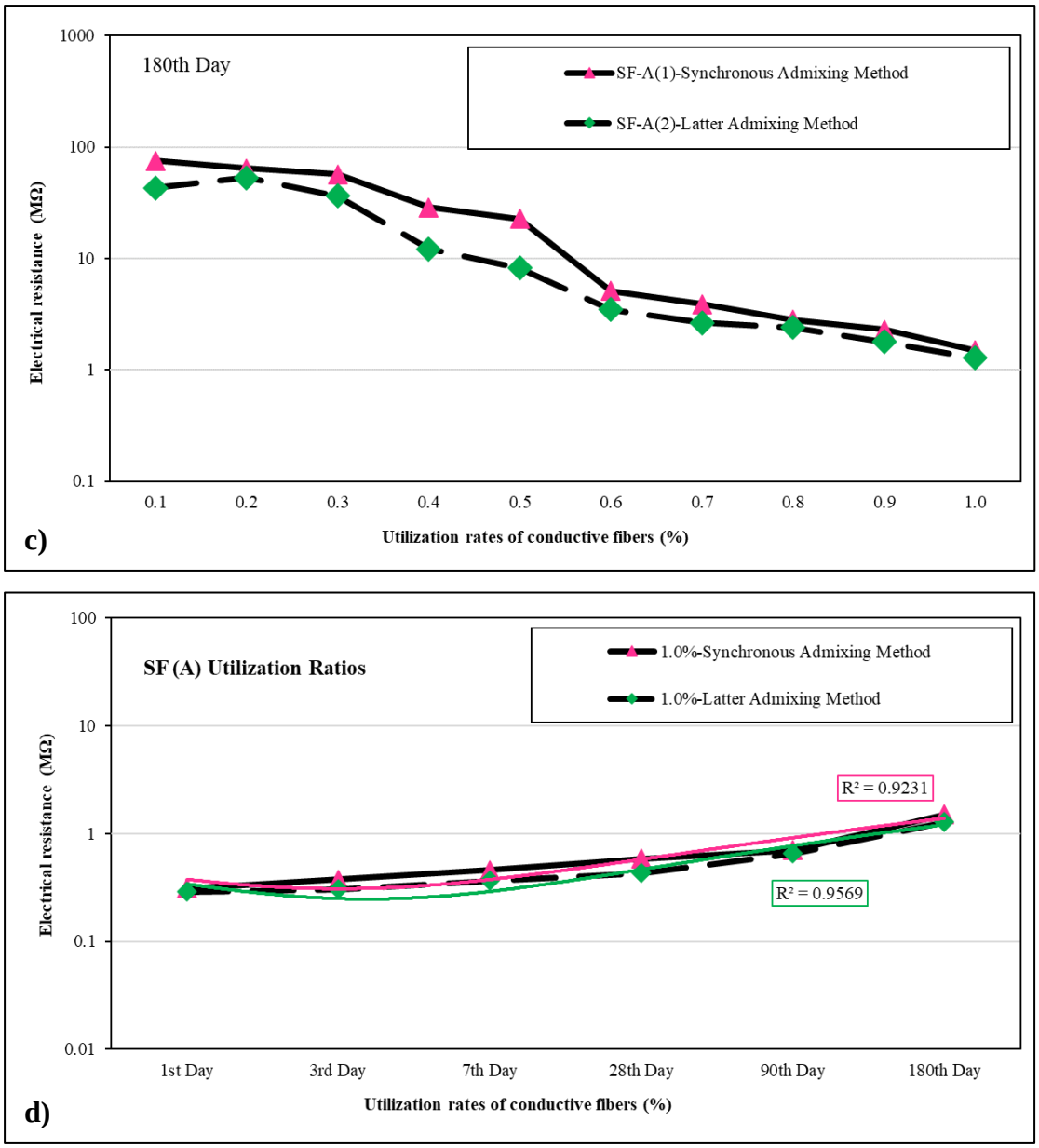

Figure 4.15. Age-dependent ER results of SF-based composites produced with a) The synchronous admixing method, and b) The latter admixing method, Effect of dispersion methods on c) 180-day ER results, d) SF-based composites having the lowest ER results with age

In Figure 4.15-a and b, the effects of the SF utilization rate and the mixing method on the electrical performance of the composites are shown. In Figure 4.15-a, the 1-day ER of the composites was measured below 1000 kΩ with the addition of SF using the synchronous admixing method beyond the utilization rate of 0.6%. In Figure 4.15-b, the 1-day ER of the composites was measured below 1000 kΩ with the addition of SF using the latter admixing method beyond the utilization rate of 0.5%. Regardless of the mixing method,

ER results exceeded the performance upper limit of 1000 kΩ in the long term and had insulative performance. Although ER values decreased with up to 1.0% SF addition, it was not possible to identify a percolation threshold because ER was not in the expected range. The effect of dispersion methods on 180-day ER results is shown in Figure 4.15-c. Although neither dispersion method provided the desired long-term performance, the ER values consistently decreased with incorporating SF. ER results were lower using the latter admixing method than the synchronous admixing method for the same SF content. In the synchronous admixing method, in which SF was mixed with a dry mixture, electrical conductivity did not improve, similar to the CF- and MCF-based mixtures. This inadequate conductivity performance was related to the segregation of fibers because of SF's high specific gravity and uniformity in some parts of the matrices. Literature studies mentioned that SF incorporated into cementitious matrices ranged from 0.25 - 5.0% by weight of the total cementitious materials [114,116,159,166,191,235]. However, lower ER values were obtained between 0.58 and 1.5% SF usage. Shi et al. [159] observed that 0.58% SF addition showed better electrical conductivity performance than 1.0% carbon black addition. However, it was also reported that SF was generally less effective than other conductive materials in the literature [114–116,166,235]. Consistent with the literature, the electrical conductivity did not obtain the expected performance range, even though the ER value decreased with SF addition up to 1.0%. Therefore, the SF content was suggested to exceed 1.0% to achieve further ER reductions. However, increasing SF beyond 1.0% might raise the overall cost of cementitious composites with ESD capability Because of the unexpected insufficient performance of SF, studies suggested that SFs should be combined with other conductive materials rather than alone [235]. The age-dependent electrical performance of SF-based composites with the lowest ER results is shown in Figure 4.15-d for different mixing methods. For both mixing methods, the ER results had similar behavior over time, increased to MΩ levels after 180 days at all mixtures. As a result, the ER results of composites, which SF incorporated, were unsuitable for developing electrostatic discharge-capable composites for flooring or other construction industry applications. To summarize the results obtained using different conductive materials and mixing methods, the percolation thresholds, the best utilization rates, and the lowest 180-day ER results are given in Table 4.21.

Table 4.21. Comparative percolation thresholds, the best utilization rates of conductive materials, and lowest long-term ER results based on different mixing methods

Conductive material	**Mixing method**	**Percolation threshold (%)**	**The best utilization rate (%)**	**Lowest 180-day ER (kΩ)**
CF	Synchronous admixing method	0.6	1.0	15.55
	Latter admixing method	0.3	0.6	0.20
MCF	Synchronous admixing method	1.0	1.0	909
	First admixing method	0.8	1.0	600
SF	Synchronous admixing method	-	1.0	1500
	Latter admixing method	-	1.0	1280

Cementitious composites had insulating properties, with MΩ level ER value within a short period. In the case of using conductive materials, composites could exhibit electrical conductivity capability. Al-Dahawi et al. [158] studied the electrical resistivity of cementitious composites containing various conductive materials over 180 days and claimed that resistivity increased with curing age. This increase was attributed to the continuous hydration reaction, which reduced porosity and moisture content while gradually surrounding the conductive fillers. So, a denser matrix led to a disrupted conductive pathway and higher resistivity over time. The electrical conductivity performance of mixtures was also influenced by factors like the percolation threshold, optimal fiber content, fiber length, fiber dispersion, and matrix microstructure [163]. Suppose efficient conductive pathways could not be created with conductive materials in the matrix; the electrical conductivity might also be negatively affected by factors such as curing age, moisture air voids, water content, and temperature [158].

4.2.3.2. Electrical Resistance Results of Cylindrical Samples

One of the other experimental methods to measure the electrical resistance of composites was determined by the AC method. Unlike the coating design, the ER results were measured from three parts of the cylindrical sample and evaluated in two aspects. The effect of utilization rates of conductive materials on electrical performance and the dispersion of the conductors between parts. ER values of three cylindrical parts measured from the cylindrical sample of

CF-, MCF-, and SF-based mixtures after 1, 3, 7, 28, 90, and 180 days of curing. ER results of MCF-based mixtures using the synchronous admixing method measured considering the age and parts obtained are given in Table 4.22.

As seen from Table 4.22, the ER value decreased on all measurement days as the amount of MCF increased in the mixtures prepared by the synchronous admixing method. Based on the ER results, the lowest resistance value was obtained from a 1.0% MCF-based mixture. However, the ER values of the samples increased continuously over time regardless of the conductive rates. While electrical resistance increased linearly in the first seven days, ER increased parabolically after the 28^{th} day. These increases occurred at different levels between parts of the cylinder. Among the ER results of the cylinder parts, the highest values were measured from the top, bottom, and middle layers. The main reason for this difference was that the conductive materials were not distributed homogeneously in the whole matrix. Although the ER values were close to each other in the bottom and middle parts, differences were observed due to the inhomogeneous distribution. In addition, the top part had quite a higher ER than other parts due to the direct exposure to external environmental conditions. Since the optimum conductive pathways could not be created in the matrix, the ER result of the samples showed a constant tendency to increase. ER results of MCF-based mixtures using the first admixing method measured considering age and parts are given in Table 4.23.

Table 4.22. ER results of the MCF-based mixtures using the synchronous admixing method, Ω

Sample	Ratio, %	Parts of the cylinder	1st day	3rd day	7th day	28th day	90th day	180th day
Reference	0.0	Bottom	521	785	1500	19820	162000	226000
		Middle	552	768	1350	17600	168000	223000
		Top	1600	50600	90300	190000	626000	773000
C1(1)	0.1	Bottom	410	598	1235	9870	91900	171000
		Middle	361	531	851	3820	22600	98200
		Top	1550	37000	88000	184000	539000	625000
C2(1)	0.2	Bottom	385	547	1180	7920	84000	164700
		Middle	347	504	822	3700	46500	147800
		Top	1160	31600	84600	178000	511000	603400
C3(1)	0.3	Bottom	379	519	1020	6100	81900	159800
		Middle	334	525	806	3630	40900	135000
		Top	1030	28500	80900	161500	478000	595300
C4(1)	0.4	Bottom	367	497	949	4230	67200	147600
		Middle	339	484	761	2540	14200	56700
		Top	925	23900	73500	147400	469000	541200
C5(1)	0.5	Bottom	353	481	888	2590	58700	135400
		Middle	345	472	685	2120	10700	45800
		Top	537	21340	69880	132500	425500	512700
C6(1)	0.6	Bottom	340	472	855	2750	51000	127600
		Middle	336	454	634	2280	11300	44320
		Top	458	18300	64700	113000	411000	498400
C7(1)	0.7	Bottom	324	463	817	2550	47800	112000
		Middle	315	442	663	2060	10600	40100
		Top	446	16400	62700	101900	399500	451200
C8(1)	0.8	Bottom	317	454	750	2100	40700	99500
		Middle	321	422	723	2170	9040	36300
		Top	425	13430	58400	98000	385000	417000
C9(1)	0.9	Bottom	276	417	620	1960	37100	91200
		Middle	247	411	806	1600	8900	28200
		Top	417	10500	49200	97500	361200	399300
C10(1)	1.0	Bottom	265	405	581	1730	33900	85700
		Middle	246	401	720	1650	7600	21500
		Top	398	9800	42300	89000	344000	376500

Table 4.23. ER results of the MCF-based mixtures using the first admixing method, Ω

Sample	Ratio, %	Parts of the cylinder	1st day	3rd day	7th day	28th day	90th day	180th day
Reference	0.0	Bottom	521	785	1500	19820	162000	226000
		Middle	552	768	1350	17600	168000	223000
		Top	1600	50600	90300	190000	626000	773000
C1(2)	0.1	Bottom	314	504	867	4730	39900	177000
		Middle	312	674	855	4820	23000	34400
		Top	336	6330	58900	171000	158000	374000
C2(2)	0.2	Bottom	305	489	809	4510	22200	84000
		Middle	297	474	798	4110	18700	23500
		Top	329	4890	52200	166000	151000	361000
C3(2)	0.3	Bottom	302	475	794	3570	16800	22100
		Middle	291	458	787	2560	12100	15900
		Top	317	4180	43100	130000	143000	353000
C4(2)	0.4	Bottom	287	438	760	3340	12800	21800
		Middle	287	434	757	2200	11300	14900
		Top	300	3750	38900	125000	141000	328000
C5(2)	0.5	Bottom	278	425	754	3260	11900	18300
		Middle	276	423	749	2160	10500	13700
		Top	297	3660	36800	123000	128000	326000
C6(2)	0.6	Bottom	270	420	750	3160	11600	17000
		Middle	256	417	725	2100	9560	12200
		Top	281	3570	35900	119000	117000	298000
C7(2)	0.7	Bottom	261	413	729	3030	11500	16300
		Middle	251	402	719	2040	8910	11900
		Top	266	3160	33800	105000	111000	288000
C8(2)	0.8	Bottom	253	404	718	3010	11300	15700
		Middle	248	395	708	1890	8630	11800
		Top	266	2850	31000	101000	110000	281000
C9(2)	0.9	Bottom	242	401	665	2970	11200	13200
		Middle	242	383	691	1870	8540	10200
		Top	255	2730	28800	95100	104000	255000
C10(2)	1.0	Bottom	236	385	638	2840	10700	11400
		Middle	219	376	621	1840	8130	9800
		Top	249	2670	27500	89400	97000	234000

As seen from Table 4.23, the ER decreased on all measurement days as the amount of MCF increased in the mixtures prepared by the first admixing method. Based on the ER results, the lowest resistance value was obtained from a 1.0% MCF-based mixture. However, the ER values of the samples increased continuously over time regardless of the conductive rates. While ER increased linearly in the first seven days, ER increased parabolically after the 28th day. ER values increased at lower rates in higher fiber contents. These increases occurred at different levels between parts of the cylinder. Although the parts had similar ER results in the first-day measurements of the samples, the ER results differed on continuous measurement days. According to the ER results of the cylinder parts, the highest values were measured from the top, bottom, and middle layers, respectively. Although the bottom and middle parts had similar ER values until the 28th day, the ER value of the top part increased at a higher level as of the 28th day. In addition, it was determined that the top part of the ER value of the 1% MCF addition increased approximately 24 times compared to the other layers, especially in the 90th-day measurements. Therefore, electrical conductivity could not be sustained with MCF additions in the long term. The main reason for this difference was that the conductive materials were not distributed homogeneously in the whole matrix. The top part had quite a higher ER than others due to direct exposure to external environmental conditions. Since the optimum conductive pathways could not be created in the matrix, the ER value of the samples showed a constant tendency to increase.

Moreover, the mixing method impacted the ER values of MCF-based mixtures. Among the two mixing methods, the ER results of the mixtures prepared using the first admixing method were lower than the synchronous admixing method on all measurement days. Although the ER values of all mixtures increased over time regardless of the mixing method, this increase was higher in the synchronous admixing method. The main reason was that MCFs created fewer electrical networks using the synchronous admixing method, where they were added to the dry mixture. The lowest ER results were obtained from the middle part regardless of the mixing method in ER measurements between parts of the cylinder. It was determined that more fibers were dispersed into the matrix in the middle part. However, ER values increased in all parts over time, and thus, sustainability of the conductivity could not be achieved. Based on these experimental results, the coating system was designed with a 1 cm thickness, which played a crucial role in sustaining conductivity performance by facilitating the distribution of conductive

materials to a whole part of the matrix. Based on the ER results of coating and cylindrical specimen measurements, optimum MCF ratios were selected depending on the mixing method in single conductor incorporations, as shown in Table 4.24. The ratios were chosen by considering the ER results of both specimens, the cost of the coating design, and the ability to achieve electrical conductivity performance in double and triple addition of the conductor.

Table 4.24. Selected ratios of milled carbon fiber for the double and triple incorporations

Ratio (%)	**The synchronous admixing method**	**The first admixing method**
0.2	C2(1)	C2(2)
0.4	C4(1)	C4(2)
0.6	C6(1)	C6(2)
1.0	C10(1)	C10(2)

ER results of CF-based mixtures using the synchronous admixing method measured considering age and parts obtained are given in Table 4.25.

Table 4.25. ER results of the CF-based mixtures using the synchronous admixing method, Ω

Sample	Ratio, %	Parts of the cylinder	1st day	3rd day	7th day	28th day	90th day	180th day
Reference	0.0	Bottom	521	785	1500	19820	162000	226000
		Middle	552	768	1350	17600	168000	223000
		Top	1600	50600	90300	190000	626000	773000
B1(1)	0.1	Bottom	443	489	616	2200	24400	25500
		Middle	464	502	650	2530	21300	27900
		Top	845	1280	2250	13700	134000	203000
B2(1)	0.2	Bottom	305	385	609	2060	11600	15500
		Middle	310	379	612	2080	10100	13800
		Top	481	650	1880	12920	104000	161000
B3(1)	0.3	Bottom	296	360	512	1250	3830	4910
		Middle	302	353	504	1200	3510	4030
		Top	406	557	950	9260	10000	16200
B4(1)	0.4	Bottom	291	348	412	1200	2960	3710
		Middle	298	334	425	1230	2660	3470
		Top	383	548	850	4410	7300	13600
B5(1)	0.5	Bottom	285	335	372	1130	2860	3270
		Middle	278	325	404	956	2480	3580
		Top	337	540	658	2610	5800	10300
B6(1)	0.6	Bottom	281	330	365	883	2730	3130
		Middle	275	314	385	800	2650	3270
		Top	289	517	604	1580	3840	6900
B7(1)	0.7	Bottom	274	314	358	800	1680	2240
		Middle	275	304	367	776	1790	1960
		Top	277	477	556	1350	2590	3400
B8(1)	0.8	Bottom	267	303	350	796	986	1880
		Middle	264	300	338	709	974	1560
		Top	270	460	520	1250	2450	2900
B9(1)	0.9	Bottom	255	289	327	700	905	1030
		Middle	259	295	324	602	886	990
		Top	265	444	502	1220	2350	2670
B10(1)	1.0	Bottom	250	275	320	400	800	844
		Middle	252	285	316	444	796	935
		Top	257	434	499	905	1200	2100

As seen from Table 4.25, the ER results decreased on all measurement days as the amount of CF increased in the mixtures prepared by the synchronous admixing method. However, ER values decreased significantly with the addition of 0.3% CF. Based on the ER results, the lowest resistance value was obtained from a 1.0% CF-based mixture. However, the ER values of the samples increased with measurement time regardless of the conductive rates. This increment increased at a lower level compared to MCF-based mixtures. The CF was more effective in reducing the resistance value than MCF-based mixtures using the synchronous admixing method between the carbon-based fibers. Unlike MCF addition, the ER results increased until the 180^{th} day.

Although similar ER values were measured from each part of the cylinder, the values varied with the 90^{th} day's measurement. It could be concluded that the conductors were distributed homogeneously. However, the ER values of the upper part increased at a higher rate than the other two parts after the 90^{th} day. The reason was related to the direct exposure of the layer to external environmental conditions. In addition, the w/c ratio was relatively higher than other parts due to the bleeding in the top layer of the cylinder. This also caused the higher void content in the system, resulting in higher ER values. In general, although a conductive network was formed in the matrix, this conductive network was not at a level that provided constant conductivity due to the increasing ER value. The ER results of CF-based mixtures using the latter admixing method measured considering age and parts obtained are given in Table 4.26.

Table 4.26. ER results of the CF-based mixtures using the latter admixing method, Ω

Sample	Ratio, %	Parts of the cylinder	1st day	3rd day	7th day	28th day	90th day	180th day
Reference	0.0	Bottom	521	785	1500	19820	162000	226000
		Middle	552	768	1350	17600	168000	223000
		Top	1600	50600	90300	190000	626000	773000
B1(2)	0.1	Bottom	289	296	320	440	716	770
		Middle	284	293	315	428	660	750
		Top	297	300	325	437	625	735
B2(2)	0.2	Bottom	275	284	307	410	656	755
		Middle	274	279	305	405	630	704
		Top	269	282	331	420	677	717
B3(2)	0.3	Bottom	235	255	288	300	527	630
		Middle	236	240	280	294	517	598
		Top	253	260	287	305	587	604
B4(2)	0.4	Bottom	231	249	272	286	499	582
		Middle	228	233	256	278	437	518
		Top	245	250	275	296	535	511
B5(2)	0.5	Bottom	206	214	246	274	327	327
		Middle	206	204	240	264	316	319
		Top	210	221	254	289	355	324
B6(2)	0.6	Bottom	183	194	212	236	248	257
		Middle	185	188	204	216	231	252
		Top	193	205	227	265	278	270
B7(2)	0.7	Bottom	170	182	201	224	233	246
		Middle	165	175	198	206	215	234
		Top	185	194	210	244	273	252
B8(2)	0.8	Bottom	163	170	187	215	217	235
		Middle	161	169	175	202	208	244
		Top	177	187	201	235	264	267
B9(2)	0.9	Bottom	161	166	172	203	208	222
		Middle	150	163	169	195	201	215
		Top	153	178	185	217	243	237
B10(2)	1.0	Bottom	155	159	165	188	200	206
		Middle	155	157	177	184	197	202
		Top	165	174	180	198	214	208

As seen from Table 4.26, the ER results decreased significantly for all measurement days with the increase in the amount of CF in mixtures prepared using the latter admixing method. Considering the ER results, the lowest resistance value was obtained from the 1.0% CF addition. Compared to the reference mixture, the ER remained as ohms for all addition ratios of CF. Although ER increased over time, all measurements remained at the ohm level at the end of the 180th day. Therefore, the targeted ER level in the matrix was achieved using incorporating carbon fiber by the latter admixing method. Among the ER results of cylindrical parts, the results were determined at similar levels. In mixtures prepared using the first admixing method, it could be concluded that the conductive fibers were homogeneously distributed to the matrix and all parts. Therefore, electrical conductivity was maintained with the 180th day. In addition, it was determined that the mixing method affected the ER values of CF-based mixtures. Among the two mixing methods, the ER values of the mixtures prepared using the latter admixing method remained lower on all measurement days. Compared to the synchronous admixing method, the latter admixing method remained at the ohm level even at the end of the 180th day and maintained electrical conductivity The achievability of homogeneous fiber distribution was determined between the two mixing methods by adding carbon fibers to the mortar mixture. In addition, compared to the other mixing method, the time-dependent ER values of the top layer did not increase significantly in the mixtures using the latter admixing method. Although the upper layer was exposed to external environmental conditions, it continued to maintain its electrical conductivity performance until the 180th day.

According to measurements from the coating surface and parts of the cylindrical, effective results were obtained from CF-based mixtures among carbon-based fibers regardless of the mixing method and ratio. Therefore, using carbon fiber as the main conductor in the double and triple conductor combinations significantly changed the electrical conductivity performance of the mixtures. Since the latter admixing method showed superior electrical conductivity performance, using only this method when preparing mixtures in double and triple conductor combinations using CF was decided. The ratios showing the best electrical conductivity performance depending on the latter admixing method in single conductor additions are given in Table 4.27.

Table 4.27. Selected ratios for the double and triple incorporations

Ratio (%)	**The latter admixing method**
0.2	B2(2)
0.4	B4(2)
0.6	B6(2)
1.0	B10(2)

ER results of SF-based mixtures using the synchronous admixing method measured considering age and parts obtained are given in Table 4.28. As seen from Table 4.28, the ER values decreased for all measurement days as the amount of steel fiber increased in mixtures prepared using the synchronous admixing method. Considering the ER results, the lowest resistance value was obtained from the mixture to which SF was added at a rate of 1.0%. However, the ER values of the samples had increased parabolically over time, regardless of the fiber content. This increase occurred at different levels for the parts of the mixtures. On all measurement days, the top part had a considerably higher resistance value than the other two. The ER in the top parts increased to the kΩ level after the first-day measurements. Although the ER value of the top part was lower than the reference sample, it could not be concluded that the electrical conductivity performance was maintained in this part. The fact that the bottom and middle parts had similar ER values between the parts indicated that the steel fiber had settled to the bottom due to its specific density in the matrix mixture. It was measured that the ER rose to the kΩ level with the curing time in the bottom and middle part where the fibers were distributed densely, but these values met the performance criterion. The high ER of the top part was attributed to two reasons. It was the inability to homogeneously distribute in the matrix mixture and the collapse of the steel fiber in the matrix due to the technical specification of the steel fiber used. Another reason was that the part was directly affected by external environmental conditions due to its inadequate electrical conductivity network. The ER results of SF-based mixtures using the latter admixing method measured considering age and parts obtained are given in Table 4.29.

Table 4.28. ER results of the SF-based mixtures using the synchronous admixing method, Ω

Sample	Ratio, %	Parts of the cylinder	1st day	3rd day	7th day	28th day	90th day	180th day
Reference	0.0	Bottom	521	785	1500	19820	162000	226000
		Middle	552	768	1350	17600	168000	223000
		Top	1600	50600	90300	190000	626000	773000
A1(1)	0.1	Bottom	397	679	1360	6980	59900	73900
		Middle	389	631	1270	6730	58300	77400
		Top	1540	49900	60100	203000	322000	425000
A2(1)	0.2	Bottom	379	665	1210	6560	39500	55600
		Middle	359	640	1010	6400	37600	59750
		Top	1340	41400	54420	202500	319000	435000
A3(1)	0.3	Bottom	371	648	1180	6470	38200	47600
		Middle	352	637	959	6020	36500	49100
		Top	1250	40400	53600	200000	305000	429000
A4(1)	0.4	Bottom	338	583	824	5800	28900	32100
		Middle	323	576	810	5560	34500	36900
		Top	1070	34700	50200	191200	291000	417000
A5(1)	0.5	Bottom	312	517	786	5650	26580	30500
		Middle	319	505	728	5710	26270	28100
		Top	1010	29400	48700	184000	287000	370000
A6(1)	0.6	Bottom	285	494	732	5450	23000	27800
		Middle	268	427	774	5170	21200	29000
		Top	950	22800	45800	233000	276000	355900
A7(1)	0.7	Bottom	269	473	706	5300	21200	23100
		Middle	245	499	803	5160	23500	23500
		Top	960	18900	43500	374000	257000	346800
A8(1)	0.8	Bottom	240	437	659	4570	16000	18300
		Middle	239	423	624	4970	19200	20500
		Top	880	15400	40100	420000	229000	335600
A9(1)	0.9	Bottom	230	444	608	4030	14500	14600
		Middle	247	442	567	4690	13300	13800
		Top	815	14300	38200	428000	207000	307500
A10(1)	1.0	Bottom	216	408	595	3820	11000	11500
		Middle	234	468	530	3200	10000	12000
		Top	705	12400	35800	469000	202000	305800

As seen from Table 4.29, the ER values decreased for all measurement days as the amount of steel fiber increased in mixtures prepared using the latter admixing method. Considering the ER results, the lowest resistance value was obtained from the mixture to which SF was added at a rate of 1.0%. Although the parts had similar ER results in the first-day measurements of the samples, the ER results increased parabolically over time, regardless of the fiber content. This increase occurred at different levels between the parts of the mixtures. Among the ER results of the cylinder parts, the highest values were measured from the top, bottom, and middle parts, respectively. Although the ER results in the upper part were lower than the reference mixture, the values increased to the kΩ level after the first day. However, the ER value of the lower layer also differed significantly from the middle layer with time. The continuous increase in ER and the significant difference in ER values between layers indicated that the electrical conductivity performance could not be achieved in the single use of steel fiber. By incorporating steel fibers into the mortar mixture, it was concluded that the fibers were concentrated in the middle layer. The upper and bottom layers lost their electrical conductivity performance over time due to low concentrations of fibers and environmental effects. In addition, the mixing method directly affected the ER values of SF-based mixtures. Among the two mixing methods, the ER values of the mixtures prepared using the latter admixing method remained lower on all measurement days. Though the ER values of all mixtures increased over time regardless of the mixing method, this increase was higher using the synchronous admixing method. Although there were differences between layers, the lowest ER values were obtained from the measurements taken from the middle layer regardless of the mixing method. In addition, the highest ER values were measured from the top part. Therefore, it could not be concluded that the fibers were homogeneously distributed between both mixing methods. One of the reasons steel fibers could not be homogeneously distributed was that the steel fiber had a higher density than the raw materials in the matrix, and its straight shape decreased the adherence between fibers and matrix.

Table 4.29. ER results of the SF-based mixtures using the latter admixing method, Ω

Sample	Ratio, %	Parts of the cylinder	1st day	3rd day	7th day	28th day	90th day	180th day
Reference	0.0	Bottom	521	785	1500	19820	162000	226000
		Middle	552	768	1350	17600	168000	223000
		Top	1600	50600	90300	190000	626000	773000
A1(2)	0.1	Bottom	370	497	1265	17400	69500	122000
		Middle	366	467	886	2060	8090	20700
		Top	333	6140	34240	165000	200000	296000
A2(2)	0.2	Bottom	364	493	1270	16100	67000	118000
		Middle	366	449	830	2010	7900	18500
		Top	361	5400	31600	163000	198000	276500
A3(2)	0.3	Bottom	350	471	1060	13900	67000	114700
		Middle	350	424	829	2080	7970	20100
		Top	376	5330	31700	161000	193000	270100
A4(2)	0.4	Bottom	332	422	930	12500	60600	107300
		Middle	332	400	819	1980	7630	19200
		Top	321	5200	30800	153000	192000	236000
A5(2)	0.5	Bottom	321	419	910	11900	44000	99500
		Middle	320	397	772	1840	7450	18700
		Top	315	4900	27600	145000	189000	224300
A6(2)	0.6	Bottom	323	394	870	9300	43400	96200
		Middle	306	363	682	1760	7160	18900
		Top	285	4070	25500	142000	187000	223700
A7(2)	0.7	Bottom	322	370	836	9700	41500	92100
		Middle	314	352	662	1510	7050	17600
		Top	276	3460	24800	135000	187000	225400
A8(2)	0.8	Bottom	318	393	750	8500	30900	84500
		Middle	307	348	582	1660	6840	15400
		Top	288	3540	22060	131000	178000	207800
A9(2)	0.9	Bottom	316	351	730	7400	26000	79800
		Middle	301	329	579	1380	6500	15700
		Top	279	3490	18000	128000	170000	203900
A10(2)	1.0	Bottom	305	343	700	6500	23500	75800
		Middle	296	326	490	1220	5400	14850
		Top	247	3320	16200	12000	166000	198700

Based on the ER results of coating and cylindrical specimen measurements, optimum SF ratios were selected depending on the mixing method in single conductor incorporations given in Table 4.30. The ratios were chosen by considering both specimens' ER results, the coating design cost, and the ability to achieve electrical conductivity performance in double and triple addition of the conductors.

Table 4.30. Selected ratios for the double and triple incorporations

Ratio (%)	**The synchronous admixing method**	**The latter admixing method**
0.2	A2(1)	A2(2)
0.4	A41)	A4(2)
0.6	A6(1)	A6(2)

Regardless of the mixing method, carbon fiber was the most effective fiber type. The highest ER values were measured from SF mixtures on all measurement days. For this reason, CF was taken as the main conductor in the double and triple combinations of fibers. However, considering the high costs of carbon fibers, the aim was to reduce the amount of carbon fiber in the double and triple combinations. In addition, the fact that MCFs and SFs had lower ER values in the middle part played an essential role in determining the optimum thickness of the coating design. The homogeneous and dense dispersion of fibers throughout the matrix were important factors in the development of electrically conductive networks. For this reason, the thickness of the coating was decided to be 1 cm to obtain the maximum level of electrical conductivity performance from the design. In this way, the coating design developed a single layer, and its cost remained economical compared to other chemical flooring systems.

4.2.4. Microstructure of Composites with Single Conductive Material Incorporation

The first stage of the thesis aimed to obtain the electrical conductivity performance from a single use of carbon fiber, milled carbon fiber, and steel fiber usage in a cementitious matrix. Therefore, the dispersion of the conductives in the matrix was examined. In this

context, the effect of micron-sized MCFs on the electrical conductivity performance in different mixing methods and usage rates was investigated by microstructure analysis. According to the ER results, the lowest values could not be obtained from one mixing method among the MCF-based mixtures. For this reason, the samples to be analyzed were carried out using the ratios used in double and triple addition, taking into account the 28^{th}-day ER results. In this context, the microstructure of C2 (0.2%), C4 (0.4%), C6 (0.6%) and C10 (1.0%) samples was determined among the mixtures using synchronous admixing method. Among selected ratios, EDX analysis was not performed on the mixture containing 0.2% MCF to observe the microstructural change in the matrix with fiber content. The EDX analysis performed with the spectrums in the image is shown in Figure 4.16.

Since conductors were incorporated into the cementitious main matrix at different ratios, similar formations were expected between the microstructure of the matrix. In addition, the highest content of elements at all points belonged to oxygen. Oxygen formation was related to keeping the sample under laboratory conditions until the measurement day. In Figure 4.16, the C element increased at the spectrums of specimens with the increase in the MCF content. It was predicted that the carbon element increased in the matrix due to using carbon-based materials. In Figure 4.16-a, the SEM image and EDX analysis of 0.4% MCF-based mixture are shown. A rough surface formed in the examined area. Among the spectrums, the highest C content was obtained from this point. Apart from the oxygen element, Ca, C, and Si formed the main elements. Although the structure formed was not determined clearly in the selected area, it was thought that C-S-H gels were dense due to the type of main elements and the 28-day-age sample. In Figure 4.16-b, the SEM image and EDX analysis of 0.6% MCF-based mixture are shown. In the image, interlocking spiral structures and flat and rectangular plates were formed. Among the spectrums, the highest C content was obtained from this point. Apart from the oxygen element, Ca, C, and Al formed as a main element. The higher content of the C element was related to the increase in the amount of MCF in the system at the spectrum. Apart from this, the high content of the Ca element was related to the helical structure of C-S-H gels in the system, while the appearance of the Al element was related to the formation of gibbsite, which can occur in plate forms due to the CAC usage. The appearance of the plate could also be detected in the formation of portlandite.

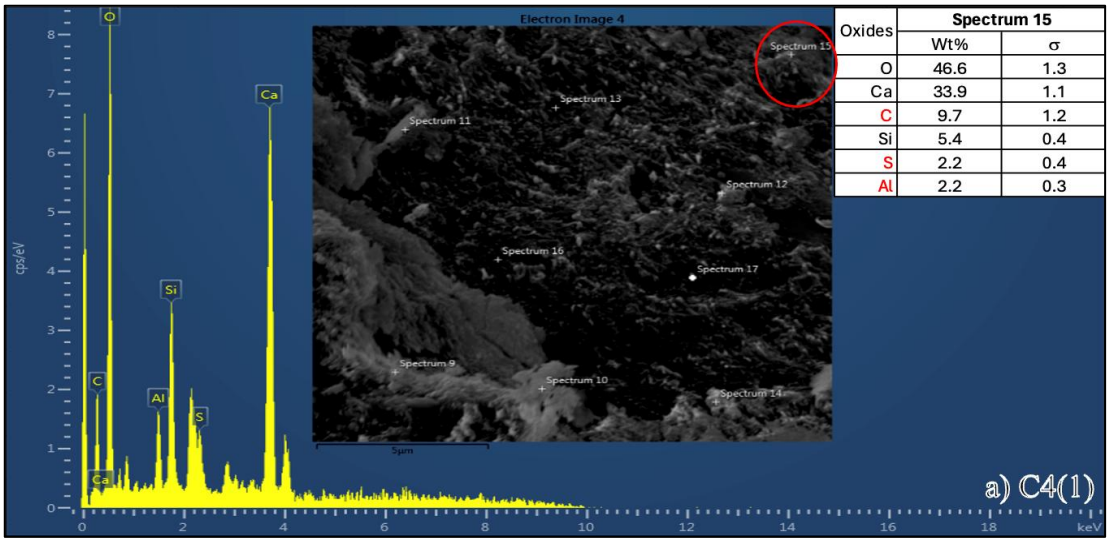

Oxides	Spectrum 15	
	Wt%	σ
O	46.6	1.3
Ca	33.9	1.1
C	9.7	1.2
Si	5.4	0.4
S	2.2	0.4
Al	2.2	0.3

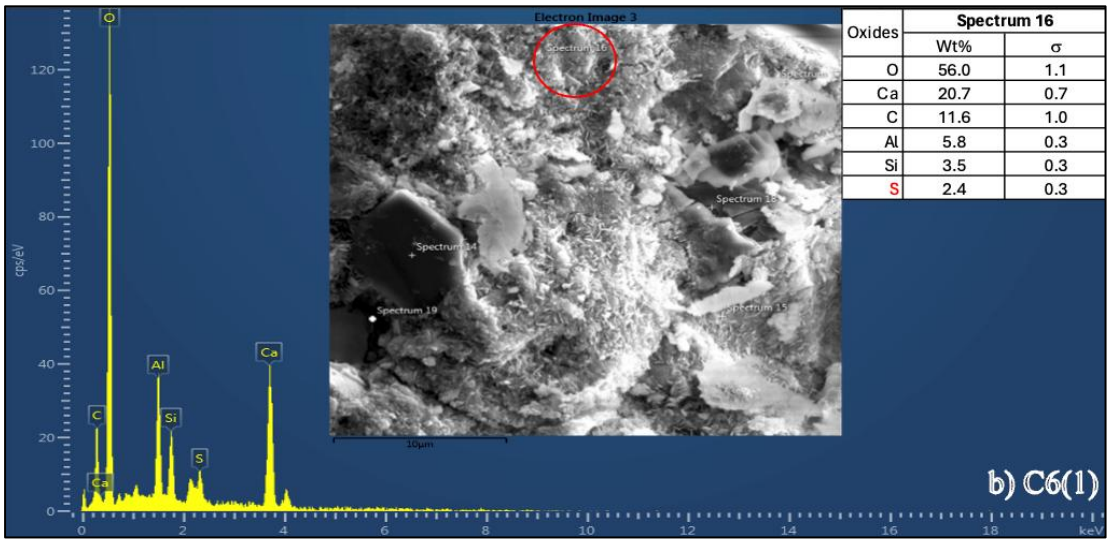

Oxides	Spectrum 16	
	Wt%	σ
O	56.0	1.1
Ca	20.7	0.7
C	11.6	1.0
Al	5.8	0.3
Si	3.5	0.3
S	2.4	0.3

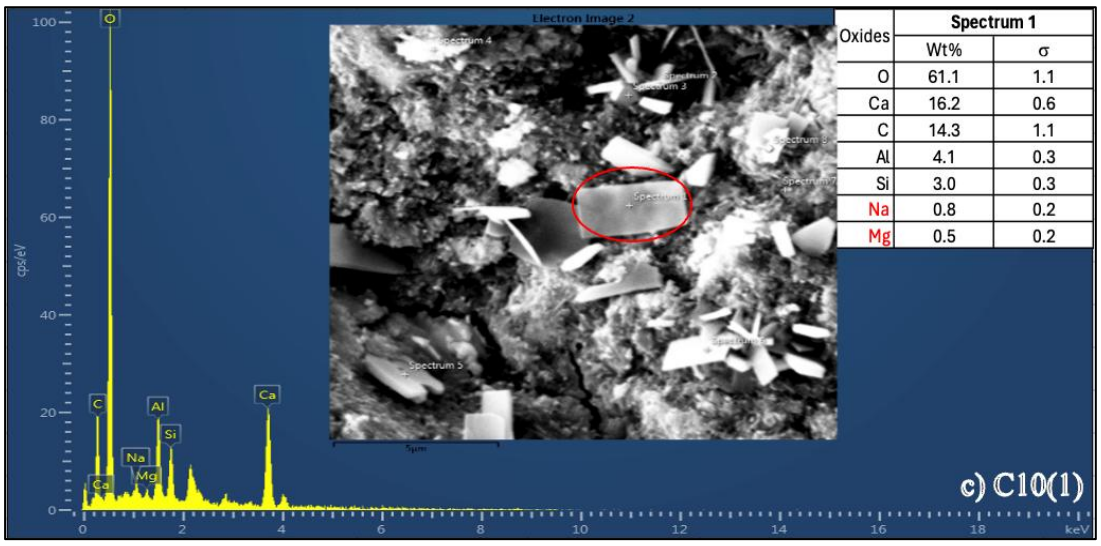

Oxides	Spectrum 1	
	Wt%	σ
O	61.1	1.1
Ca	16.2	0.6
C	14.3	1.1
Al	4.1	0.3
Si	3.0	0.3
Na	0.8	0.2
Mg	0.5	0.2

Figure 4.16. EDX analysis of MCF-based composites which performed the best electrical performance and manufactured by synchronous admixing method

In Figure 4.16-c, the SEM image and EDX analysis of the 1.0% MCF-based mixture were given. In the image, similar plate-like formations, varieties of needles, and spiral structures were found. Among the spectrums, the highest C content was obtained from this point. Apart from the oxygen element, Ca, C, and Al formed as a main element. The highest C content was measured from the 1.0% MCF addition among the selected specimens. The other main elements, seen in a traditional cementitious matrix, formed at predicted rates in the same area upon forming the C element.

In addition, the microstructure of C4 (0.4%), C6 (0.6%), and C10 (1.0%) samples were determined among the first admixing method using mixtures. The EDX analysis performed with the spectrums in the image taken at a 5 μm scale is shown in Figure 4.17. The C element increased at the spectrums of specimens with the increase in the MCF content. It was predicted that the carbon element increased in the matrix due to using carbon-based materials. Compared to the synchronous admixing method, higher C content was measured with using the first admixing method.

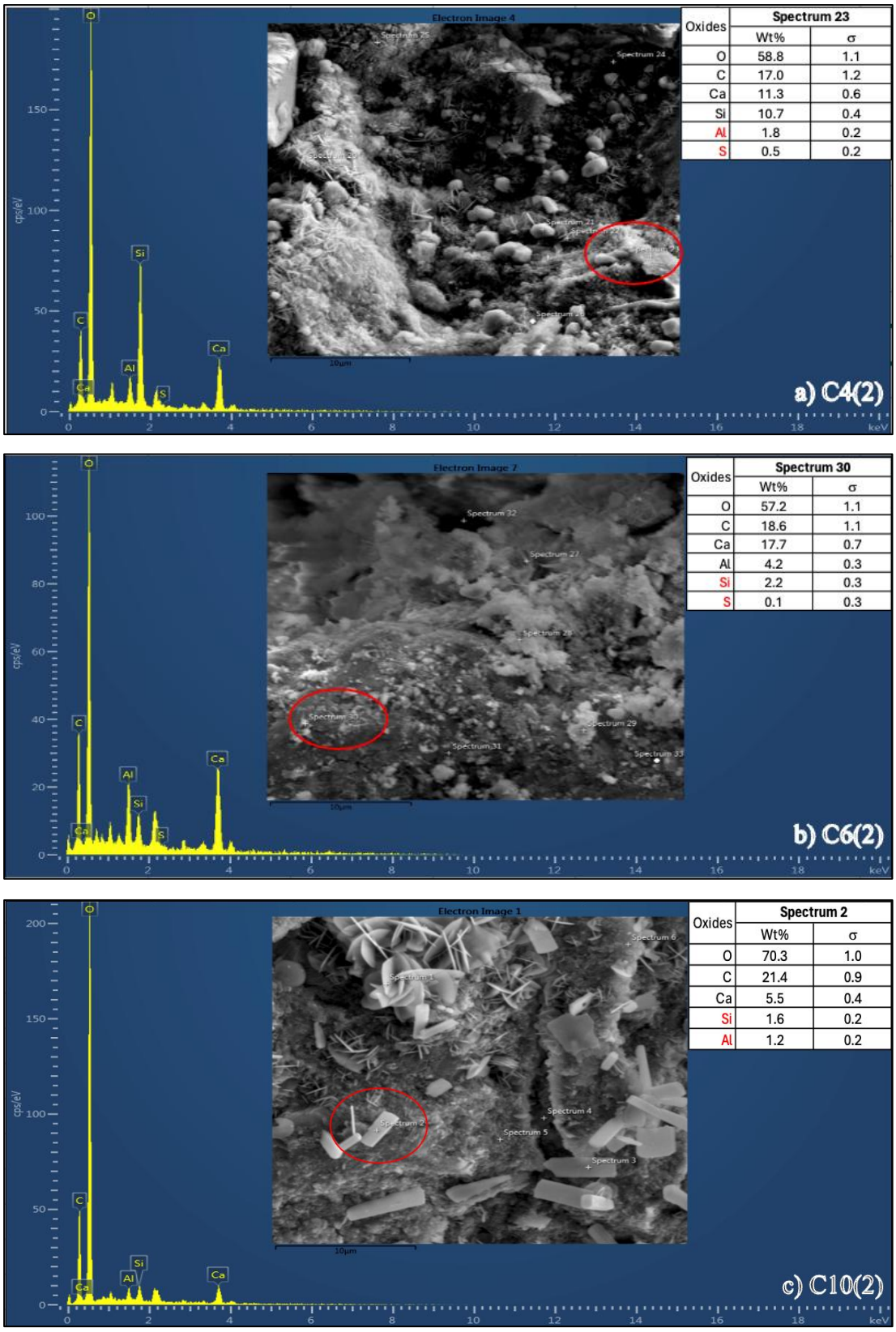

Figure 4.17. EDX analysis of MCF-based composites which performed the best electrical performance and manufactured by first admixing method

In Figure 4.17-a, the SEM image and the EDX analysis of the 0.4% MCF-based mixture were shown. Elevation differences were seen in the examined area. Numerous smooth, plate-like formations of varying sizes and thicknesses were also observed. Some areas contained intertwined, thinner, oval-shaped formations. The spectrum analysis showed that this point had the highest carbon content. Apart from the oxygen element, C, Ca, and Si formed as a main element. It was thought that C-S-H gels were dense due to the type of main elements and the 28-day-age sample. In addition, small stone-like formations in the examined area were related to the formation of portlandite due to the PC-rich system. The high silica content was related to the silica fumes used in the matrix. In Figure 4.17-b, the SEM image and the EDX analysis of the 0.6% MCF-based mixture are shown. This area had a cloudy and rough surface, unlike the other samples examined. Although the structures formed were not clearly understood, the EDX analysis of the spectrum with the highest C content was included. Apart from the oxygen element, C, Ca, and Al formed the main elements. In the formation here, C-S-H gel was present in a large matrix region, and the Al element was also observed due to the use of CAC. In Figure 4.17-c, the SEM image and the EDX analysis of 1.0% MCF-based mixture were shown. In the examined area, various-size/thickness smooth plate-like formations were observed to a large extent. There were also regions where plate-like formations with thinner and oval shapes were intertwined. Among the spectrums, the highest C content was obtained from this point. Apart from the oxygen element, C, Ca, and Si formed as main elements. It was thought that C-S-H gels were dense due to the type of main elements and the 28-day-age sample. The C content reached 21.4% in the matrix. Among the selected samples, the lowest ER results were obtained using 1.0% MCF, regardless of the mixing method. Although the MCF length was 100-μm, the dispersion of the fibers was examined by SEM analysis. The SEM images of samples prepared by the synchronous admixing method and incorporating 1.0% of MCF are shown in the Figure 4.18.

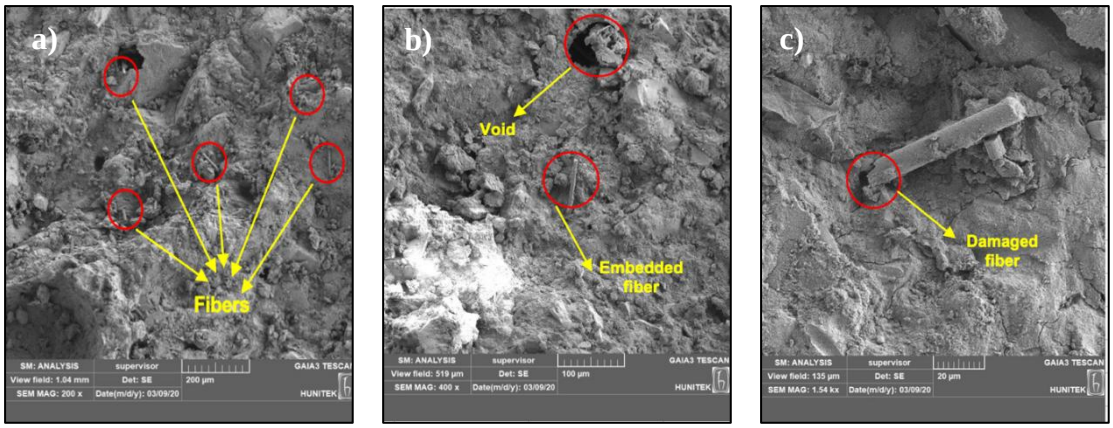

Figure 4.18. SEM images of MCF-based (1.0%) composites prepared by the synchronous admixing method: a) General view of fibers in a selected area, b) Non-homogenous distribution of the fibers in a selected area, c) View of reaction products on a fiber

In general, the ER results were coherent with the SEM images. In Figure 4.18-a, hardly dispersed fibers were concentrated only in certain parts at a 200 μm scale. Some fibers were on the surface, while others were found embedded in the matrix. In addition, a large diameter pores were also formed. Likely, embedded fibers and denser microstructure with continuous hydration reaction prevented electrical conductivity performance in the matrix. The insufficient length size and lower number of fibers in the selected area also caused higher ER results of the mixture. Another SEM image was taken from a different region, provided at 100 μm scale in Figure 4.18-b. With the increase in the scale, the number of fibers decreased to only one fiber. However, it was observed in the large-scale pores in the area under study. Despite using 1.0% MCF in the mixture, the number of fibers was scarce. Here, the effect of the mixing method on the mixture was significant. In Figure 4.18-c, broken or damaged fiber was seen at a 20 μm scale. Adding MCFs to the dry mix during mixing caused damage to the fibers. For this reason, ER values increased significantly over time in mixtures using the synchronous admixing method. The SEM images of samples prepared by the first admixing method and incorporating 1.0% of MCF are given in Figure 4.19.

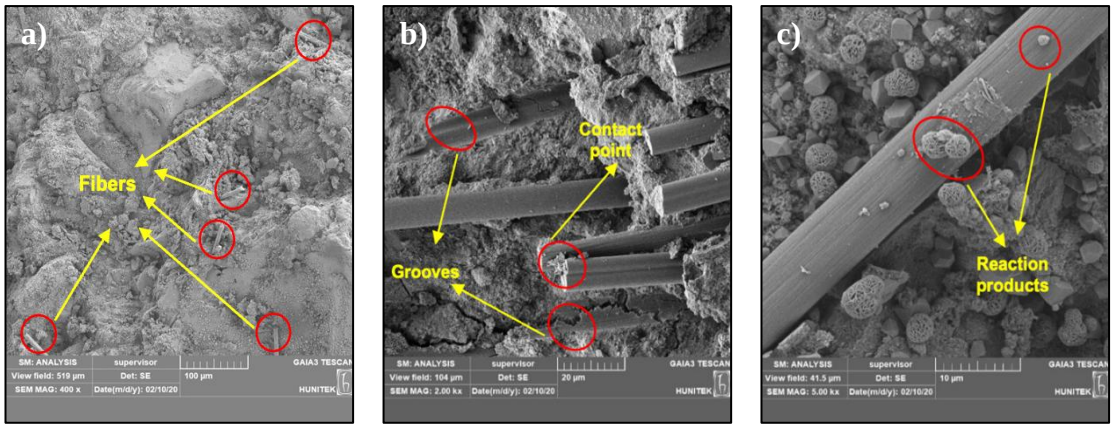

Figure 4.19. a) General view of fibers in a selected area, b) Non-homogenous distribution of the fibers in a selected area, c) View of reaction products on a fiber

In general, the ER results were concordant with the SEM images. In Figure 4.19-a, just a few fibers were seen in certain parts of the selected SEM area. The electrical conductivity deteriorated due to embedded fibers in the matrix and the denser microstructure. Additionally, the length of the MCFs and low utilization rate caused the higher ER results of the mixture. Although no form of agglomeration was observed in Figure 4.19-b, MCFs were dispersed non-homogeneously in the matrix. SEM images indicated that the MCFs had grooves or small channels of varying widths and depths along the fiber axis. These surface defects likely improved mechanical interlocking and created stronger interfacial bonds between the MCFs and the hydrated cement paste. In addition, these formations provided nucleation sites for hydration products, resulting in a denser microstructure, higher compressive strength, and increased ER values. In Figure 4.19-c, hydration products were shown on the MCFs. The improved adherence between the fiber and cementitious mortar mixture enhanced mechanical performance; at the same time, the hydration products also hindered the conductive path and resulted in higher ER results. The effect of micron-sized CFs on the electrical conductivity performance in different mixing methods and usage rates was investigated by microstructure analysis. Although both mixing methods positively influenced electrical conductivity, the lowest ER results were measured with the latter admixing method. In this context, the microstructure of B6 (0.6%), B8 (0.8%), and B10 (1.0%) samples were determined among the mixtures using the synchronous admixing method. The SEM images of CF-based composites prepared by the synchronous admixing method are shown in Figure 4.20.

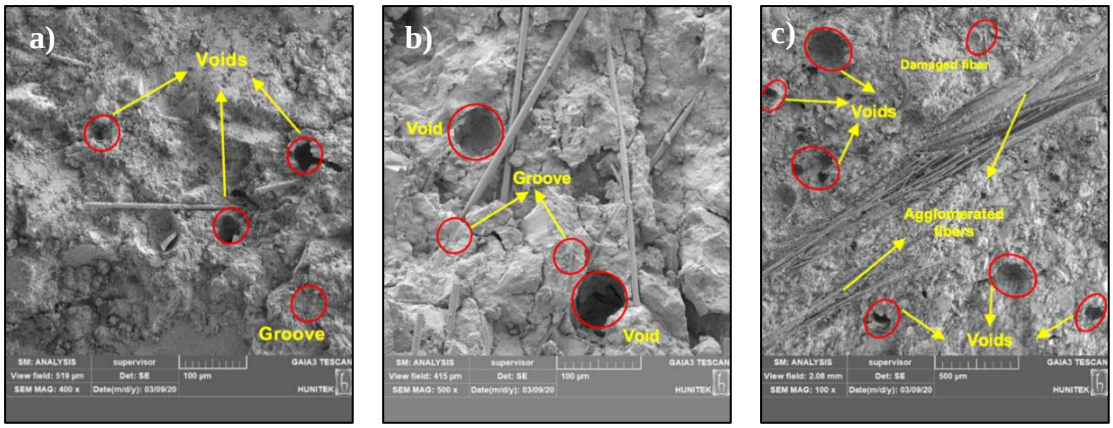

Figure 4.20. SEM images of CF-based cementitious composites prepared by the synchronous admixing method at different CF utilization rates: a) General view of fibers in a selected area, b) Contact point of fibers in a selected area, c) Agglomerated fibers in a selected area

Because the percolation threshold was identified as 0.6%, and the lowest ER value was measured at the 1.0% CF addition based on the ER results of the CF-based mixtures, the 0.6%, 0.8%, and 1.0% contents were selected to investigate the dispersion of the CFs in matrices. In Figure 4.20-a, fibers were dispersed ununiformly, some fibers were embedded, and large voids were also seen in the matrix. In Figure 4.20-b, as the number of fibers increased in the area, more contact of the fibers was seen. CFs also had grooved and small channels of different widths and depths in the matrix. These surface defects and channels likely enhanced mechanical interlocking, leading to better interfacial bonding between fibers and hydrated cement paste. As the content of CF increased to 1.0%, fiber agglomerations became much more apparent, as observed in Figure 4.20-c. Though more CFs were found in this area, electrical conductivity was prevented due to fiber agglomeration. The matrices also had protruding and damaged fibers, indicating that the synchronous admixing process caused fiber damage. In summary, the synchronous admixing method did not disperse CFs uniformly, regardless of the CF utilization rate. Large-diameter voids, uneven dispersion, and agglomeration of the fibers in all matrices negatively impacted overall conductivity performance. The SEM images of CF-based composites prepared by the latter admixing method are shown in Figure 4.21.

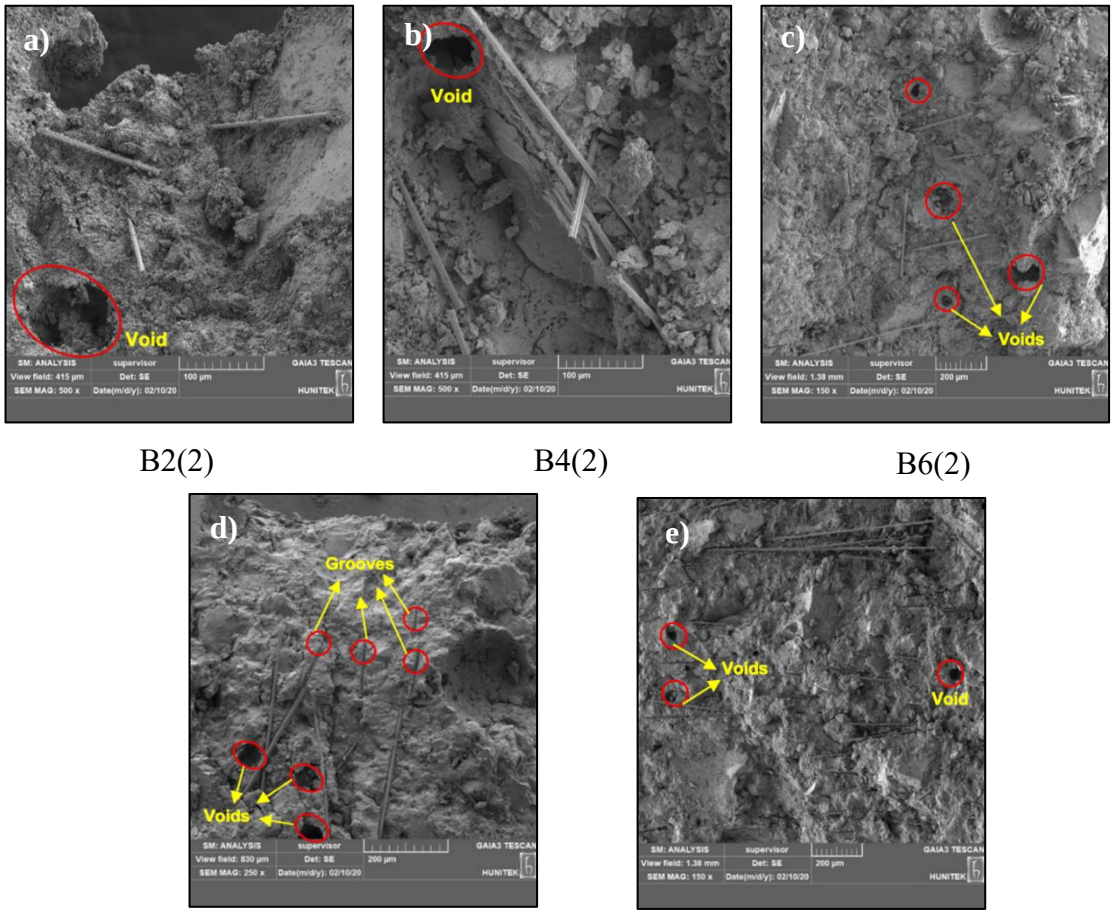

Figure 4.21. SEM images of CF-based cementitious composites prepared by the latter admixing method at different CF utilization rates

Because the percolation threshold was identified as 0.3%, and the lowest ER value was measured at the 0.6% CF addition based on the ER results of the CF-based mixtures, the 0.2%, 0.4%, 0.6%, 0.8%, and 1.0% contents were selected to investigate the dispersion of the CFs in matrices. In Figure 4.21, fiber-to-fiber contacts optimally increased when CFs were dispersed uniformly regardless of CF content, improving electrical conductivity. It was observed that SEM images were consistent with ER results. Chen et al. [142] stated that electrical conductivity was improved with the increase of CF content. While the conductivity improved significantly with initial increases in fiber content, the rate of improvement slowed after reaching an optimal CF level, indicating that exceeding this level did not enhance conductivity performance further. In the thesis study, more fibers were dispersed at a 1.0% CF content, but a similar ER value was also measured with 0.6% CF content. On the other hand, although different-sized voids were observed

in the matrix, conductive pathways remained, and electrical conductivity was not negatively affected due to optimized mixing and effective fiber-to-fiber contact.

Unlike the MCF and CF-based mixtures, microstructure analysis was not conducted on SF-based mixtures. The addition of 35-mm steel fibers to the matrix challenged the observation of the dispersion of conductors within the matrix. Thus, SEM and EDX analyses were not applied. Instead, the effect of the mixing method and usage rate on the electrical conductivity of SF-based mixtures was evaluated by analyzing the ER values measured from plate and cylinder samples.

4.3. Double Addition of Conductive Materials into the Cementitious Matrix

After the individual additions of the conductive materials, the ratios and mixing methods that resulted in the lowest ER value and cost of the mixture were considered. Based on these ratios, conductor fibers were added to the matrix mixture in three combinations: carbon fiber-milled carbon fiber, carbon fiber-steel fiber, and milled carbon fiber-steel fiber.

4.3.1. Flow Diameter and Flow Time Values of Composites with Double Conductive Material Incorporation

The effect of the combination of two conductive materials on the flow diameter and flow time of the matrix was examined. Among mixtures, the samples indicated with “CB22” had both carbon fiber and milled carbon fiber, the samples indicated with “AB22” had both carbon fiber and steel fiber, and the samples indicated with “CA22” had both milled carbon fiber and steel fiber. While carbon fiber was incorporated into the mixture only by the latter admixing method, steel and milled carbon fiber were incorporated into the mixture by both admixing methods in double conductor additions. The flow diameter and flow time results for mini-slump tests of carbon fiber and milled carbon fiber-based mixtures are shown in Figure 4.22.

Four groups were prepared using a combination of milled carbon fiber and carbon fiber. In each group, milled carbon fiber content was increased at the constant carbon fiber content. As seen in Figure 4.22-a, the flow diameters of the mixtures were adversely affected by the combined use of CF and MCF regardless of the mixing method. Flow diameters significantly reduced between the mixtures with the increase in carbon fiber. However, the increase of the MCF content at the same CF content had a more negative effect on the fluidity of the mixtures. In Figure 4.22-b, the flow times of mixtures showed similar behaviour to the flow diameter results regardless of the mixing method. The flow time of the mixture increased approximately two times compared to the reference sample with the use of both CF and MCF. Among the mixtures, the highest diameter and lowest time were measured from the mixture CB22(2), while the lowest diameter and highest time were measured from the mixture CB1010(1). The workability losses of the mixtures were related to the carbon-based fibers usage and their water-holding properties. In addition, adding milled carbon fiber using the synchronous admixing method adversely affected the flow diameters and times in all mixtures more than the first admixing method.

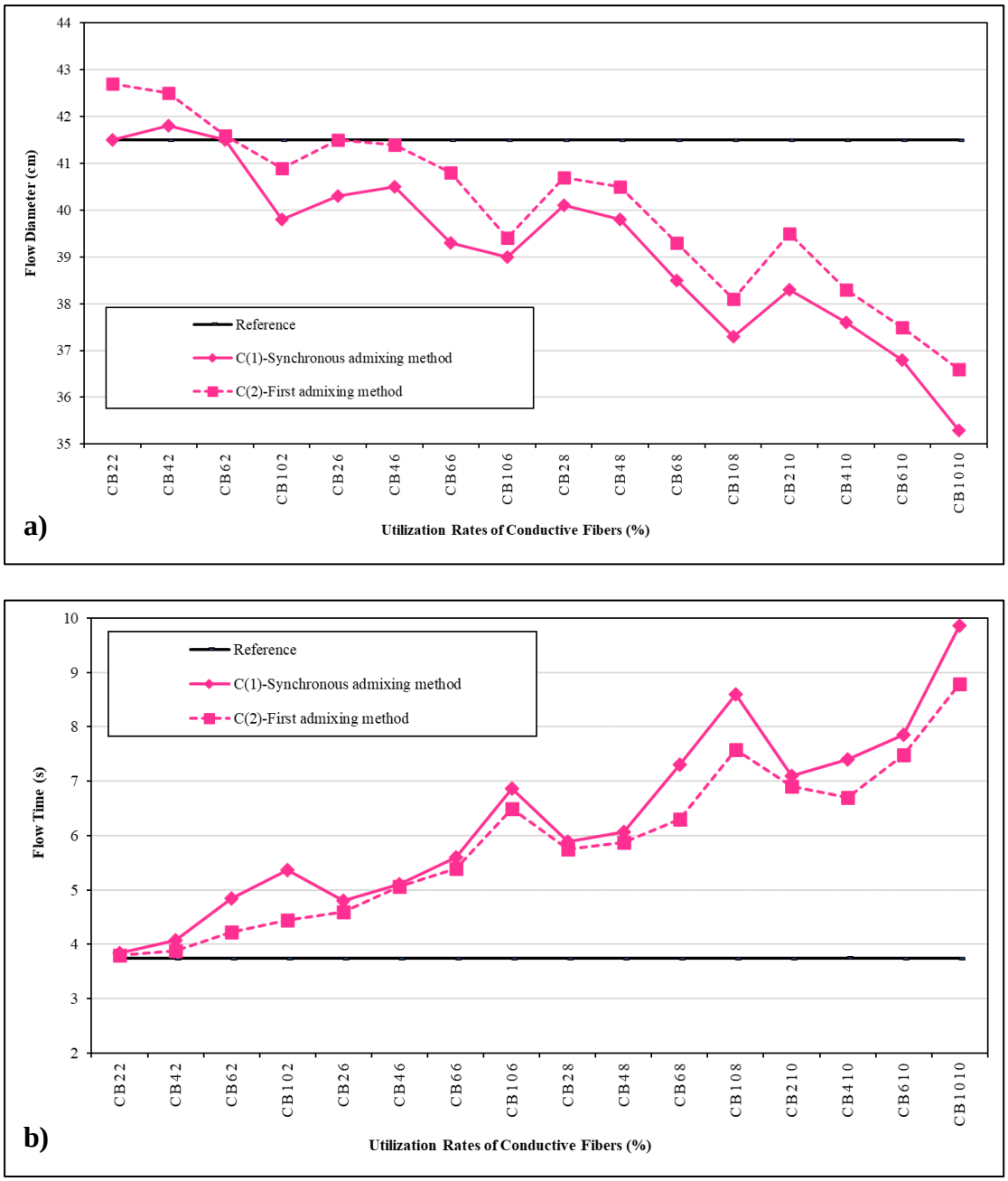

Figure 4.22. a) Flow diameter, and b) Flow time results for carbon fiber and milled carbon fiber-based mixtures

The flow diameter and flow time results for mini-slump tests of carbon fiber and steel fiber-based mixtures are shown in Figure 4.23. In combination with steel fiber and carbon fiber, four groups were prepared. Steel fiber content was increased in each group at the constant carbon fiber content.

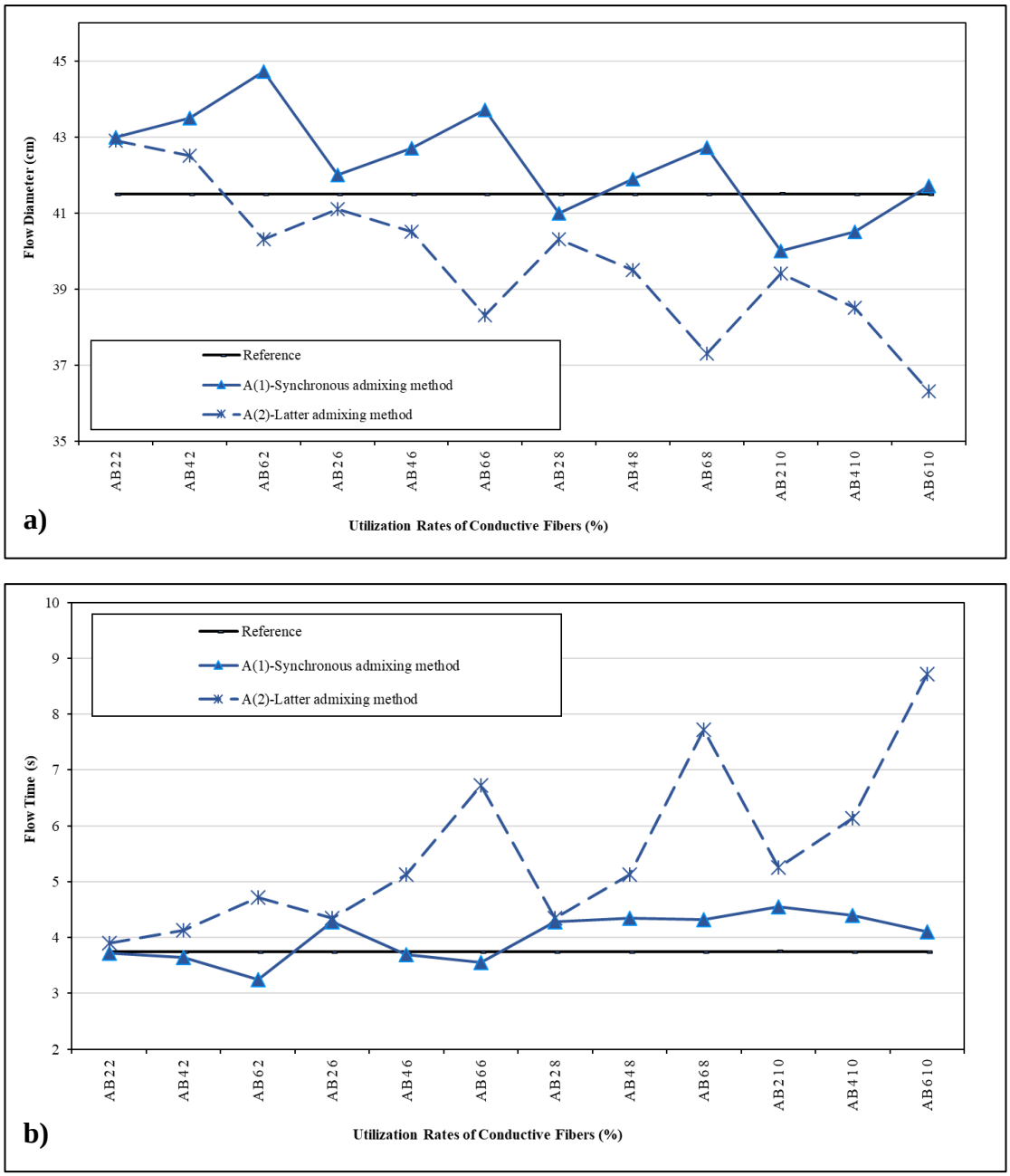

Figure 4.23. a) Flow diameter, and b) Flow time results for carbon fiber and steel fiber-based mixtures

As seen in Figure 4.23-a, steel fiber content with the mixing method directly affected the flow diameter of the mixtures. Increasing the amount of steel fiber at the same carbon fiber content increased flow diameters in the synchronous admixing method. Although higher carbon fiber content reduced the flow diameters of the mixtures, a similar flow diameter value was measured in the AB610(1) sample with the reference sample. While the flow diameters of the mixtures decreased with the carbon fiber content, they exhibited a higher flow diameter than the reference mixture when steel fibers were used. This

discrepancy was attributed to the collapsing of steel fibers in the dry mixture, or the technical properties of the steel fibers may have indirectly affected the workability. However, the opposite behavior was observed in both steel fiber and carbon fiber addition with the latter admixing method. With a higher steel and carbon fiber content in the mixtures, the flow diameters decreased significantly. The flow diameter was measured for the AB610(2) mixture as 36.3 cm. Adding steel fiber to the mortar mixture with carbon fiber resulted in better adherence and more homogeneous dispersion. However, the decreased flowability caused by the carbon fiber could not be compensated by simultaneously adding steel fiber. In Figure 4.23-b, similar behavior was also observed in the flow time results. The flow time for mixtures using the synchronous admixing method varied between 3 and 5 seconds. As the steel fiber content increased in the mixture, the flow time decreased regardless of the carbon fiber content. Although the flow time increased with the higher carbon fiber in the mixtures, it was similar to the reference mixture. On the other hand, the flow time increased with the higher amount of steel and carbon fiber in the latter admixing method. The highest flow time of the mixture was measured to be approximately 2.5 times longer in the AB610(2) sample than that of the reference mixture. The content of steel fiber and the mixing method directly affected the workability of the mixture.

The flow diameter and flow time results for mini-slump tests of milled carbon fiber and steel fiber-based mixtures are shown in Figure 4.24. While both mixing methods were used in milled carbon fiber additions, only the synchronous admixing method was preferred in steel fiber additions in terms of workability concerns. Three groups were prepared in combination with steel fiber and milled carbon fiber. Milled carbon fiber content was increased in each group at the constant steel fiber content.

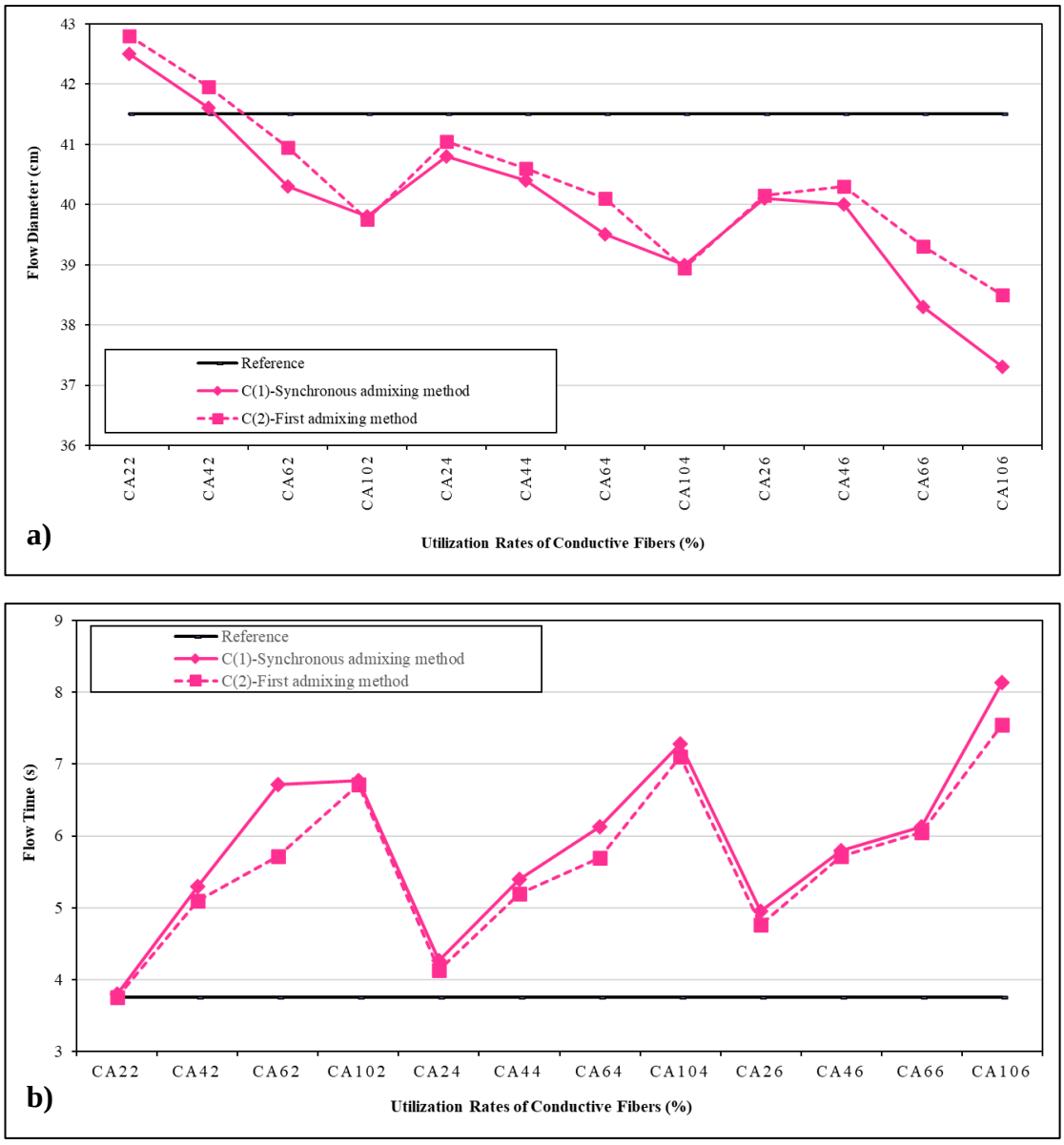

Figure 4.24. a) Flow diameter, and b) Flow time results for milled carbon fiber-steel fiber-based mixtures

As seen from Figure 4.24-a, increasing the amount of steel fiber at the same carbon fiber content decreased flow diameters. The lowest flow diameter was obtained from the CA106(1) sample using 0.6% SF and 1.0% MCF. Although higher diameters were measured in mixtures using the first admixing method, the mixing method of MCF did not significantly change the diameters of the mixtures among all mixtures. Due to the fact that MCF was carbon-based and had water-holding properties, the diameters of the mixtures were affected regardless of the mixing method. In Figure 4.24-b, a similar behavior was also observed in the flow time. As both the MCF and SF content increased

in the mixture, the flow times of the mixtures increased. The flow time of the mixtures was measured as 8.13 seconds in the CA106(1) mixture.

4.3.2. Compressive Strength Results of Composites with Double Conductive Material Incorporation

Average compressive strength results of mixtures containing a combination of the carbon fiber-milled carbon fiber, carbon fiber-steel fiber, and milled carbon fiber-steel fiber were measured for different curing ages of 1, 3, 7, 28, and 90 days. The compressive strength results of the combination of the carbon fiber-milled carbon fiber were shown in Figure 4.25 for different curing ages.

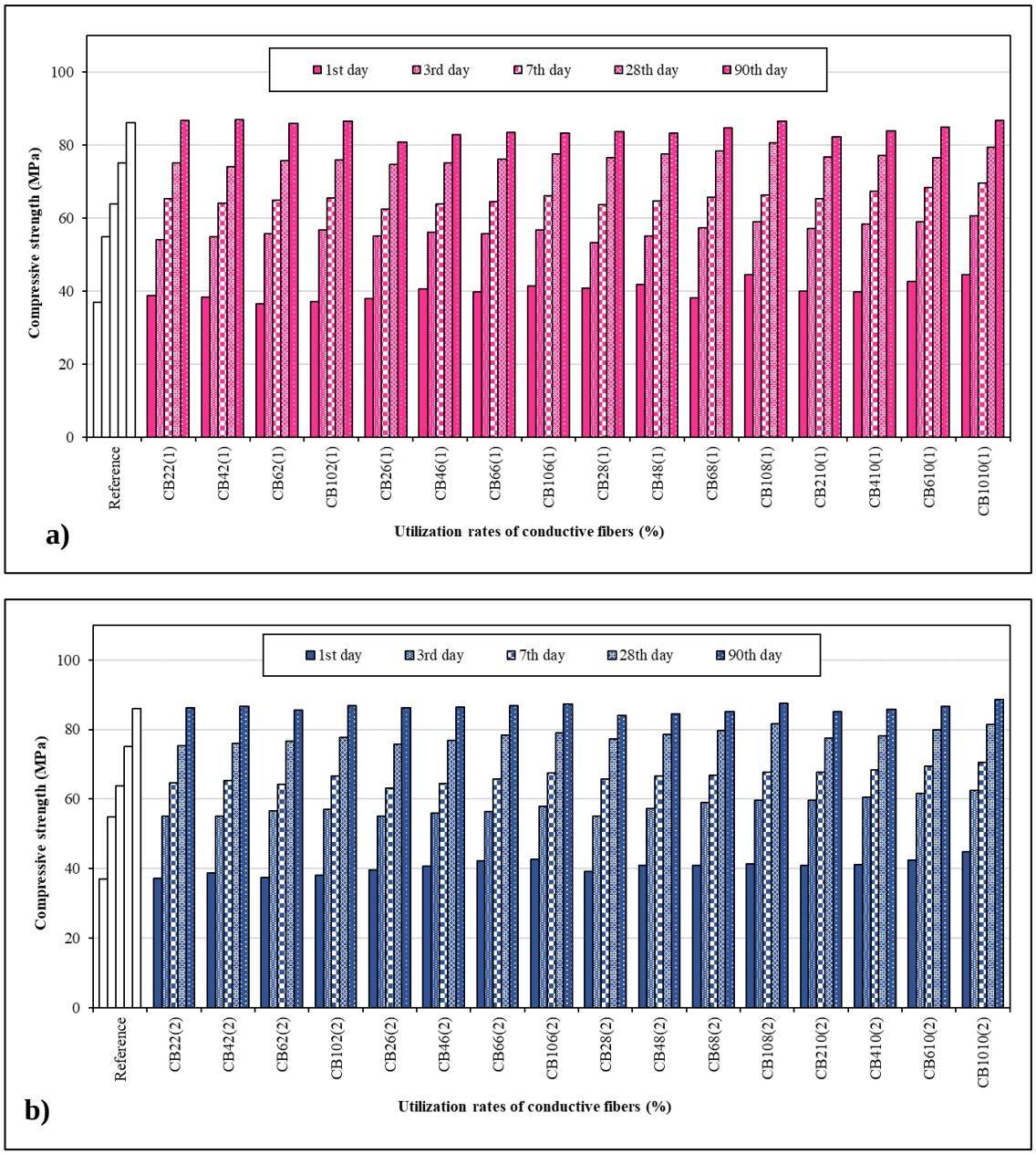

Figure 4.25. Compressive strength results of the mixtures by preparing, a) The synchronous admixing method, b) The first admixing method

Independently from the type of conductive fiber and mixing method, all specimens showed an incremental trend in compressive strength results with rates similar to those of age. It was measured in the general sense that all mixtures reached 40-50%, 50-60%, 70-75%, and 85-90% of their ultimate compressive strength (90-day strength values) after 1, 3, 7, and 28 days, respectively. As seen from Figure 4.25-a, the differences between compressive strengths of the combination of CF and MCF at different rates were observed by incorporating MCF into a matrix with a synchronous admixing method. Four groups

were prepared, and the MCF was increased for the same CF content in each group. According to the results on different curing days, combining MCF and CF content enhanced the compressive strength. The higher content of both conductive materials in the mixture improved compressive strength at all ages. The highest compressive strength increment was measured for the first day. CF was incorporated into a matrix using the latter admixing method, and MCF was incorporated into a matrix using the synchronous admixing method, which did not adversely affect compressive strength. In Figure 4.25-b, the differences between compressive strengths of the combination of CF and MCF at different rates were observed by incorporating MCF into a matrix with the first admixing method. Four groups were prepared, and the MCF content was increased to the same carbon fiber content in each group. The differences in the compressive strengths of the mixtures were similar to the mixtures using the synchronous admixing method. The combined use of MCF and CF with the higher content of fibers in the matrix improved the compressive strength positively. Unlike other mixing method, higher strength results were obtained in all mixtures for all measurement days by adding MCF using the first admixing method. From here, the incorporation of carbon fiber with the latter admixing method and the incorporation of MCF with the first admixing method dispersed the fibers more homogeneously into the matrix, improving the compressive strength of the mixtures. The compressive strength results of the combination of the carbon fiber-steel fiber are shown in Figure 4.26 for different curing ages.

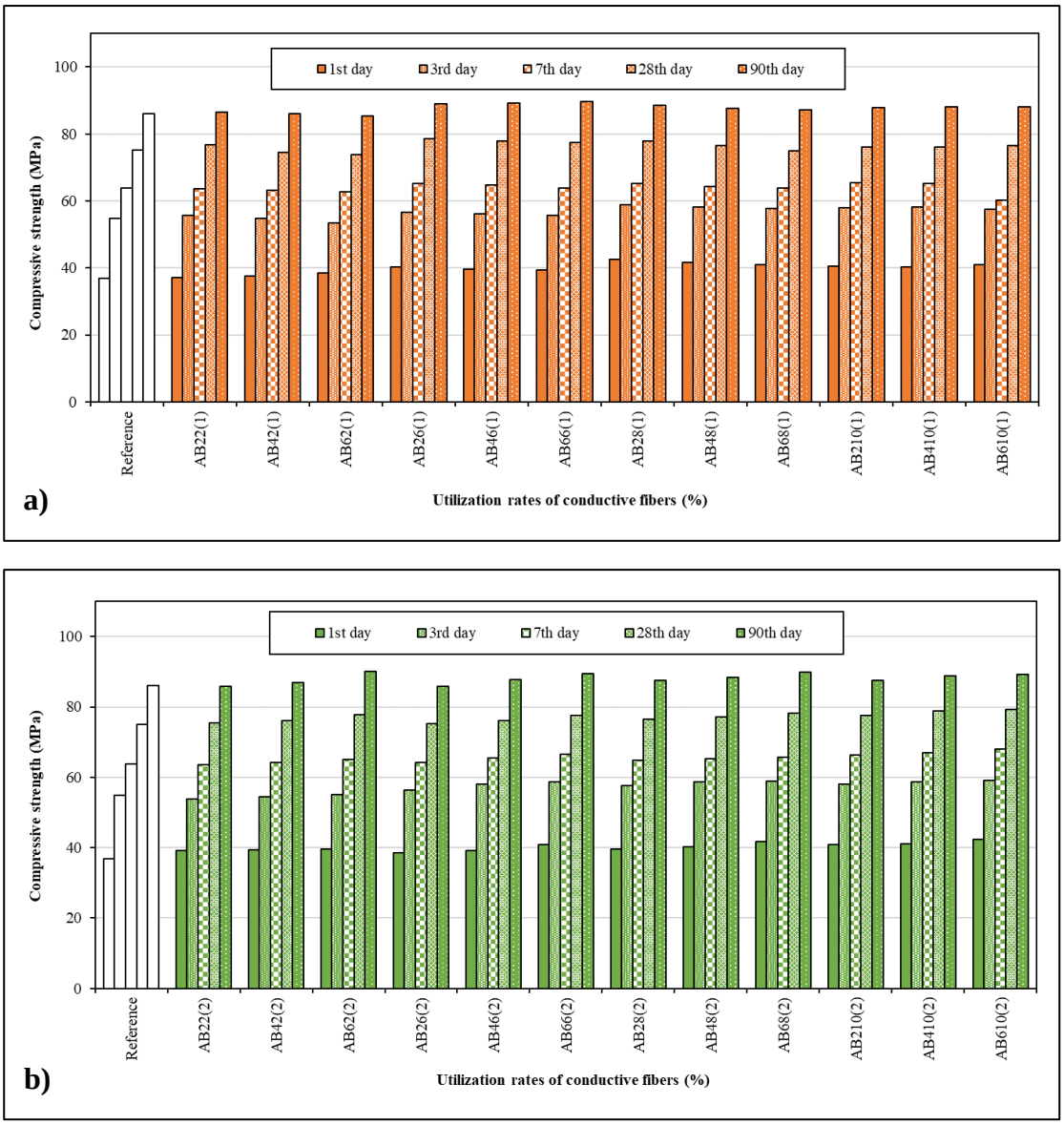

Figure 4.26. Compressive strength results of the mixtures by preparing, a) The synchronous admixing method, b) The latter admixing method

Independently from the type of conductive fiber and mixing method, all specimens showed an incremental trend in compressive strength results with rates similar to those of age. As seen from Figure 4.26-a, the differences between compressive strength results of the combination of CF and SF at different rates were observed by incorporating SF into a matrix with a synchronous admixing method. Four groups were prepared, and the SF content was increased at the same CF content in each group. According to the results on different curing days, increasing the CF content positively affected the strengths. The highest compressive strengths were obtained using 1.0% CF, and the highest increments were obtained for first day. However, higher SF content at the same CF content did not

significantly change the strength values on all measurement days. While the strength differences were higher in the first day measurements, the strength values were at similar levels at the end of the 90th day. It had been determined that the negative effect of steel fiber decreased depending on the curing time. The effect of both conductors on the compressive strength was decreased after 28 days. In Figure 4.26-b, the differences between compressive strengths of the combination of CF and SF at different rates were observed by incorporating SF into a matrix with the latter admixing method. Four groups were prepared, and the SF content was increased at the same CF content in each group. According to the results of the mixtures on different curing days, the combination of SF and CF content positively affected the compressive strength. The higher content of both conductive materials in the mixture improved compressive strength at all ages. The highest compressive strength increment was measured in the first day. However, the incorporation of SFs into the matrix with the latter admixing method had a positive effect on the strength. Although higher CF content in both mixtures affected the strength positively, the strength values varied depending on the SF ratio and admixing method in the SF combination. The addition of CF and SF into the mortar mixture with the latter admixing method provided homogeneous dispersion into the matrix, resulting in higher strength. Although the strength values of the mixtures were at similar levels at the end of the 90th day, the highest strength was obtained from the AB610(2) mixture. The compressive strength results of the combination of the milled carbon fiber-steel fiber are shown in Figure 4.27 for different curing ages.

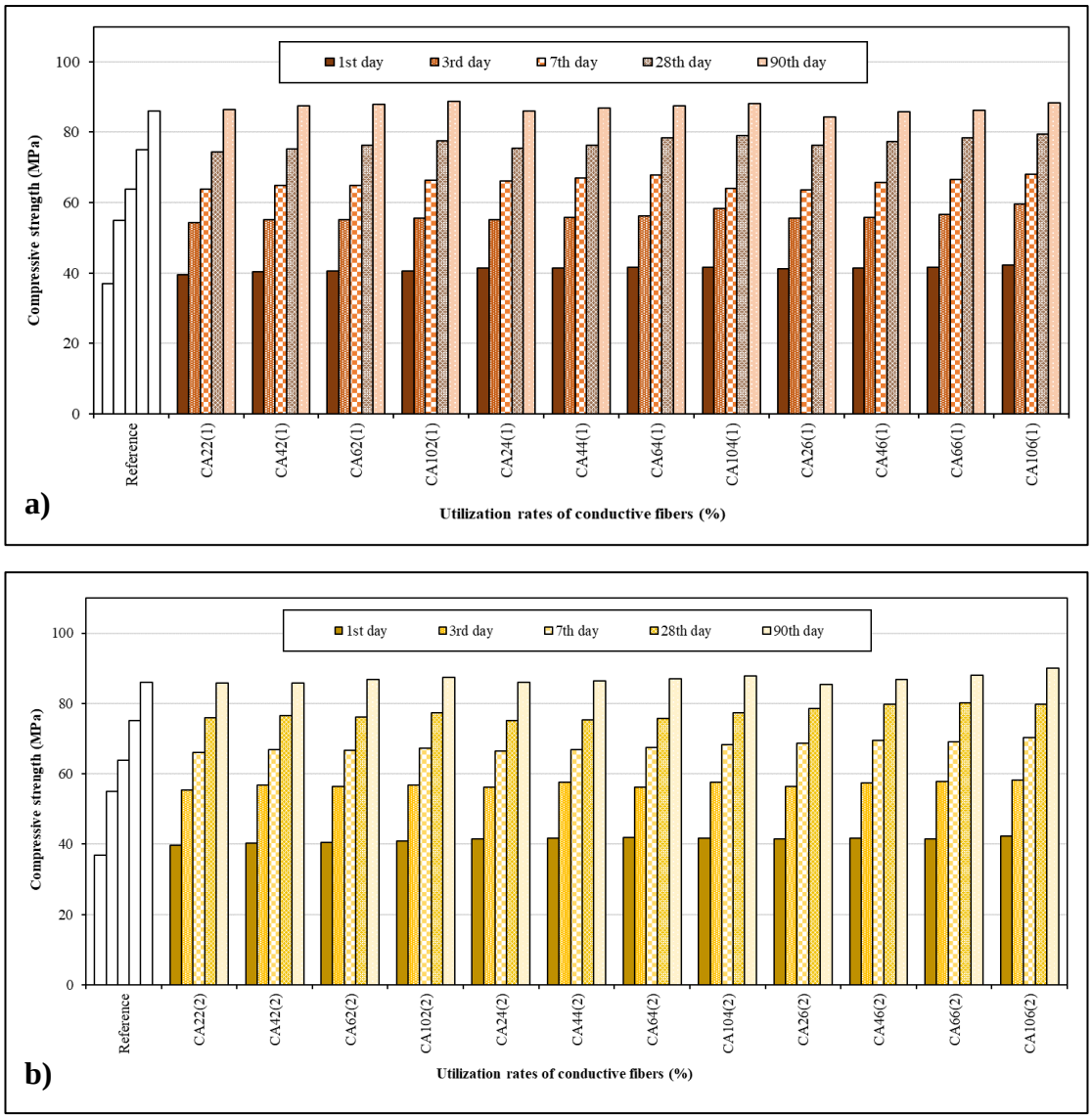

Figure 4.27. Compressive strength results of the mixtures by preparing, a) The synchronous admixing method, b) The first admixing method

Independently from the type of conductive fiber and mixing method, all specimens showed an incremental trend in compressive strength results with rates similar to those of age. Although the method of adding SF caused a small increment in strength from the first day, the synchronous admixing method was preferred, considering the workability of the mixtures. For this reason, SF was added to the SF and MCF mixture only using the synchronous admixing method. Since similar results were obtained in both mixtures, MCFs were added to the mixtures using both synchronous and first admixing methods in steel and MCF mixtures. As seen from Figure 4.27-a, the differences between compressive strength values of the combination of MCF and SF at different rates were

observed by incorporating MCF into a matrix with a synchronous admixing method. Three groups were prepared, and the MCF content was increased at the same SF content in each group. According to the results on different curing days, increasing the MCF content with SF positively affected the strengths. The higher content of both conductive materials in the mixture improved compressive strength at all ages. Compared to the strength results of the reference mixture on all days, adding fibers at different ratios had the most positive effect on the first-day measurements. Using the synchronous admixing method, the compressive strength increased with increased MCF content. In Figure 4.27-b, the differences between compressive strength values of the combination of MCF and SF at different rates were observed by incorporating MCF into a matrix with the first admixing method. Three groups were prepared, and the MCF content was increased at the same SF content in each group. According to the results on different curing days, similar strength values were measured with the synchronous and first admixing methods. However, slightly higher compressive strength was measured in the first admixing method used mixtures. Compared to the strength values of the reference mixture among all days, the addition fibers at different ratios had the most positive effect on the first-day measurements. In general, the mixing method did not significantly affect the compressive strength of the mixtures in the combination of milled carbon fiber with steel fiber.

4.3.3. Electrical Resistance Results of Composites with Double Conductive Material Incorporation

4.3.3.1. Electrical Resistance Results of Coating Samples

The electrical resistance of the mixtures was determined using two experimental devices. After determining the optimal ratios for each fiber through single incorporation, conductors were combined in double: carbon fiber-milled carbon fiber, carbon fiber-steel fiber, and milled carbon fiber-steel fiber. Average electrical resistances (ER) were measured from the coating sample of related mixtures after 1, 3, 7, 28, 90, and 180 days of curing. The ER results of the reference sample without any conductive material were 15.4, 20.8, 33.2, 65.4, 75.3, and 104.5 MΩ after 1, 3, 7, 28, 90, and 180 days of curing, respectively. It had insulative performance even after the first day without conductive

material addition. The ER results of the carbon fiber-milled carbon fiber-based mixtures until 180th day are shown in Figure 4.28.

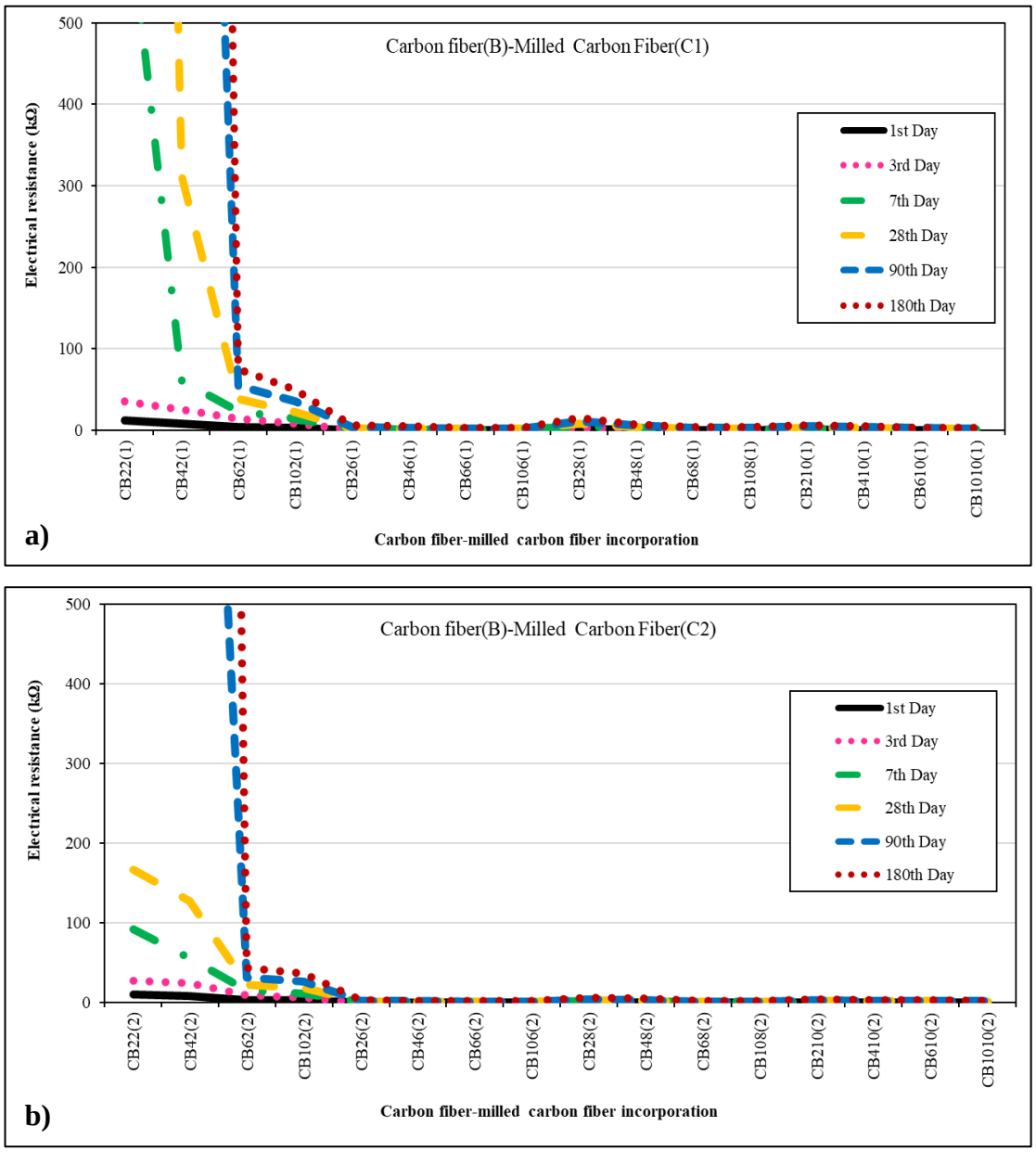

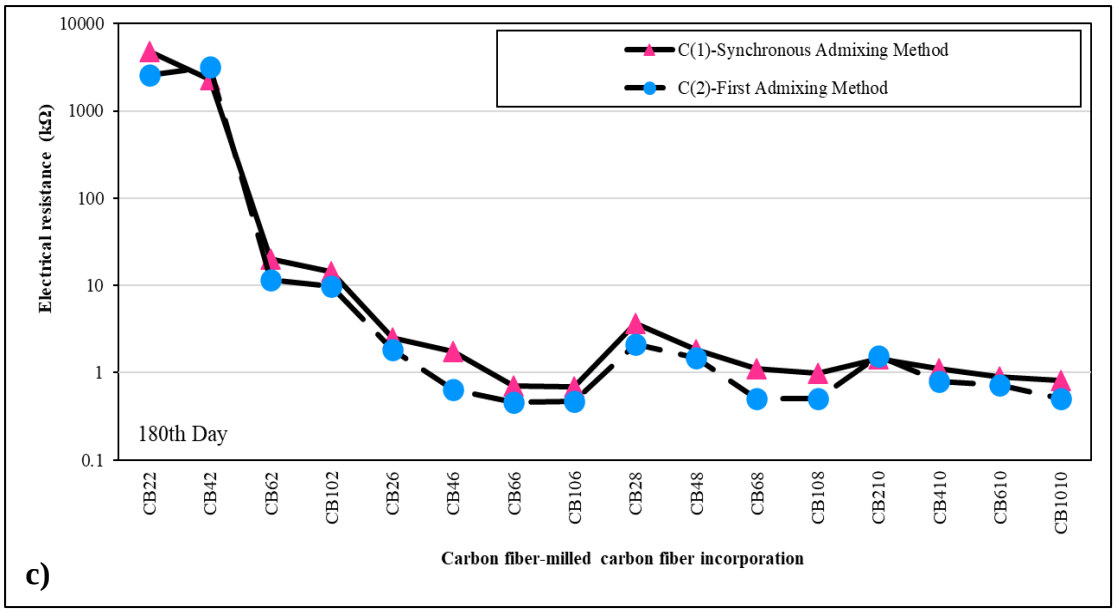

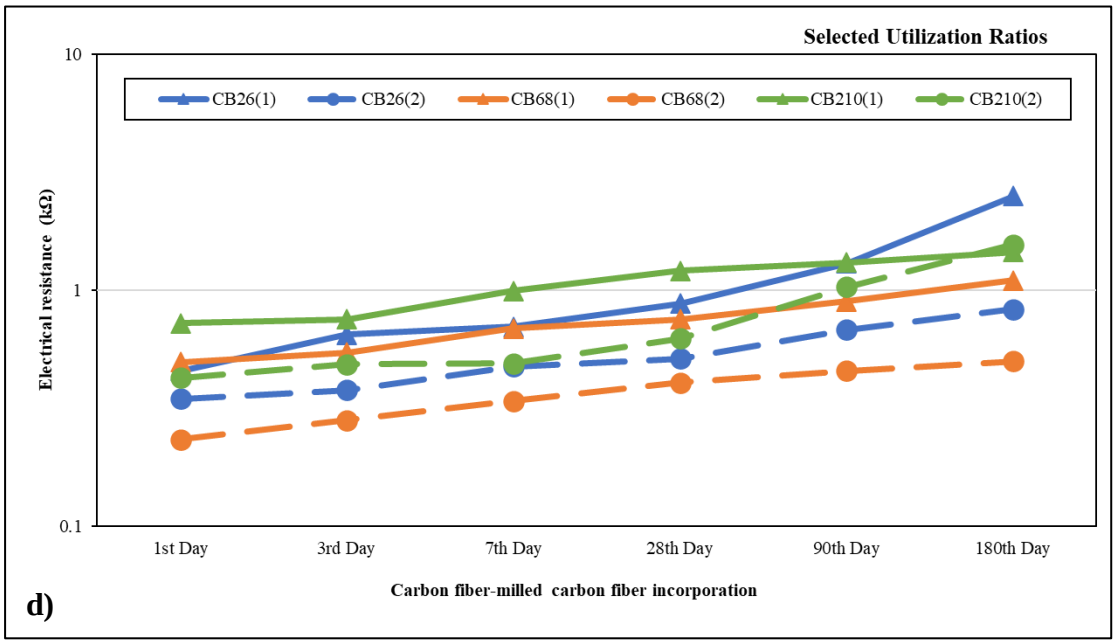

Figure 4.28. Age-dependent ER results of carbon fiber-milled carbon fiber-based composites produced with a) The synchronous admixing method, and b) The first admixing method, Effect of dispersion methods on c) 180-day ER results, d) Selected samples having the lowest ER results with age

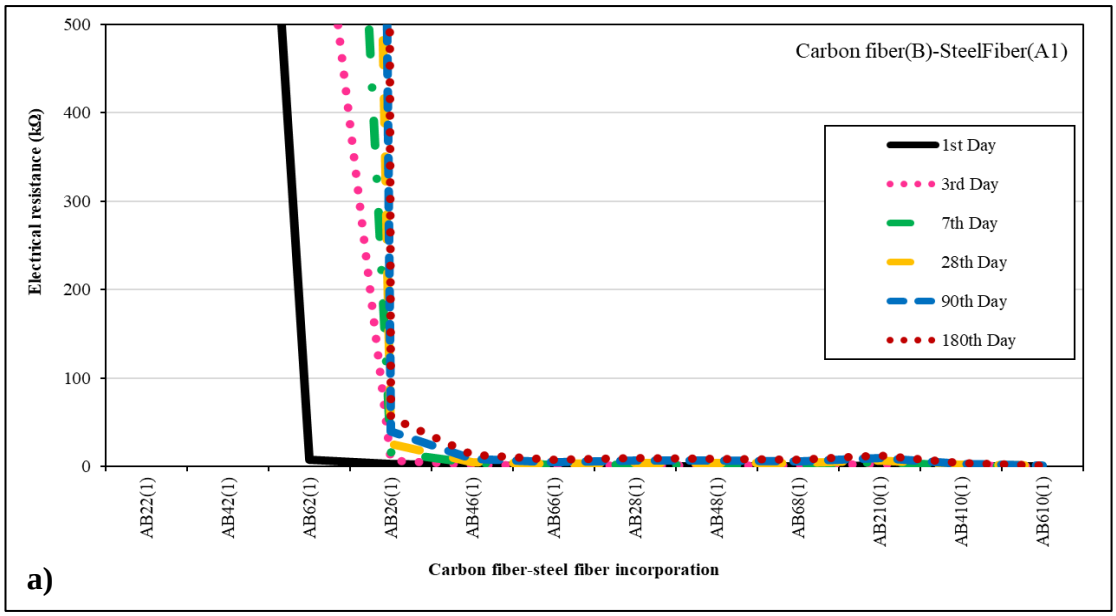
Carbon fiber(B)-SteelFiber(A1)
Electrical resistance (kΩ)
500
400
300
200
100
0
1st Day
3rd Day
7th Day
28th Day
90th Day
180th Day
AB22(1)
AB42(1)
AB62(1)
AB26(1)
AB46(1)
AB66(1)
AB28(1)
AB48(1)
AB68(1)
AB210(1)
AB410(1)
AB610(1)
Carbon fiber-steel fiber incorporation

a)

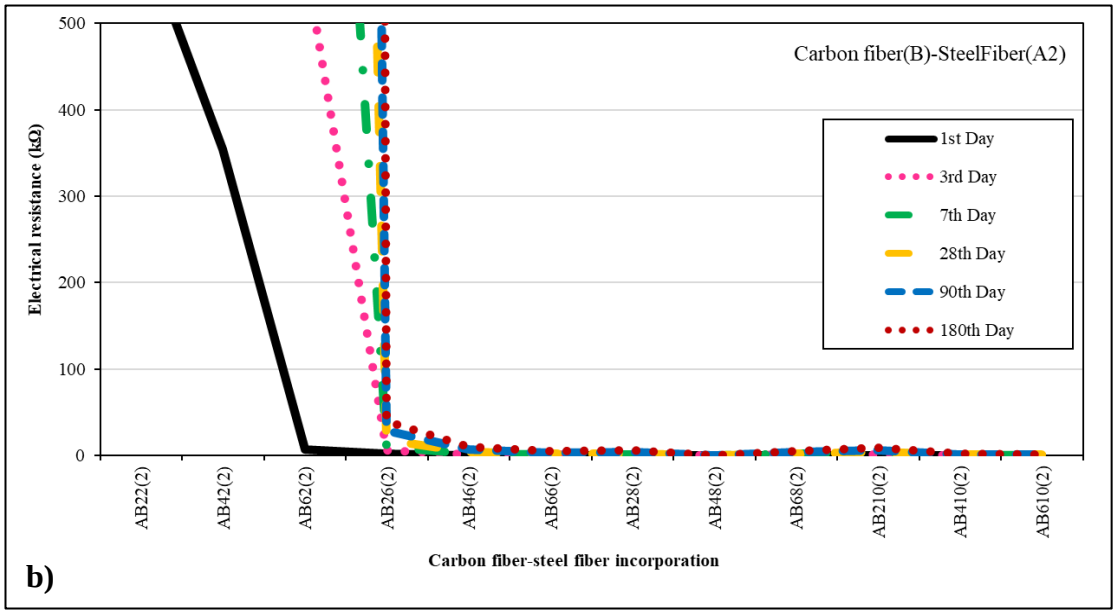
Carbon fiber(B)-SteelFiber(A2)
Electrical resistance (kΩ)
500
400
300
200
100
0
1st Day
3rd Day
7th Day
28th Day
90th Day
180th Day
AB22(2)
AB42(2)
AB62(2)
AB26(2)
AB46(2)
AB66(2)
AB28(2)
AB48(2)
AB68(2)
AB210(2)
AB410(2)
AB610(2)
Carbon fiber-steel fiber incorporation

b)

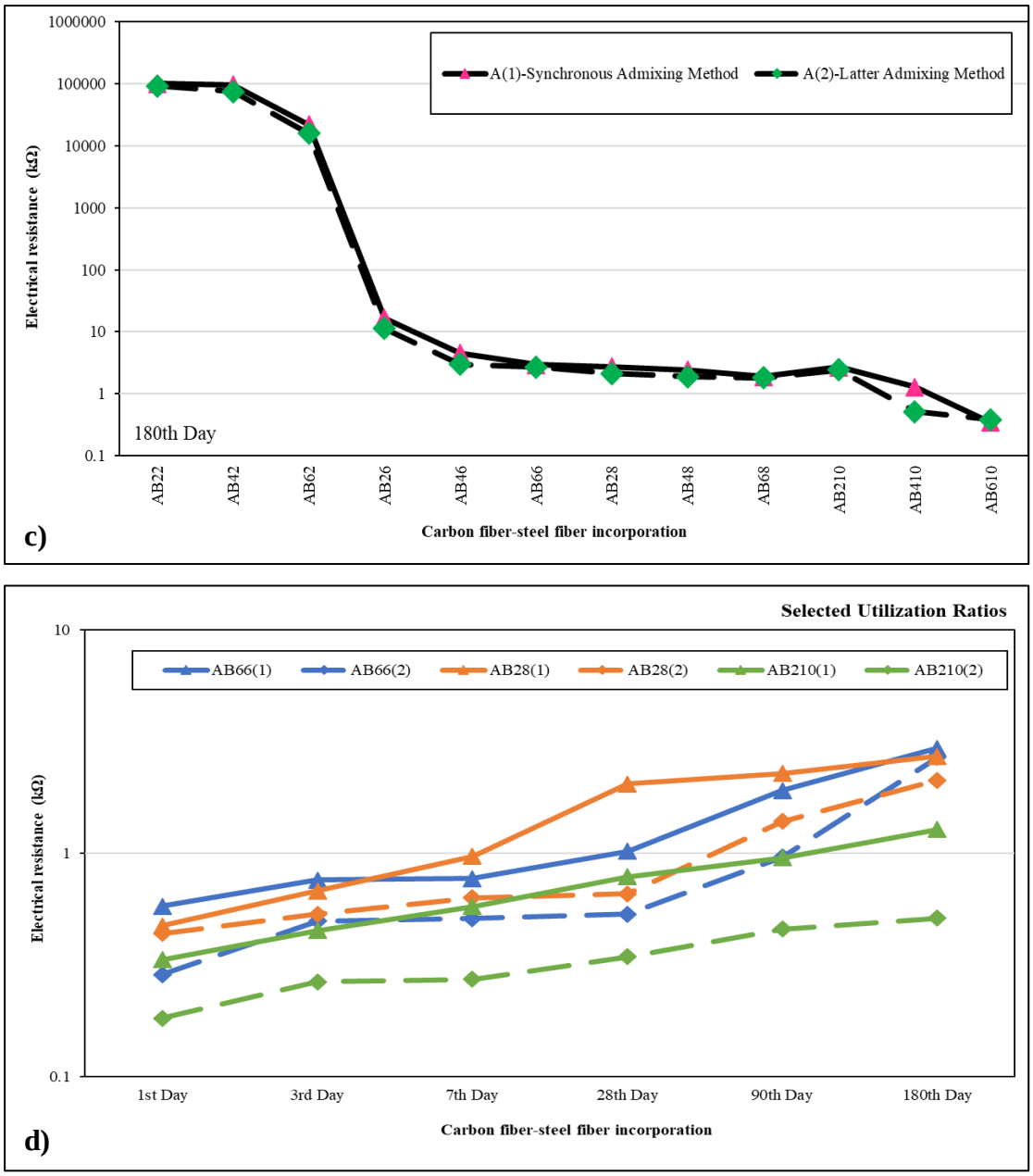

Figure 4.29. Age-dependent ER results of carbon fiber-steel fiber-based composites produced with a) The synchronous admixing method, and b) The latter admixing method, Effect of dispersion methods on c) 180-day ER results, d) Selected samples having the lowest ER results with age

Although all mixtures showed electrical conductivity performance, one of the most critical criteria in developing coating design for floor applications was the development of cost-effective coatings. Therefore, selections were made by considering the lowest conductor ratio in the matrix. In Figure 4.28-c, ER values of all mixtures at the end of 180 days are shown. While similar ER results were obtained for the same content, lower

ER values were measured in MCF-based mixtures prepared by the first admixing method. As in single additions, MCFs were distributed more homogeneously using the first admixing method and formed an effective conductive network. Apart from this result, the lowest ER values were obtained at 0.8% and 1.0% CF content in both mixing methods. Among all the mixtures, the most effective mixtures were selected based on economic criteria as CB26 (0.2% MCF, 0.6% CF), CB68 (0.6% MCF, 0.8% CF), and CB210 (0.2% MCF, 1.0% CF) mixtures. In Figure 4.28-d, ER values of selected mixtures increased depending on the measurement day. However, the ER values of all mixtures remained below 10 kΩ even after the 180th day. This result showed that the mixtures could maintain electrical performance in the long term. Ternary additions were made by considering this conductor ratio. The ER results of the carbon fiber-steel fiber-based mixtures until 180th day are shown in Figure 4.29.

In Figure 4.29-a and b, the differences in ER results were observed based on the mixing method. Regardless of the mixing method, the composites showed conductive performance with a resistance value below the performance limit of 100 kΩ in the long term except for 0.2% CF-based mixtures. Despite the increased SF content and 0.2% CF content, the ER value of the mixtures decreased but remained above the performance criteria. Regardless of the mixing method, a conductive network was formed, and its conductivity was maintained in the long term by adding 0.6% CF to mixtures containing steel and carbon fiber. The minimum conductor usage was taken as a basis for the coating design to be cost-effective. Since CF was more costly than SF and MCF, the lowest CF content was preferred. When similar results were observed between mixtures with the same CF content, the lowest usage ratio of the second conductor was preferred. In Figure 4.29-c, ER values of all mixtures at the end of 180 days are shown. Based on the results, the long-term ER values of mixtures containing 0.2% CF increased to 100 MΩ, showing insulating performance. The ER values decreased to below 10 kΩ at the end of the 180 days, attributed to adding carbon fiber to the matrix. Between mixing methods, slightly lower ER values were measured in the mixtures prepared with the latter admixing method. In addition, the lowest ER value was obtained from the AB610(2) mixture in all mixtures. However, the most effective mixtures were selected based on economic criteria as AB66 (0.6% SF, 0.6% CF), AB28 (0.2% SF, 0.8% CF), and AB210 (0.2% MCF, 1.0% CF) mixtures. In Figure 4.29-d, ER values of selected mixtures increased depending on the

measurement day. However, the ER values of all mixtures remained below 10 kΩ even after the 180th day. This result showed that the mixtures could maintain electrical performance in the long term. Triple additions were made by considering this conductor ratio. The ER results of the milled carbon fiber-steel fiber-based mixtures until the 180th day are shown in Figure 4.30.

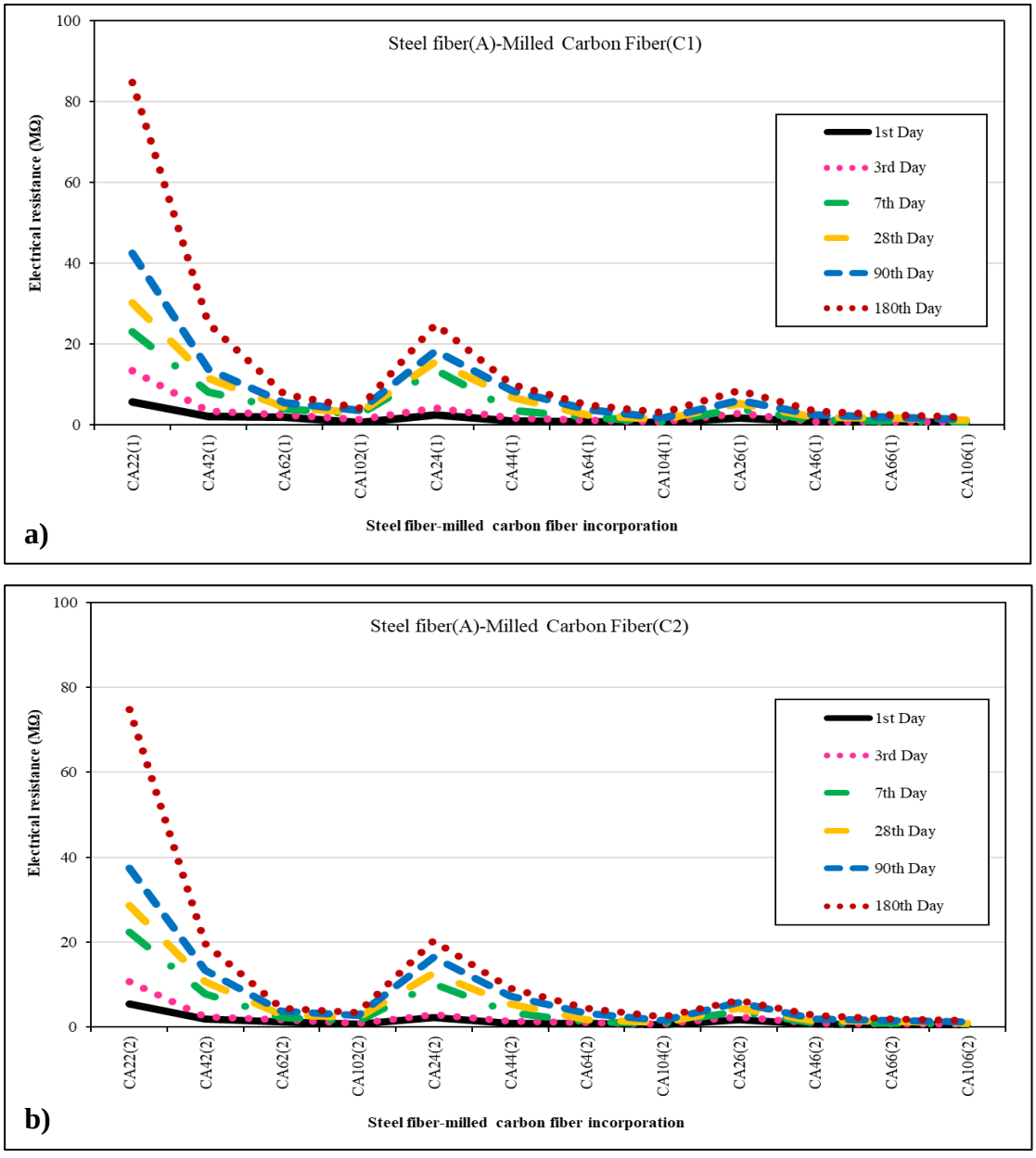

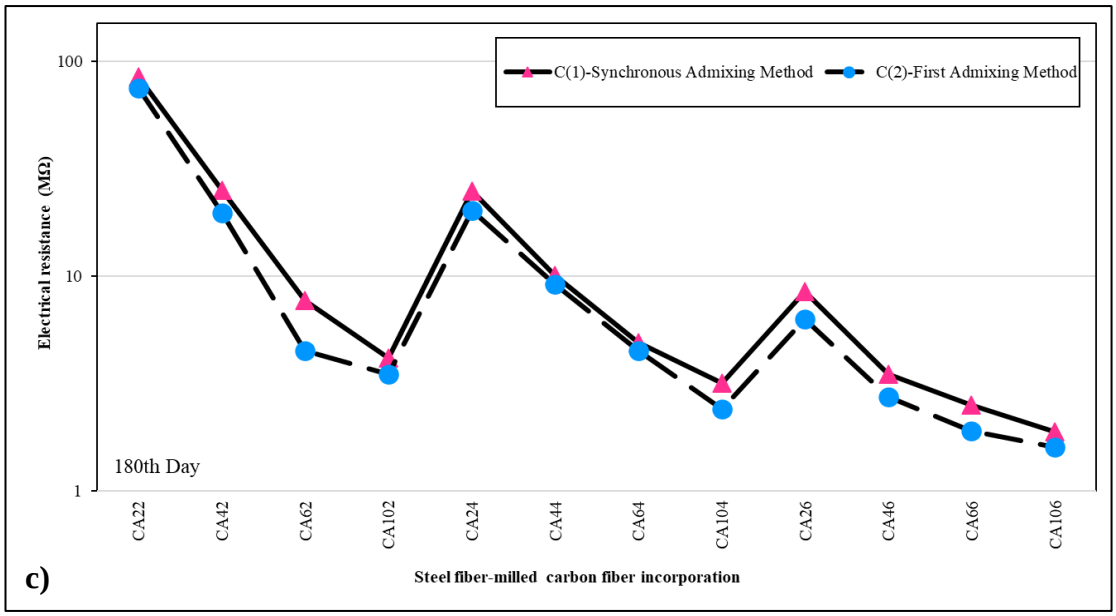

Figure 4.30. Age-dependent ER results of milled carbon fiber-steel fiber-based composites produced with a) The synchronous admixing method, and b) The first admixing method, Effect of dispersion methods on c) 180-day ER results, d) Selected samples having the lowest ER results with age

In Figure 4.30-a and b, the differences in ER results were observed based on the mixing method. Regardless of the mixing method, ER values decreased significantly with increasing conductor content in the mixtures. However, the composites showed insulator performance with a resistance value higher than performance limit of 1 MΩ in the long term. Although increasing the MCF content in both admixing methods was more effective

in decreasing the ER value, the conductivity performance could not be maintained in the long term. The SF content contributed to a decrease in the ER values. However, the higher SF content caused to an increase in ER value depending on time. The admixing method of MCF slightly changed the ER values. In Figure 4.30-c, ER values of all mixtures at the end of 180 days are shown. Based on the results, the long-term ER values of all mixtures changed between 1 – 100 MΩ and showed insulating performance. Lower ER results were measured in mixtures using the first admixing method among the mixing methods. The lowest ER value was measured from the CA106 (1.0%MCF, 0.6%SF) mixture. It was determined that the type and content of the conductors were not suitable for triple additions due to the higher conductive ratio in the mixture and the higher long-term ER value. Since all mixtures had ER values at the MΩ level, selecting the mixtures with the lowest conductive ratio was decided. Therefore, the most effective mixtures were selected based on economic criteria as CA42 (0.4% MCF, 0.2% SF) and CA64 (0.6% MCF, 0.4% SF) mixtures. In Figure 4.30-d, ER values of selected mixtures increased depending on the measurement day. Regardless of the mixing method, the 1-day ER value of the mixtures increased from around 1 MΩ to 5 MΩ at the end of 180 days. The performance criteria were not achieved by double adding milled carbon fiber and steel fiber. Triple additions were chosen based on this criterion.

4.3.3.2. Electrical Resistance Results of Cylindrical Samples

One of the other experimental methods for the electrical resistance values was determined by the AC method. Unlike the coating design, the ER values were measured from three parts of the cylindrical sample to determine whether the conductive materials were distributed homogeneously into the matrix mixture. The ER values of three cylindrical parts were measured from the cylindrical samples after 1, 3, 7, 28, 90, and 180 days of curing. ER results of carbon fiber-milled carbon fiber-based mixtures measured considering age and parts obtained are given in Table 4.31 and Table 4.32. In Table 4.31, milled carbon fibers were added to the mixture using the synchronous admixing method. In contrast, milled carbon fibers were added to the mixture using the first admixing method, as given in Table 4.32.

Table 4.31. ER results of the carbon fiber-milled carbon fiber-based mixtures using the synchronous admixing method, Ω

Sample	Ratio, %		Parts of the cylinder	1st day	3rd day	7th day	28th day	90th day	180th day
	MCF	CF							
Reference	0.0	0.0	Bottom	521	785	1500	19820	162000	226000
			Middle	552	768	1350	17600	168000	223000
			Top	1600	50600	90300	190000	626000	773000
CB22(1)	0.2	0.2	Bottom	318	354	382	945	2330	4590
			Middle	314	343	374	932	2240	4430
			Top	335	356	448	1370	4430	8578
CB42(1)	0.4		Bottom	306	318	375	927	2170	4235
			Middle	303	306	364	914	2110	4200
			Top	324	321	397	1280	4090	7867
CB62(1)	0.6		Bottom	240	357	474	1250	2850	3548
			Middle	233	343	467	1210	2690	3476
			Top	235	374	530	1590	4430	8209
CB102(1)	1.0		Bottom	206	287	339	829	1400	2100
			Middle	204	279	327	817	1260	2089
			Top	220	296	360	963	1640	1875
CB26(1)	0.2	0.6	Bottom	189	327	356	530	559	573
			Middle	185	296	333	520	538	546
			Top	188	323	355	541	578	592
CB46(1)	0.4		Bottom	171	229	257	292	312	334
			Middle	163	219	238	279	306	321
			Top	179	257	268	312	366	385
CB66(1)	0.6		Bottom	262	268	298	341	409	438
			Middle	257	264	289	326	397	402
			Top	269	276	318	382	453	474
CB106(1)	1.0		Bottom	282	312	358	397	541	567
			Middle	260	307	327	371	516	538
			Top	296	318	345	397	578	603
CB28(1)	0.2	0.8	Bottom	318	322	345	360	385	398
			Middle	308	319	363	375	382	385
			Top	326	339	343	355	386	389

Table 4.31. ER results of the carbon fiber-milled carbon fiber-based mixtures using the synchronous admixing method, Ω (continued)

CB48(1)	0.4	0.8	Bottom	274	288	301	303	307	311
			Middle	264	272	298	302	304	307
			Top	289	322	327	342	368	392
CB68(1)	0.6		Bottom	206	213	246	262	274	278
			Middle	202	210	248	256	269	272
			Top	231	252	267	285	305	308
CB108(1)	1.0		Bottom	322	343	362	392	444	451
			Middle	315	338	355	371	410	433
			Top	345	362	372	385	485	497
CB210(1)	0.2	1.0	Bottom	195	218	226	239	281	298
			Middle	191	205	275	293	321	335
			Top	199	217	289	317	345	378
CB410(1)	0.4		Bottom	185	214	219	220	269	278
			Middle	178	202	268	267	298	300
			Top	197	225	278	296	339	351
CB610(1)	0.6		Bottom	174	202	215	203	241	246
			Middle	162	198	253	244	278	285
			Top	181	205	265	289	317	330
CB1010(1)	1.0		Bottom	168	201	222	236	238	244
			Middle	165	188	215	231	236	241
			Top	186	193	206	218	227	236

Table 4.32. ER results of the carbon fiber-milled carbon fiber-based mixtures using the synchronous admixing method, Ω

Sample	Ratio, %		Parts of the cylinder	1st day	3rd day	7th day	28th day	90th day	180th day
	MCF	CF							
Reference	0.0	0.0	Bottom	521	785	1500	19820	162000	226000
			Middle	552	768	1350	17600	168000	223000
			Top	1600	50600	90300	190000	626000	773000
CB22(2)	0.2	0.2	Bottom	301	342	379	751	1627	3678
			Middle	305	333	362	732	1645	3549
			Top	345	352	375	1050	3530	7584
CB42(2)	0.4		Bottom	298	304	356	627	1870	3346
			Middle	293	299	344	619	1830	3278
			Top	307	314	368	880	3359	6800
CB62(2)	0.6		Bottom	244	287	347	640	1650	3043
			Middle	236	278	321	635	1549	3132
			Top	254	303	348	795	3130	6150
CB102(2)	1.0		Bottom	211	275	318	629	1267	2005
			Middle	226	266	316	608	1148	1982
			Top	233	289	340	683	1550	2060
CB26(2)	0.2	0.6	Bottom	181	282	336	496	524	558
			Middle	180	288	323	488	538	556
			Top	184	301	334	501	536	573
CB46(2)	0.4		Bottom	179	228	236	268	328	345
			Middle	182	232	239	270	311	318
			Top	174	234	237	282	354	356
CB66(2)	0.6		Bottom	192	248	254	273	358	389
			Middle	169	246	255	268	367	374
			Top	186	233	248	277	353	387
CB106(2)	1.0		Bottom	188	222	263	288	358	385
			Middle	174	197	238	254	314	369
			Top	197	218	257	296	366	392
CB28(2)	0.2	0.8	Bottom	246	267	338	371	391	403
			Middle	238	248	363	388	390	412
			Top	255	274	355	377	385	424

Table 4.32. ER results of the carbon fiber-milled carbon fiber-based mixtures using the synchronous admixing method, Ω (continued)

CB48(2)	0.4	0.8	Bottom	262	281	298	301	305	322
			Middle	264	283	289	296	300	315
			Top	279	298	317	322	326	338
CB68(2)	0.6		Bottom	244	249	255	265	278	290
			Middle	238	243	248	258	274	289
			Top	247	258	264	276	288	303
CB108(2)	1.0		Bottom	233	242	248	255	261	266
			Middle	238	244	254	264	272	279
			Top	245	248	262	275	277	287
CB210(2)	0.2	1.0	Bottom	190	215	222	245	267	289
			Middle	189	209	234	250	264	281
			Top	192	212	256	278	301	305
CB410(2)	0.4		Bottom	180	191	205	222	249	277
			Middle	182	188	209	234	245	268
			Top	186	195	208	242	278	294
CB610(2)	0.6		Bottom	166	188	207	218	241	256
			Middle	162	184	203	214	247	255
			Top	171	196	214	243	275	288
CB1010(2)	1.0		Bottom	164	185	199	235	239	244
			Middle	162	188	203	232	237	240
			Top	179	193	206	244	246	253

As seen from Tables 4.31 and 4.32, the ER results decreased on all measurement days as the number of conductors increased in the mixtures. Both admixing methods of the milled carbon fiber positively affected the conductivity of the mixtures. ER values of the mixtures were quite similar to those of the admixing methods. Here, the CF content and the method of admixing CF into the mixture, mainly using the latter admixing method, had been significant factors in achieving electrical conductivity. After analyzing all ER results, it was observed that the long-term ER values of the mixtures increased to the kΩ level when the amount of MCF was increased in the mixing group where CF was used at a rate of 0.2%. Apart from this, ER values decreased as the MCF content increased at the same CF content among the mixing groups. Based on the ER results, the lowest resistance value was obtained from a CB1010 (1.0% MCF, 1.0% CF) mixture. Although the ER

values of the mixtures increased with the curing time, the rate of increase was relatively low. It concluded that the mixtures would maintain their conductivity in the long term. The ER value between cylindrical parts was approximately the same as the CF content, and MCF increased in the mixture. Among the ER values of cylindrical parts, the highest ER was measured from the upper part. Although the ER values of the parts increased depending on the external weather conditions, the homogeneous distribution of the conductors prevented the loss of conductivity performance. It concluded that the conductors were distributed homogeneously in the matrix. The ER results of carbon fiber-steel fiber-based mixtures measured considering age and parts obtained are given in Table 4.33 and Table 4.34. In Table 4.33, steel fibers were added to the mixture using the synchronous admixing method. In contrast, steel fibers were added to the mixture using the latter admixing method as given in Table 4.34.

Table 4.33. ER results of the carbon fiber-steel fiber-based mixtures using the synchronous admixing method, Ω

Sample	Ratio, %		Parts of the cylinder	1st day	3rd day	7th day	28th day	90th day	180th day
	SF	CF							
Reference	0.0	0.0	Bottom	521	785	1500	19820	162000	226000
			Middle	552	768	1350	17600	168000	223000
			Top	1600	50600	90300	190000	626000	773000
AB22(1)	0.2	0.2	Bottom	274	349	387	734	2070	4168
			Middle	281	342	378	716	1570	4056
			Top	267	323	340	689	1710	4584
AB42(1)	0.4		Bottom	261	314	374	789	1050	2846
			Middle	252	310	367	764	999	2778
			Top	276	319	389	783	1140	4150
AB62(1)	0.6		Bottom	315	393	437	485	820	2647
			Middle	303	385	421	446	860	2800
			Top	295	381	433	471	1150	4056
AB26(1)	0.2	0.6	Bottom	271	301	426	448	661	1456
			Middle	287	325	450	567	968	1589
			Top	311	321	477	634	1010	2430
AB46(1)	0.4		Bottom	265	289	325	411	639	788
			Middle	253	300	357	445	802	932
			Top	245	269	328	455	863	1001
AB66(1)	0.6		Bottom	311	314	372	425	682	802
			Middle	298	303	374	457	877	905
			Top	290	312	384	437	898	987
AB28(1)	0.2	0.8	Bottom	234	269	308	345	398	679
			Middle	235	262	278	364	409	656
			Top	248	281	307	357	437	802
AB48(1)	0.4		Bottom	250	279	321	378	455	688
			Middle	254	294	356	421	521	765
			Top	254	313	363	451	620	849
AB68(1)	0.6		Bottom	261	291	327	370	489	673
			Middle	257	304	340	372	545	715
			Top	268	299	355	420	599	804

Table 4.33. ER results of the carbon fiber-steel fiber-based mixtures using the synchronous admixing method, Ω (continued)

AB210(1)	0.2	1.0	Bottom	169	231	269	281	332	455
			Middle	179	226	274	289	338	462
			Top	189	245	279	305	344	489
AB410(1)	0.		Bottom	199	251	291	312	340	456
			Middle	212	249	282	318	402	455
			Top	221	267	302	342	410	459
AB610(1)	0.6		Bottom	187	240	268	311	368	410
			Middle	184	236	283	307	376	405
			Top	387	396	288	339	401	428

As seen from Tables 4.33 and 4.34, the ER value decreased on all measurement days as the number of conductors increased in the mixtures. Both admixing methods of the milled carbon fiber positively affected the conductivity of the mixtures. ER values of the mixtures were quite similar to those of the admixing methods. There was no difference between mixing methods because of the presence of carbon fiber in the matrix. After analyzing all ER results, higher conductor content significantly decreased the ER values of the mixtures. Increasing the CF content decreased the ER value significantly. However, the ER values of the mixtures increased with measurement time. The rate of increase in ER values ascended with higher steel fiber ratios in the mixture. However, the addition of SF with the latter admixing method showed a lower increase in ER depending on measurement time among the mixing methods. In addition, it was observed that the long-term ER values of the mixtures increased to the around kΩ level when the amount of MCF was increased in the mixing group where carbon fiber was used at a rate of 0.6%. Therefore, the minimum CF usage to achieve sustainable conductivity was determined to be 0.8%. Within 0.8% CF addition to the matrix, the resistance increase rate was relatively low, and it concluded that the mixtures would maintain their conductivity performance in the long term. Based on the ER results, the lowest resistance value was obtained from an AB610 (0.6% SF, 1.0%CF) mixture. Although ER differences were observed between cylindrical parts, these differences decreased with increasing CF content. With 0.8% CF content, the ER values of the layers were approximately similar. Among the ER results of cylindrical parts, the highest ER values were measured from the upper part, and the lowest ER values were measured from the bottom. The difference was related to the

dispersion of SFs in the matrix. Additionally, external environmental conditions caused higher resistance to be measured in the top layer. However, similar ER values between layers with 0.8% carbon fiber content showed that both conductors were homogeneously dispersed in the matrix, and the conductivity performance was unaffected.

Table 4.34. ER results of the carbon fiber-steel fiber-based mixtures using the latter admixing method, Ω

Sample	**Ratio, %**		**Parts of the cylinder**	**1st day**	**3rd day**	**7th day**	**28th day**	**90th day**	**180th day**
	SF	**CF**							
Reference	0.0	0.0	Bottom	521	785	1500	19820	162000	226000
			Middle	552	768	1350	17600	168000	223000
			Top	1600	50600	90300	190000	626000	773000
AB22(2)	0.2	0.2	Bottom	294	338	487	666	1510	3566
			Middle	298	315	477	708	1700	3800
			Top	298	323	496	827	2480	4670
AB42(2)	0.4		Bottom	278	339	380	722	1489	2500
			Middle	286	347	376	706	1500	2512
			Top	292	345	345	734	1668	3880
AB62(2)	0.6		Bottom	256	315	364	689	999	1780
			Middle	249	310	357	664	1100	1666
			Top	278	319	389	701	1440	1877
AB26(2)	0.2	0.6	Bottom	264	327	378	438	761	1375
			Middle	275	325	385	447	855	1486
			Top	289	338	417	532	985	1734
AB46(2)	0.4		Bottom	258	271	333	388	742	875
			Middle	258	277	338	392	755	901
			Top	269	291	345	421	823	965
AB66(2)	0.6		Bottom	247	282	345	415	725	798
			Middle	257	286	382	435	727	809
			Top	241	271	309	429	810	835
AB28(2)	0.2	0.8	Bottom	244	266	300	367	382	638
			Middle	240	258	288	356	377	641
			Top	252	277	316	378	391	633

Table 4.34. ER results of the carbon fiber-steel fiber-based mixtures using the latter admixing method, Ω (continued)

AB48(2)	0.4	0.8	Bottom	237	266	308	382	418	636
			Middle	234	260	308	386	445	657
			Top	245	258	331	397	462	672
AB68(2)	0.6		Bottom	258	286	318	346	417	614
			Middle	251	291	330	342	437	622
			Top	254	306	343	352	518	685
AB210(2)	0.2	1.0	Bottom	245	250	258	279	311	379
			Middle	239	253	274	283	308	388
			Top	257	245	279	292	337	396
AB410(2)	0.4		Bottom	199	251	291	312	340	354
			Middle	212	249	282	318	402	358
			Top	221	267	302	362	452	387
AB610(2)	0.6		Bottom	164	222	253	284	347	380
			Middle	171	231	245	282	362	384
			Top	195	238	274	302	373	401

The ER results of steel fiber-milled carbon fiber-based mixtures measured considering age and parts obtained are given in Table 4.35 and Table 4.36. In Table 4.35, milled carbon fibers were added to the mixture using the synchronous admixing method. In contrast, milled carbon fibers were added to the mixture using the first admixing method as given in Table 4.36. Steel fiber was added to the mixture using the latter admixing method.

Table 4.35. ER results of the steel fiber-milled carbon fiber-based mixtures using the synchronous admixing method, Ω

Sample	Ratio, %		Parts of the cylinder	1st day	3rd day	7th day	28th day	90th day	180th day
	MCF	SF							
Reference	0.0	0.0	Bottom	521	785	1500	19820	162000	226000
			Middle	552	768	1350	17600	168000	223000
			Top	1600	50600	90300	190000	626000	773000
CA22(1)	0.2	0.2	Bottom	452	578	876	1188	2950	8500
			Middle	473	603	850	1160	2870	8100
			Top	890	1027	1260	1572	4000	10300
CA42(1)	0.4		Bottom	366	488	640	980	2368	6540
			Middle	375	509	718	878	2110	6100
			Top	810	930	1140	1348	3670	8245
CA62(1)	0.6		Bottom	391	462	670	920	1990	5700
			Middle	401	496	748	930	1840	5680
			Top	387	610	890	1169	2910	7710
CA102(1)	1.0		Bottom	374	419	751	887	1310	3450
			Middle	376	420	728	850	1040	3125
			Top	376	578	820	984	2270	4620
CA24(1)	0.2	0.4	Bottom	399	437	722	870	1020	2820
			Middle	400	426	750	890	1047	2763
			Top	425	520	860	1040	1820	3459
CA44(1)	0.4		Bottom	391	462	770	820	990	1479
			Middle	401	436	712	830	940	1430
			Top	387	610	814	980	1610	2500
CA64(1)	0.6		Bottom	376	455	726	760	835	1120
			Middle	364	423	689	748	801	1057
			Top	388	461	754	812	901	1642
CA104(1)	1.0		Bottom	326	437	512	588	663	1440
			Middle	329	425	525	576	647	1400
			Top	331	448	533	592	684	1860
CA26(1)	0.2	0.6	Bottom	356	391	470	543	699	900
			Middle	334	356	490	514	620	878
			Top	386	409	550	634	713	1235

Table 4.35. ER results of the steel fiber-milled carbon fiber-based mixtures using the synchronous admixing method, Ω (continued)

CA46(1)	0.4	0.6	Bottom	304	317	449	520	675	814
			Middle	295	342	466	548	660	807
			Top	311	371	480	570	690	786
CA66(1)	0.6		Bottom	296	320	345	490	607	658
			Middle	289	321	342	470	590	639
			Top	271	280	349	520	664	702
CA106(1)	0.2		Bottom	264	288	310	420	478	590
			Middle	256	276	304	403	472	540
			Top	268	279	318	390	500	600

As seen from Tables 4.35 and 4.36, the ER value decreased on all measurement days as the number of conductors increased in the mixtures. Both admixing methods of the milled carbon fiber positively affected the conductivity of the mixtures. After analyzing all ER results, higher conductor content decreased the ER values of the mixtures. Among fiber types, MCF was more effective in reducing resistance. However, the ER results of the mixtures increased with the measurement time. The lowest ER value was measured from CA106 (1.0% MCF, 0.6%SF). In addition, it was observed that the long-term ER values of the mixtures increased to the around kΩ level except for the CA106 mixture. It was concluded that the SF and MCF combination could not maintain electrical conductivity. In addition, the rate of increase in ER values ascended with higher SF ratios in the mixture. However, the higher MCF with the first admixing method showed a lower increase in ER depending on measurement time among the mixing methods. However, differences were observed between the ER values of the cylinder parts. Although ER differences were observed between cylindrical parts, these differences decreased with increasing MCF content. At the same time, the ER results between parts were similar in the first-day measurements. In addition, differences were observed between the parts as the measurement time. Among the ER values of the cylindrical parts, the highest ER values were measured from the upper part, and the lowest ER values were measured from the bottom part. Although there was no significant difference between the mixing methods, adding MCF to the mixture with the first admixing method resulted in a lower difference. The differences showed that the conductors were not distributed homogeneously, and the conductive paths formed by the conductors were lost or

negatively affected due to time and environmental effects. Time-dependent ER results and conductivity behaviors of coatings and cylindrical samples in double conductor additions were consistent with experimental results.

Table 4.36. ER results of the steel fiber-milled carbon fiber-based mixtures using the first admixing method, Ω

Sample	Ratio, %		Parts of the cylinder	1st day	3rd day	7th day	28th day	90th day	180th day
	MCF	SF							
Reference	0.0	0.0	Bottom	521	785	1500	19820	162000	226000
			Middle	552	768	1350	17600	168000	223000
			Top	1600	50600	90300	190000	626000	773000
CA22(2)	0.2	0.2	Bottom	425	506	765	1076	2710	7889
			Middle	413	483	740	1130	2645	7456
			Top	650	827	1190	1350	3800	8990
CA42(2)	0.4		Bottom	388	520	592	747	956	1488
			Middle	374	540	611	780	875	1560
			Top	393	750	930	1250	1880	2400
CA62(2)	0.6		Bottom	342	439	623	720	903	1234
			Middle	350	430	618	680	804	1107
			Top	390	480	820	986	1240	1866
CA102(2)	1.0		Bottom	333	408	546	680	878	1132
			Middle	326	425	558	642	840	1150
			Top	368	472	715	895	1030	1580
CA24(2)	0.2	0.4	Bottom	399	442	708	952	1110	1720
			Middle	412	433	737	907	1145	1744
			Top	455	516	850	1130	1681	2250
CA44(2)	0.4		Bottom	339	420	592	710	950	1345
			Middle	347	440	611	780	925	1420
			Top	388	452	730	980	1300	1989
CA64(2)	0.6		Bottom	342	439	623	820	990	1143
			Middle	350	430	618	880	970	1260
			Top	370	680	820	1090	1240	1677

Table 4.36. ER results of the steel fiber-milled carbon fiber-based mixtures using the first admixing method, Ω (continued)

CA104(2)	1.0	0.4	Bottom	345	488	637	830	952	1088
			Middle	354	491	626	840	980	1045
			Top	347	560	760	950	1010	1540
CA26(2)	0.2	0.6	Bottom	404	466	608	730	895	987
			Middle	403	480	609	710	830	935
			Top	416	527	698	850	990	1200
CA46(2)	0.4		Bottom	397	424	579	760	824	889
			Middle	383	446	563	745	833	867
			Top	410	488	685	857	980	1078
CA66(2)	0.6		Bottom	346	452	508	687	750	825
			Middle	359	430	526	695	730	844
			Top	365	470	547	714	880	934
CA106(2)	0.2		Bottom	306	432	503	560	630	689
			Middle	308	442	505	579	652	695
			Top	323	458	580	590	694	725

Among the double conductor combinations, the most effective results were obtained from mixtures containing carbon fiber-milled carbon fiber, steel fiber-ground carbon fiber, and ground carbon fiber-steel fiber, respectively. A higher conductor ratio in the mixture caused ER values to decrease significantly on all measurement days. However, using CF and its ratio significantly changed the conductivity of the matrix and maintained its long-term conductivity. The combination of MCF and SF was ineffective in obtaining electrical conductivity. When the conductor ratio was selected in triple additions, a low content of conductor usage was preferred to obtain the mixture economically.

4.2.4. Microstructure of Composites with Double Conductive Material Incorporation

In the second stage of the thesis, it was aimed to obtain the electrical conductivity performance from a double use of carbon fiber, milled carbon fiber, and steel fiber in a cementitious matrix as carbon fiber-milled carbon fiber, carbon fiber-steel fiber, and

milled carbon fiber-steel fiber. At this stage, the best electrical conductivity performance mixtures were preferred for examination, focusing on those with the lowest fiber ratio to optimize the mixing cost in double additions. Among milled carbon fiber-carbon fiber-based mixtures, SEM, mapping, and EDX analyses were conducted to determine the microstructure of the CB26(1) sample. SEM analysis was applied to the 28-day sample, and images taken from different scales are shown in Figure 4.31.

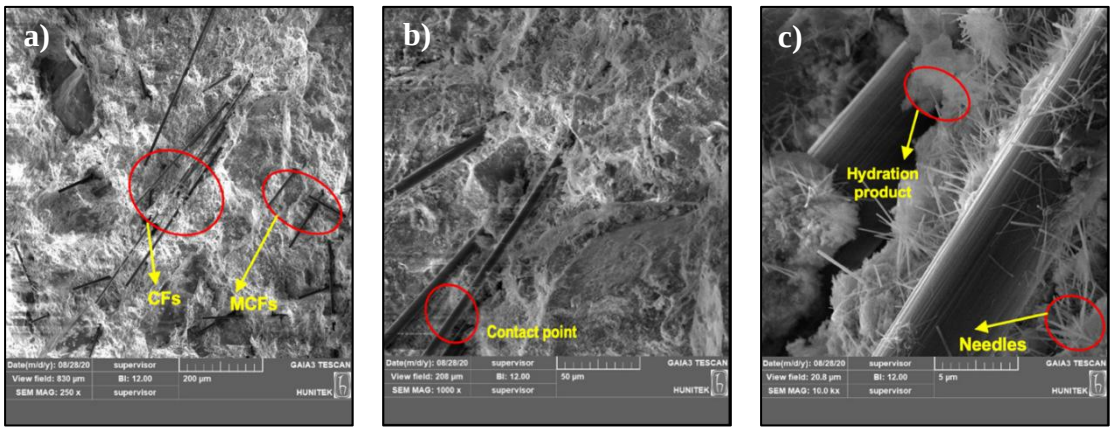

Figure 4.31. SEM images of CB26(1) mixture at different scales a) 250 x, b)1 kx, c) 10 kx

As seen in Figure 4.31-a, CFs were found at a 250-x scale in the area, which belonged to 0.6% CF and 0.2% MCF addition. Fibers were dispersed in the matrix in a line and messy. There were differences in fiber sizes. These differences were related to the CF and MCF lengths. Grooves and embedded fibers were also seen in the matrix. According to ER results, electrically conductive networks were created in the matrix and maintained conductivity performance in the long term. In Figure 4.31-b, embedded fibers were found in the matrix at a 1-kx scale. In addition, contact points were created between fibers. In Figure 4.31-c, two fibers were found in the matrix at a 10-kx scale. In addition to the fibers, needle-like structures and gel formation appeared to surround the matrix. The resulting needle structure positively affected the adherence between the fiber and the cement paste, allowing the fibers to be placed regularly in the matrix. This formation also positively improved the mechanical performance of the mixture. The continuation of the hydration reaction and the resulting hydration products did not cause a loss of fiber conductivity. Additionally, the mapping analysis performed on this scale and the result of the elemental analysis of the matrix are shown in Figure 4.32.

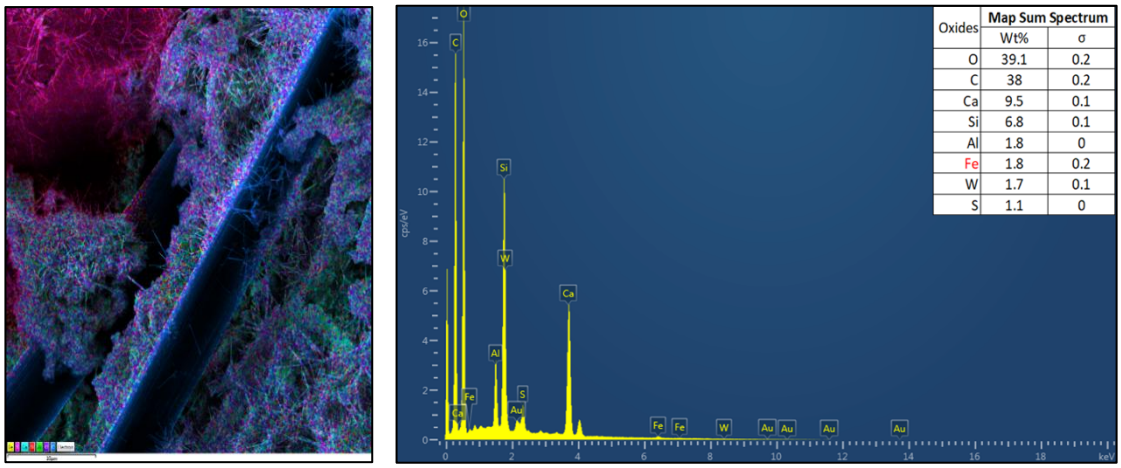

Oxides	Map Sum Spectrum	
	Wt%	σ
O	39.1	0.2
C	38	0.2
Ca	9.5	0.1
Si	6.8	0.1
Al	1.8	0
Fe	1.8	0.2
W	1.7	0.1
S	1.1	0

Figure 4.32. Elemental analysis of CB26(1) mixture performed by mapping method

In Figure 4.32, the intensity of the elements in the area was shown with colors by the mapping method made in the examined area. The C element was shown in blue, the Ca element was shown in a light blue color, the Si element was shown in red, and the Al element was shown in a green color. In the examination, the elements were found in the ratio of C (38.0%), Ca (9.5%), Si (6.8%) and Al (1.8%), respectively. The high percentage of C element after O element in elemental analysis was related to the magnification of the matrix at the 5 µm scale and the two carbon fibers in the image. However, there was a blue color among the colorings except for the red color of the area. The result estimated that the needle structures formed around the fiber consist of ettringite and C-S-H gel due to the combined presence of Si, Ca, C, and Al. Additionally, the EDX analysis performed on the structures in the image is shown in Figure 4.33.

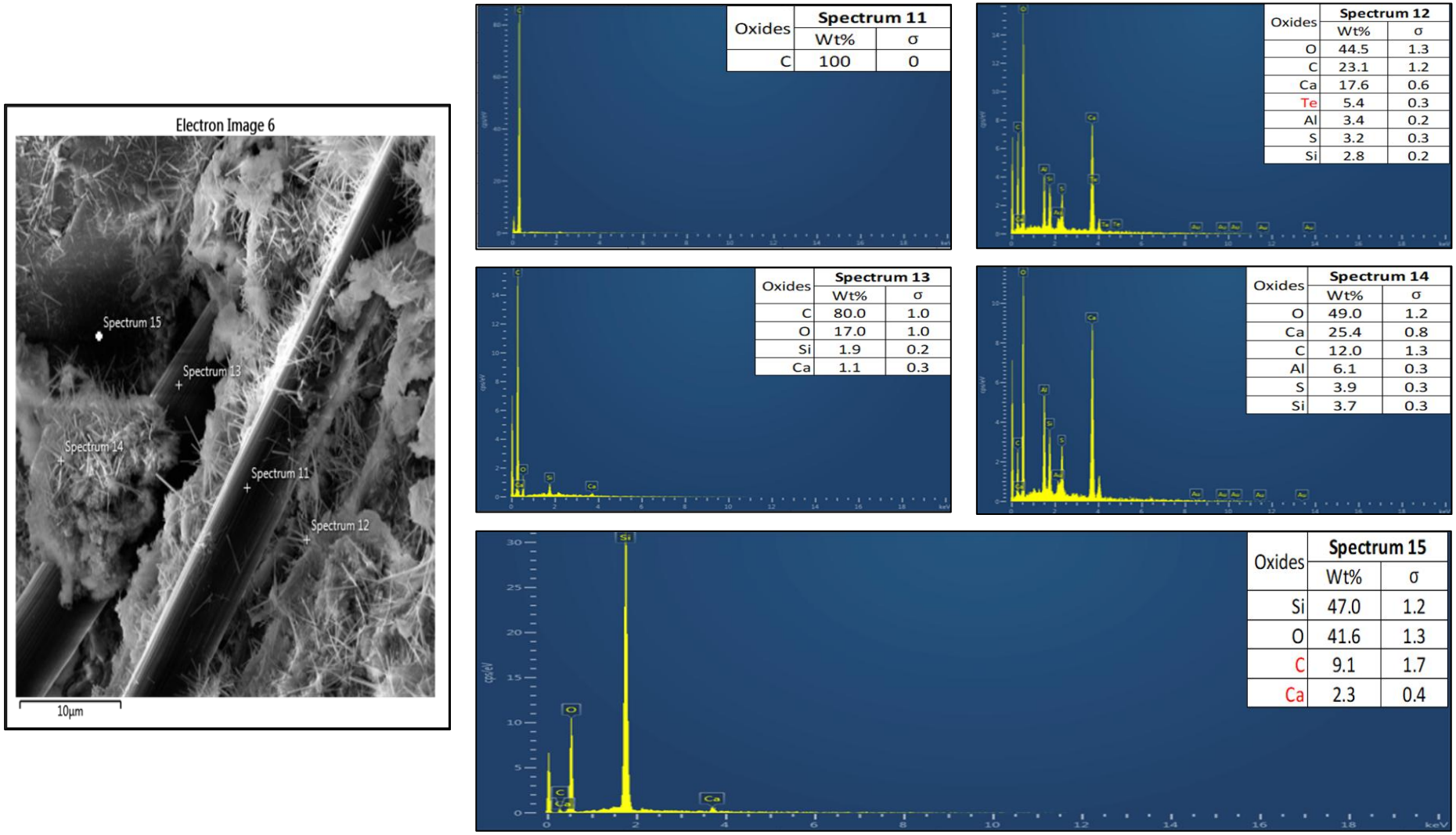

Figure 4.33. EDX analysis of CB26(1) composite with different spectrums

In Figure 4.33, five spectrums were selected in the examined area. Two points were taken on the fiber, two from the needle structure around the fiber and the last from the flat surface where the Si element was densely encountered. The percentage of the C element at two points on the carbon fiber was determined to be 80% and 100%. The presence of Ca and Si in the part where the percentage of the C element decreases indicated gel formation around it. It was determined that the highest content of Ca and C elements was found at two points on the needle structure. While the Ca element was found in raw materials, the high carbon content in the needle structure originated from carbon-based fibers. Apart from this, 47% silicon was measured at the point taken from the red color area and related to silicate formations.

Among steel fiber-carbon fiber mixtures, the AB28(1) sample was selected. In this context, SEM, mapping, and EDX analyses were conducted to determine the microstructure of the AB28(1) sample. SEM analysis was applied to the 28-day sample, and images taken from different scales are shown in Figure 4.34.

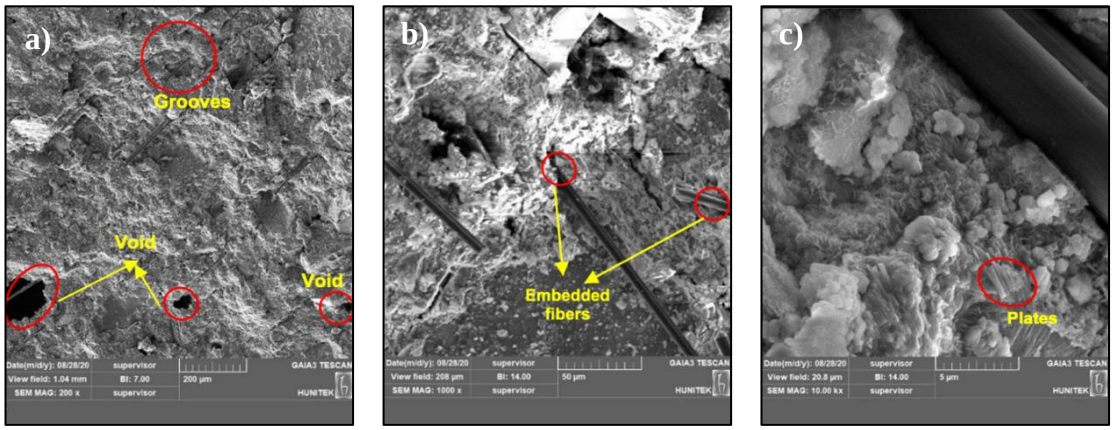

Figure 4.34. SEM images of AB28 (1) mixture at different scales a) 200x, b) 1 kx, c) 10 kx

As seen from Figure 4.34-a, dispersed CFs in a line and grooves were also found at a 200-x scaled area that belongs to 0.8% CF addition. No difference in fiber sizes could be detected from the image. The main reason was that SF was used in the mixture instead of MCF. In the image, the fibers were embedded into the mortar and dispersed sequentially line in the matrix. Although a microscale void was visible in the matrix, the CF appeared

to cross the void. Grooves and some fibers were also seen in the matrix. According to ER results, electrically conductive networks were created in the matrix and maintained conductivity performance in the long term. Figure 4.34-b, embedded fibers were found in the matrix at a 1-kx scale. The small distance between fibers indicated that conductive paths could transmit electrostatic charges. Additionally, no deterioration in fiber surface and size was detected. In Figure 4.34-c, hydration products were observed with the CF in the area at the 10-kx scale. Structures formed by cluttering thin oval or rectangular plates on top of each other in the matrix attracted attention. Additionally, the mapping analysis performed on this scale and the result of the elemental analysis of the matrix are shown in Figure 4.35.

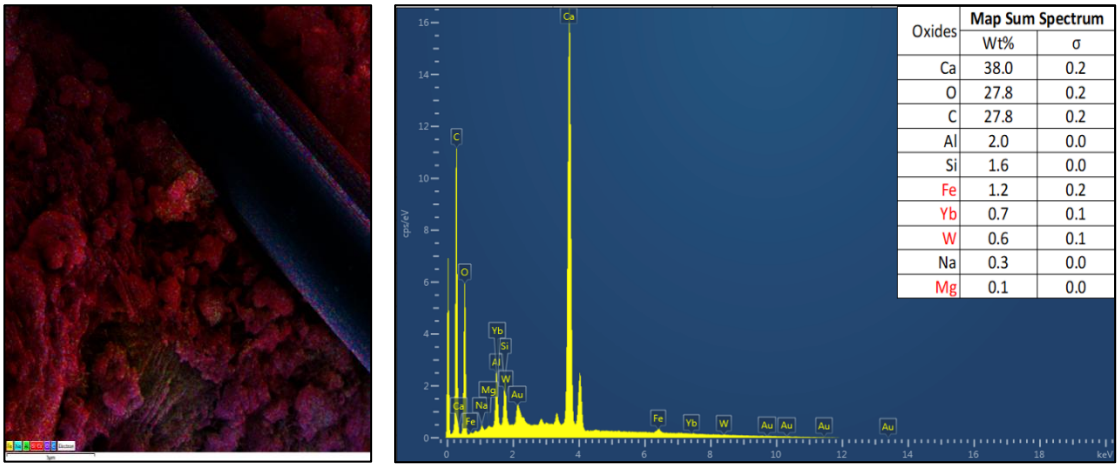

Oxides	Map Sum Spectrum	
	Wt%	σ
Ca	38.0	0.2
O	27.8	0.2
C	27.8	0.2
Al	2.0	0.0
Si	1.6	0.0
Fe	1.2	0.2
Yb	0.7	0.1
W	0.6	0.1
Na	0.3	0.0
Mg	0.1	0.0

Figure 4.35. Elemental analysis of AB28(1) mixture performed by mapping method

In Figure 4.35, the intensity of the elements in the area was shown with colors by the mapping method made in the examined area. The C element was shown in blue, the Ca and Si element in red, and the Al element in green. There were high amounts of Ca (38.0%) and C (27.8%) elements in the examination, except for the O element. While The C content was high due to the low scale of the examined area and the carbon fiber found in this area, the high Ca content was related to the hydration products in the matrix. The structures except from fiber were seen as red. Considering that this area indicated Si and Ca elements, it was concluded that C-S-H gel or ettringite was formed. Additionally, the EDX analysis performed on the structures in the image is shown in Figure 4.36.

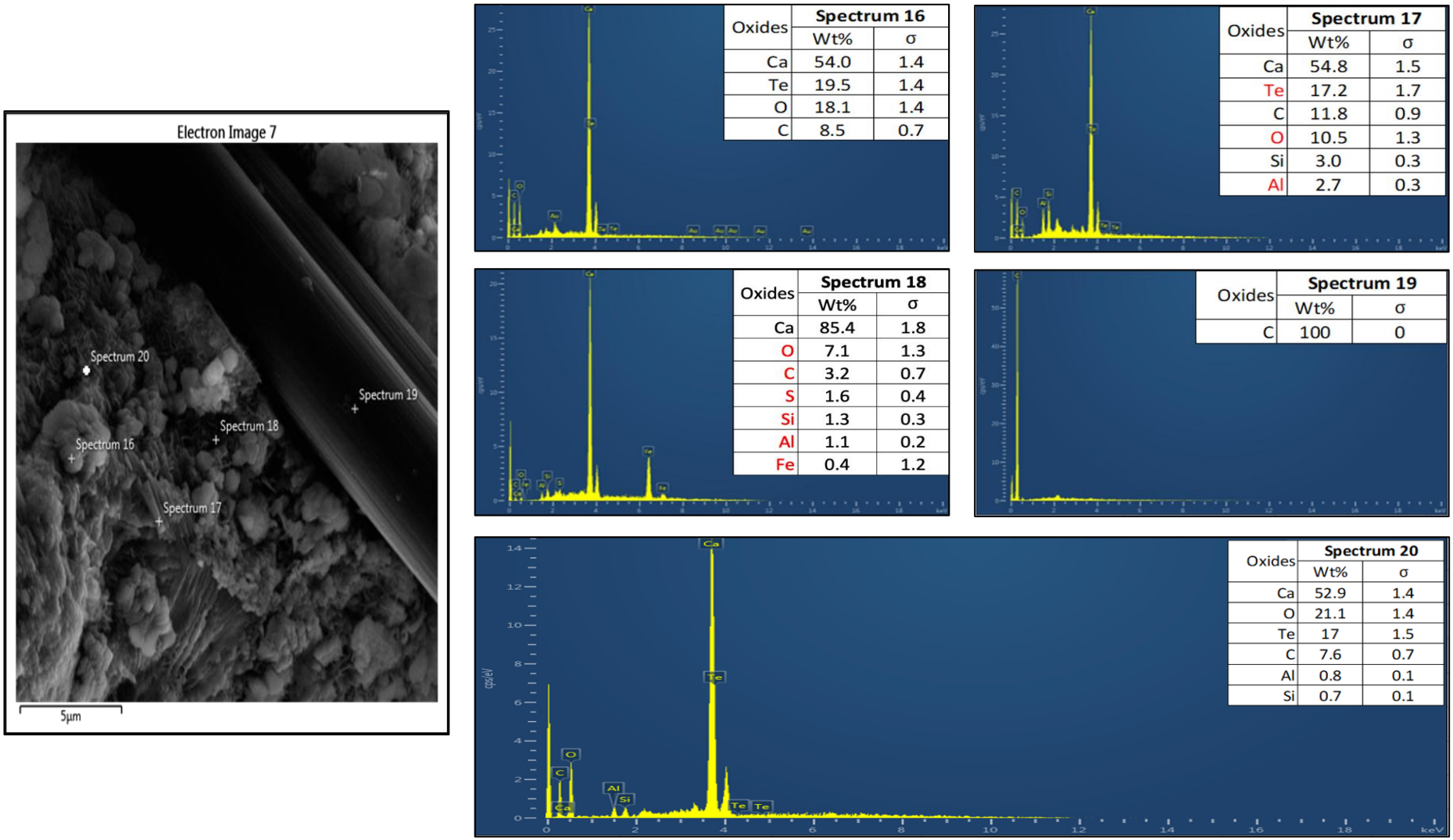

Figure 4.36. EDX analysis of AB28(1) composite with different spectrums

In Figure 4.36, five spectrums were selected in the examined area. One point was taken from the fiber, one from the cluttered tubular plates, one from the more rounded and cottony structure, another from the thin flat plates, and the last from the part that looks darker compared to the other structures. The percentage of C element at the point taken on the fiber was determined as 100%. The Ca element varied between 52-85% in the other spectrums. Although formations in different shapes were observed, high Ca content was attributed to hydration products.

Among the mixtures containing steel fiber and milled carbon fiber, SEM, mapping, and EDX analyses were conducted to determine the microstructure of the CA42(1) sample. SEM analysis was applied to the 28-day sample, and images taken from different scales are shown in Figure 4.37.

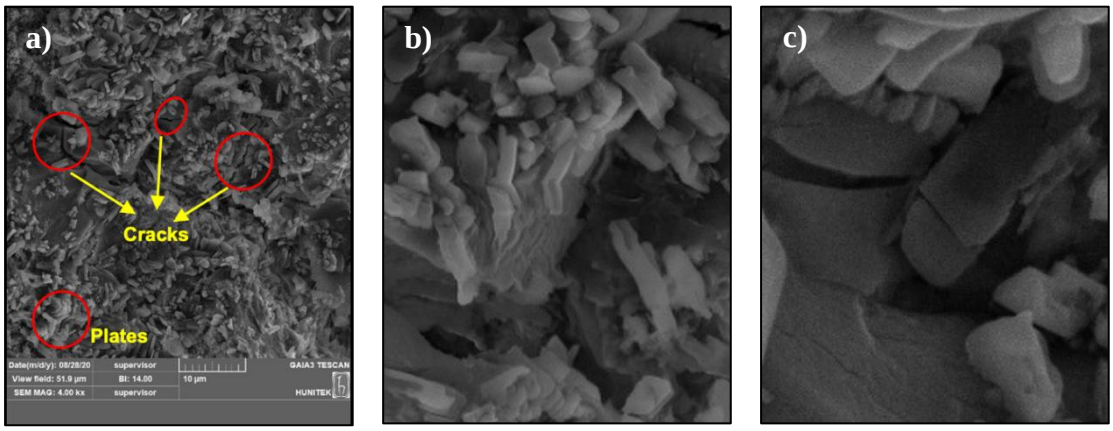

Figure 4.37. SEM images of CA42(1) mixture at different scales a) 4 kx, b) 10 kx, c) 20 kx

Although no carbon fiber was in the CA42(1) mixture, 0.4% MCF was used. As seen in Figure 4.37-a, the presence of fibers could not be observed in the microstructure images. Therefore, fiber dispersion in the matrix could not be mentioned for this examined area. There was a bumpy structure, and small-sized plates were formed on this structure at a 4-kx scale. These plates were spread throughout the examined area. Additionally, microcracks formed in some parts of the matrix. In Figure 4.37-b, the same shapes of plates were on the uneven surface, and these plates were generally arranged vertically. In Figure 4.37-c, similar structures and flat and sharp structures were seen at the 20-kx scale. Plate formations were

seen in C-S-H gel formations. Additionally, the mapping analysis performed on this scale and the result of the elemental analysis of the matrix are shown in Figure 4.38.

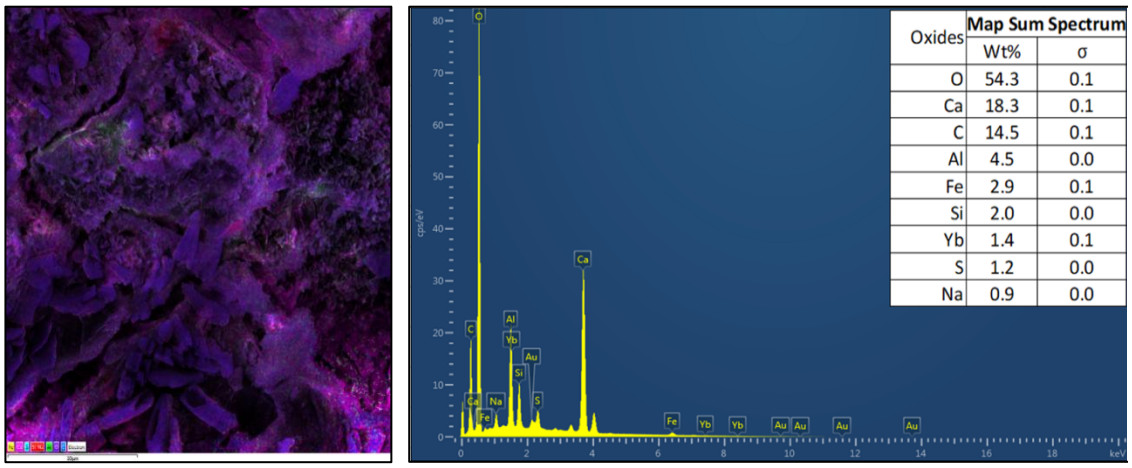

Oxides	Map Sum Spectrum	
	Wt%	σ
O	54.3	0.1
Ca	18.3	0.1
C	14.5	0.1
Al	4.5	0.0
Fe	2.9	0.1
Si	2.0	0.0
Yb	1.4	0.1
S	1.2	0.0
Na	0.9	0.0

Figure 4.38. Elemental analysis of CA42(1) mixture performed by mapping method

In Figure 4.38, the intensity of the elements in the area was shown with colors by the mapping method made in the examined area. The Ca element was shown in purple, the C element in blue, the Si element in red, and the Al element in green color. In the examination, there were high amounts of Ca (18.3%), C (14.5%), Al (4.5%), and Si (2.0%) elements except from the O element, respectively. According to colors, the field generally consisted of a mixture of pink and blue colors. While the plate-like structures had pink primary colors, the needle structures in the remaining parts were mainly blue and sometimes green. Additionally, the EDX analysis performed on the structures in the image is given in Figure 4.39.

In Figure 4.39, six spectrums were selected in the examined area. One point was taken from the tubular plate surface, one point was taken from the inside of the plate, two points were taken from the flat and shiny surface, one point was taken from the vertically adjacent part, and the final one was taken from the inside of the crack. The highest element content was measured from Ca and C elements, apart from O elements, in spectrums. The high content of element C was due to carbon-based milled carbon fibers. The elements such as Al and Si, measured with the Ca element in high amounts, belong to hydration products. C and Ca elements, detected at higher rates than other elements throughout the matrix, led to the pink color formation.

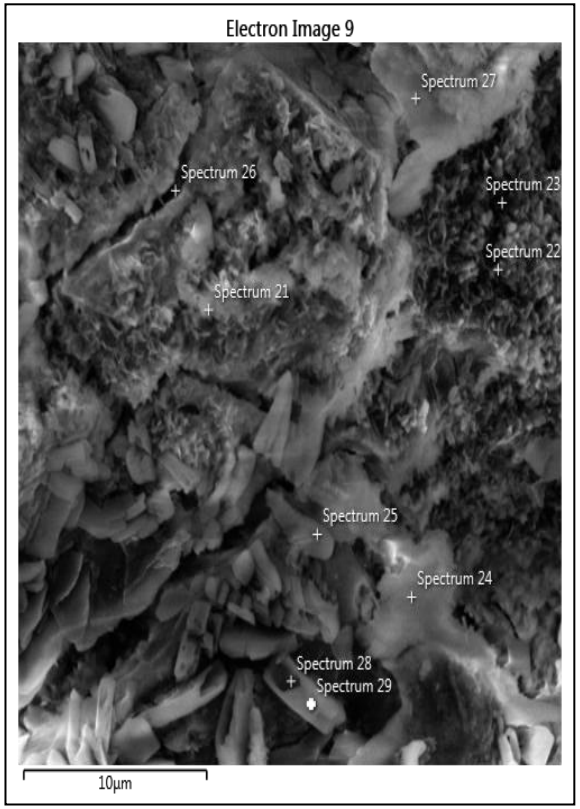

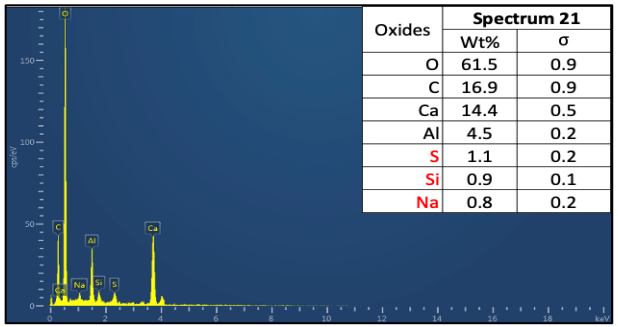

Oxides	Spectrum 21	
	Wt%	σ
O	61.5	0.9
C	16.9	0.9
Ca	14.4	0.5
Al	4.5	0.2
S	1.1	0.2
Si	0.9	0.1
Na	0.8	0.2

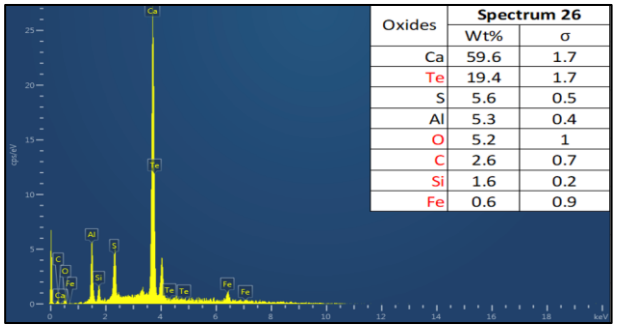

Oxides	Spectrum 26	
	Wt%	σ
Ca	59.6	1.7
Te	19.4	1.7
S	5.6	0.5
Al	5.3	0.4
O	5.2	1
C	2.6	0.7
Si	1.6	0.2
Fe	0.6	0.9

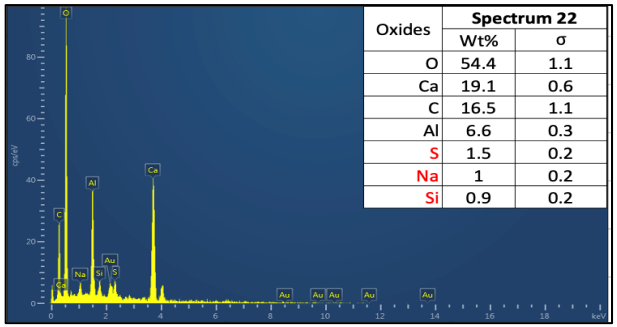

Oxides	Spectrum 22	
	Wt%	σ
O	54.4	1.1
Ca	19.1	0.6
C	16.5	1.1
Al	6.6	0.3
S	1.5	0.2
Na	1	0.2
Si	0.9	0.2

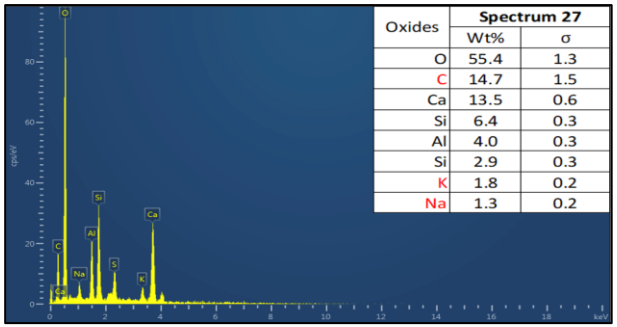

Oxides	Spectrum 27	
	Wt%	σ
O	55.4	1.3
C	14.7	1.5
Ca	13.5	0.6
Si	6.4	0.3
Al	4.0	0.3
Si	2.9	0.3
K	1.8	0.2
Na	1.3	0.2

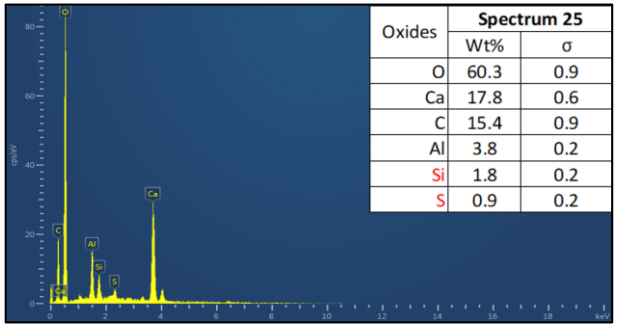

Oxides	Spectrum 25	
	Wt%	σ
O	60.3	0.9
Ca	17.8	0.6
C	15.4	0.9
Al	3.8	0.2
Si	1.8	0.2
S	0.9	0.2

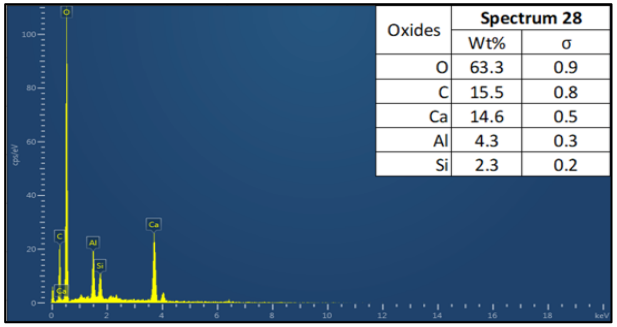

Oxides	Spectrum 28	
	Wt%	σ
O	63.3	0.9
C	15.5	0.8
Ca	14.6	0.5
Al	4.3	0.3
Si	2.3	0.2

Figure 4.39. EDX analysis of CA42(1) composite with different spectrums

4.4. Triple Addition of Conductive Materials into the Cementitious Matrix

After the triple additions of the conductive materials, ratios and mixing methods were determined by considering the lowest conductor content in the mixtures. Based on these ratios, the three conductive materials were added to the mixture in different proportions.

4.4.1. Flow Diameter and Flow Time Values of Composites with Triple Conductive Material Incorporation

The effect of the combination of three conductive materials on the flow diameter and flow time of the matrix was examined. In triple additions, CF was incorporated into the mixture only by the latter admixing method, and SF and MCF were incorporated into the mixture only by the synchronous admixing method due to workability concerns. Flow diameter and flow time results for mini-slump tests of triple conductor-based mixtures are shown in Figure 4.40.

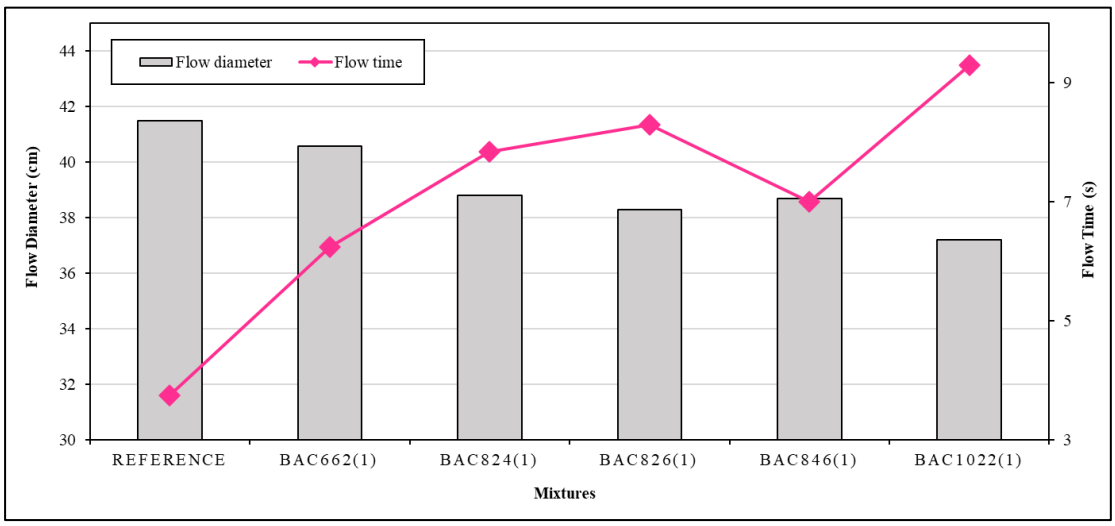

Figure 4.40. Flow diameter and flow time results for triple conductor incorporation-based mixtures

As seen from Figure 4.40, the values were similar to the previous experimental results. Additionally, there was a direct relationship between the flow diameters and flow times

of the mixtures. Compared to the reference mixture, the workability of all mixtures was negatively affected by conductive usage. Triple conductor incorporations were made, taking into account the CF ratios of the mixtures. Experimental results showed that as CF and MCF content increased in the mixture, the flow diameter decreased, and the flow time increased. However, adding SF using the synchronous admixing method improved an increase in flow diameters and a decrease in flow times. The lowest flow diameter was measured from the reference sample among all mixtures. However, the flow diameter and flow times were similar to the experimental results of single and double additions. Therefore, the workability of the mixtures was found suitable for ready-mix use in the field.

4.4.2. Compressive Strength Results of Composites with Triple Conductive Material Incorporation

The average compressive strength values of mixture combinations of all conductive fibers were measured for different curing ages of 1, 3, 7, 28, and 90 days. The compressive strength results of the combination of conductive fibers are shown in Figure 4.41 for different curing ages.

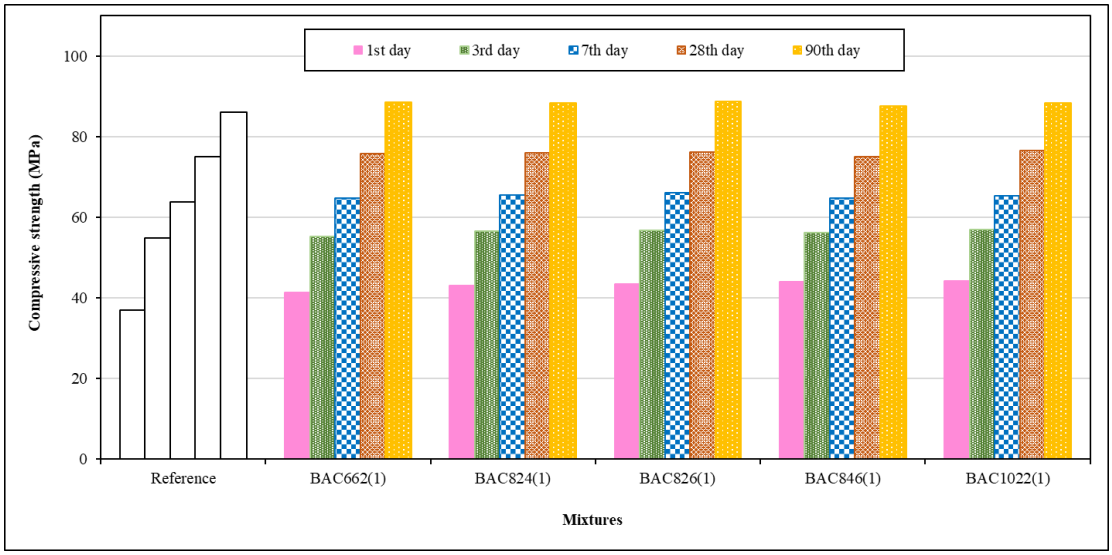

Figure 4.41. Compressive strength results of the triple conductor incorporation-based mixtures

In Figure 4.41, the short- and long-term mechanical performance of the mixtures was better than the reference mixture. All triple conductors-based mixtures had a higher than 40 MPa value on the first day. According to experimental results, mechanical strengths were positively affected by increasing the CF and MCF content in the mixtures, while increasing the SF content had a slightly negative effect. This was related to SF being added to the matrix using the synchronous admixing method. However, the negative effect of SF on the mixtures was compensated according to the strength results of the reference mixture.

4.4.3. Electrical Resistance Results of Composites with Triple Conductive Material Incorporation

4.4.3.1. Electrical Resistance Results of Coating Samples

The electrical resistance values of the mixtures were determined using two experimental devices. After determining the lowest conductor usage and mixing methods for double incorporation, conductors were combined in triple. Average electrical resistance (ER) values were measured from the coating sample of related mixtures after 1, 3, 7, 28, 90, and 180 days of curing. ER results of the reference sample without any conductive material were 15.4, 20.8, 33.2, 65.4, 75.3, and 104.5 MΩ after 1, 3, 7, 28, 90, and 180 days of curing, respectively. The ER results of triple conductive material-based mixtures until the 180th day are shown in Figure 4.42.

As seen in Figure 4.42-a, the ER values of all mixtures remained below 300 kΩ on all measurement days. With 0.8% CF addition in the mixture, the ER values remained below 100 kΩ in the long term. The mixtures maintained their electrical conductivity performance in the early and long term. While higher CF content significantly reduced the electrical resistance value, increasing the MCF content contributed to the decrease in the resistance value. However, the higher SF content in the mixture did not improve or cause an increase in the ER value of the mixtures. In Figure 4.42-b, the lowest value was measured from the BAC1022(1) mixture according to the 180-day ER results of the mixtures. ER value was lower than other mixtures due to the 1.0% CF addition and the low use of other conductors. Therefore, only the BAC1022(1) mixture was selected for

moisture and temperature experiments among the triple conductors' additions. Figure 4.42-c shows the ER values of the BAC1022(1) mixture depending on time. The ER value of the mixture was measured as 1.87 kΩ after 180 days. It was concluded that the mixture would maintain its electrical conductivity in the long term.

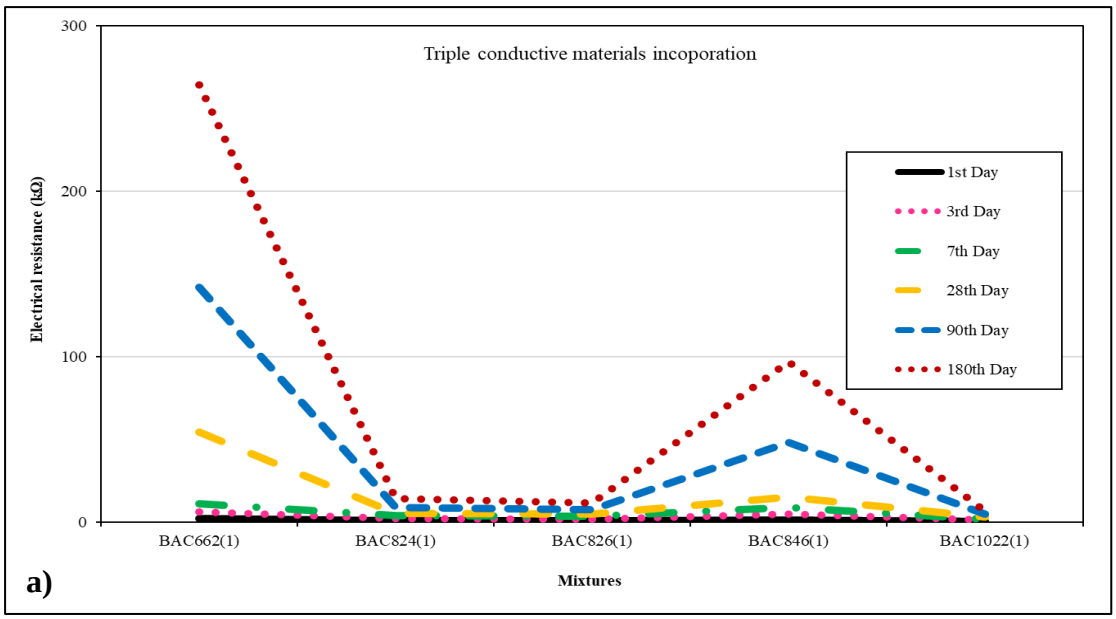

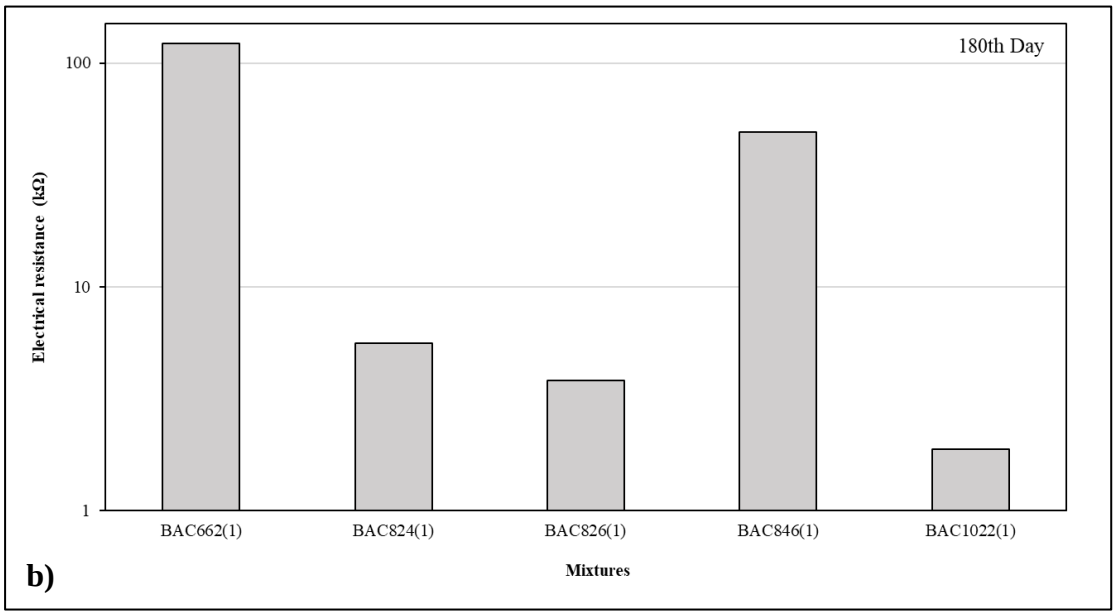

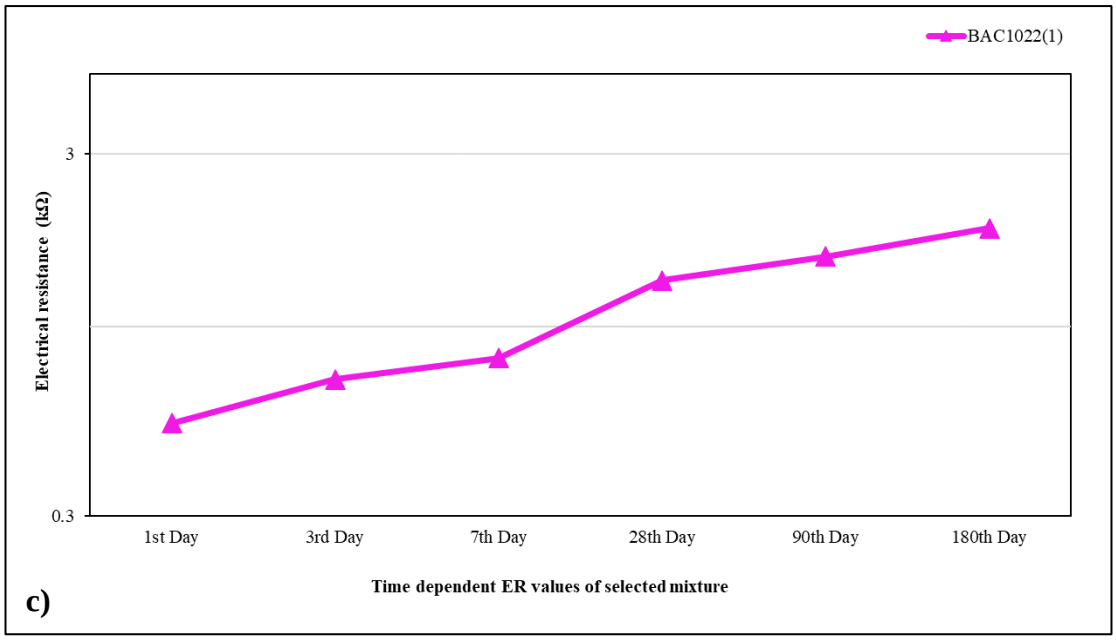

Figure 4.42. a) Age-dependent ER results of triple conductive incorporation-based composites, b) Effect of dispersion methods on 180-day ER results, c) Selected sample having the lowest ER results with age

4.4.3.2.Electrical Resistance Results of Cylindrical Samples

One of the other experimental methods for the electrical resistance values was determined by the AC method. Unlike the coating design, the ER values were measured from three parts of the cylindrical sample to determine whether the conductive materials were distributed homogeneously into the matrix mixture. The electrical resistance (ER) values of three cylindrical parts were measured from the cylindrical samples after 1, 3, 7, 28, 90, and 180 days of curing. The ER results of triple conductive materials-based mixtures measured considering age and parts obtained are given in Table 4.37.

Table 4.37. ER results of the triple conductive materials incorporation-based mixtures, Ω

Sample	Ratio, %			Parts of the cylinder	1st day	3rd day	7th day	28th day	90th day	180th day
	CF	SF	MCF							
Reference	0.0	0.0	0.0	Bottom	521	785	1500	19820	162000	226000
				Middle	552	768	1350	17600	168000	223000
				Top	1600	50600	90300	190000	626000	773000
BAC662(1)	0.6	0.6	0.2	Bottom	230	254	291	305	355	402
				Middle	227	249	284	300	342	398
				Top	239	252	277	313	365	421
BAC824(1)	0.8	0.2	0.4	Bottom	176	201	231	274	307	318
				Middle	168	197	221	275	290	309
				Top	174	183	224	278	296	312
BAC826(1)		0.2	0.6	Bottom	174	189	217	248	283	298
				Middle	171	188	209	251	286	302
				Top	177	195	214	256	284	297
BAC846(1)		0.4	0.6	Bottom	171	196	220	266	297	315
				Middle	164	195	216	256	294	322
				Top	183	215	265	283	315	345
BAC1022(1)	1.0	0.2	0.2	Bottom	143	195	214	269	292	305
				Middle	140	187	209	262	287	297
				Top	150	192	235	273	294	306

In Table 4.37, the ER values of all mixtures were relatively low compared to the reference mixture. Although the ER values of all mixtures increased, the ER values remained below 500 Ω at the end of 180 days. As in the plate measurements, the ER values of the cylindrical parts decreased with higher CF content. Although the MCF content also contributed to the decrease in the ER value, a partial increase in the ER value was observed with the addition of SF. The rate of increase in the ER values of the mixtures decreased significantly with the higher CF. In addition, the ER values were measured at similar levels in the cylindrical parts. The mixtures maintained their electrical conductivity performance in the long term. It was concluded that all types of fibers were distributed homogeneously in the matrix. The BAC1022(1) sample was chosen considering the mixtures' lowest conductor usage and ER value.

4.4.4. Microstructure of Composites with Triple Conductive Material Incorporation

The third stage of the thesis aimed to obtain the electrical conductivity performance by using carbon fiber, milled carbon fiber, and steel fiber in a cementitious matrix as triple incorporation. At this stage, the best electrical conductivity performance mixtures were preferred for examination, focusing on those with the lowest fiber ratio to optimize the mixing cost in triple additions. In this context, SEM, mapping, and EDX analyses were conducted to determine the microstructure of the BAC1022(1) sample among the mixtures. SEM analysis was applied to the 28-day sample, and images taken from different scales are shown in Figure 4.43.

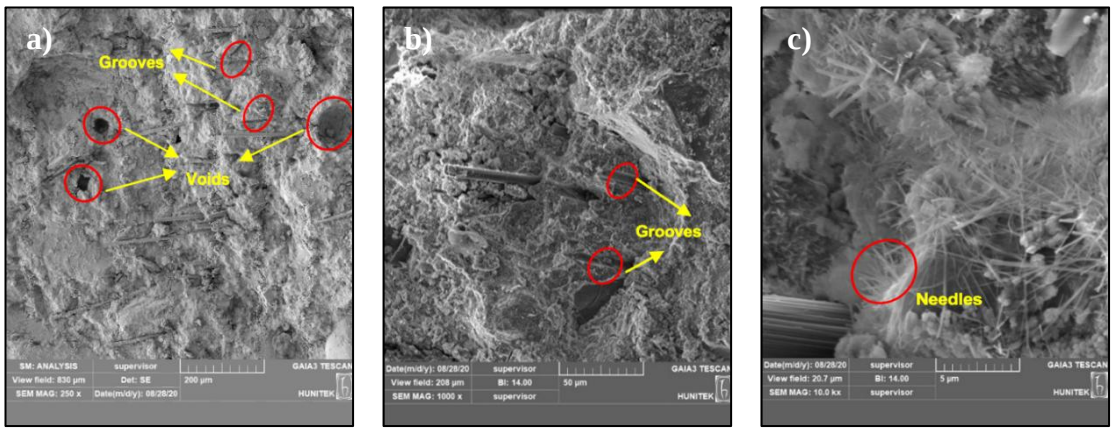

Figure 4.43. SEM images of BAC1022(1) mixture at different scales a) 250 x, b) 1 kx, c) 10 kx

As seen from Figure 4.43-a, carbon fibers dispersed in a line and grooves were also found at a 250-x scale in the area that belongs to 1.0% CF and 0.2% MCF addition. Therefore, size differences between some fibers were detected in the image. At the same time, the fibers were dispersed in the matrix in a line and at the same intervals. While some fibers were embedded in the mortar mixture, some were visible on the matrix surface. There were also different sizes of voids in the matrix. Although it was known that voids negatively affected electrical conductivity performance, the conductivity was maintained in the long term according to the ER result of the mixture. A logical relationship was found between the ER result of the mixture and the SEM image. Figure 4.43-b, embedded

fibers were found in the matrix at a 1-kx scale. In addition, grooves were also seen in the matrix. Additionally, no deterioration in fiber surface and size was detected. In Figure 4.43-c, hydration products were observed with the carbon fiber in the area at the 10-kx scale. Thin and long needle structures intertwined could be seen in the matrix. Additionally, the mapping analysis performed on this scale and the result of the elemental analysis of the matrix are shown in Figure 4.44.

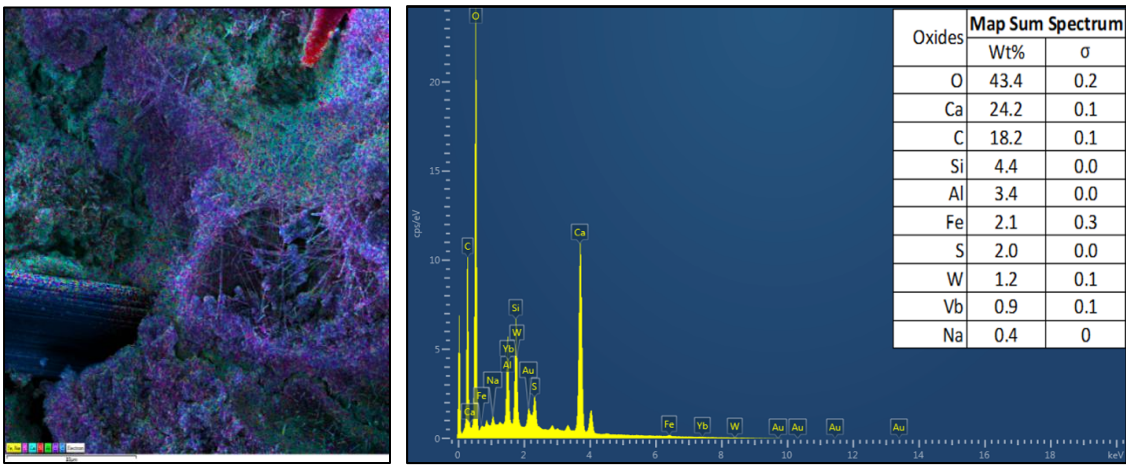

Oxides	Map Sum Spectrum	
	Wt%	σ
O	43.4	0.2
Ca	24.2	0.1
C	18.2	0.1
Si	4.4	0.0
Al	3.4	0.0
Fe	2.1	0.3
S	2.0	0.0
W	1.2	0.1
Vb	0.9	0.1
Na	0.4	0

Figure 4.44. Elemental analysis of BAC1022(1) mixture performed by mapping method

In Figure 4.44, the intensity of the elements in the area was shown with colors by the mapping method made in the examined area. The C element was shown in blue, the Ca element in light blue, the Si element in red, and the Al element in green color. In the examination, there were high amounts of Ca (24.2%), C (18.2%), Si (4.4%), and Al (3.4%) elements except from the O element, respectively. According to colors, the field generally consisted of a mixture of red and blue colors. The analysis showed that the C element was mainly dispersed in the fiber and matrix, while the Ca element was dispersed on the needle structure. The high level of Ca element was due to hydration products. Additionally, the EDX analysis performed on the structures in the image is shown in Figure 4.45.

In Figure 4.45, six spectrums were selected in the examined area. The first point was taken on the fiber, two points were taken from the flat and smooth surface of the matrix, one was taken from the area where very short-sized indentations occur, one point was taken from the thin and long-sized needle structure, and the one point was taken from the

crack-like part that was darker in color than the other structures. The C content was 100% at the point taken from the fiber. Flat and smooth surfaces had a high amount of Ca element between 23% and 43.8%, while the C rate varied between 0 and 9.0%. It concluded that the formation structure was completely gel and contained relatively less C element. The spectrum of shorter-sized structures contained 50.3% Ca, 8.8% C, and 7.6% Si elements. The high level of Ca was attributed to hydration gels, and Si content was attributed to the silica fume used in the matrix. The spectrum of thin and long-sized needle structures contained 31.0% Ca, 9.0% C, and 8.3% Si elements. The large, darker structure spectrum contained 58.5% Ca, 17.8% Si, and 5.3% Al elements. In spectrum 38, the results showed gel accumulation, and even though there was a gap in the part, there was a gel structure underneath. The high level of Al element was related to the formation of gibbsite, ettringite, or monosulfate due to using CAC in the mixture.

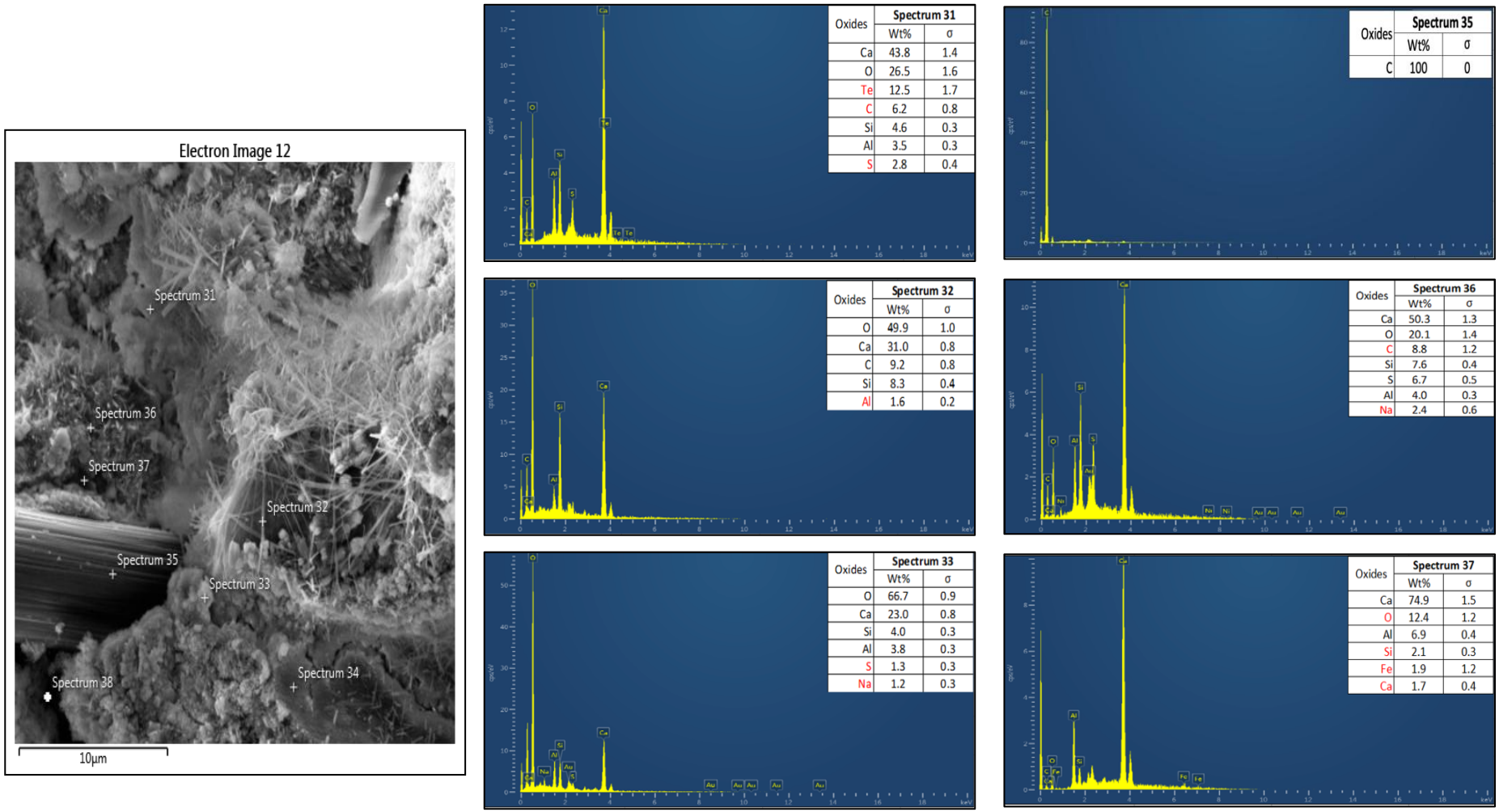

Figure 4.45. EDX analysis of BAC1022(1) composite with different spectrums

4.5. Effects of the Laboratory, Humidity, and Temperature on the Properties of the Cementitious Mixtures

At this stage of the thesis study, the effect of ambient temperature and humidity on the electrical conductivity performance of samples was determined. These mixtures were selected from different proportions of single, double, and triple conductive incorporations. In this context, reference mixture, B6(2) and B10(2) mixtures were selected from single addition of carbon fiber, CB26(1), CB68(1), and CB210(1) mixtures were selected from double addition of carbon fiber-milled carbon fiber, AB66(1), AB28(1), and AB210(1) were selected from double addition of carbon fiber-steel fiber, BAC1022(1) was selected from triple addition of all type of fibers. Among mixtures, a single addition of steel fiber and milled carbon fiber and a double addition of milled carbon fiber-steel fiber could not maintain electrical conductivity performance in the long term. So, moisture and temperature tests were not applied to these mixtures. In order to determine the effect of moisture and temperature, three different samples were prepared from each mixture. At this stage, the mixtures' flow diameter, flow time, and compressive strength values were not measured. In order to determine the effect of humidity and temperature factors on electrical conductivity behavior, the microstructures of the mixtures, together with their ER values, were examined.

4.5.1. Electrical Resistance Results of Selected Composites

4.5.1.1. Electrical Resistance Results of Coating Samples

The electrical resistance results of the mixtures were determined with two experimental devices. After selecting the mixtures from single, double, and triple conductor incorporations, the ER values of mixtures were determined based on different ambient factors. Average electrical resistance (ER) values were measured from the coating sample of related mixtures after 1, 3, 7, 28, 90, and 180 days of curing. The ER results of the selected mixtures until the 180^{th} day are given in Table 4.38.

Table 4.38. ER results of coating mixtures in different ambient conditions, kΩ

Sample	**Condition**	**1st day**	**3rd day**	**7th day**	**28th day**	**90th day**	**180th day**
Reference Mixture	First	15400	20800	33200	65400	75300	104500
	Lab.	16650	19800	34100	67950	77500	108900
	50 °C	82300	108000	209000	275000	327000	388000
	%100 RH	7.410	9.050	11.950	18.680	26.050	40.800
B6(2)	First	0.155	0.141	0.144	0.156	0.183	0.201
	Lab.	0.226	0.350	0.377	0.417	0.515	0.554
	50 °C	0.340	0.351	0.364	0.478	0.529	0.576
	%100 RH	1.530	2.250	2.520	2.66	3.520	3.625
B10(2)	First	0.180	0.173	0.192	0.259	0.299	0.370
	Lab.	0.133	0.240	0.268	0.312	0.418	0.526
	50 °C	0.213	0.252	0.290	0.357	0.455	0.679
	%100 RH	1.870	2.160	2.280	2.910	2.970	3.179
CB26(1)	First	0.456	0.648	0.701	0.876	1.300	2.500
	Lab.	0.560	0.865	1.102	1.360	1.815	2.680
	50 °C	0.570	0.842	1.200	1.453	2.018	2.890
	%100 RH	0.487	0.605	1.367	1.416	2.830	3.265
CB68(1)	First	0.496	0.545	0.687	0.754	0.897	1.100
	Lab.	0.567	0.614	0.678	0.690	0.885	0.925
	50 °C	0.351	0.381	0.478	0.725	1.010	1.230
	%100 RH	0.735	0.960	1.240	1.700	2.370	2.680
CB210(1)	First	0.724	0.754	0.994	1.210	1.310	1.450
	Lab.	0.461	0.556	0.564	0.638	0.886	1.255
	50 °C	0.106	0.137	0.278	0.356	0.404	0.518
	%100 RH	0.435	0.687	0.907	1.210	1.940	2.253
AB66(1)	First	0.581	0.759	0.770	1.020	1.910	2.950
	Lab.	0.540	0.809	0.886	1.167	2.205	3.456
	50 °C	0.404	0.680	0.822	0.984	1.680	2.874
	%100 RH	2.630	2.680	3.520	4.160	5.030	6.752
AB28(1)	First	0.474	0.678	0.970	2.040	2.280	2.720
	Lab.	0.239	0.281	0.425	0.492	0.603	1.100
	50 °C	0.228	0.239	0.294	0.354	0.452	0.615
	%100 RH	0.560	0.676	0.882	1.400	2.260	3.366

Table 4.38. The ER results of coating mixtures in different ambient conditions, kΩ (continued)

AB210(1)	First	1.300	1.810	1.880	2.120	2.280	2.690
	Lab.	0.475	0.584	0.604	0.708	0.866	1.545
	50 °C	0.197	0.216	0.246	0.324	0.359	0.458
	%100 RH	0.341	0.370	0.515	0.789	1.620	2.355
BAC1022(1)	First	0.540	0.814	1.060	1.320	1.740	2.150
	Lab.	0.253	0.259	0.262	0.371	0.445	0.564
	50 °C	0.321	0.334	0.365	0.381	0.402	0.553
	%100 RH	0.410	0.479	0.687	1.870	2.690	3.450

In Table 4.38, the differences in ER results of mixtures were changed between those kept in a laboratory environment, those kept in a 100% RH condition, and those kept at 50 °C for 3 hours before measurement. At the same time, the ER results of the first mixtures prepared in the conductive additions of the mixtures are also given in the table. Among all mixtures, the difference in ER values was seen the most in the reference sample. The ER values were similar between the first prepared sample and those kept in laboratory conditions. At the end of 180 days, the ER value of the reference mixture increased to 108 MΩ. However, a significant increase in ER values was observed in those kept at 50 °C before measurement. At the end of 180 days, the ER value of the reference mixture increased to 388 MΩ. However, keeping the reference sample continuously in a 100% RH environment significantly reduced the ER values, and the reference mixture showed electrical conductivity performance. This behavior was observed in the reverse in conductors-based mixtures. The ER results of the conductor-based samples were similar between those first prepared and those kept in laboratory conditions. From this, it concluded that the mixtures were repeatable. In addition, no significant change was observed in ER values due to keeping the samples at 50 °C before measurement. It showed a similar or lower ER value than the laboratory condition. Among the environmental conditions, the most negatively affected the ER values was keeping samples under 100% RH condition. Although the ER values of the mixtures were similar to other environmental conditions on the first measurement days, the ER values increased significantly with time. In contrast, the ER values of all mixtures under 50 °C temperature were approximately 5 kΩ after 180 days.

In literature studies, it has been stated that the effects of humidity and temperature factors on the electrical conductivity performance of mixtures vary depending on factors such as fiber ratio, technical properties of the fiber, cement type, and chemical additives [154]. Regarding Table 4.38, the coatings were more negatively affected under 100% RH conditions with single CF additions. Apart from this, it was seen that the electrical conductivity performance of the coatings kept at 50 °C was not negatively affected. The possible pores in the matrix could affect the ER values of the mixtures. Here, it concluded that the mixture became fully saturated with water over time, filling the pores and negatively affecting the conductivity. The results of literature studies conducted on the effect of temperature on coating performance were as follows: Abtahi et al. [236] stated that carbon fiber, which had a high melting temperature (approximately 1000 °C) among conductive materials, was resistant to high temperatures due to this structural resistance. As a result of this study, the carbon fibers exposed to a temperature of 50 °C were not affected by the temperature and maintained their conductivity performance. However, it could be said that the reduction of extra water in the environment positively affected conductivity performance. Fan [237] stated that the matrix contained 0.5% carbon fiber and 0, 5, 10, 15, 20, 25, and 30% graphite, and the ER values of mixtures were measured between 10 - 50 °C and 20 - 60% RH conditions. As a result of the study, it was stated that the developed composite could be used against different temperatures. In the temperature range of 10 – 50 °C, resistance values decreased with increasing temperature. In the same way, between 20 and 60% RH, the resistance values gradually decreased as the relative humidity increased. Apart from this, Shifeng et al. [238] found that the ER value decreased with increased temperature below a specific critical temperature value. However, the ER value increased at the same rate as the temperature increased beyond the critical temperature value. This was attributed to the increase in current due to the fact that electrons move faster with the increase in temperature and carry more energy to transfer. On the other hand, it had been stated that the internal tensions between the carbon fiber and the cement matrix caused the connection between the fibers to break. It was also stated that as the temperature increased, the unreacted water in the matrix evaporated, and the ER value increased due to the decrease in the electrical conductivity of water and ions. In addition, Han et al. [139] mentioned that the resistance values of the composite change depending on temperature. Temperature change had two effects on conductivity. On the one hand, temperature change due to thermal expansion and cold contraction affected the detection performance by changing the gap between conductive materials and the

dispersion of the conductive network. On the other hand, temperature differences changed the electron transfer barrier and the effect of tunneling composite on conductivity performance. Due to these two interactions, the resistance of the composite increased with increasing or decreasing temperature. Within a specific temperature range, resistance decreased with increasing temperature. However, the sensing performance and the repeatability of this performance did not vary monotonically with increasing temperature. At temperatures of -40, -20, 0, 20, 40, 60, and 80 °C, the sensing performance of the composite was best between 20 and 40 °C, slightly worse between 60 and 80 °C, and worst performance below 0 °C. Different results were obtained from studies on temperature in the literature. In conclusion, all conductors-based mixtures maintained their electrical conductivity in the short and long term under different environmental conditions. It is clear that the coating to be developed will maintain its conductivity performance under important ambient factors such as temperature and humidity in indoor environments.

4.5.1.2. Electrical Resistance Results of Cylindrical Samples

One of the other experimental methods for the electrical resistance values was determined by the AC method. Unlike the coating design, the ER values were measured from three parts of the cylindrical sample to determine whether the conductive materials were distributed homogeneously into the matrix mixture. ER values of mixtures were determined based on different ambient factors. Average electrical resistance (ER) values were measured from the three cylindrical parts of related mixtures after 1, 3, 7, 28, 90, and 180 days of curing. The ER results of the selected mixtures until the 180^{th} day are given for the bottom part of the cylindrical sample in Table 4.39, for the middle part of the cylindrical sample in Table 4.40, and for the top part of the cylindrical sample in Table 4.41.

Table 4.39. ER results of the bottom part of cylindrical mixtures in different ambient conditions, Ω

Bottom							
Sample	**Factors**	**1st day**	**3rd day**	**7th day**	**28th day**	**90th day**	**180th day**
Reference mixture	First	521	785	1500	19820	162000	226000
	Lab.	471	634	1380	18140	155000	222100
	50 °C	1200	5090	8310	20400	181000	345000
	%100 RH	257	367	455	624	1040	2300
B6(2)	First	183	194	212	236	248	257
	Lab.	204	213	225	270	294	315
	50 °C	191	202	216	250	283	309
	%100 RH	195	209	212	241	276	291
B10(2)	First	155	159	165	188	200	206
	Lab.	152	157	169	191	215	226
	50°C	100	134	155	177	198	235
	%100 RH	162	198	253	311	348	389
CB26(1)	First	189	327	356	530	559	573
	Lab.	188	319	357	517	568	582
	50 °C	160	183	203	218	253	312
	%100 RH	208	297	384	426	602	725
CB68(1)	First	206	213	246	262	274	278
	Lab.	195	217	243	267	291	322
	50°C	92.7	110	146	168	170	176
	%100 RH	171	227	253	287	349	395
CB210(1)	First	195	218	226	239	281	298
	Lab.	182	211	224	237	275	292
	50 °C	173	177	201	212	236	267
	%100 RH	212	229	249	287	317	331
AB66(1)	First	311	314	372	425	682	802
	Lab.	192	267	348	374	671	788
	50 °C	144	223	317	352	389	412
	%100 RH	205	264	310	347	410	433

Table 4.39. ER results of the bottom part of cylindrical mixtures in different ambient conditions, Ω (continued)

AB28(1)	First	234	269	308	345	398	679
	Lab.	231	267	302	342	405	433
	50 °C	136	170	191	203	240	274
	%100 RH	219	249	287	290	292	310
AB210(1)	First	169	231	269	281	332	455
	Lab.	205	234	268	299	329	366
	50 °C	87.2	158	244	252	264	287
	%100 RH	188	215	245	325	375	322
BAC1022(1)	First	143	195	214	269	292	305
	Lab.	114	175	202	253	297	314
	50 °C	70.9	144	169	202	235	271
	%100 RH	155	208	249	268	299	324

According to Table 4.39, Table 4.40, and Table 4.41, the ER behavior of the mixtures between the cylinder and coating samples was similar. Regardless of the parts, the ER values of all the first prepared samples and those kept in the laboratory were similar. ER values of the reference mixture under different conditions varied in the long term. The ER value of the reference sample kept at 50 °C for 3 hours increased compared to the laboratory environment. However, the ER value of the reference mixture was kept under 100% RH, which showed reverse behavior in the long-term and conductive properties. Among the cylinder parts of the reference mixture, the highest ER values were measured from the top part, regardless of the ambient condition.

Table 4.40. ER results of the middle part of cylindrical mixtures in different ambient conditions, Ω

Middle							
Sample	**Factors**	**1st day**	**3rd day**	**7th day**	**28th day**	**90th day**	**180th day**
Reference mixture	First	552	768	1350	17600	168000	223000
	Lab.	540	740	1380	15130	153240	215600
	50°C	946	4177	6270	19250	170000	301300
	%100 RH	228	336	444	642	965	2380
B6(2)	First	185	188	204	216	231	252
	Lab.	208	215	231	249	287	303
	50°C	191	207	217	238	273	299
	%100 RH	190	200	209	227	268	288
B10(2)	First	155	157	177	184	197	202
	Lab.	156	162	175	202	218	230
	50°C	102	132	149	174	197	233
	%100 RH	163	184	250	277	307	375
CB26(1)	First	185	296	333	520	538	546
	Lab.	180	284	327	508	541	573
	50°C	168	180	203	215	242	288
	%100 RH	202	274	388	419	581	710
CB68(1)	First	202	210	248	256	269	272
	Lab.	194	211	237	262	301	337
	50°C	109	140	156	164	172	180
	%100 RH	174	221	249	292	328	382
CB210(1)	First	191	205	275	293	321	335
	Lab.	178	208	216	235	260	288
	50°C	164	173	197	213	234	272
	%100 RH	207	225	237	269	309	335
AB66(1)	First	298	303	374	457	877	905
	Lab.	190	259	320	329	669	875
	50°C	140	215	308	339	360	394
	%100 RH	187	259	298	337	405	438

Table 4.40. ER results of the middle part of cylindrical mixtures in different ambient conditions, Ω (continued)

AB28(1)	First	235	262	278	364	409	656
	Lab.	220	258	300	326	397	428
	50°C	134	167	194	202	234	388
	%100 RH	208	230	273	297	303	325
AB210(1)	First	179	226	274	289	338	462
	Lab.	186	216	270	296	315	360
	50°C	99.1	139	235	244	255	284
	%100 RH	172	201	237	308	367	404
BAC1022(1)	First	140	187	209	262	287	297
	Lab.	117	167	200	249	279	308
	50°C	76	133	166	198	231	266
	%100 RH	159	198	235	267	295	327

The ER values of all parts of the conductor-based mixtures remained at Ω level in the short and long term, regardless of the environmental condition. However, the lower ER values were measured in those kept under 50 °C among ambient conditions. It concluded that the amount of unreacted water in the large voids evaporated and positively affected the conductivity. However, it was observed that ER values increased more under 100% RH conditions continuously compared to other environmental conditions. The voids were filled with water under continuous 100% RH conditions, affecting the ER values negatively. However, the difference between ER values was insignificant, and the conductivity was maintained long-term regardless of the ambient conditions. Additionally, the ER values were similar between cylindrical parts in conductors-based mixtures. From this, it can be stated that the conductive materials were dispersed homogeneously, and static charges were transmitted at every point of the matrix.

Table 4.41. ER results of the top part of cylindrical mixtures in different ambient conditions, Ω

Top							
Sample	**Factors**	**1st day**	**3rd day**	**7th day**	**28th day**	**90th day**	**180th day**
Reference mixture	First	1600	50600	90300	190000	626000	773000
	Lab.	1350	4477	85780	186000	621000	768500
	50 °C	1068	5600	8460	30800	700590	827655
	%100 RH	218	354	457	648	1050	2900
B6(2)	First	193	205	227	265	278	270
	Lab.	197	217	251	281	304	312
	50 °C	185	199	215	249	284	308
	%100 RH	197	214	235	252	297	324
B10(2)	First	165	174	180	198	214	208
	Lab.	164	177	183	205	221	235
	50 °C	107	137	162	183	205	241
	%100 RH	201	235	256	265	308	366
CB26(1)	First	188	323	355	541	578	592
	Lab.	193	331	374	433	571	601
	50 °C	169	193	209	237	256	300
	%100 RH	216	289	397	444	617	744
CB68(1)	First	231	252	267	285	305	308
	Lab.	219	257	281	296	313	345
	50 °C	111	134	152	170	181	202
	%100 RH	192	232	268	317	375	423
CB210(1)	First	199	217	289	317	345	378
	Lab.	181	209	235	247	284	300
	50 °C	178	183	205	224	245	280
	%100 RH	217	238	249	275	347	386
AB66(1)	First	290	312	384	437	898	987
	Lab.	196	281	384	470	728	893
	50 °C	154	237	312	369	418	456
	%100 RH	210	264	303	346	430	449

Table 4.41. ER results of the top part of cylindrical mixtures in different ambient conditions, Ω (continued)

AB28(1)	First	248	281	307	357	437	802
	Lab.	228	276	296	348	410	449
	50 °C	142	178	199	215	258	287
	%100 RH	228	239	283	301	314	348
AB210(1)	First	189	245	279	305	344	489
	Lab.	203	249	265	282	338	377
	50 °C	114	186	242	272	291	301
	%100 RH	177	203	259	291	385	406
BAC1022(1)	First	150	192	235	273	294	306
	Lab.	129	185	208	258	299	322
	50 °C	72.3	152	169	221	251	285
	%100 RH	175	219	234	272	305	339

In this thesis stage, reference mixture and nine different conductor-based mixtures, which showed the best electrical conductivity, were examined under different environmental conditions. According to the results, all of the mixtures with single, double, and triple conductor additions maintained their electrical conductivity performance in the long term under different environmental conditions. Therefore, mixtures were selected based on the lowest conductor ratio among single, double, and triple conductor additions. In this context, B6(2) was selected from the single addition of carbon fiber, AB28(1) was selected from the double addition of carbon fiber-steel fiber, CB26(1) was selected from the double addition of carbon fiber-milled carbon fiber, and BAC1022(1) was selected from the triple addition of all types of conductors for sulfuric acid resistance test of mixtures.

4.5.2. Microstructure of Selected Composites

In this thesis stage, microstructure analysis was conducted to examine the change in ER under ambient conditions for the mixtures demonstrating the best electrical conductivity performance, which contains single, double, and triple conductive materials. In this context, ten samples were tested under different environmental conditions. According to

the ER values, the BAC1022(1) sample was selected among the mixtures due to its minimal effect from different environmental conditions and triple conductor content. Since the microstructure of the BAC1022(1) sample under laboratory conditions was examined in Section 4.4.4., the microstructure of two samples kept at 100% RH and 50 °C conditions were analyzed. In this context, SEM, mapping, and EDX analyses were conducted to determine the microstructure of the BAC1022(1) sample among the selected mixtures. SEM analysis was applied to the 28-day sample, which was broken after being kept at 50 °C for 3 hours, and images taken from different scales are shown in Figure 4.46.

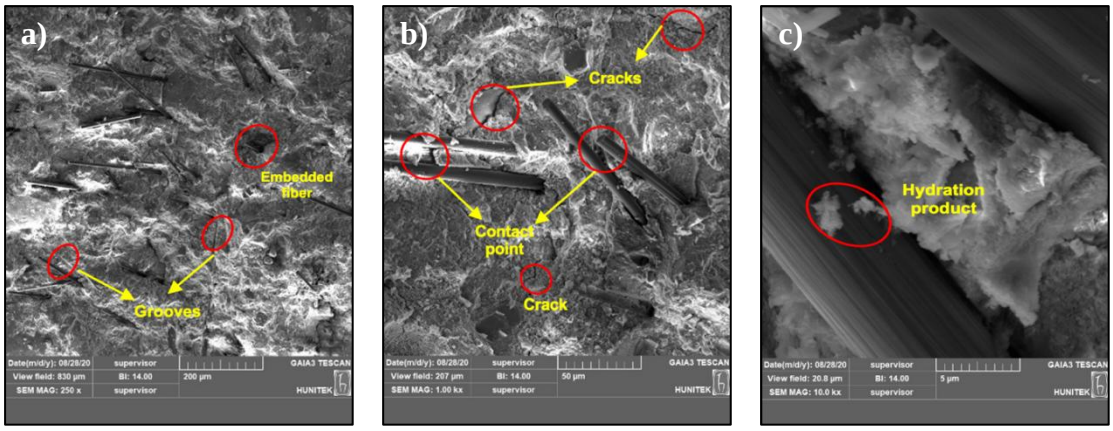

Figure 4.46. SEM images of BAC1022(1) mixture kept at 50 °C at different scales a) 250 x, b) 1 kx, c) 10 kx

As seen from Figure 4.46-a, dispersed CFs in a disorganized way were found at a 250-x scale in the area that belongs to 1.0% CF and 0.2% MCF addition. Therefore, differences in fiber size were observed in the matrix. Although the SEM image was bright, some fibers were embedded in the matrix, some were on the surface, and some touched each other at certain points. The number of fibers at the 250-x scale was the reason for the positive effect on electrical conductivity. It was observed that the amount of fiber in the matrix kept at 50 °C for 3 hours was at the expected level, and the conductivity was not negatively affected. In Figure 4.46-b, embedded fibers and grooves were found in the matrix at a 1-kx scale. Embedded fibers were quite close to each other. In addition to the fiber dispersion, microcracks were also observed on the matrix surface. The crack formation was related to the effect of temperature. In Figure 4.46-c, cloudy shape hydration products were observed between two fibers in the area at the 10-kx scale. The

hydration product on the fiber indicated that adherence could be achieved between the fiber and mortar and that the hydration products surround the fibers. Additionally, the mapping analysis performed on this scale and the result of the elemental analysis of the matrix are shown in Figure 4.47.

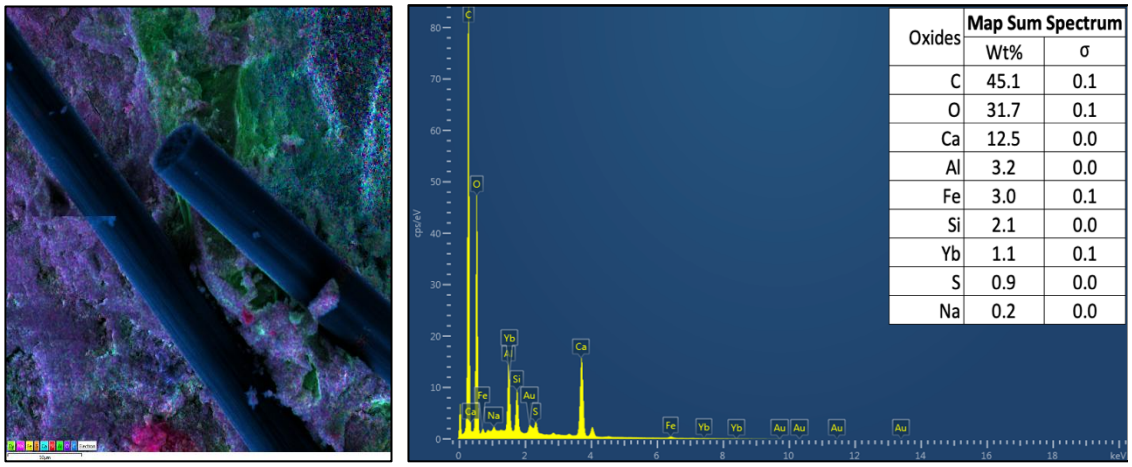

Oxides	Map Sum Spectrum	
	Wt%	σ
C	45.1	0.1
O	31.7	0.1
Ca	12.5	0.0
Al	3.2	0.0
Fe	3.0	0.1
Si	2.1	0.0
Yb	1.1	0.1
S	0.9	0.0
Na	0.2	0.0

Figure 4.47. Elemental analysis of BAC1022(1) mixture kept at 50 °C performed by mapping method

In Figure 4.47, the intensity of the elements in the area was shown with colors by the mapping method made in the examined area. The C element was shown in blue, the Ca element in light blue, the Si element in red, and the Al element in green color. In the examination, there were high amounts of C (45.1%), Ca (12.5%), Al (3.2%), and Si (2.1%) elements except from the O element, respectively. Two main color formations were observed in the matrix: blue and green. Al-based formations resulting from CAC were detected in the matrix, along with C-S-H gel formation from hydration products. The samples were kept at 50 °C for 3 hours on the measurement day after the first day. It was concluded that temperature increases could transform the reaction products and result in Al-based phases in the matrix. Additionally, the EDX analysis performed on the structures in the image is shown in Figure 4.48.

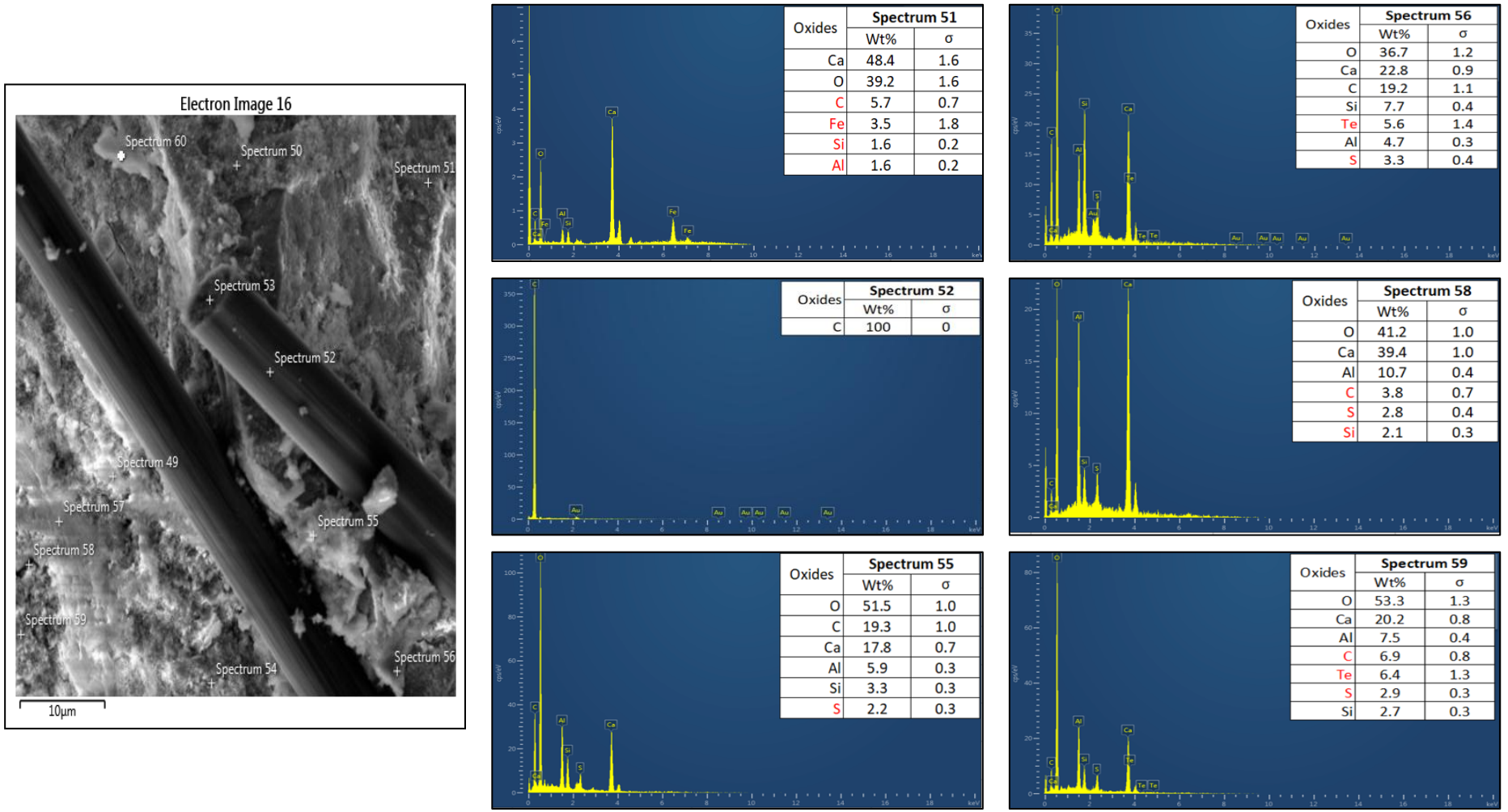

Figure 4.48. EDX analysis of BAC1022(1) composite kept at 50 °C with different spectrums

In Figure 4.48, six spectrums were selected in the examined area. Among these spectrums, one point was taken on the fiber, two points were taken from the flat and smooth surface of the matrix, two points were taken from similar structures, and the other spectrum was taken from the small, darker point. The C content was 100% at both points taken from the fiber. Among the points taken from the flat and smooth surface, 16.2 to 22.8% of the Ca element and 13.9 to 19.3% of the C element were found. The presence of minor elements indicated that a more complex structure had been formed. Among the points taken from the remaining matrix parts, 18.4 to 48.4% Ca element, 5.7 to 11.9% C element and 9.0% Al element were found. Differences in contents were predicted to be related to temperature. SEM analysis was also applied to the 28-day sample, which was broken after being kept in the water (100% RH) until measurement day, and images taken from different scales are shown in Figure 4.49.

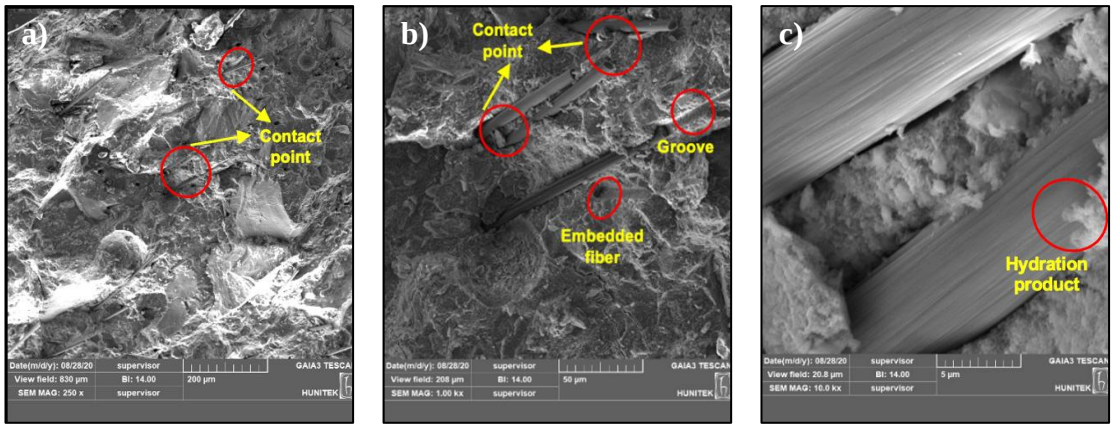

Figure 4.49. SEM images of BAC1022(1) mixture kept at 100% RH at different scales a) 250 x, b) 1 kx, c) 10 kx

As seen from Figure 4.49-a, numerous grooves were found with dispersed CFs in a disorganized way at a 250-x scaled area that belongs to 1.0% CF and 0.2% MCF addition. Although the SEM image was bright, more flattening structures were observed in the sample, which was kept under 100% RH throughout the measurement period. The appearance of grooves indicated the presence of fibers and left traces during the sample preparation. In Figure 4.49-b, embedded fibers and grooves were clearly found in the matrix at a 1-kx scale. Even though the fibers were embedded in the matrix, the distance between fibers and grooves was relatively short. In addition, some of the fibers touched each other at certain points. Therefore, the placement of fibers at the 1-kx scale was the

reason for the positive effect on electrical conductivity. Based on short- and long-term ER results, the electrical conductivity behavior did not negatively affect the samples kept at 100% RH condition throughout the measurement period. In Figure 4.49-c, cloudy shape hydration products were observed between two fibers in the area at the 10-kx scale. This appearance resembled the same matrix kept at 50 °C for 3 h before the measurement. The hydration product on the fiber indicated that adherence could be achieved between the fiber and mortar and that the hydration products surround the fibers. However, the alignment of the fibers and the short distance contributed to the maintenance of conductivity. Compared to the sample kept under 50 °C, no crack formation was observed in the matrix because the matrix was constantly kept at 100% RH condition, and the hydration reaction continued continuously. Additionally, the mapping analysis performed on this scale and the result of the elemental analysis of the matrix are shown in Figure 4.50.

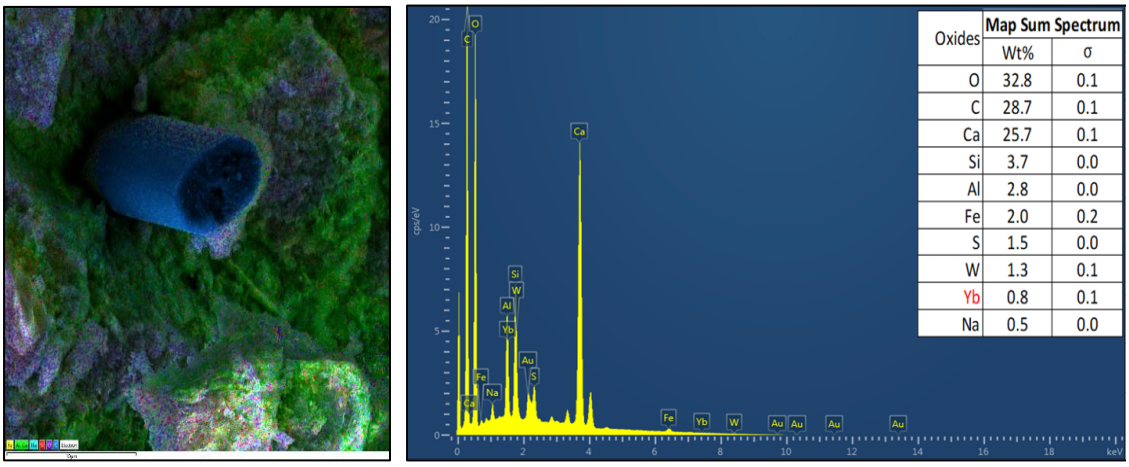

Oxides	Map Sum Spectrum	
	Wt%	σ
O	32.8	0.1
C	28.7	0.1
Ca	25.7	0.1
Si	3.7	0.0
Al	2.8	0.0
Fe	2.0	0.2
S	1.5	0.0
W	1.3	0.1
Yb	0.8	0.1
Na	0.5	0.0

Figure 4.50. Elemental analysis of BAC1022(1) mixture kept at 100% RH performed by mapping method

In Figure 4.50, the intensity of the elements in the area was shown with colors by the mapping method made in the examined area. The C element was shown in blue, the Ca and Al elements were shown in green, and Si was shown in red color. In the examination, there were high amounts of C (28.7%), Ca (25.7%), Si (3.7%), and Al (2.8%) elements except from the O element, respectively. In the matrix, two main color formations were observed, blue and green, and a minor color formation was observed, red. According to color differences, the carbon fiber was colored blue. In contrast, other structures in the

matrix were colored green. Ca and Al elements in green indicated hydration products that developed due to the continuation of the hydration reaction. Here, the silicate products from the PC system and the aluminate products from the CAC system were represented. Additionally, the EDX analysis performed on the structures in the image is shown in Figure 4.51.

In Figure 4.51, six different spectrums were selected in the examined area. Among these spectrums, two points were taken on the fiber; one was taken under the dark place of the fiber, and the other was taken from similar structures. The C content ranged between 84.5 - 100% at both points taken from the fiber. While the C element was 100% at the point taken from the fiber, the C level decreased at the points in the inner part, and in addition, it contained low amounts of Ca and Si elements. Hydration products around the fiber caused a decrease in the C content. In the dark side of the fiber, 41.2% Ca and 10.8% C elements were found. Although the part was shown as a void around the fiber, the gel structure was formed with a high Ca content. Other points mainly contained 17.5 to 45.8% Ca and 8.5% to 20.7% C elements. Differences in contents were predicted to be related to samples kept in the water during measurement time.

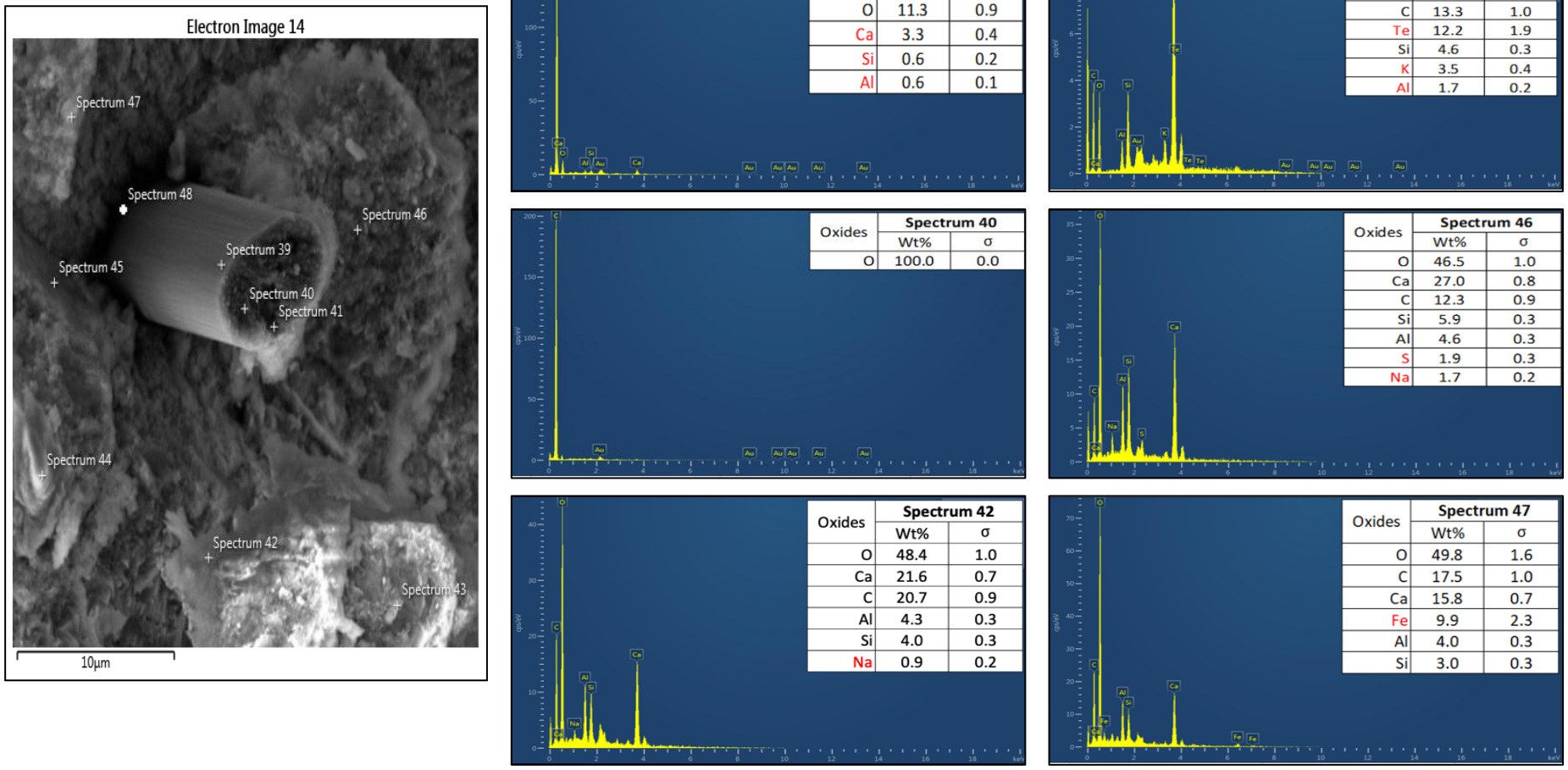

Oxides	Spectrum 39	
	Wt%	σ
C	84.3	0.9
O	11.3	0.9
Ca	3.3	0.4
Si	0.6	0.2
Al	0.6	0.1

Oxides	Spectrum 45	
	Wt%	σ
Ca	45.8	1.5
O	18.9	1.4
C	13.3	1.0
Te	12.2	1.9
Si	4.6	0.3
K	3.5	0.4
Al	1.7	0.2

Oxides	Spectrum 40	
	Wt%	σ
O	100.0	0.0

Oxides	Spectrum 46	
	Wt%	σ
O	46.5	1.0
Ca	27.0	0.8
C	12.3	0.9
Si	5.9	0.3
Al	4.6	0.3
S	1.9	0.3
Na	1.7	0.2

Oxides	Spectrum 42	
	Wt%	σ
O	48.4	1.0
Ca	21.6	0.7
C	20.7	0.9
Al	4.3	0.3
Si	4.0	0.3
Na	0.9	0.2

Oxides	Spectrum 47	
	Wt%	σ
O	49.8	1.6
C	17.5	1.0
Ca	15.8	0.7
Fe	9.9	2.3
Al	4.0	0.3
Si	3.0	0.3

Figure 4.51. EDX analysis of BAC1022(1) composite kept at 100% RH with different spectrums

4.6. Sulfuric Acid Resistance of the Selected Cementitious Mixtures

During the thesis study, the samples showing the best electrical conductivity performance among the mixtures prepared using single, double, and triple conductive materials were exposed to environmental factors such as humidity, temperature, and laboratory. Among the mixtures, samples that were least negatively affected by different environmental conditions and had the lowest conductor content were selected. In this context, B6(2) was selected from the single addition of carbon fiber, AB28(1) was selected from the double addition of carbon fiber-steel fiber, CB26(1) was selected from the double addition of carbon fiber-milled carbon fiber, and BAC1022(1) was selected from the triple addition of all types of conductors for sulfuric acid resistance test of mixtures. Apart from the acid resistance of samples, the pure PC sample was also immersed in a sulfuric acid solution to compare the acid resistance of both mixtures. To determine the acid resistance, the re-prepared samples were kept in laboratory condition for seven days after casting and immersed in sulfuric acid solution.

4.6.1. Compressive Strength Results of Selected Composites After Sulfuric Acid Test

The effect of the sulfuric acid solution on the mechanical properties of the mixtures was determined by measuring the compressive strengths of the samples. This measurement was conducted on the 7^{th} day before immersing the samples in the sulfuric acid solution. Subsequently, the compressive strengths were assessed again on the 28^{th} day, following a 21-day immersion period in the acid solution. The average compressive strength results of the selected samples are shown in Figure 4.52.

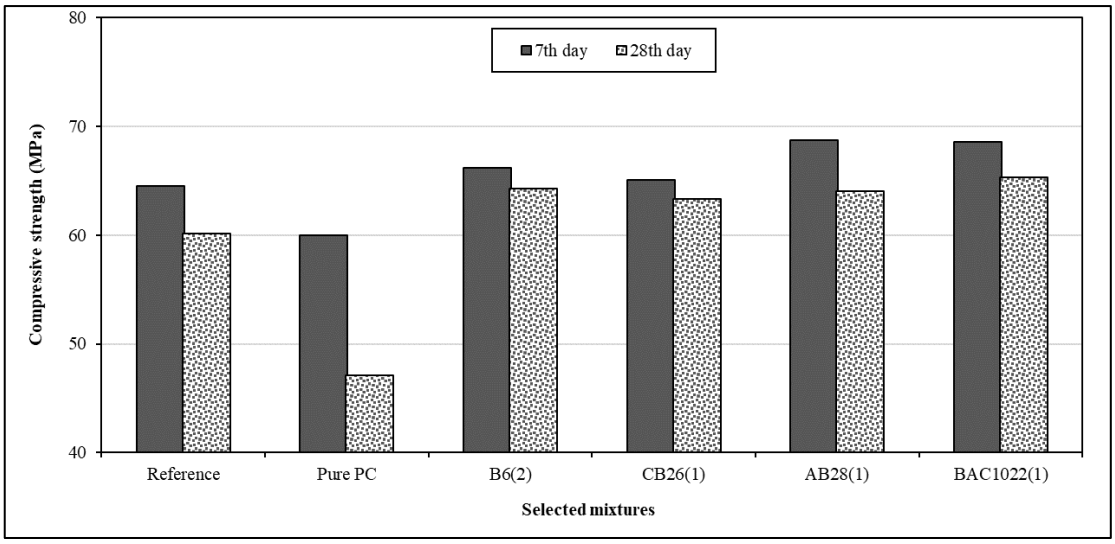

Figure 4.52. Compressive strength results of the selected mixtures after acid resistance test

A negative effect in compressive strength was observed at the end of the 21-day acid test of all mixtures. In Figure 4.52, the reduction in compressive strength was measured between 2.76 and 21.48% after 21 days. Among the mixtures, only PC used sample was most affected by the acid solution. It has been investigated for years in the literature that concrete prepared using standard PC has poor resistance to chemical attacks such as aggressive acids [239]. The reaction with sulfuric acid in the solution and free calcium hydroxide (CH) in the concrete causes gypsum to be released into the environment. The gypsum products then react with calcium aluminate (C_3A) to produce the ettringite mineral. This formation causes the concrete volume to increase a few times and large volume expansions. As a result, significant deformations in structures are observed due to increased internal pressure [240]. Therefore, the 21.48% decrease measured in the PC-based mixture immersed in the acid solution for 21 days was consistent with the results of the literature. On the other hand, the strength losses in mixtures prepared using the ternary system were measured between 2.76 and 6.78%. The strength losses remained at a much lower level compared to PC due to the use of CAC in the ternary system. It was stated in the literature that CAC cements could be used in sewer applications where acid attacks occur frequently due to their superior acid resistance [239]. In acidic solutions with a pH above 4, the AH_3 compound was released and acts as a barrier against acid attack, thus protecting the concrete. In addition, the use of CAC reduced the acid effect in concrete more than the use of PC. Therefore, the strength losses occurred similarly

among ternary-based mixtures due to the main matrix. Among the mixtures, the lowest strength loss was measured in the CB26(1) sample, while the highest strength loss was measured in the reference sample.

4.6.2. Electrical Resistance Results of Selected Composites After Sulfuric Acid Test

4.6.2.1. Electrical Resistance Results of Coating Samples

The change in the electrical conductivity performance of mixtures containing conductors was determined in the case of a sulfuric acid attack. In addition, the effect of sulfuric acid exposure in the early and long term on the electrical resistance value of the selected samples was determined. Therefore, two different methods were used to determine the acid resistance. First, 180-day casting samples were directly immersed in a sulfuric acid solution. As a second method, selected samples were recast for sulfuric acid testing. The prepared coatings were kept under laboratory conditions for the first seven days and then immersed in the sulfuric acid solution for 7-day periods up to 90 days. At the end of each period, the surface of the coatings was cleaned with water and kept at 50 °C for 24 hours. The electrical resistance behavior of selected samples was compared with that of a pure PC-based mixture without conductors. The average ER results of selected mixtures until the 90^{th} day are given in Table 4.42.

Table 4.42. ER results of selected coating samples in sulfuric acid solution, Ω

Sample		**Pure PC**	**Reference**		**B6(2)**		**CB26(1)**		**AB28(1)**		**BAC1022**	
Resistance (Ω)		**Acid Test**	**First Casting**	**Acid Test**	**First Casting**	**Acid Test**	**First Casting**	**Acid Test**	**First Casting**	**Acid Test**	**First Casting**	**Acid Test**
Test Day	**Acid Test Day**											
1st day	-	271*10^5	-	16.2*10^6	-	583	-	275	-	411	-	465
3rd day	-	80.6*10^5	-	25.3*10^6	-	625	-	460	-	417	-	221
7th day	1st day	97.8*10^5	9.4*10^7	47.8*10^6	445	849	977	730	998	577	642	376
14th day	7th day	2.6*10^7	10.3*10^7	2.9*10^7	133	815	804	715	872	789	577	317
21st day	14th day	14.2*10^7	10.7*10^7	4.53*10^7	332	487	753	877	766	612	439	372
28th day	21st day	15.3*10^7	11.2*10^7	6.72*10^7	128	352	769	391	835	751	229	300
35th day	28th day	18.7*10^7	11.9*10^7	9.47*10^7	219	326	635	313	836	408	421	461
42nd day	35th day	20.1*10^7	13.4*10^7	11.1*10^7	166	308	479	619	788	859	272	226
49th day	42nd day	22.7*10^7	15.9*10^7	13.1*10^7	170	268	476	562	555	604	188	301
56th day	49th day	25.3*10^7	16.7*10^7	14.8*10^7	197	235	493	645	563	338	208	298
63rd day	56th day	26.7*10^7	17.0*10^7	15.2*10^7	255	348	458	752	591	635	250	449
70th day	63rd day	28.4*10^7	17.4*10^7	16.1*10^7	261	374	479	781	610	722	304	456
77th day	70th day	30.1*10^7	18.2*10^7	17.4*10^7	299	405	502	803	655	745	356	488
84th day	77th day	36.4*10^7	22.7*10^7	18.9*10^7	312	446	548	811	683	773	446	529
91st day	84th day	40.8*10^7	23.5*10^7	20.4*10^7	348	481	592	866	710	856	523	655
98th day	91st day	44.2*10^7	27.8*10^7	23.9*10^7	356	524	629	921	767	903	564	700

As seen from Table 4.42, although the ER values of the samples increased, the electrical conductivity behavior of conductor-based mixtures was preserved at the end of the 90th-day immersion in acid solution. Except for the conductor-based mixtures, ER values of reference and PC sample immersed in the acid solution, which were at the MΩ level before the sulfuric acid test, increased continuously at the GΩ level during the acid time. However, the ER value of the pure PC-based mixture increased approximately two times compared to the reference mixture. There was no significant difference between ER values when the reference mixture was exposed to the sulfuric acid solution in the early and long term. However, while the exposure of the reference mixture to sulfuric acid attack after the 180-day curing period increased the ER value more during the first 7-day periods, this rate of increase decreased over time. In the reference sample exposed to sulfuric acid attack after the 7-day curing period, the ER value increased at a lower rate from the first period. This was related to the ER value of the 180-day reference sample increased to MΩ level over time, without acid attack. As for conductor-based mixtures, although the resistance values of the conductor-contained coatings changed in the sulfuric acid solution, superconductivity behavior was observed by remaining at the Ω level after 90 days. Among the conductors-based samples, exposure to the sulfuric acid solution in the early and long terms did not significantly change the ER values. Though the ER values of samples decreased until the 56th-day measurements in both ages, the ER values increased after the 56th day. The main reason for the decline was that more fibers remained on the coating surface due to the deterioration caused by coatings immersed in the sulfuric acid solution until the 56th day. As the immersion time in the sulfuric acid solution continued, ER values increased due to further corrosion of the matrix and a lower number of fibers. Based on the ER values at the end of 90 days of immersion in sulfuric acid solution, the age of exposure to the sulfuric acid solution during the service life of the coatings using the lowest fiber ratio was not an obstacle to the electrical conductivity performance of the coatings due to preserved electrical conductivity. Conductor-based coatings gained 40-50% of their compressive strength within the first day. In conclusion, incorporating conductors into the ternary-based cementitious matrix was resistant to acid attack and preserved its conductivity. The deformations of the surface appearance of the coatings after acid attack are shown between Figures 4.53 and 4.56.

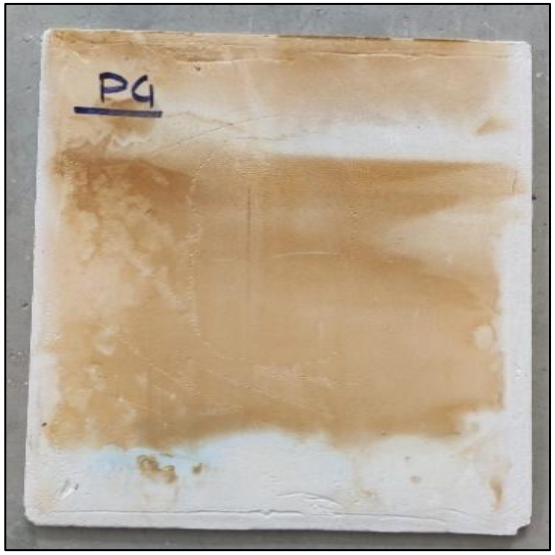

7-day PC sample

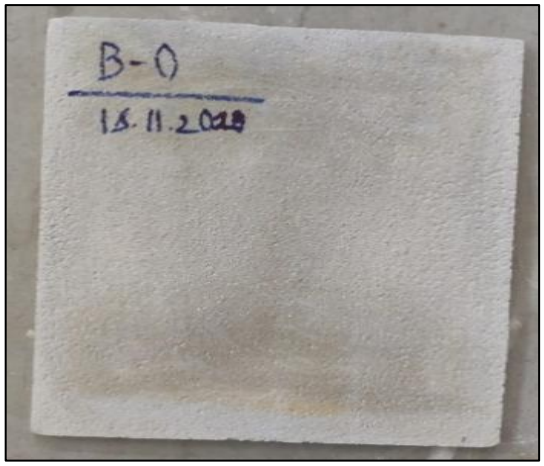

180-day reference sample

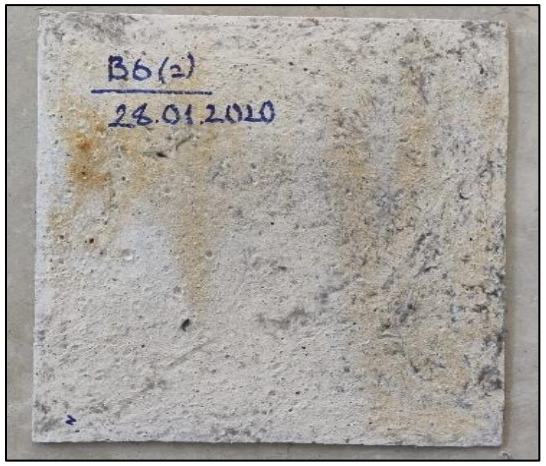

180-day B6(2) sample

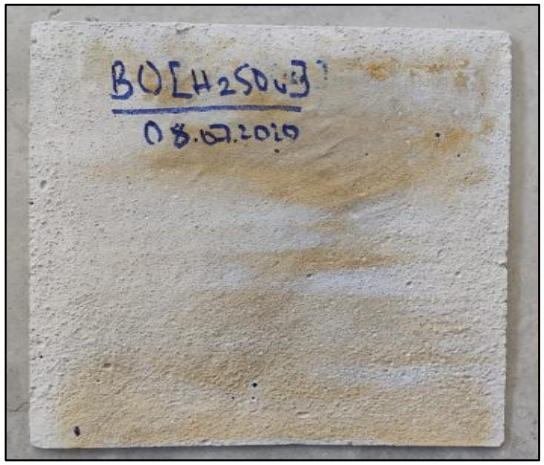

7-day reference sample

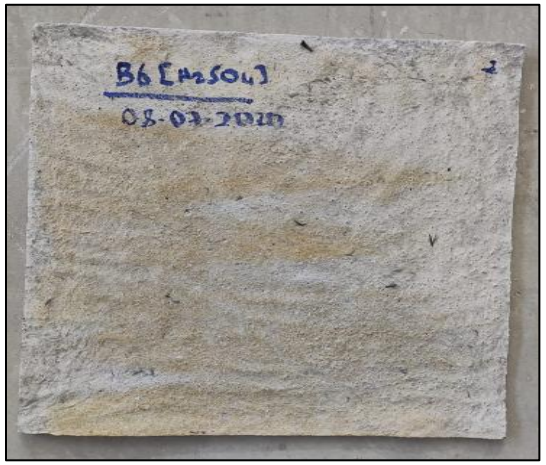

7-day B6(2) sample

Figure 4.53. Surface views of PC, reference, and B6(2) samples immersed in sulfuric acid solution after the 56th day

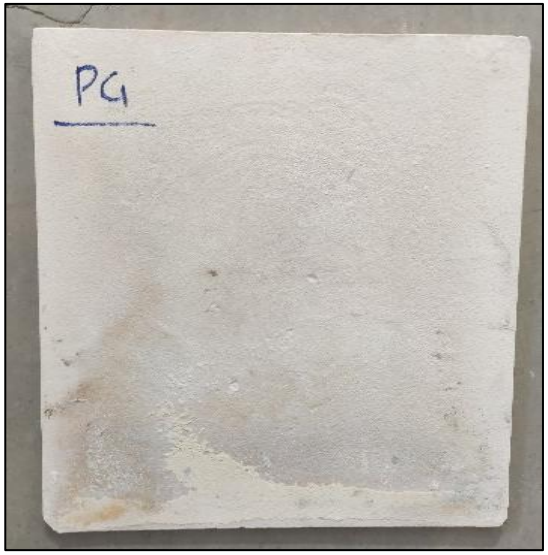

7-day PC sample

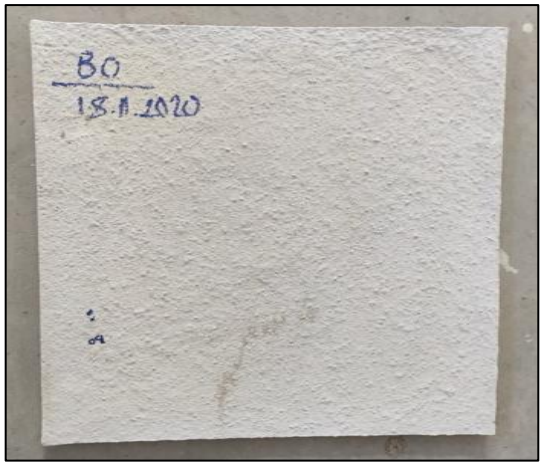

180-day reference sample

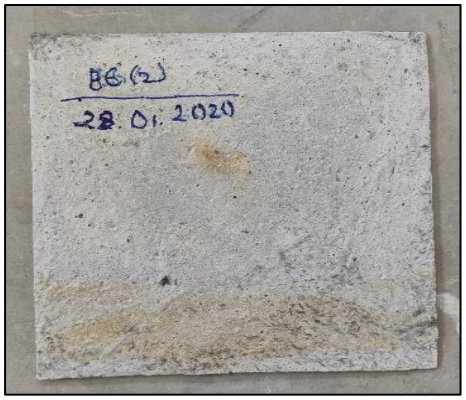

180-day B6(2) sample

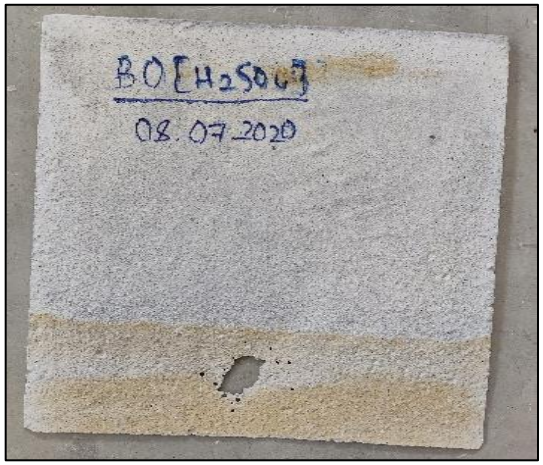

7-day reference sample

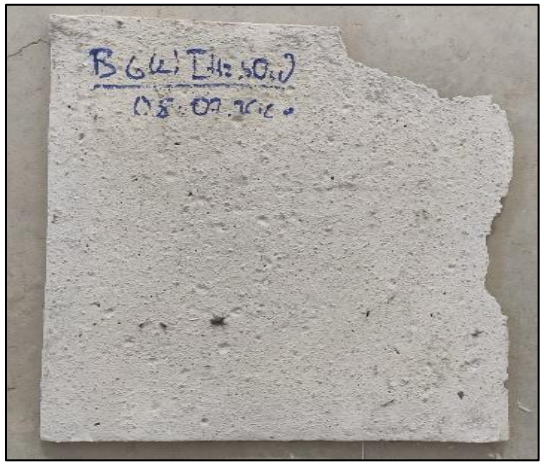

7-day B6(2) sample

Figure 4.54. Surface views of PC, reference, and B6(2) samples immersed in sulfuric acid solution after the 90th day

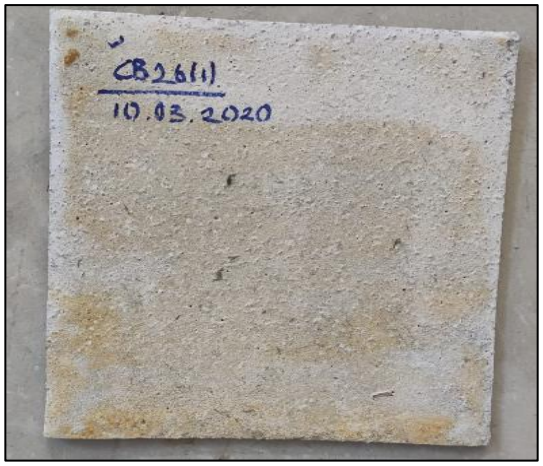

180-day CB26(1) sample

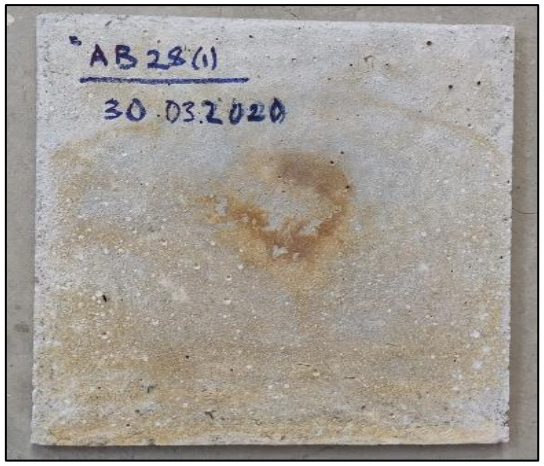

180-day AB28(1) sample

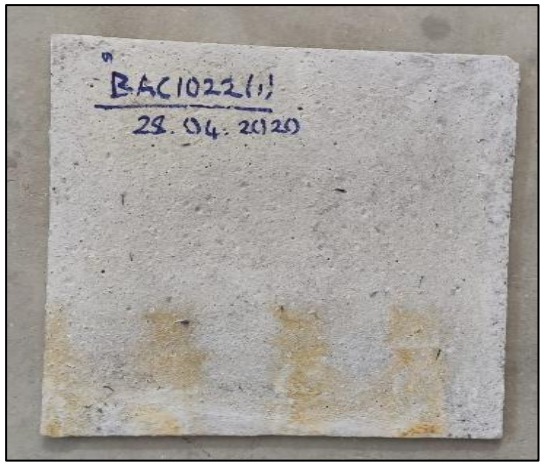

180-day BAC1022(1) sample

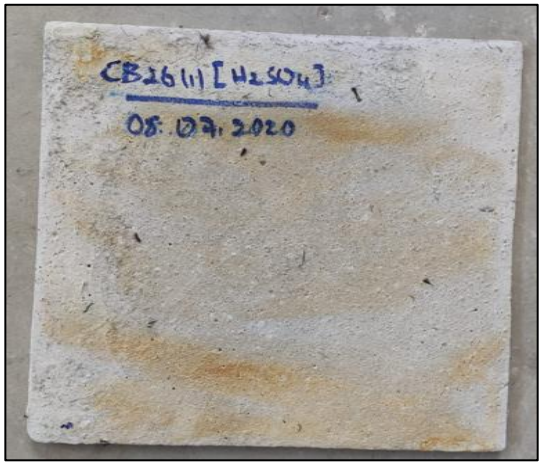

7-day CB26(1) sample

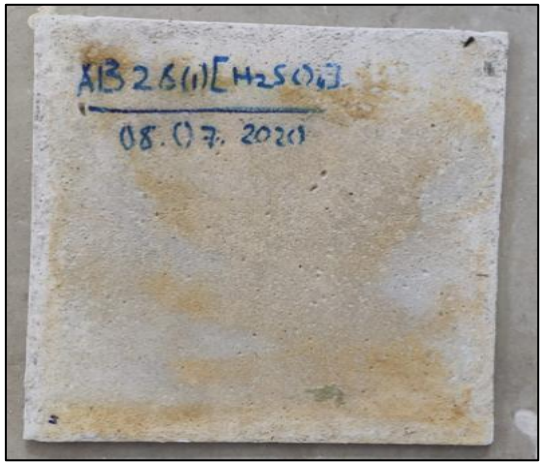

7-day AB28(1) sample

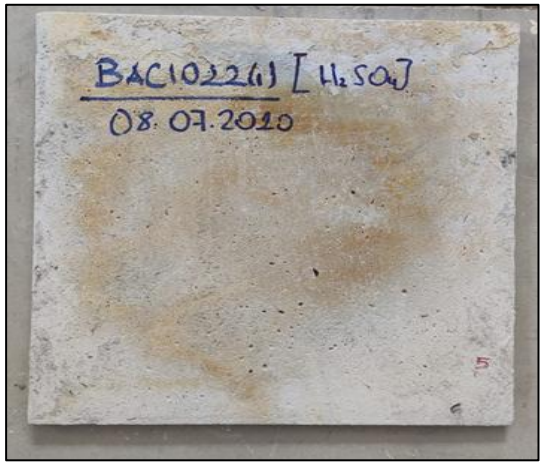

7-day BAC1022(1) sample

Figure 4.55. Surface views of CB26(1), AB28(1), and BAC1022(1) samples immersed in sulfuric acid solution after the 56th day

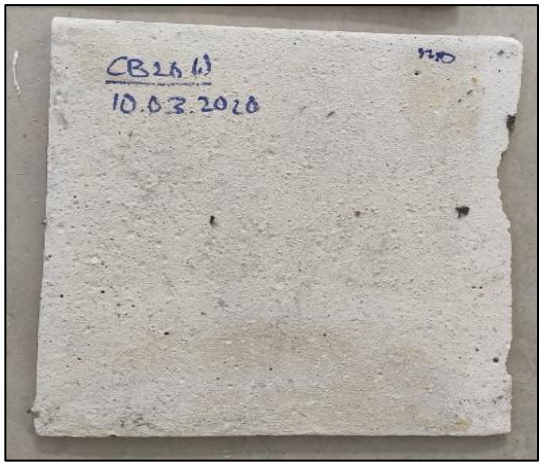

180-day CB26(1) sample

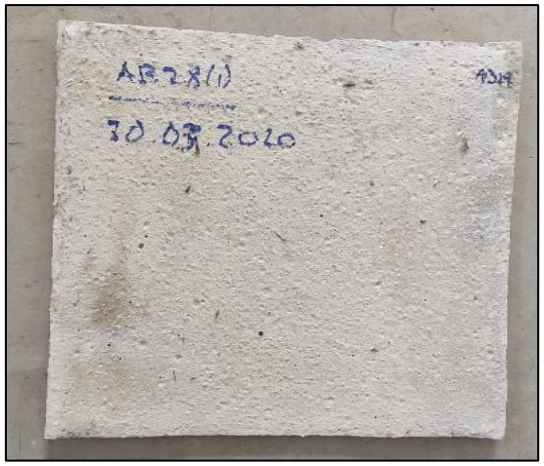

180-day AB28(1) sample

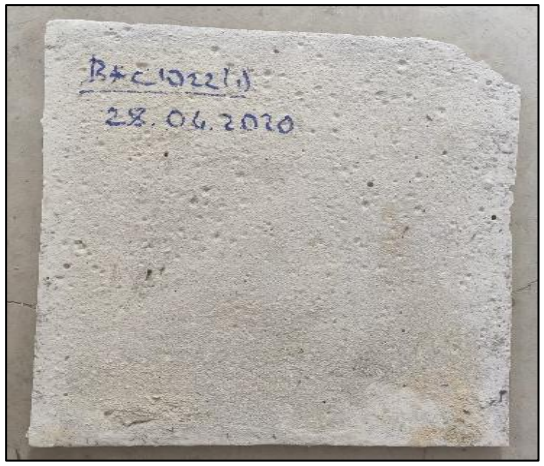

180-day BAC1022(1) sample

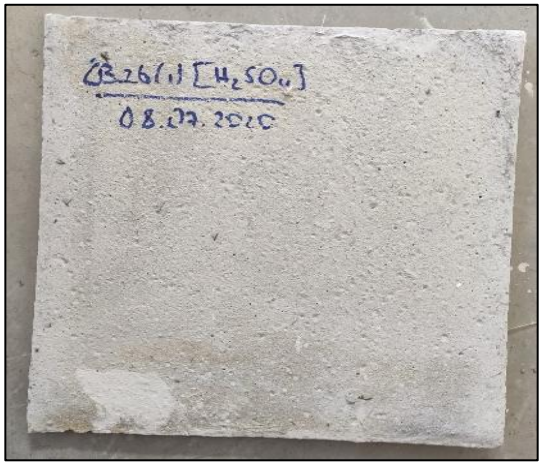

7-day CB26(1) sample

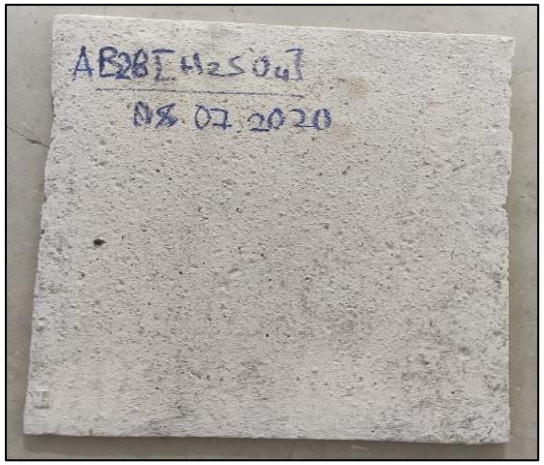

7-day AB28(1) sample

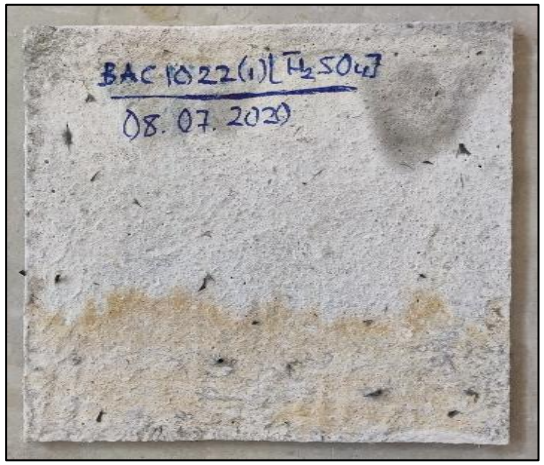

7-day BAC1022(1) sample

Figure 4.56. Surface views of CB26(1), AB28(1), and BAC1022(1) samples immersed in sulfuric acid solution after the 90th day

As seen in Figure 4.53 and Figure 4.54, discolorations and deteriorations were observed on the surface of some coatings after 56 days of sulfuric acid test. After removing coatings from the acid solution and cleaning them, they were kept at 50 °C for one day, and staining was observed on the surfaces. While the PC sample was affected the most during this test process, there was almost no color change in the reference sample kept in sulfuric acid after the 180-day curing period. On the other hand, color changes were visible in the reference sample immersed in sulfuric acid solution at an early age (7^{th} day). Considering the surface appearance of conductor-based mixtures, the B6(2) sample was most affected in both groups. It was observed that fibers rise to the surface with the effect of sulfuric acid solution and clump at certain points during the cleaning of the coatings. This showed that the acid solution leaked into the matrix more easily and negatively affected the matrix's acid resistance. There was a logical relationship between ER results and coating appearances. Due to the higher number of fibers remaining on the surface, electrical resistance values decreased compared to the first-day measurements.

As seen in Figure 4.55 and Figure 4.56, discolorations, deteriorations, and damages were observed on the surface of all coatings after 90 days of sulfuric acid test. While no holes, gaps, or damages were observed in the coatings exposed to the acid solution for 56 days, damage was detected in some samples at the end of the 90^{th} day. Among the mixtures without conductors' addition, the reference mixture, which was exposed to sulfuric acid attack early, was most affected by the acid solution. No deterioration, damage, or color change was observed after exposure to acid attack after the 180-day curing period of the same sample. It was thought that the main reason was the strength of the reference sample after 180 days. After 90 days of the acid test, coloring on the PC-based coating surface disappeared due to the deformation of the layer. The fact that the 7^{th}-day PC-based mixture had a better surface appearance than the 7^{th}-day reference mixture was in contrast to the compressive strength results. Apart from this, the most negatively affected coating at early and later ages was observed in the B6(2) sample among all samples. Among the conductor-based samples, acid attacks most affected the 7-day coatings. Surface deformations were acceptable in 180-day coatings. In addition, the fibers and agglomerations seen on the coating surfaces on the 56^{th} day decreased on the 90^{th} day. ER values of the coatings increased as the thickness of the coatings and the amount of fiber decreased.

4.6.2.2. Electrical Resistance Results of Cylindrical Samples

In addition to the effect of sulfuric acid attack on the electrical resistance of the coatings, the electrical conductivity behavior of cylindrical samples under sulfuric acid solution was determined. Therefore, the electrical resistance behavior of selected samples was compared with that of a pure PC-based and reference mixture without conductors. Selected samples were recast for acid testing. The prepared cylindricals were kept under laboratory conditions for the first seven days and then immersed in the sulfuric acid solution for 7-day periods up to 90 days. At the end of each period, the surface of the coatings was cleaned with water and kept at 50 °C for 24 hours. Average electrical resistance (ER) values were measured from the three cylindrical parts of related mixtures 90 days of sulfuric acid test. The ER results of the selected mixtures until the 90^{th} day are given in Table 4.43 and Table 4.44.

Table 4.43. ER results of cylindrical PC, reference, and B6(2) samples in sulfuric acid solution, Ω

Sample		**PC**			**Reference**			**B6(2)**		
Resistance (Ω)		**Bottom**	**Middle**	**Top**	**Bottom**	**Middle**	**Top**	**Bottom**	**Middle**	**Top**
Test Day	**Acid Test Day**									
1st day	-	261	256	259	315	313	317	187	202	216
3rd day	-	292	295	344	522	543	3710	193	192	206
7th day	1st day	456	467	824	1040	1120	4500	209	212	219
14th day	7th day	511	507	639	2170	200	5060	206	210	217
21st day	14th day	3200	3150	5880	2800	2880	5270	205	206	209
28th day	21st day	4290	4750	6540	2070	3680	5470	181	201	208
35th day	28th day	6080	6220	7180	3590	4190	6000	178	194	207
42nd day	35th day	7060	6480	7770	3780	4360	6630	175	187	204
49th day	42nd day	7290	6750	8540	5150	6360	8630	171	184	199
56th day	49th day	7950	7400	9000	6190	7160	9820	171	180	198
63rd day	56th day	8150	7680	12500	8190	7900	10400	174	182	194
70th day	63rd day	8870	8450	13800	8430	8660	12900	175	184	200
77th day	70th day	9340	8950	15600	8890	9100	14100	176	183	198
84th day	77th day	11500	9580	17920	9400	10500	16380	179	188	194
91st day	84th day	13200	11400	20900	11500	13400	18200	183	185	196
98th day	91st day	15800	13600	22100	14300	15700	20150	182	187	199

Table 4.44. ER results of cylindrical CB26(1), AB28(1), and BAC1022(1) samples in sulfuric acid solution, Ω

Sample		**CB26(1)**			**AB28(1)**			**BAC10222(1)**		
Resistance (Ω)		**Bottom**	**Middle**	**Top**	**Bottom**	**Middle**	**Top**	**Bottom**	**Middle**	**Top**
Test Day	**Acid Test Day**									
1st day	-	208	211	213	202	214	230	156	170	182
3rd day	-	234	243	254	220	237	256	178	209	218
7th day	1st day	265	271	282	245	276	288	205	218	225
14th day	7th day	239	248	264	219	237	251	194	202	215
21st day	14th day	214	222	236	208	229	228	192	183	208
28th day	21st day	197	205	222	191	212	214	181	174	198
35th day	28th day	184	192	209	170	180	203	175	171	192
42nd day	35th day	168	189	196	134	162	194	164	169	185
49th day	42nd day	164	177	189	121	145	188	159	145	171
56th day	49th day	157	169	183	119	146	180	152	139	158
63rd day	56th day	131	118	136	118	120	136	141	133	128
70th day	63rd day	138	127	145	124	138	144	147	138	133
77th day	70th day	137	135	147	128	134	140	146	137	139
84th day	77th day	138	132	144	126	135	147	148	139	144
91st day	84th day	140	135	146	128	138	148	149	142	146
98th day	91st day	143	138	145	130	139	150	150	143	148

As seen from Table 4.43 and Table 4.44, although the ER values of the samples increased, the electrical conductivity behavior of conductor-based mixtures was preserved at the end of the 90th-day immersion in sulfuric acid solution. Except for the conductor-based mixtures, ER values of reference and PC samples immersed in the acid solution, which were at the Ω level before the sulfuric acid test, increased continuously at the kΩ level during the acid time. While there was a significant difference between the ER values of the reference mixture and the PC-based mixture until the 14th measurement day, similar ER values were measured at the end of the 90th day. All parts of both mixtures were significantly affected by the sulfuric acid attack. Among the parts of the cylindricals, the highest ER values were measured from the top part. However, ER values of the lower and middle parts were measured at similar levels. The main reason was that the upper part was directly exposed to the sulfuric acid solution. While the ER values of the mixtures increased quickly in the first seven days due to laboratory conditions, the ER values decreased after acid immersion, with differences between 1 and 3%. The main reason for the reduction of ER value within sulfuric acid immersion time was that conductive materials came to the surface due to corrosion. According to ER values at the end of 90 days, conductors-based mixtures maintained electrical conductivity behavior. In addition, no significant differences were observed between the ER values of the conductor-based parts. Incorporating conductive materials lessened the ER differences between the parts, which did not change with the sulfuric acid solution. Although exposure of the layers to acid solution negatively affected the surfaces, ER values remained at similar levels due to the fibers remaining on the surface. Homogeneous fiber dispersion between parts remained the same before and after the sulfuric acid attack except for the reference sample. The deformations of the surface appearance of the cylindrical after the acid attack are shown in Figure 4.57 and Figure 4.58.

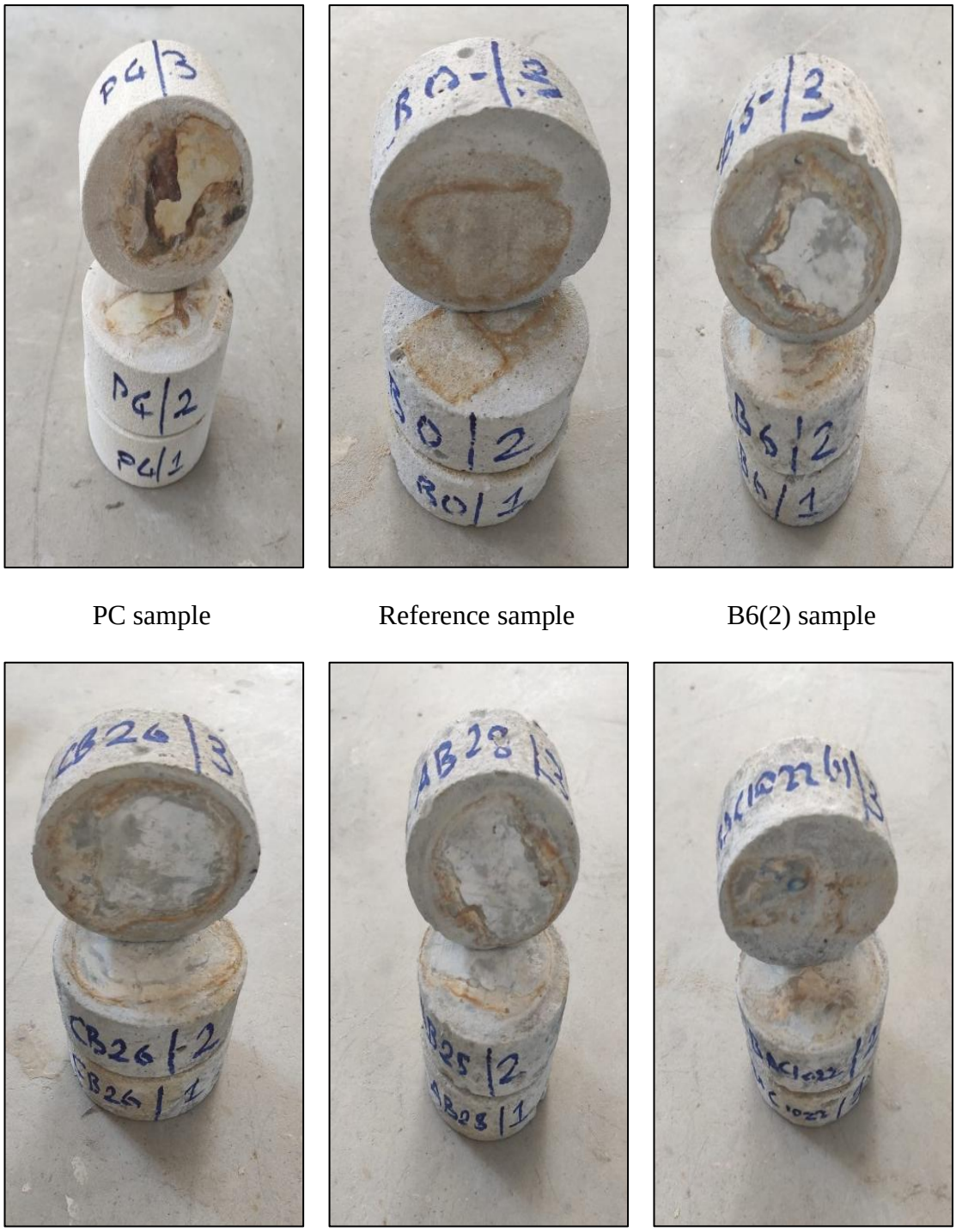

Figure 4.57. Views of the cylindrical surface immersed in sulfuric acid solution after 56th day

PC sample

Reference sample

B6(2) sample

CB26(1) sample

AB28(1) sample

BAC1022(1) sample

Figure 4.58. Views of the cylindrical surface immersed in sulfuric acid solution after 90th day

As seen in Figure 4.57 and Figure 4.58, discolorations and deteriorations were observed on the surface of cylindrical parts after 56 days and 90 days of the sulfuric acid test,

respectively. Deteriorations on the surfaces and their surroundings also occurred because the samples were removed from the solution every seven days and then kept at 50 °C for one day after cleaning with water. In the Figures, surface degradation, corrosion, color changes, and reductions in sample sizes increased during acid attack. Deterioration occurred more in the parts that touch each other. In conclusion, although continuous acid exposure of conductor-based mixtures using ternary systems did not adversely affect the electrical conductivity performance, continuous acid solution exposure should be prevented because it negatively affected the acid resistance of mixtures and surfaces.

4.6.3. Microstructure of Selected Composites After Sulfuric Acid Test

In this stage of the thesis, microstructure analysis was conducted to examine the change in ER under sulfuric acid solution for the mixtures demonstrating the best electrical conductivity performance, which contains single, double, and triple conductive materials. According to the ER values, the BAC1022(1) sample was selected among the mixtures due to its minimal effect from different environmental conditions and triple conductor content. In this context, SEM, mapping, and EDX analyses were conducted to determine the effect of sulfuric acid attack on the microstructure of the BAC1022(1) sample. SEM analysis was applied to the 28-day sample, which was broken after being kept at 50 °C for one day, and images taken from different scales are shown in Figure 4.59.

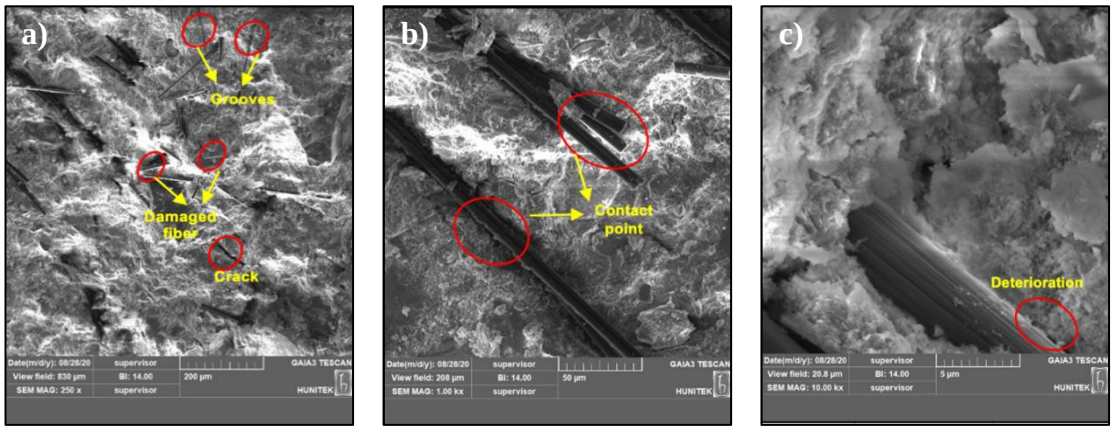

Figure 4.59. SEM images of BAC1022(1) mixture immersed in sulfuric acid solution at different scales a) 250 x, b) 1 kx, c) 10 kx

As seen from Figure 4.59-a, the dispersion of numerous fibers on the matrix surface, clumps, and grooves were observed in some areas at a 250-x scaled in the area that belongs to 1.0% CF and 0.2% MCF addition. Although numerous fibers belong to CFs, a few MCFs were also seen on the surface of the matrix. Although the SEM image was bright, some fibers were embedded in the matrix, some were on the surface, and some touched each other at certain points. The brightness of the SEM picture was attributed to the corrosion of the matrix after the acid solution, and the SEM device sent high beams to capture images after the acid solution. The excessive fiber appearance on the surface was due to the high fiber content, and the fibers came to the surface more after being exposed to the sulfuric acid solution. However, the increased number of fibers also contributed to improving electrical conductivity. In Figure 4.59-b, embedded fibers and grooves were found in the matrix at a 1-kx scale. Embedded fibers were quite close to each other in the matrix. Numerous fibers were found at the 1-kx scale. The small distance between fibers showed that conductive paths can transmit electrostatic charges. In addition to the fiber dispersion, microcracks were observed on the matrix surface. The crack formation was related to the acid attack and related expansion mechanism. In Figure 4.59-c, cloudy shape hydration products were observed between two fibers in the area at the 10-kx scale. There was a shift in the matrix during imaging. After applying the acid solution, the structure's appearance within the matrix became flatter. Except for this, the hydration products on the fiber indicated that adherence can be achieved between the fiber and mortar and that the hydration products surround the fibers. Additionally, the mapping analysis performed on this scale and the result of the elemental analysis of the matrix are shown in Figure 4.60.

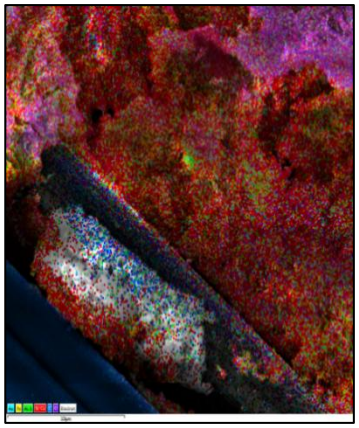

a) All elements

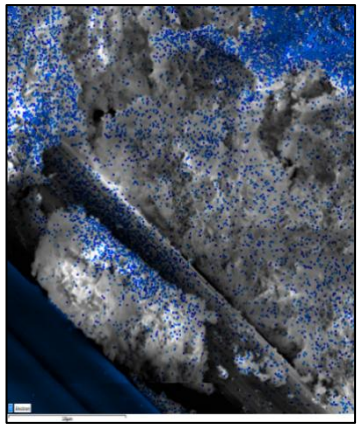

b) C element

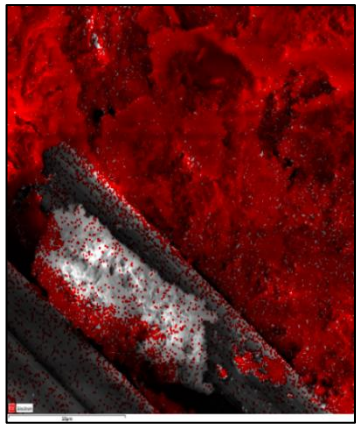

c) Ca element

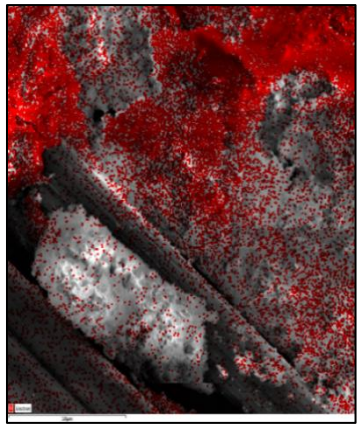

d) Si element

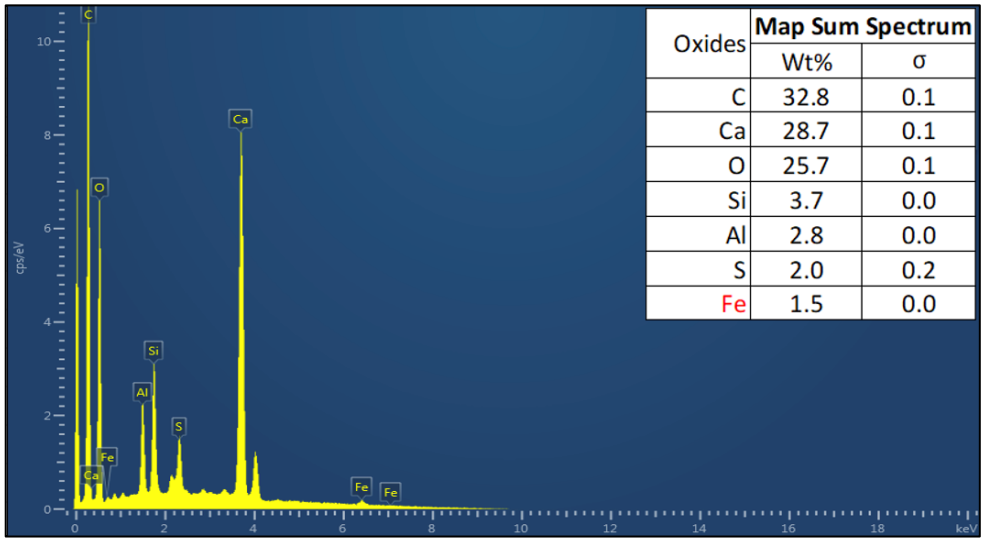

Oxides	Map Sum Spectrum	
	Wt%	σ
C	32.8	0.1
Ca	28.7	0.1
O	25.7	0.1
Si	3.7	0.0
Al	2.8	0.0
S	2.0	0.2
Fe	1.5	0.0

Figure 4.60. Elemental analysis of BAC1022(1) mixture immersion in sulfuric acid solution performed by mapping method and EDX analysis

In Figure 4.60, the intensity of the elements in the area was shown with colors by the mapping method made in the examined area. In Figure 4.60-a, the C element was shown in blue, the Ca and Si elements in red, and the Al and S elements in green color. In the examination, there were high amounts of C (32.9%), Ca (29.7%), Si (3.2%), and Al (2.1%) elements except from the O element, respectively. In the matrix, two main color formations were observed, red and blue, and a minor color formation was observed, green. Apart from the O element, the main elements were C and Ca. The C element was detected in high concentrations due to the fibers in the matrix. In contrast, the Ca element was detected in high concentrations due to the products formed by the reaction of a combination of PC, CAC, and CŚ. In Figure 4.60-b, the C element sections were colored blue using the mapping method. While the adjacent fibers at the edge of the image were shown entirely in blue, the fiber remaining inside the matrix was depicted with less intensity in blue. The decrement was related to the reaction products around the fiber. In Figure 4.60-c, the sections containing the Ca element were colored red using the mapping method. Except for the fibers, the Ca element was present throughout the entire matrix. The content of the Ca element in the matrix, immersed in an acid solution for 21 days following a 7-day curing period, increased due to the heightened ettringite content. This increase resulted from the reaction between calcium hydroxide (CH) and calcium aluminate (C_3A) in the environment. In Figure 4.60-d, the Si element sections were colored red using the mapping method. The Ca element could be detected throughout the matrix, except in the fibers, while the Si element was detected in areas similar to those containing the C element. The Si element was present due to hydration reaction products.

5. CONCLUSION

This thesis has contributed to the field of civil engineering by developing a comprehensive understanding of anti-static flooring systems. The research has provided valuable insights into developing cementitious composites with electrostatic discharge capability.

Within the scope of the doctoral thesis, the aim is to develop a new-generation high-performance anti-static protection capability of cementitious composites that can exhibit different performance characteristics simultaneously. These composites are intended to have long-term electrical conductivity performance independent of ambient temperature, humidity conditions, and the hydration level of the cementitious binder system. The composites possess early and long-term high/normal strength properties, high flowability, resistance to harmful solutions, crack-free surfaces, and cost-effectiveness compared to composite designs used for the same purpose and a thickness of 1 cm.

The development of the composite consisted of two main stages. The first stage included the development of a cementitious binder matrix with early and final-age high strength, high workability and flowability, and crack-free surfaces. In this context, different combinations of Portland cement, calcium aluminate cement, and calcium sulfate source with mineral and chemical additives were used to develop early-age high-strength mixtures. The second part included the development of cementitious mixtures with early and long-term anti-static protection capability by incorporating different types of conductors into the main matrix and determining composite performances under various environmental conditions. In this context, different combinations of carbon fiber, milled carbon fiber, and steel fiber were used to develop the anti-static capability of mixtures in the early and long term. Then, the performance properties of the mixtures showing the highest electrical conductivity performance with the lowest conductor content were tested under different moisture and temperature conditions. The early and long-term acid resistance was evaluated in the final stage according to performance characteristics.

Empirical test methods were used to determine the physical, mechanical, and electrical properties of the mixtures. The rheological assessment was conducted using the flow table method. Mechanical assessments in the early and long term were carried out through the compressive strength test. Electrical conductivity was evaluated using the electrical resistance test in both the early and long term. Additionally, the microstructure of the structures formed in the matrix and the dispersion of conductive materials were assessed through microstructure testing.

In the first stage of this study, a cementitious mixture was developed to which conductive materials would be added. The following conclusions had been drawn from the experimental works performed on the cementitious pastes within the scope of the first stage of this thesis study:

- The early age of the high strength of the cementitious composites was achieved in four stages. Initially, the workability and flowability performance of the mixtures were assessed using only early age high-strength Portland cement, without the addition of chemical and mineral additives. In this first stage, the mixture with a water-to-cement ratio of 0.35 and a sand-to-cement ratio of 0.6 exhibited the highest 6-hour compressive strength, measured at 26.10 MPa.

- Early age high-strength Portland Cement was replaced with different rates of Calcium Aluminate Cement from various suppliers in specific proportions. Ternary system mixtures were then obtained by adding calcium sulfate at different rates to prevent sudden setting. Among all types of CAC, the highest compressive strength at 3 and 6 hours was achieved using Secar 51 (with 51% Al_2O_3). Specifically, in the ternary combination of 40% PC, 60% CAC, and 0.20 CŚ ratio, the compressive strengths were determined to be 44.00 MPa and 55.00 MPa, respectively. Considering the economic cost criterion for the coating design to compete with other designs, it had been determined that the most suitable CAC type was Isıdaç 40 (40% Al_2O_3). The highest compressive strength for 3 and 6

hours was determined to be 20.90 and 28.17 MPa in the ternary combination of 60% PC, 40% CAC, and 0.15 CŚ ratio.

- In the second stage of the experimental study, silica fume was added to the system at different rates based on the proportion of the ternary system. While similar results were obtained at 2 and 3-hour strengths between 0.5-2.0% silica fume ratios, the compressive strength decreased by approximately 25% beyond 2.0% silica fume content. Based on the results, the 2 and 3-hour highest compressive strength was obtained as 26.87 and 27.57 MPa from the mixture containing 0.5% silica fume addition.

- In the third stage of the experimental study, various chemical additives were added to the system at different rates to improve the matrix performance. Among the chemical additives, the high-range water range-reducing agent improved the workability and flowability of the matrix the most. Among the HRWRA types supplied by different companies, the workability performance of ternary systems was improved the most by EBA 1047 type HRWRA obtained from BASF company. Using the setting accelerator and setting retarder effectively improved the matrix's early age and high strength. Based on the compressive strength results and workability behavior, the best performance was achieved, with 2 and 3-hour compressive strengths of 29.00 MPa and 29.95 MPa, respectively, in the sample using 2.5% silica fume and 2.0% HRWRA, 0.2% SRA, and 0.5% SA by the weight of cement (PC+CAC).

- In the fourth stage of the experimental study, the mixing time and mixing process of ingredients were determined. It had been observed that the process stages of chemical additives were added to the mixture, and the mixing time significantly affected the flowability and caused noticeable changes in compressive strength. Based on the results, the flow diameter was measured as 41.5 cm, and the slump flow time was measured as 3.75 seconds in the final main mixture. In terms of mechanical performance at the early age, no strength could be measured at 1 hour, the 2-hour compressive strength was measured as 32.73 MPa for 2 hours, 36.90 MPa for one day, and 86.10 MPa for 90^{th} day in the final main mixture.

In the second stage of this thesis study, conductive materials were added to the cementitious main matrix individually, in double, and in triple combinations. The aim was to develop a composite that could resist various environmental conditions and exposure to harmful solutions while maintaining low conductivity and anti-static protection. This approach also aimed to ensure the economic viability of the composite compared to similar designs. The following conclusions had been drawn from the experimental works performed on single conductors incorporated into cementitious composites within the scope of the second stage of this thesis study:

- The ER value of the reference mixture measured from the coating sample was measured as 15.4 MΩ on the first day and 104.5 MΩ at the end of 180 days. ER values of the reference mixture measured from the cylindrical sample were measured as 1.60 kΩ on the first day and 773 kΩ at the end of 180 days. The reference mixture showed insulating properties without containing conductive materials.

- The best flow diameter was 44.75 cm for the A10(1) mixture. Adding MCF and CF to the reference mixture negatively affected the fluidity, while adding SF had a positive effect.

- Regardless of the conductive material type, ER results followed a decreasing trend with adding CF, MCF, and SF content to the mixtures. However, the continuous hydration reaction increased the ER values of all mixtures measured from both coating and cylinder samples. In terms of conductivity performance, the lowest ER values were measured from carbon fiber, milled carbon fiber, and steel fiber-based mixtures, respectively. In that order, the electrical conductivity performance was primarily influenced by the admixing method, conductor type, and conductor content.

- The lowest 180-day ER result among coating samples was measured as 200.5 Ω from the B6(2) sample prepared with the latter admixing method. Among cylindrical samples, the lowest 180-day ER result was obtained as 202 Ω from the B10(2) sample prepared with the latter admixing method.

- Similar levels of ER were measured from the cylinder parts of the samples where the conductors were dispersed homogeneously, and electrical conductivity was achieved. While there was a significant difference in ER values between the cylindrical parts of the samples where the conductors were not dispersed homogeneously, the highest ER values were measured from the top cylindrical part. It was determined by SEM analysis that the fibers in the mixtures showing high conductivity performance in microstructure analysis were homogeneously distributed in the matrix and were compatible with ER results.

- The most effective mixing method for the best homogeneous dispersion of conductive materials was the latter admixing method for the CF- and SF-based composites and the first admixing method for the MCF-based composites.

The conductor ratios showing the highest electrical conductivity were determined, and the conductors were added to the matrix as carbon fiber-steel fiber, carbon fiber-milled carbon fiber, and carbon fiber-steel fiber. The following conclusions had been drawn from the experimental works performed on double conductors incorporated into cementitious composites within the scope of the second stage of this thesis study:

- The mixtures' flow diameter and flow times were negatively affected by a higher content of carbon-based fibers in the matrix regardless of the mixing method and the higher content of steel fibers added by the latter method. However, steel fibers were positively affected by the increasing content when added by the synchronous method. The increase of the milled carbon fiber content at the same conductor content had a more negative effect on the fluidity of the mixtures.

- Except for the admixing method of fibers, the higher content of both conductive materials and the double addition of conductors in the mixture improved compressive strength at all ages. Different admixing methods had a slight difference in the compressive strength performance of mixtures. Incorporating carbon fiber with the latter admixing method, the incorporation of milled carbon fiber with the first admixing method, and the incorporation of steel fiber with the latter admixing method had more positive effects on strength than other methods.

- Regardless of the mixing method, long-term electrical conductivity values were below 100 kΩ, which had the highest performance limit, achieved in all mixtures by increasing the amount of carbon fiber in the double additions. The combination of milled carbon fiber and steel fiber was ineffective in obtaining electrical conductivity performance. Among coating and cylindrical samples, the lowest 180-day ER result was measured from the combination of carbon fiber and milled carbon fiber. It was observed that carbon fibers can form conductive networks even at a 0.2% ratio. In addition, the increased amount of milled carbon fibers helped the conductive network expand, and the transmission of electrostatic discharge became more efficient.

- Among the cylindrical and coating samples to which conductors were double incorporated, the incorporation of carbon fiber with the latter admixing method, the incorporation of milled carbon fiber with the first admixing method, and the incorporation of steel fiber with the latter admixing method had a more positive effect on the electrical conductivity performance than the other methods. Based on ER values of cylindrical layers and microstructural analysis, carbon fiber and milled carbon fibers were dispersed homogeneously in the matrix.

To ensure the economic productivity of the matrix, conductors were incorporated into the triple mixture, considering the lowest conductor content and selecting the appropriate mixing method to maintain the flowability of the matrix. The following conclusions had been drawn from the experimental works performed on triple conductors incorporated into cementitious composites within the scope of the second stage of this thesis study:

- Compared to the reference mixture, the workability of all mixtures was negatively affected by conductive usage. While carbon and milled carbon fiber decreased flowability, adding steel fiber using the synchronous admixing method caused increased flowability.

- All triple conductors-based mixtures had a higher than 40 MPa value on the first day. Compressive strengths of triple conductor additions were positively affected by increasing the carbon and milled carbon fiber content in the mixtures while increasing the steel fiber content had a slightly negative effect.

- With 0.8% carbon fiber addition in the mixture, ER values remained below 100 kΩ in the long term. Among coating and cylindrical samples, the lowest value was measured from the BAC1022(1) mixture according to the 180-day ER results of the mixtures. From microstructure analysis, it was determined that the conductors were dispersed homogeneously.

Among the mixtures with single, double, and triple conductor incorporations, ten samples with the best electrical conductivity performance were identified, and these samples were tested under humidity and temperature conditions. The following conclusions had been drawn from the experimental works performed to determine environmental effects on selected cementitious composites within the scope of the second stage of this thesis study:

- It had been determined that the electrical resistance (ER) values of all selected samples, in which electrical conductivity was achieved, did not change significantly under laboratory, humidity, and temperature conditions, thus maintaining their conductivity behavior. Among the environmental conditions, the most negatively affected the ER values was keeping samples under 100% RH condition.

- In terms of economic considerations, the mixtures with the lowest conductive content were selected for the acid resistance test: B6(2) sample for single addition of carbon fiber, AB28(1) sample for double addition of carbon fiber-steel fiber, CB26(1) sample for double addition of carbon fiber-milled carbon fiber, and BAC1022(1) sample for triple addition.

In the final stage, the mixtures with the lowest conductor ratio among single, double, and triple conductor incorporations were selected, and the effects on the performance immersed in the sulfuric acid solution in the short and long term were determined. Sulfuric acid testing was also applied to the reference and PC-based mixture, except for the conductor addition. The following conclusions had been drawn from the experimental works performed to determine acid resistance on selected cementitious composites within the scope of the second stage of this thesis study:

The reduction in compressive strength was measured between 2.76 – 6.78% from conductor-based mixtures after 21 days of acid solution. The sulfuric acid solution most affected the PC-based mixture, with a 21.48% reduction after the acid test. Among the mixtures, the lowest strength loss was measured in the CB26(1) sample, while the highest was in the reference sample.

- Although the ER values of the samples increased, the electrical conductivity behavior of conductor-based mixtures was preserved at the end of the 90^{th}-day immersion in sulfuric acid solution. Except for the conductor-based mixtures, ER values of reference and PC samples immersed in the acid solution, which were at the MΩ level before the acid test, increased continuously at the GΩ level during the acid time.

- After 90 days of sulfuric acid immersion, coloring, size reduction, and surface degradation were detected in all mixtures. However, the curing age at which the mixtures were exposed to acid solution affected the acid resistance of the coating samples. 180-day mixtures showed higher sulfuric acid resistance compared to 7-day mixtures. No deterioration, damage, or color change was observed after exposure to acid attack after the 180-day curing period of the same sample.

- Considering the surface appearance of conductor-based mixtures, the B6(2) sample was most affected in early and long terms. It was observed that fibers rise to the surface with the effect of sulfuric acid solution and clump at certain points

during the cleaning of the coatings. Microstructural analysis showed numerous fiber dispersions on the matrix surface.

- According to the performance characteristics of the mixtures with the best electrical conductivity performance at the lowest fiber ratio under sulfuric acid solution, the best result was obtained from the BAC1022(1) sample.

A cementitious composite had been developed that was suitable for use in solving the ESD problem in floor applications of critical structures. It had superior performance properties and economical anti-static protection compared to the coating designs currently used in the sector.

6. FUTURE STUDIES

Based on the results of the thesis study, additional research can be conducted on the following topics:

Transitioning to mass production and commercializing the composite tested in the laboratory for flooring systems in critical structures

Improving the surface appearance of the cementitious composite and achieving a smooth surface

REFERENCE

[1] S.H. Voldman, A Review of Electrostatic Discharge (ESD) in Advanced Semiconductor Technology, Microelectronics Reliability, 44 (**2004**) 33–46. https://doi.org/10.1016/j.microrel.2003.10.004.

[2] W. Boxleitner, How to Defeat Electrostatic Discharge, IEEE Spectrum, 26 (**1989**) 36–40. https://doi.org/10.1109/6.30778.

[3] C. Diaz, S.M. Kang, C. Duvvury, Tutorial Electrical Overstress and Electrostatic Discharge, IEEE Transactions on Reliability, 44 (**1995**) 2–5.

[4] B.A. Unger, Electrostatic Discharge Failures of Semiconductor Devices, in: 19th International Reliability Physics Symposium, IEEE, Las Vegas, NV, USA, **1981**: pp. 193–200. https://doi.org/10.1109/IRPS.1981.362995.

[5] S.H. Voldman, The State of the Art of Electrostatic Discharge Protection: Physics, Technology, Circuits, Design, Simulation, and Scaling, IEEE Journal of Solid-State Circuits, 34 (**1999**) 1272–1282.

[6] T. Diep, R. Cline, Application Report Electrostatic Discharge (ESD), Texas Instruments. https://www.ti.com/lit/an/ssya010a/ssya010a.pdf?ts=1723188301801 (accessed **August 9, 2024**).

[7] M.A. Kelly, G.E. Servais, T. V. Pfaffenbach, An Investigation of Human Body Electrostatic Discharge, in: The 19th International Symposium for Testing & Failure Analysis, Los Angeles, **1993**: pp. 167–173.

[8] W.D. Greason, Electrostatic Discharge Characteristics for The Human Body and Circuit Packs, Journal of Electrostatics, 59 (**2003**) 285–300. https://doi.org/10.1016/S0304-3886(03)00090-1.

[9] Hong Tian, J.J.K. Lee, Electrostatic Discharge Damage of MR Heads, IEEE Transactions on Magnetics, 31 (**1995**) 2624–2626. https://doi.org/10.1109/20.490073.

[10] R.N. Fisher, Static Control Measures-ESD Control Handbook, http://solutions.3m.com/3MContentRetrievalAPI/BlobServlet?locale=en_US&lmd=1154017253000&assetId=1114279231283&assetType=MMM_Image&blobAttribute=ImageFile (accessed **August 9, 2024**).

[11] M.B. Talawar, A.P. Agrawal, M. Anniyappan, D.S. Wani, M.K. Bansode, G.M. Gore, Primary Explosives: Electrostatic Discharge Initiation, Additive Effect and Its Relation to Thermal and Explosive Characteristics, Journal of Hazardous Materials, 137 (**2006**) 1074–1078. https://doi.org/10.1016/j.jhazmat.2006.03.043.

[12] K. Gotlib-Vainstein, I. Gouzman, O. Girshevitz, A. Bolker, N. Atar, E. Grossman, C.N. Sukenik, Liquid Phase Deposition of a Space-Durable, Antistatic SnO_2 Coating on Kapton, ACS Applied Materials and Interfaces, 7 (**2015**) 3539–3546. https://doi.org/10.1021/am5072817.

[13] H. Kumral, Kimyasallarla Çalışmalarda Statik Elektrik Tehlikeleri ve Korunma Yöntemleri, IKMIB - Istanbul Chemicals and Chemical Products Exporters' Association, https://www.ikmib.org.tr/files/images/muhtelif6/Kimyasallarla%20%C3%87al%C4%B1%C5%9Fmalarda%20Statik%20Elektrik%20Tehlikeleri%20ve%20%C3%96nlemler.pdf. (accessed **August 4, 2024**).

[14] J. Markarian, New Developments in Antistatic and Conductive Additives, Plastics, Additives and Compounding, 10 (**2008**) 22–25. https://doi.org/https://doi.org/10.1016/S1464-391X(08)70172-7.

[15] P. Şengün, Synthesis of Designed Al-and Ga-Doped Zinc Oxide (ZnO) Particles and Their Application for Antistatic Coatings, Master of Science, Graduate School of Sciences of Eskişehir Technical University, **2018**.

[16] A., Stokki, R. Karlsson, Electrically Conductive Floor Coverings, U.S. 7,811,476. https://patents.google.com/patent/US7811476B2/en?oq=US+7%2C811%2C476+ (accessed **August 9, 2024**).

[17] B., Ramme, J., Noegel, R., Setchell, R. Bischke, Electrically Conductive Concrete and Controlled Low-Strength Materials, U.S. 20020162484A1. https://patents.google.com/patent/US20020162484A1/en?oq=US2002%2F0162484+A1+ (accessed **August 9, 2024**).

[18] G.B., Pye, R.E., Myers, M.R., Arnott, J.J., Beaudoin, P.J. Tumidajski, Conductive Concrete Composition, U.S. 6503318B2. https://patents.google.com/patent/US6503318B2/en?oq=US+6%2C503%2C318++ (accessed **August 9, 2024**).

[19] ANSI/ESD S6.1, The Protection of Electrostatic Discharge Susceptible Items - Grounding, American National Standards Institute, **2019**.

[20] NFPA 99, Care Center of Patients with Risks of Fire, Explosion, and Electricity, National Fire Protection Association, **2015**.

[21] FAA-STD-019f, Lighting and Surge Protection, Grounding, Bonding, and Shielding Requirements for Facilities and Electronic Equipment, Federal Aviation Administration, **2017**.

[22] ASTM F150-06, Electrical Resistance of Conductive and Static Dissipative Resilient Flooring, American Society for Testing Materials, **2018**.

[23] Makina ve Kimya Endüstrisi Kurumu, Makina ve Kimya Endüstrisi Kurumu İş Sağlığı ve Güvenliği Yönergesi, Ankara, **2002**.

[24] Y. Chang, J. Liang, Study on the Preparation and the Construction Technology of Anti-Static and Anti-Corrosion Self-Levelling Floor Coating, Advanced Materials Research, 168-170 (**2011**) 981–984. https://doi.org/10.4028/www.scientific.net/AMR.168-170.981.

[25] D.D.L. Chung, Composite Materials, Second Edition, Springer, London, **2010**. https://doi.org/10.1007/978-1-84882-831-5.

[26] W.D. Greason, G.S.P. Castle, The Effects of Electrostatic Discharge on Microelectronic Devices: A Review, IEEE Transactions on Industry Applications, 20 (**1984**) 247–252.

[27] A. Karlsson, R., Stokki, Electrically Conductive Floor Coverings, 1544258A1. https://patents.google.com/patent/EP1544258A1/en (accessed **August 9, 2024**).

[28] B. Ramme, Electrically Conductive Concrete and Controlled Low Strength Materials Having Spent Carbon Sorbent, U.S. 20070240620A1. https://patents.google.com/patent/US20070240620A1/en?oq=US+2007%2F0240620+A1+ (accessed **August 9, 2024**).

[29] C.Y. Lee, S.R. Wang, Application of Four-Electrode Method to Analysis Resistance Characteristics of Conductive Concrete, World Academy of Science, Engineering and Technology, 72 (**2010**) 101–105. https://doi.org/10.5281/zenodo.1076782.

[30] H. Wang, J. Yang, H. Liao, X. Chen, Electrical and Mechanical Properties of Asphalt Concrete Containing Conductive Fibers and Fillers, Construction and Building Materials, 122 (**2016**) 184–190. https://doi.org/10.1016/j.conbuildmat.2016.06.063.

[31] P.K., Mehta, P.J.M. Monteiro, Concrete Microstructure, Properties, and Materials, Third Edition, The McGraw-Hill Company, Berkeley, **2006**. https://doi.org/10.1036/0071462899.

[32] S. Griffiths, B.K. Sovacool, D.D. Furszyfer Del Rio, A.M. Foley, M.D. Bazilian, J. Kim, J.M. Uratani, Decarbonizing the Cement and Concrete Industry: A Systematic Review of Socio-Technical Systems, Technological Innovations, and Policy Options, Renewable and Sustainable Energy Reviews, 180 (**2023**). https://doi.org/10.1016/j.rser.2023.113291.

[33] M.G. Alexander, K. Stanish, Durability Design and Specification of Reinforced Concrete Structures Using a Multi-Factored Approach, in: Third International Conference on Construction Materials: Performance, Innovations and Structural Implications and Mindess Symposium, University of British Columbia, Vancouver, **2005**.

[34] P.K. Mehta, R.W. Burrows, Building Durable Structures in the 21st Century, Concrete International, 23 (**2001**) 57–63.

[35] N. Koçu, M. Dereli, Yapı Cephelerini Görsel Yönden Olumsuz Olarak Etkileyen Sorunlar ve Nedenlerin Analizi, IV. Ulusal Çatı&Cephe Kaplamalarında Çağdaş Malzeme ve Teknolojiler Sempozyumu, https://www.cativecephe.com/yayin/643/yapi-cephelerini-gorsel-yonden-olumsuz-olarak-etkileyen-sorunlar-ve-nedenlerin-analizi_18972.html. (accessed **August 4, 2024**).

[36] F. Dehn, Concrete Repair According to the New European Standard, in: Measuring, Monitoring and Modeling Concrete Properties, Springer, Dordrecht, **2006**: pp. 619–624. https://doi.org/10.1007/978-1-4020-5104-3_75.

[37] S. Trost, Using Maturity Testing for Airfield Concrete Pavement Construction and Repair, Innovative Pavement Research Foundation, Skokie, **2006**.

[38] F. Parker, W. Lee Shoemaker, PCC Pavement Patching Materials and Procedures, Journal of Materials in Civil Engineering, 3 (**1991**) 29–47. https://doi.org/10.1061/(ASCE)0899-1561(1991)3:1(29).

[39] P. Zia, M.L. Leming, S.H. Ahmad, SHRP-C/FR-91-103: High Performance Concretes, a State-of-the-Art Report, National Search Council Strategic Highway Research, Washington, https://ntrl.ntis.gov/NTRL/dashboard/searchResults/titleDetail/PB92130087.xhtml (accessed **August 4, 2024**).

[40] S., Kurtz, P., Blaguru, G., Consolazio, A. Maher, FHWA 2001-015: Fast Track Concrete for Construction Repair, Center for Advanced Infrastructure & Transportation, Trenton, New Jersey. https://cait.rutgers.edu/wp-content/uploads/2018/05/fhwa-nj-2001-015.pdf (accessed **August 4, 2024**).

[41] Federal Highway Administration (FHWA), Manual of Practice: Materials and Procedures for Rapid Repair of Partial-Depth Spalls in Concrete Pavements, United States Department of Transportation. https://highways.dot.gov/research/publications/infrastructure/FHWA-RD-99-152 (accessed **August 4, 2024**).

[42] J. Warner, J. Trout, Paving Repair Finds a Four-Hour Champion, Concrete Construction Magazine, 46 (**2001**) 69–70. https://www.concreteconstruction.net/how-to/materials/paving-repair-finds-a-four-hour-champion_o (accessed **August 4, 2024**).

[43] Michigan Department of Transportation (MDOT), Qualification Procedure for Prepackaged Hydraulic Fast-Set Materials for Patching Structural Concrete, MDOT Quality Assurance and Quality Control, **2003**.

[44] E. Larmie, Rehabilitation and Maintenance of Road Pavements Using High Early Strength Concrete, Master of Science, Faculty of the Graduate School of the University of Maryland, **2005**.

[45] S. Arslan, Applicability of Cold Mix Asphalt in Rapid Runway Repair, Master of Science, The Graduate School of Natural and Applied Sciences of Dokuz Eylül University, **2005**.

[46] M. Şahmaran, M. Al-Emam, G. Yıldırım, Y.E. Şimşek, T.K. Erdem, M. Lachemi, High-Early-Strength Ductile Cementitious Composites with Characteristics of Low Early-Age Shrinkage for Repair of Infrastructures, Materials and Structures, 48 (**2015**) 1389–1403. https://doi.org/10.1617/s11527-013-0241-z.

[47] A.K. Yasin, R. Bayuaji, T.E. Susanto, A Review in High Early Strength Concrete and Local Materials Potential, in: IOP Conference Series: Materials Science and Engineering, Institute of Physics Publishing, **2017**. https://doi.org/10.1088/1757-899X/267/1/012004.

[48] TS EN 14647, Calcium Aluminate Cement - Composition, Specifications and Conformity Criteria, Türk Standartları Enstitüsü, **2008**.

[49] G.J. Snelus, T. Gibb, J.C. Swann, H. Smith, W. Whamond, Limestone-Bauxite Cement, British Patent 10312, **1888**.

[50] J. Bied, Recherches Industrielles sur les Chaux, Ciments et Mortiers, Dunod, Paris, **1926**.

[51] J. Bied, Aluminous Cement, British Patent 8193, **1909**.

[52] H.S. Spackman, E.W. Lazell, Cementitious Material, US903020A. https://patents.google.com/patent/US903020A/en?oq=US903020A (accessed **August 9, 2024**).

[53] P. Barnes, J. Bensted, Structure and Performance of Cements, Second Edition, CRC Press, **2002**. https://doi.org/10.1201/9781482295016.

[54] A.M. Neville, J.J. Brooks, Concrete Technology, Second Edition, Prentice Hall, Canada, **2010**.

[55] P.C. Hewlett, Lea's Chemistry of Cement and Concrete, Fourth Edition, Elsevier, Oxford, **2006**.

[56] K.L. Scrivener, A. Capmas, Calcium Aluminate Cements, in: P.C. Hewlett (Ed.), Lea's Chemistry of Cement and Concrete, Fourth Edition, Elsevier, **1998**. https://doi.org/10.1016/B978-0-7506-6256-7.X5007-3.

[57] J. Bizzozero, K.L. Scrivener, Limestone Reaction in Calcium Aluminate Cement-Calcium Sulfate Systems, Cement and Concrete Research, 76 (**2015**) 159–169. https://doi.org/10.1016/j.cemconres.2015.05.019.

[58] Ö. Kırca, Temperature Effect on Calcium Aluminate Cement Based Composite Binders, Doctor of Philosophy, The Graduate School of Natural and Applied Sciences of Middle East Technical University, **2006**.

[59] J.H. Ideker, K.L. Scrivener, H. Fryda, B. Touzo, Calcium Aluminate Cements, in: Lea's Chemistry of Cement and Concrete, Fifth Edition, Elsevier, **2019**: pp. 537–584. https://doi.org/10.1016/B978-0-08-100773-0.00012-5.

[60] E. Adesanya, A. Ezu, H. Nguyen, C. Rößler, H. Sreenivasan, K. Ohenoja, P. Kinnunen, M. Illikainen, Hydration of Blended Ladle Slag and Calcium Aluminate Cement, Journal of Building Engineering, 66 (**2023**) 105855. https://doi.org/10.1016/j.jobe.2023.105855.

[61] A.F. Bentivegna, Multi-Scale Characterization, Implementation, and Monitoring of Calcium Aluminate Cement Based-Systems, Doctor of Philosophy, Faculty of the Graduate School of The University of Texas at Austin, **2012**.

[62] Çimsa Company, Isıdaç 40, Technical Data Sheet. https://cimsa.com.tr/urun/aluminates-isidac-40/ (accessed **August 4, 2024**).

[63] S.M. Bushnell-Watson, J.H. Sharp, The Application of Thermal Analysis to The Hydration and Conversión Reactions of Calcium Alumínate Cements, Materiales de Construcción, 42 (**1992**) 13–32. https://doi.org/10.3989/mc.1992.v42.i228.694.

[64] A.J. Majumdar, R.N. Edmonds, B. Singh, Hydration of Secar 71 Aluminous Cement in Presence of Granulated Blast Furnace Slag, Cement and Concrete Research, 20 (**1990**) 7–14. https://doi.org/10.1016/0008-8846(90)90111-A.

[65] N. Ukrainczyk, T. Matusinović, Thermal Properties of Hydrating Calcium Aluminate Cement Pastes, Cement and Concrete Research, 40 (**2010**) 128–136. https://doi.org/10.1016/j.cemconres.2009.09.005.

[66] J.P. Gevaudan, J. Osio-Norgaard, W. V Srubar, Alternative Cements: Recent Developments and Future Directions, in: Proceedings of the Architectural Engineering Conference, American Society of Civil Engineers, Tysons, Virginia, **2019**: pp. 294–308.

[67] H.M. Son, S. Park, H.Y. Kim, J.H. Seo, H.K. Lee, Effect of $CaSO_4$ on Hydration and Phase Conversion of Calcium Aluminate Cement, Construction and Building Materials, 224 (**2019**) 40–47. https://doi.org/10.1016/j.conbuildmat.2019.07.004.

[68] S. Lamberet, Durability of Ternary Binders Based on Portland Cement, Calcium Aluminate Cement and Calcium Sulfate, Docteur es Sciences, Institut des Matériaux, Université de Lyon, **2005**.

[69] N.C. Collier, Transition and Decomposition Temperatures of Cement Phases - A Collection of Thermal Analysis Data, Ceramics – Silikaty, 60 (**2016**) 338–343. https://doi.org/10.13168/cs.2016.0050.

[70] V.S. Ramachandran, R.M. Paroli, J.J. Beaudoin, A.H. Delgado, Handbook of Thermal Analysis of Construction Materials, First Edition, Noyes Publications, New York, **2002**.

[71] P. Gu, J.J. Beaudoin, E.G. Quinn, R.E. Myers, Early Strength Development and Hydration of Ordinary Portland Cement/Calcium Aluminate Cement Pastes, Advanced Cement Based Materials, 6 (**1997)** 53-58. https://doi.org/10.1016/S1065-7355(97)00008-4.

[72] L. Amathieu, T.A. Bier, K.L. Scrivener, Mechanisms of Set Acceleration of Portland Cement Through CAC Addition, in: R.J. Mangabhai, F.P. Glasser (Eds.), Proceedings of the International Conference on Calcium Aluminate Cements (CAC), IOM Communications, Edinburgh, **2001**: p. 21.

[73] Sorrentino F., Crystallization of Cao–Al_2O_3–Fe_2O_3–SiO_2 Melts and the Phase Composition of High Alumina Cement, Doctor of Phisolophy, University of Aberdeen, **1973**.

[74] F. Paulik, J. Paulik, M. Arnold, Thermal Decomposition of Gypsum, Thermochimica Acta, 200 (**1992**) 195–204. https://doi.org/10.1016/0040-6031(92)85115-C.

[75] H. Minard, S. Garrault, L. Regnaud, A. Nonat, Mechanisms and Parameters Controlling the Tricalcium Aluminate Reactivity in The Presence of Gypsum, Cement and Concrete Research, 37 (**2007**) 1418–1426. https://doi.org/10.1016/j.cemconres.2007.06.001.

[76] D. Torréns-Martín, L. Fernández-Carrasco, M.T. Blanco-Varela, Conduction Calorimetric Studies of Ternary Binders Based on Portland Cement, Calcium Aluminate Cement and Calcium Sulphate, Journal of Thermal Analysis and Calorimetry, 114 (**2013**) 799–807. https://doi.org/10.1007/s10973-013-3003-9.

[77] D.L. Hudson-Lamb, C.A. Strydom, J.H. Potgieter, The Thermal Dehydration of Natural Gypsum and Pure Calcium Sulphate Dihydrate (Gypsum), Thermochimica Acta, 282–283 (**1996**) 483–492. https://doi.org/10.1016/0040-6031(95)02819-6.

[78] N. Ukrainczyk, M. Ukrainczyk, J. Sipusic, T. Matusinovic, XRD and TGA Investigation of Hardened Cement Paste, 11th Conference on Materials, Processes, Friction and Wear MATRIB'06, Vela Luka (**2006**) 22–24.

[79] R. Trauchessec, J.M. Mechling, A. Lecomte, A. Roux, B. Le Rolland, Impact of Anhydrite Proportion in A Calcium Sulfoaluminate Cement and Portland Cement Blend, Advances in Cement Research, 26 (**2014**) 325–333. https://doi.org/10.1680/adcr.13.00051.

[80] G. Tzouvalas, N. Dermatas, S. Tsimas, Alternative Calcium Sulfate-Bearing Materials as Cement Retarders: Part I. Anhydrite, Cement and Concrete Research, 34 (**2004**) 2113–2118. https://doi.org/10.1016/j.cemconres.2004.03.020.

[81] L. Xu, P. Wang, G. Zhang, Calorimetric Study on the Influence of Calcium Sulfate on the Hydration of Portland Cement-Calcium Aluminate Cement Mixtures, Journal of Thermal Analysis and Calorimetry, 110 (**2012**) 725–731. https://doi.org/10.1007/s10973-011-1920-z.

[82] S.K. Kuthadi, Laboratory Scale Study of Calcium Sulfate Hydration Forms, Master of Science, The Faculty of the Department of Chemistry Western Kentucky University, **2014**. http://digitalcommons.wku.edu/theses/1467.

[83] S. Zhang, X. Xu, S.A. Memon, Z. Dong, D. Li, H. Cui, Effect of Calcium Sulfate Type and Dosage on Properties of Calcium Aluminate Cement-Based Self-Leveling Mortar, Construction and Building Materials, 167 (**2018**) 253–262. https://doi.org/10.1016/j.conbuildmat.2018.01.146.

[84] C. Evju, S. Hansen, Expansive Properties of Ettringite in A Mixture of Calcium Aluminate Cement, Portland Cement and B-Calcium Sulfate Hemihydrate, Cement and Concrete Research, 31 (**2001**) 257–261. https://doi.org/10.1016/S0008-8846(00)00495-6.

[85] C. Evju, S. Hansen, The Kinetics of Ettringite Formation and Dilatation in A Blended Cement with β-Hemihydrate and Anhydrite as Calcium Sulfate, Cement and Concrete Research, 35 (**2005**) 2310–2321. https://doi.org/10.1016/j.cemconres.2004.09.012.

[86] G.C. Sang, J.P. Liu, Study of Properties of Portland and Aluminate Cementitious Composited Grouting Material, Materials Research Innovations, 14 (**2010**) 200–205. https://doi.org/10.1179/143307510X12719005364387.

[87] I. Martin, C. Patapy, M. Cyr, Impact of Calcium Sulfate Type and Additions on Hydration and Properties of Ettringite-Based Systems, in: The 14th International Congress on the Chemistry of Cement, Beijing, **2015**: pp. 18–21.

[88] E. Qoku, T.A. Bier, G. Schmidt, J. Skibsted, Impact of Sulphate Source on the Hydration of Ternary Pastes of Portland Cement, Calcium Aluminate Cement and Calcium Sulphate, Cement and Concrete Composites, 131 (**2022**). https://doi.org/10.1016/j.cemconcomp.2022.104502.

[89] A. Puri, G. Voicu, A. Badanoiu, Expansive Binders in the Portland Cement - Calcium Aluminate Cement - Calcium Sulfate System, Revista de Chimie, 61 (**2010**) 740–744.

[90] L. Fernández-Carrasco, E. Vázquez, Reactions of Fly Ash with Calcium Aluminate Cement and Calcium Sulphate, Fuel, 88 (**2009**) 1533–1538. https://doi.org/10.1016/j.fuel.2009.02.018.

[91] M. Idrees, O. Ekincioglu, M.S. Sonyal, Hydration Behavior of Calcium Aluminate Cement Mortars with Mineral Admixtures at Different Curing Temperatures, Construction and Building Materials, 285 (**2021**). https://doi.org/10.1016/j.conbuildmat.2021.122839.

[92] G. Li, W. Wang, G. Zhang, Effects of Slag on the Degradation Mechanism of Ordinary Portland Cement-Calcium Aluminate Cement-Gypsum Ternary Binder Under the Multiple Erosive Ions, Construction and Building Materials, 324 (**2022**). https://doi.org/10.1016/j.conbuildmat.2022.126661.

[93] Y. Liao, S. Wang, K. Wang, S. Al Qunaynah, S. Wan, Z. Yuan, P. Xu, S. Tang, A Study on the Hydration of Calcium Aluminate Cement Pastes Containing Silica Fume Using Non-Contact Electrical Resistivity Measurement, Journal of Materials Research and Technology, 24 (**2023**) 8135–8149. https://doi.org/10.1016/j.jmrt.2023.05.080.

[94] V. Mallikarjuna Reddy, M. Seshagiri Rao, P. Srilakshmi., B. Sateesh Kumar., Effect of w/c Ratio on Workability and Mechanical Properties of High Strength Self Compacting Concrete, International Journal of Engineering Research and Development, 7 (**2013**) 06–13.

[95] S. Aggoun, M. Cheikh-Zouaoui, N. Chikh, R. Duval, Effect of Some Admixtures on the Setting Time and Strength Evolution of Cement Pastes at Early Ages, Construction and Building Materials, 22 (**2008**) 106–110. https://doi.org/10.1016/j.conbuildmat.2006.05.043.

[96] S. Alsadey, Effects of Super Plasticizing and Retarding Admixtures on Properties of Concrete, in: International Conference on Innovations in Engineering and Technology (ICIET'2013), Bangkok, **2013**: pp. 271–274. https://doi.org/http://dx.doi.org/10.15242/IIE.E1213607.

[97] A.R. Saglam, N. Parlak, M.H. Özkul, Polikarboksilat Esaslı Kimyasal Katkıların Beton Üretiminde Kullanımı, in: 2. Yapılarda Kimyasal Katkılar Sempozyumu, TMMOB İnşaat Mühendisleri Odası, Ankara, **2007**: pp. 107–120.

[98] M. Niziurska, J. Małolepszy, G. Malata, The Influence of Lithium Carbonate on Phase Composition of Calcium Aluminate Cement Paste, Procedia Engineering, 108 (**2015**) 363–370. https://doi.org/10.1016/j.proeng.2015.06.159.

[99] E. Gödek, B. Felekoğlu, K. Tosun Felekoğlu, Polycarboxylate-Based Superplasticizer Selection for Ready-Mixed Concrete Industry and Performance in Self-Compacting Concrete Production, Afyon Kocatepe University Journal of Sciences and Engineering, 15 (**2015**) 8–18. https://doi.org/10.5578/fmbd.9448.

[100] İ., Demir, Ö. Sevim, Effect of Sulfate on Cement Mortars Containing Li_2SO_4, $LiNO_3$, Li_2CO_3 and LiBr, Construction and Building Materials, 156 (**2017**) 46–55. https://doi.org/10.1016/j.conbuildmat.2017.08.148.

[101] X. Li, J. Hao, New Preparation of Super-Early-Strength Grouting Materials by Ternary Complex System, Advances in Cement Research, 30 (**2018**) 139–147. https://doi.org/10.1680/jadcr.17.00077.

[102] J. Zhang, D. Cai, Study on the Effects of the Types and Addition Time of Chemical Admixtures on Cement Performance, Chemical Engineering Transactions, 62 (**2017**) 1051–1056. https://doi.org/10.3303/CET1762176.

[103] S. Gwon, S.Y. Jang, M. Shin, Combined Effects of Set Retarders and Polymer Powder on the Properties of Calcium Sulfoaluminate Blended Cement Systems, Materials, 11 (**2018**). https://doi.org/10.3390/ma11050825.

[104] L. Coppola, D. Coffetti, E. Crotti, R. Dell'Aversano, G. Gazzaniga, T. Pastore, Influence of Lithium Carbonate and Sodium Carbonate on Physical and Elastic Properties and on Carbonation Resistance of Calcium Sulphoaluminate-Based Mortars, Applied Sciences, 10 (**2019**) 176. https://doi.org/10.3390/app10010176.

[105] E.A.R. Trout, The History of Calcareous Cements, in: P.C. Hewlett, M. Liska (Eds.), Lea's Chemistry of Cement and Concrete, Fifth Edition, Elsevier, **2019**: pp. 1–29. https://doi.org/10.1016/C2013-0-19325-7.

[106] W. Chuang, J. Geng-sheng, L. Bing-liang, P. Lei, F. Ying, G. Ni, L. Ke-zhi, Dispersion of Carbon Fibers and Conductivity of Carbon Fiber-Reinforced Cement-Based Composites, Ceramics International, 43 (**2017**) 15122–15132. https://doi.org/10.1016/j.ceramint.2017.08.041.

[107] F. Reza, G.B. Batson, J.A. Yamauro, J.S. Lee, Volume Electrical Resistivity of Carbon Fiber Cement Composites, ACI Materials Journal, 98 (**2001**) 25–34. https://doi.org/10.14359/10157.

[108] F. Vossoughi, Electrical Resistivity of Carbon Fiber Reinforced Concrete, University of California. https://www.researchgate.net/profile/Fariborz_Vossoughi/publication/241729614_Electrical_Resistivity_of_Carbon_Fiber_Reinforced_Concrete/links/0c96052e1504c7c896000000/Electrical-Resistivity-of-Carbon-Fiber-Reinforced-Concrete.pdf (accessed **August 4, 2024**).

[109] P.-W. Chen, D.D.L. Chung, Carbon Fiber Reinforced Concrete for Smart Structures Capable of Non-Destructive Flaw Detection, Smart Materials and Structures, 2 (**1993**) 22–30. https://doi.org/10.1088/0964-1726/2/1/004.

[110] H. Dehghanpour, K. Yilmaz, F. Afshari, M. Ipek, Electrically Conductive Concrete: A Laboratory-based Investigation and Numerical Analysis Approach, Construction and Building Materials, 260 (**2020**) 119948. https://doi.org/10.1016/j.conbuildmat.2020.119948.

[111] S. Yehia, C.Y. Tuan, D. Ferdon, B. Chen, Conductive Overlay for Bridge Deck Deicing: Mixture Proportioning. Optimization and Properties, Acids Materials Journals, 97 (**2000**) 172–181. https://doi.org/10.14359/821.

[112] W. Dong, W. Li, Z. Tao, K. Wang, Piezoresistive Properties of Cement-Based Sensors: Review and Perspective, Construction and Building Materials, 203 (**2019**) 146–163. https://doi.org/10.1016/j.conbuildmat.2019.01.081.

[113] N. Banthia, S. Djeridane, M. Pigeon, Electrical Resistivity of Carbon and Steel Micro-Fiber Reinforced Cements, Cement and Concrete Research, 22 (**1992**) 804–814. https://doi.org/10.1016/0008-8846(92)90104-4.

[114] L. Wang, F. Aslani, A Review on Material Design, Performance, and Practical Application of Electrically Conductive Cementitious Composites, Construction and Building Materials, 229 (**2019**) 116892. https://doi.org/10.1016/j.conbuildmat.2019.116892.

[115] J. Wu, J. Liu, F. Yang, Three-Phase Composite Conductive Concrete for Pavement Deicing, Construction and Building Materials, 75 (**2015**) 129–135. https://doi.org/10.1016/j.conbuildmat.2014.11.004.

[116] S. Düzağaç, Investigation the Effect of Gradation on Conductivity at Electrically Conductive Stone Mastic Asphalt Mixtures, Master of Science, Graduate School of Natural and Applied Sciences of Afyon Kocatepe University, **2019**.

[117] A. Sassani, A. Arabzadeh, H. Ceylan, S. Kim, S.M.S. Sadati, K. Gopalakrishnan, P.C. Taylor, H. Abdualla, Carbon Fiber-based Electrically Conductive Concrete for Salt-Free Deicing of Pavements, Journal of Cleaner Production, 203 (**2018**) 799–809. https://doi.org/10.1016/j.jclepro.2018.08.315.

[118] A. Gambo, G. Ozgur, E. Sevkat, Electrical Resistance Heating for Deicing and Snow Melting Applications: Experimental Study, Cold Regions Science and Technology, 160 (**2019**) 128–138. https://doi.org/10.1016/j.coldregions.2019.02.004.

[119] J. Donnini, T. Bellezze, V. Corinaldesi, Mechanical, Electrical and Self-Sensing Properties of Cementitious Mortars Containing Short Carbon Fibers, Journal of Building Engineering, 20 (**2018**) 8–14. https://doi.org/10.1016/j.jobe.2018.06.011.

[120] E. Zornoza, G. Catalá, F. Jiménez, L.G. Andión, P. Garcés, Electromagnetic Interference Shielding with Portland Cement Paste Containing Carbon Materials and Processed Fly Ash, Materiales de Construcción, 60 (**2010**) 21–32. https://doi.org/10.3989/mc.2010.51009.

[121] B.K. Baldwin, Electrically Conductive Concrete: Properties and Potential, Construction Canada, 98 (**1998**) 28–29.

[122] D. Micheli, A. Vricella, R. Pastore, A. Delfini, R. Bueno Morles, M. Marchetti, F. Santoni, L. Bastianelli, F. Moglie, V. Mariani Primiani, V. Corinaldesi, A. Mazzoli, J. Donnini, Electromagnetic Properties of Carbon Nanotube Reinforced Concrete Composites for Frequency Selective Shielding Structures, Construction and Building Materials, 131 (**2017**) 267–277. https://doi.org/10.1016/j.conbuildmat.2016.11.078.

[123] L. Bertolini, F. Bolzoni, T. Pastore, P. Pedeferri, Effectiveness of A Conductive Cementitious Mortar Anode for Cathodic Protection of Steel in Concrete, Cement and Concrete Research, 34 (**2004**) 681–694. https://doi.org/10.1016/j.cemconres.2003.10.018.

[124] J. Carmona, P. Garcés, M.A. Climent, Efficiency of A Conductive Cement-based Anodic System for the Application of Cathodic Protection, Cathodic Prevention and Electrochemical Chloride Extraction to Control Corrosion in Reinforced Concrete Structures, Corrosion Science, 96 (**2015**) 102–111. https://doi.org/10.1016/j.corsci.2015.04.012.

[125] H. Shifeng, X. Dongyu, C. Jun, X. Ronghua, L. Lingchao, C. Xin, Smart Properties of Carbon Fiber Reinforced Cement-based Composites, Journal of Composite Materials, 41 (**2007**) 125–131. https://doi.org/10.1177/0021998306063378.

[126] G.H. Nalon, J.C.L. Ribeiro, E.N.D. de Araújo, L.G. Pedroti, J.M.F. de Carvalho, R.F. Santos, A. Aparecido-Ferreira, Effects of Different Kinds of Carbon Black Nanoparticles on the Piezoresistive and Mechanical Properties of Cement-based Composites, Journal of Building Engineering, 32 (**2020**) 101724. https://doi.org/10.1016/j.jobe.2020.101724.

[127] Z.-Q. Shi, D.D.L. Chung, Carbon Fiber-Reinforced Concrete for Traffic Monitoring and Weighing in Motion, Cement and Concrete Research, 29 (**1999**) 435–439. https://doi.org/10.1016/S0008-8846(98)00204-X.

[128] S. Wu, P. Pan, M. Chen, Y. Zhang, Analysis of Characteristics of Electrically Conductive Asphalt Concrete Prepared by Multiplex Conductive Materials, Journal of Materials in Civil Engineering, 25 (**2013**) 871–879. https://doi.org/10.1061/(ASCE)MT.1943-5533.0000565.

[129] D.N. Çelik, G. Yıldırım, A. Al-Dahawi, H. Ulugöl, B. Han, M. Şahmaran, Self-Monitoring of Flexural Fatigue Damage in Large-Scale Steel-Reinforced Cementitious Composite Beams, Cement and Concrete Composites, 123 (**2021**). https://doi.org/10.1016/j.cemconcomp.2021.104183.

[130] A. Al-Dahawi, O. Ozturk, F. Emami, G. Yıldırım, S. Mustafa, Effect of Mixing Methods on the Electrical Properties of Cementitious Composites Incorporating Different Carbon-based Materials, Construction and Building Materials, 104 (**2016**) 160–168. https://doi.org/10.1016/j.conbuildmat.2015.12.072.

[131] G. Yıldırım, M.H. Sarwary, A. Al-Dahawi, O. Öztürk, Ö. Anıl, M. Şahmaran, Piezoresistive Behavior of CF- and CNT-based Reinforced Concrete Beams Subjected to Static Flexural Loading: Shear Failure Investigation, Construction and Building Materials, 168 (**2018**) 266–279. https://doi.org/10.1016/j.conbuildmat.2018.02.124.

[132] K. Keller, Electrical System Grounding and Bonding, in: Electrical Safety Code Manual, Elsevier, **2010**: pp. 91–122. https://doi.org/10.1016/b978-1-85617-654-5.00005-4.

[133] X. Tian, H. Hu, Test and Study on Electrical Property of Conductive Concrete, Procedia Earth and Planetary Science, (**2012**) 83–87. https://doi.org/10.1016/j.proeps.2012.01.014.

[134] C. Weir, M.L. Pantoya, G. Ramachandran, T. Dallas, D. Prentice, M. Daniels, Electrostatic Discharge Sensitivity and Electrical Conductivity of Composite Energetic Materials, Journal of Electrostatics, 71 (**2013**) 77–83. https://doi.org/10.1016/j.elstat.2012.10.002.

[135] J. Terwoert, Occupational Exposure to Epoxy Resins, European Agency for Safety and Health at Work. https://oshwiki.osha.europa.eu/en/themes/occupational-exposure-epoxy-resins (accessed **August 6, 2024**).

[136] H. Dehghanpour, K. Yilmaz, Investigation of Specimen Size, Geometry and Temperature Effects on Resistivity of Electrically Conductive Concretes, Construction and Building Materials, 250 (**2020**) 118864. https://doi.org/10.1016/j.conbuildmat.2020.118864.

[137] A.S. El-Dieb, M.A. El-Ghareeb, M.A.H. Abdel-Rahman, E.S.A. Nasr, Multifunctional Electrically Conductive Concrete Using Different Fillers, Journal of Building Engineering, 15 (**2018**) 61–69. https://doi.org/10.1016/j.jobe.2017.10.012.

[138] J. Han, J. Pan, J. Cai, X. Li, A Review on Carbon-based Self-Sensing Cementitious Composites, Construction and Building Materials, 265 (**2020**) 120764. https://doi.org/10.1016/j.conbuildmat.2020.120764.

[139] D.G. Meehan, Shoukai Wang, D.D.L. Chung, Electrical-Resistance-based Sensing of Impact Damage in Carbon Fiber Reinforced Cement-Based Materials, Journal of Intelligent Material Systems and Structures, 21 (**2010**) 83–105. https://doi.org/10.1177/1045389X09354786.

[140] H. Dehghanpour, K. Yilmaz, The Relationship Between Resistances Measured by Two-Probe, Wenner Probe and C1760-12 ASTM Methods in Electrically Conductive Concretes, SN Applied Sciences, 2 (**2020**) 1–10. https://doi.org/10.1007/s42452-019-1811-7.

[141] B. Chen, K. Wu, W. Yao, Conductivity of Carbon Fiber Reinforced Cement-Based Composites, Cement and Concrete Composites, 26 (**2004**) 291–297. https://doi.org/10.1016/S0958-9465(02)00138-5.

[142] Z. Zhou, N. Xie, X. Cheng, L. Feng, P. Hou, S. Huang, Electrical Properties of Low Dosage Carbon Nanofiber/Cement Composite: Percolation Behavior and Polarization Effect, Cement and Concrete Composites, 109 (**2020**) 103539. https://doi.org/10.1016/j.cemconcomp.2020.103539.

[143] A. Sassani, H. Ceylan, S. Kim, K. Gopalakrishnan, A. Arabzadeh, P.C. Taylor, Influence of Mix Design Variables on Engineering Properties of Carbon Fiber-Modified Electrically Conductive Concrete, Construction and Building Materials, 152 (**2017**) 168–181. https://doi.org/10.1016/j.conbuildmat.2017.06.172.

[144] L. Fiala, J. Toman, J. Vodička, V. Ráček, Experimental Study on Electrical Properties of Steel-Fibre Reinforced Concrete, In: Procedia Engineering, Elsevier, **2016**: pp. 241–248. https://doi.org/10.1016/j.proeng.2016.07.362.

[145] S. Zhu, D.D.L. Chung, Numerical Assessment of the Methods of Measurement of the Electrical Resistance in Carbon Fiber Reinforced Cement, Smart Materials and Structures, 16 (**2007**) 1164–1170. https://doi.org/10.1088/0964-1726/16/4/026.

[146] G. Vijayaraghavan, Mark Brown, Malcolm Barnes, Static Electricity and Protection, in: Practical Grounding, Bonding, Shielding and Surge Protection, Elsevier, **2004**: pp. 55–61. https://doi.org/10.1016/B978-0-7506-6399-1.X5000-X.

[147] NFPA 70, National Electrical Code, National Fire Protection Association, Quincy, **2017**.

[148] EN 1081+A1, Resilient, Laminate and Modular Multilayer Floor Coverings-Determination of the Electrical Resistance, European Standard, **2020**.

[149] J.-M. Chiou, Q. Zheng, D.D.L. Chung, Electromagnetic Interference Shielding by Carbon Fibre Reinforced Cement, Composites, 20 (**1989**) 379–381. https://doi.org/10.1016/0010-4361(89)90663-0.

[150] H.O.U. Zuofu, L.I. Zhuoqiu, W. Jianjun, Electrical Conductivity of the Carbon Fiber Conductive Concrete, Journal of Wuhan University of Technology Material Science, 22 (**2006**) 346–349. https://doi.org/10.1007/s11595-005-2346-x.

[151] H. Li, H. Xiao, J. Ou, Effect of Compressive Strain on Electrical Resistivity of Carbon Black-Filled Cement-based Composites, Cement and Concrete Composites, 28 (**2006**) 824–828. https://doi.org/10.1016/j.cemconcomp.2006.05.004.

[152] S. Wen, D.D.L. Chung, Partial Replacement of Carbon Fiber by Carbon Black in Multifunctional Cement–Matrix Composites, Carbon, 45 (**2007**) 505–513. https://doi.org/10.1016/j.carbon.2006.10.024.

[153] X. Fan, D. Fang, M. Sun, Z. Li, Piezoresistivity of Carbon Fiber Graphite Cement-based Composites with CCCW, Journal of Wuhan University of Technology-Materials Science Journals, 26 (**2011**) 339–343. https://doi.org/10.1007/s11595-011-0226-0.

[154] J. Qin, W. Yao, J. Zuo, H. Cao, Assessment on the Electrical Conductivity of Additive Fillers into Carbon Fiber-Cement Based Composites, Key Engineering Materials, 492 (**2012**) 185–188. https://doi.org/10.4028/www.scientific.net/KEM.492.185.

[155] M.Y. Zakaria, A.B. Sulong, J. Sahari, H. Suherman, Effect of the Addition of Milled Carbon Fiber as A Secondary Filler on The Electrical Conductivity of Graphite/Epoxy Composites for Electrical Conductive Material, Composites Part B: Engineering, 83 (**2015**) 75–80. https://doi.org/10.1016/j.compositesb.2015.08.034.

[156] B. Han, L. Zhang, C. Zhang, Y. Wang, X. Yu, J. Ou, Reinforcement Effect and Mechanism of Carbon Fibers to Mechanical and Electrically Conductive Properties of Cement-based Materials, Construction and Building Materials, 125 (**2016**) 479–489. https://doi.org/10.1016/j.conbuildmat.2016.08.063.

[157] A. Al-Dahawi, M.H. Sarwary, O. Öztürk, G. Yildirim, A. Akin, M. Şahmaran, M. Lachemi, Electrical Percolation Threshold of Cementitious Composites Possessing Self-Sensing Functionality Incorporating Different Carbon-based Materials, Smart Materials and Structures, 25 (**2016**). https://doi.org/10.1088/0964-1726/25/10/105005.

[158] L. Shi, Y. Lu, Y. Bai, Mechanical and Electrical Characterisation of Steel Fiber and Carbon Black Engineered Cementitious Composites, Procedia Engineering, 188 (**2017**) 325–332. https://doi.org/10.1016/j.proeng.2017.04.491.

[159] G.M. Kim, S.M. Park, G.U. Ryu, H.K. Lee, Electrical Characteristics of Hierarchical Conductive Pathways in Cementitious Composites Incorporating CNT and Carbon Fiber, Cement and Concrete Composites, 82 (**2017**) 165–175. https://doi.org/10.1016/j.cemconcomp.2017.06.004.

[160] S. Jiang, D. Zhou, L. Zhang, J. Ouyang, X. Yu, X. Cui, B. Han, Comparison of Compressive Strength and Electrical Resistivity of Cementitious Composites with Different Nano- and Micro-Fillers, Archives of Civil and Mechanical Engineering, 18 (**2018**) 60–68. https://doi.org/10.1016/j.acme.2017.05.010.

[161] W. Zhang, J. Ouyang, Y. Ruan, Q. Zheng, J. Wang, X. Yu, B. Han, Effect of Mix Proportion and Processing Method on the Mechanical and Electrical Properties of Cementitious Composites with Nano/Fiber Fillers, Materials Research Express, 5 (**2018**) 15706. https://doi.org/10.1088/2053-1591/aaa60a.

[162] G. Faneca, I. Segura, J.M. Torrents, A. Aguado, Development of Conductive Cementitious Materials Using Recycled Carbon Fibres, Cement and Concrete Composites, (**2018**). https://doi.org/10.1016/j.cemconcomp.2018.06.009.

[163] T. Uygunoğlu, B. Şimşek, Investigation of Mechanical, Physical and Electrical Properties of Graphene Oxide Blended Mortars, Mühendislik Bilimleri ve Tasarım Dergisi, 7 (**2019**) 196–204. https://doi.org/10.21923/jesd.451473.

[164] T. Wang, J. Xu, E. Bai, X. Luo, H. Chen, G. Liu, S. Chang, Study on the Effects of Carbon Fibers and Carbon nanofibers on Electrical Conductivity of Concrete, IOP Conference Series: Earth and Environmental Science, 267 (**2019**) 032011. https://doi.org/10.1088/1755-1315/267/3/032011.

[165] A. Dehghani, F. Aslani, The Effect of Shape Memory Alloy, Steel, and Carbon Fibres on Fresh, Mechanical, and Electrical Properties of Cementitious Composites, Cement and Concrete Composites, (**2020**) 103659. https://doi.org/10.1016/j.cemconcomp.2020.103659.

[166] A. Akbar, V.K.R. Kodur, K.M. Liew, Microstructural Changes and Mechanical Performance of Cement Composites Reinforced with Recycled Carbon Fibers, Cement and Concrete Composites, 121 (**2021**) 104069. https://doi.org/10.1016/j.cemconcomp.2021.104069.

[167] D.D.L. Chung, Cement Reinforced with Short Carbon Fibers: A Multifunctional Material, Composites Part B: Engineering, 31 (**2000**) 511–526. https://doi.org/10.1016/S1359-8368(99)00071-2.

[168] X. Huang, Fabrication and Properties of Carbon Fibers, Materials, 2 (**2009**) 2369–2403. https://doi.org/10.3390/ma2042369.

[169] Y. Ding, Z. Chen, Z. Han, Y. Zhang, F. Pacheco-Torgal, Nano-Carbon Black and Carbon Fiber as Conductive Materials for the Diagnosing of the Damage of Concrete Beam, Construction and Building Materials, 43 (**2013**) 233–241. https://doi.org/10.1016/j.conbuildmat.2013.02.010.

[170] R. Kaur, N.C. Kothiyal, Comparative Effects of Sterically Stabilized Functionalized Carbon Nanotubes and Graphene Oxide as Reinforcing Agent on Physico- Mechanical Properties and Electrical Resistivity of Cement Nanocomposites, Construction and Building Materials, 202 (**2019**) 121–138. https://doi.org/10.1016/j.conbuildmat.2018.12.220.

[171] N.A. Mohd Radzuan, M. Yusuf Zakaria, A.B. Sulong, J. Sahari, The Effect of Milled Carbon Fibre Filler on Electrical Conductivity in Highly Conductive Polymer Composites, Composites Part B: Engineering, 110 (**2017**) 153–160. https://doi.org/10.1016/j.compositesb.2016.11.021.

[172] A.S. Ali, A.A.M. Al-Shaar, A.A. Shakir, Electrical Properties of Fibrous Self-Compacting Concrete Reinforced with Different Types of Fibers, Materials Today: Proceedings, 42 (**2021**) 2012–2017. https://doi.org/10.1016/j.matpr.2020.12.252.

[173] H.K. Kim, I.W. Nam, H.K. Lee, Enhanced Effect of Carbon Nanotube on Mechanical and Electrical Properties of Cement Composites by Incorporation of Silica Fume, Composite Structures, 107 (**2014**) 60–69. https://doi.org/10.1016/j.compstruct.2013.07.042.

[174] H. Suherman, A.B. Sulong, M.Y. Zakaria, N. Royan, J. Sahari, Electrical Conductivity and Physical Changes of Functionalized Carbon Nanotube/Graphite/Stainless Steel (SS316L)/Polypropylene Composites Immersed in an Acidic Solution, Songklanakarin Journal of Science and Technology, 40 (**2018**) 105–112. https://doi.org/10.14456/sjst-psu.2018.12.

[175] P. Payakaniti, S. Pinitsoonthorn, P. Thongbai, V. Amornkitbamrung, P. Chindaprasirt, Effects of Carbon Fiber on Mechanical and Electrical Properties of Fly Ash Geopolymer Composite, Materials Today: Proceedings, 5 (**2018**) 14017–14025. https://doi.org/10.1016/j.matpr.2018.02.054.

[176] L. Lavagna, S. Musso, G. Ferro, M. Pavese, Cement-based Composites Containing Functionalized Carbon Fibers, Cement and Concrete Composites, 88 (**2018**) 165–171. https://doi.org/10.1016/j.cemconcomp.2018.02.007.

[177] D.D. Chung, Dispersion of Short Fibers in Cement, Journal of Materials in Civil Engineering, 17 (**2005**) 379–383. https://doi.org/10.1061/(ASCE)0899-1561(2005)17:4(379).

[178] A.O. Monteiro, A. Loredo, P.M.F.J. Costa, M. Oeser, P.B. Cachim, A Pressure-Sensitive Carbon Black Cement Composite for Traffic Monitoring, Construction and Building Materials, 154 (**2017**) 1079–1086. https://doi.org/10.1016/j.conbuildmat.2017.08.053.

[179] S. Ivaturi, H. Baske, P. Ghosal, Distribution of Milled Carbon Fibers as A Function of Their Length on S-Glass Fabric and Its Effect on the Electromagnetic Properties of S-Glass Epoxy Composites, Journal of Composite Materials, 53 (**2019**) 2891–2899. https://doi.org/10.1177/0021998318819738.

[180] M.A. Notani, A. Arabzadeh, H. Ceylan, S. Kim, K. Gopalakrishnan, Effect of Carbon-Fiber Properties on Volumetrics and Ohmic Heating of Electrically Conductive Asphalt Concrete, Journal of Materials in Civil Engineering, 31 (**2019**) 1–9. https://doi.org/10.1061/(ASCE)MT.1943-5533.0002868.

[181] D.D.L. Chung, Properties of Carbon Fibers, in: Carbon Fiber Composites, Elsevier, **1994**: pp. 65–78. https://doi.org/10.1016/B978-0-08-050073-7.50008-7.

[182] B. Díaz, B. Guitián, X.R. Nóvoa, C. Pérez, Analysis of The Microstructure of Carbon Fibre Reinforced Cement Pastes by Impedance Spectroscopy, Construction and Building Materials, 243 (**2020**). https://doi.org/10.1016/j.conbuildmat.2020.118207.

[183] B. Han, S. Ding, X. Yu, Intrinsic Self-Sensing Concrete and Structures: A Review, Measurement, 59 (**2015**) 110–128. https://doi.org/10.1016/j.measurement.2014.09.048.

[184] X. Wang, Y. Wang, Z. Jin, Electrical Conductivity Characterization and Variation of Carbon Fiber Reinforced Cement Composite, Journal of Material Science, 37 (**2002**) 223–227. https://doi.org/https://doi.org/10.1023/A:1013107623281.

[185] S. Yehia, N. Qaddoumi, M. Hassan, Conductive Concrete for Electromagnetic Shielding Applications, Advances in Civil Engineering Materials, 3 (**2018**). https://doi.org/10.1520/ACEM20130107.

[186] H. Deng, H. Li, Assessment of Self-Sensing Capability of Carbon Black Engineered Cementitious Composites, Construction and Building Materials, 173 (**2018**) 1–9. https://doi.org/10.1016/j.conbuildmat.2018.04.031.

[187] C. Shi, Effect of Mixing Proportions of Concrete on Its Electrical Conductivity and the Rapid Chloride Permeability Test (ASTM C1202 or ASSHTO T277) Results, Cement and Concrete Research, 34 (**2004**) 537–545. https://doi.org/10.1016/j.cemconres.2003.09.007.

[188] A. Principigallo, K. van Breugel, G. Levita, Influence of The Aggregate on the Electrical Conductivity of Portland Cement Concretes, Cement and Concrete Research, 33 (**2003**) 1755–1763. https://doi.org/10.1016/S0008-8846(03)00166-2.

[189] A.O. Monteiro, P.B. Cachim, P.M.F.J. Costa, Self-Sensing Piezoresistive Cement Composite Loaded with Carbon Black Particles, Cement and Concrete Composites, (**2017**). https://doi.org/10.1016/j.cemconcomp.2017.04.009.

[190] K. Zhang, B. Han, X. Yu, Nickel Particle Based Electrical Resistance Heating Cementitious Composites, Cold Regions Science and Technology, 69 (**2011**) 64–69. https://doi.org/10.1016/j.coldregions.2011.07.002.

[191] J. Cao, D.D.L. Chung, Carbon Fiber Reinforced Cement Mortar Improved by Using Acrylic Dispersion as An Admixture, Cement and Concrete Research, 31 (**2001**) 1633–1637. https://doi.org/10.1016/S0008-8846(01)00599-3.

[192] Y. Huang, H. Li, S. Qian, Self-Sensing Properties of Engineered Cementitious Composites, Construction and Building Materials, 174 (**2018**) 253–262. https://doi.org/10.1016/j.conbuildmat.2018.04.129.

[193] M. Nili, V. Afroughsabet, Combined Effect of Silica Fume and Steel Fibers on The Impact Resistance and Mechanical Properties of Concrete, International Journal of Impact Engineering, 37 (**2010**) 879–886. https://doi.org/10.1016/j.ijimpeng.2010.03.004.

[194] S. Bai, L. Jiang, N. Xu, M. Jin, S. Jiang, Enhancement of Mechanical and Electrical Properties of Graphene/Cement Composite due to Improved Dispersion of Graphene by Addition of Silica Fume, Construction and Building Materials, 164 (**2018**) 433–441. https://doi.org/10.1016/j.conbuildmat.2017.12.176.

[195] W. Dong, W. Li, Y. Guo, X. He, D. Sheng, Effects of Silica Fume on Physicochemical Properties and Piezoresistivity of Intelligent Carbon Black-Cementitious Composites, Construction and Building Materials, 259 (**2020**) 120399. https://doi.org/10.1016/j.conbuildmat.2020.120399.

[196] C. Jiang, X. Zhou, S. Huang, D. Chen, Influence of Polyacrylic Ester and Silica Fume on the Mechanical Properties of Mortar for Repair Application, Advances in Mechanical Engineering, 9 (**2017**) 168781401668385. https://doi.org/10.1177/1687814016683856.

[197] S. Wen, D.D.L. Chung, Cement-Based Controlled Electrical Resistivity Materials, Journal of Electronic Materials, 30 (**2001**) 1448–1451. https://doi.org/10.1007/s11664-001-0200-2.

[198] Y. Liu, S. Yang, J. Li, F. Wang, S. Hu, Effect of w/c ratio and Antifreeze Admixture on The Frost Damage of Sulfoaluminate Cement Concrete at − 20 °C, Construction and Building Materials, 347 (**2022**). https://doi.org/10.1016/j.conbuildmat.2022.128457.

[199] Y. Liu, W. Tian, M. Wang, B. Qi, W. Wang, Rapid Strength Formation of On-Site Carbon Fiber Reinforced High-Performance Concrete Cured by Ohmic Heating, Construction and Building Materials, 244 (**2020**) 118344. https://doi.org/10.1016/j.conbuildmat.2020.118344.

[200] R. Fulham-Lebrasseur, L. Sorelli, D. Conciatori, Development of Electrically Conductive Concrete and Mortars with Hybrid Conductive Inclusions, Construction and Building Materials, 237 (**2020**) 117470. https://doi.org/10.1016/j.conbuildmat.2019.117470.

[201] H. LI, H. Xiao, J. Ou, Electrical Property of Cement-Based Composites Filled with Carbon Black Under Long-Term Wet and Loading Condition, Composites Science and Technology, 68 (**2008**) 2114–2119. https://doi.org/10.1016/j.compscitech.2008.03.007.

[202] C.T. Chen, J.J. Chang, W.C. Yeih, The Effects of Specimen Parameters on The Resistivity of Concrete, Construction and Building Materials, 71 (**2014**) 35–43. https://doi.org/10.1016/j.conbuildmat.2014.08.009.

[203] H.K. Lee, I.W. Nam, M. Tafesse, H.K. Kim, Fluctuation of Electrical Properties of Carbon-based Nanomaterials/Cement Composites: Case Studies and Parametric Modeling, Cement and Concrete Composites, 102 (**2019**) 55–70. https://doi.org/10.1016/j.cemconcomp.2019.04.008.

[204] EN 197-1, Composition, Specifications and Conformity Criteria for Common Cements, European Standard, **2012**.

[205] ASTM C150, Standard Specification for Portland Cement, American Society for Testing Materials, West Conshohocken, **2010**. https://doi.org/10.1520/C0150.

[206] ASTM C204, Standard Test Methods for Fineness of Hydraulic Cement by Air-Permeability Apparatus, American Society for Testing Materials, **2019**.

[207] ASTM C618, Standard Specification for Coal Fly Ash and Raw or Calcined Natural Pozzolan for Use in Concrete, American Society for Testing Materials, **2022**.

[208] EN 12350, Testing Fresh Concrete - Part 2: Slump Test, European Standard, **2019**.

[209] TS EN 1015-3, Methods of Test for Mortar for Masonry- Part 3: Determination of Consistence of Fresh Mortar (by Flow Table), Türk Standartları Enstitüsü, **2000**.

[210] ASTM C109, Standard Test Method for Compressive Strength of Hydraulic Cement Mortars, West Conshohocken, American Society for Testing Materials, **2001**.

[211] R.P. Spragg, J. Castro, T. Nantung, M. Paredes, J. Weiss, Variability Analysis of the Bulk Resistivity Measured Using Concrete Cylinders, Advances in Civil Engineering Materials, 1 (**2012**) 104596. https://doi.org/10.1520/ACEM104596.

[212] K. Wu, H. Han, C. Rößler, L. Xu, H.M. Ludwig, Rice Hush Ash as Supplementary Cementitious Material for Calcium Aluminate Cement – Effects on Strength and Hydration, Construction and Building Materials, 302 (**2021**). https://doi.org/10.1016/j.conbuildmat.2021.124198.

[213] I.B. Celik, The Effects of Particle Size Distribution and Surface Area Upon Cement Strength Development, Powder Technology, 188 (**2009**) 272–276. https://doi.org/10.1016/j.powtec.2008.05.007.

[214] G. Li, X. Zhao, Properties of Concrete Incorporating Fly Ash and Ground Granulated Blast-Furnace Slag, Cement and Concrete Composites, 25 (**2003**) 293–299. https://doi.org/10.1016/S0958-9465(02)00058-6.

[215] Md. Safiuddin, G. Abdel-Sayed, N. Hearn, Flexural and Impact Behaviors of Mortar Composite Including Carbon Fibers, Materials, 15 (**2022**) 1657–1677. https://doi.org/10.3390/ma15051657.

[216] S.Y. Ghanem, J. Bowling, Mechanical Properties of Carbon-Fiber–Reinforced Concrete, Advances in Civil Engineering Materials, 8 (**2019**) 20180089. https://doi.org/10.1520/ACEM20180089.

[217] D. Rieger, M. Pola, P. Franče, J. Kadlec, T. Kovářík, P. Kopačka, The Effect of Short Carbon Fibers on Rheological Behaviour and Mechanical Properties of Metakaolin-Slag Geopolymer Binder, IOP Conference Series: Materials Science and Engineering, 613 (**2019**) 012050. https://doi.org/10.1088/1757-899X/613/1/012050.

[218] N. Majain, A.B.A. Rahman, R.N. Mohamed, A. Adnan, Effect of Steel Fibers on Self-Compacting Concrete Slump Flow and Compressive Strength, IOP Conference Series: Materials Science and Engineering, 513 (**2019**) 012007. https://doi.org/10.1088/1757-899X/513/1/012007.

[219] N. Ozyurt, T.O. Mason, S.P. Shah, Correlation of Fiber Dispersion, Rheology and Mechanical Performance of FRCs, Cement and Concrete Composites, 29 (**2007**) 70–79. https://doi.org/10.1016/j.cemconcomp.2006.08.006.

[220] V. Kavya Sameera, L. Keshav, Properties and Performance of Steel Fiber Reinforced Concrete Beam Structure – Review, Materials Today: Proceedings, 66 (**2022**) 916–919. https://doi.org/10.1016/j.matpr.2022.04.643.

[221] V. Ramakrishnan, G.Y. Wu, G. Hosalli, Flexural Behavior and Toughness of Fiber Reinforced Concretes, in: International Symposium on Recent Developments in Concrete Fiber Composites, Washington, DC, **1989**: pp. 69–77.

[222] A. Alrawashdeh, O. Eren, Mechanical and Physical Characterisation of Steel Fibre Reinforced Self-Compacting Concrete: Different Aspect Ratios and Volume Fractions of Fibres, Results in Engineering, 13 (**2022**). https://doi.org/10.1016/j.rineng.2022.100335.

[223] Öztürk. O., Yıldırım. G., Keskin. Ü. S., Şahmaran. M., Multifunctional Cementitious Composites for Real-time Structural/Materials HealthMonitoring Applications, in: Uluslararası 10. Beton Kongresi, TMMOB İnşaat Mühendisleri Odası, Bursa, **2019**: pp. 521–529.

[224] D. Lu, D. Wang, J. Zhong, Highly Conductive and Sensitive Piezoresistive Cement Mortar with Graphene Coated Aggregates and Carbon Fiber, Cement and Concrete Composites, 134 (**2022**). https://doi.org/10.1016/j.cemconcomp.2022.104731.

[225] Q.S. Banyhussan, G. Yıldırım, E. Bayraktar, S. Demirhan, M. Şahmaran, Deflection-Hardening Hybrid Fiber Reinforced Concrete: The Effect of Aggregate Content, Construction and Building Materials, 125 (**2016**) 41–52. https://doi.org/10.1016/j.conbuildmat.2016.08.020.

[226] B. Chaudhuri, S. Ghosh, B. Mondal, D. Bhadra, Preparation and Characterization of Carbon Fibre Powder (CFP)-Polyvinyl Alcohol (PVA) Composite Films Showing Percolation Threshold Behaviour, Materials Science and Engineering: B 275, (**2022**) 115500. https://doi.org/10.1016/j.mseb.2021.115500.

[227] D. Wanasinghe, F. Aslani, G. Ma, Electromagnetic Shielding Properties of Cementitious Composites Containing Carbon Nanofibers, Zinc Oxide, and Activated Carbon Powder, Construction and Building Materials, 285 (**2021**). https://doi.org/10.1016/j.conbuildmat.2021.122842.

[228] T. Groetsch, M. Maghe, C. Creighton, R.J. Varley, Environmental, Property and Cost Impact Analysis of Carbon Fibre at Increasing Rates of Production, Journal of Cleaner Production, 382 (**2023**). https://doi.org/10.1016/j.jclepro.2022.135292.

[229] Z. Feng, Y. Zhou, L. Sui, Z. Zhu, Optimal Design of a Low-Cost High-Performance Hybrid Fiber Engineered Cementitious Composites, Construction and Building Materials, 345 (**2022**). https://doi.org/10.1016/j.conbuildmat.2022.128372.

[230] A.K. Thomoglou, M.G. Falara, M.E. Voutetaki, J.G. Fantidis, B.A. Tayeh, C.E. Chalioris, Electromechanical Properties of Multi-Reinforced Self-Sensing Cement-Based Mortar with MWCNTs, CFs, and PPs, Construction and Building Materials, 400 (**2023**). https://doi.org/10.1016/j.conbuildmat.2023.132566.

[231] H.V. Le, M.K. Kim, D.J. Kim, J. Park, Electrical Properties of Smart Ultra-High-Performance Concrete Under Various Temperatures, Humidities, And Age of Concrete, Cement and Concrete Composites, 118 (**2021**). https://doi.org/10.1016/j.cemconcomp.2021.103979.

[232] A.O. Monteiro, P.B. Cachim, P.M.F.J. Costa, Electrical Properties of Cement-based Composites Containing Carbon Black Particles, Materials Today: Proceedings, 2 (**2015**) 193–199. https://doi.org/10.1016/j.matpr.2015.04.021.

[233] T. Damion, P. Chaunsali, Evaluating Acid Resistance of Portland Cement, Calcium Aluminate Cement, and Calcium Sulfoaluminate Based Cement Using Acid Neutralisation, Cement and Concrete Research, 162 (**2022**). https://doi.org/10.1016/j.cemconres.2022.107000.

[234] J. Monteny, N. De Belie, L. Taerwe, Resistance of Different Types of Concrete Mixtures to Sulfuric Acid, Materials and Structures, 36 (**2003**) 242–249. https://doi.org/10.1007/BF02479618.